THE GEOLOGY, PETROLOGY AND GEOCHEMISTRY OF THE MINERALIZATION AND HYDROTHERMAL ALTERATION AT ONGEAMA, ONGOMBO AND MATCHLESS WEST EXTENSION, NAMIBIA

by

Marilena Moroni

This thesis is submitted in partial fulfilment of the requirements for the degree of Master of Science (Economic Geology) at Rhodes University, Grahamstown

November 1990

Declaration

All the work in this thesis is that of the writer, except where specific reference is made to the work of others.

Signed: Marilena Moroni

ABSTRACT

The Matchless Amphibolite Belt (Damara Orogen, Namibia) hosts several volcanogenic-exhalative, sediment-hosted stratiform cupriferous pyrite deposits. These are thought to be related to submarine volcanism during the early evolutionary stages of a narrow Damaran ocean, the Matchless Trough. The mineralized bodies examined (Ongeama, Ongombo and Matchless West Extension) are deformed and metamorphosed to low-medium grade (greenschist-amphibolite facies). They are associated with metapelite and amphibolite country rocks, and crop out as prominent limonite-rich gossans. The elongated shape of the sulphide bodies suggests a structural control. The mineralization normally consists of a variably developed massive sulphide portion, either quartz-, talc- or amphibole-bearing, and a stratigraphically overlying, extensive horizon of sulphide- and baryte-bearing exhalite (magnetite quartzite and less common talc- and actinolite-bearing schists). Lateral and vertical mineralogical changes within the mineralization match with significant variations in the element distribution. A metamorphosed and deformed alteration pipe, indicating the position of the fluid conduit, can be recognized in association with some ore bodies. The formation of quartz-muscovite and chlorite alteration envelopes (Ongeama, Matchless West Extension) and the presence of subtle mineralogical changes (Ongombo) in the immediate wallrocks, accompanied by extensive redistribution, leaching and introduction of elements from outside, suggest the hydrothermal metasomatic origin of the alteration zones. Element zoning within the mineralized bodies can be related to the original position of the vent, possibly coinciding with the intersection of the axis of the alteration pipe with the sulphide body. Cu, Zn, Au (pro parte) and Mo are enriched proximal to the vent, whereas Pb, Ba, Mn, Ag, Au, Sn, Bi and W enrichment characterizes the distal facies of the mineralization. In spite of the obliterating and disrupting effects of the regional dynamo-metamorphism, the element distribution within the mineralization and alteration zones examined is comparable with the geochemical trends observed in present-day mineralizing systems in early-stage oceanic environments (e.g. Guaymas Basin). During exploration for blind volcanogenic mineralization, the detection of hydrothermally altered rocks is fundamental in indicating the proximity to the mineralization. The localization of the alteration zone is also important in the interpretation of the regional geology of the explored area: in deformed terrains the assessment of the stratigraphic position of the alteration zone, relative to the mineralization, helps in establishing the polarity of the sequence.

AKNOWLEDGEMENTS

I want to express my sincere gratitude to people and organizations for their help in the fulfilment of my thesis:

* *the C.S.I.R. for the bursary that allowed me to study at Rhodes University;*

* *Gold Fields Namibia Ltd., for the financial and logistic support for my thesis, and friendlyness. In particular, I would like to thank Dudley Corbett for his precious advices and assistance; my field assistance Freddie Sakkie Tumuna and the field crew of the "Republic of Ongombo" for their help under the hot Namibian sun; Ina Maneschjin and Tom Evers for their assistance and nice parties.*

* *Tim Smalley, for his precious help, stimulating discussions and friendship.*

* *my supervisors Prof. F. Pirajno, Prof. R.E. Jacob and C.A. Mallinson for their careful guidance and valuable advices throughout my studies at Rhodes University. Prof. J.S. Marsh and Prof. H.V. Eales are kindly thanked for their assistance for XRF analysis and for ore polishing and micro-photography, respectively.*

* *the secretaries and the technical staff of the Geology Department , Rhodes University, namely Lori and Coleen, Abel, Frans, John Hepple, Wilberforce and Bennett.*

* *Last, but not least, my brother Franco and my friends Alfredo and Cecilia for their tireless help in typing, sticking, printing, proof-reading, etc.; my fellow students Fabrice, Angela, Duck, Derek, Link, and the other honourable members of the Society of Insulting Geologists (Rupert and Colin) for nice companionship and friendship; my family for its constant encouragement and support.*

INDEX

PART C PETROLOGY OF MINERALIZED AND BARREN ROCKS

PART D GEOCHEMISTRY OF MINERALIZATION, ALTERATION ZONE AND COUNTRY ROCKS

PART E CONCLUSIONS

LIST OF FIGURES

LIST OF TABLES

LIST OF THE APPENDICES

LIST OF PLATES

Plate 9 - *Ongeama gossan: phlogopite (?)-bearing ferruginous schist (brownish) containing gahnite (?) and magnetite.*

Plate 10 - *Ongeama deposit, alteration pipe, magnetic quartz-chlorite schist facies: aggregate of garnet, staurolite and chloritoid in chlorite-bearing quartz-rich groundmass.*

Plate 11 - *Ongeama deposit, alteration pipe, magnetic quartz-chlorite schist facies: coarse-grained skeletal garnet porphyroblast in chlorite-bearing quartzose groundmass.*

Plate 12 - *Ongeama deposit, alteration pipe magnetic muscovite facies: Fe-hydroxide-stained quartz-muscovite schist, with disseminated magnetite. Sporadic staurolite and chlorite.*

Plate 13 - *Matchless West Extension deposit: particular of a talc-quartz-rich patch of the massive sulphide gossan.*

Plate 14 - *Matchless West Extension deposit: quartz-muscovite schist from the axial zone of the alteration pipe. Fe-hydroxide-rimmed cavities after euhedral pyrite crystals are disseminated.*

Plate 15 - *Matchless West Extension deposit, upper magnetite quartzite layer: thin magnetite strings and anhedral baryte blebs in the sulphide-devoid quartz-rich groundmass.*

Plate 16 - *Matchless West Extension deposit, lower magnetite quartzite layer: typical banding induced by magnetite-rich laminae.*

Plate 17 - *Matchless West Extension deposit, ultramafic exhalites: talc-phlogopite-carbonate schist.*

Plate 18 - *Matchless West Extension deposit: same rock type as in Plate 17.*

Plate 19 - *Matchless West Extension deposit, ultramafic exhalites: assemblage of actinolite, quartz and baryte.*

Plate 20 - *Matchless West Extension deposit, ultramafic exhalites: actinolite and baryte in gossanous quartzite.*

Plate 21 - *Matchless West Extension deposit, marble-like rock: anhedral, sieve-textured carbonate crystals replacing the muscovite-bearing quartzitic-groundmass.*

Plate 21 - *Von Francois Ost 60 farm area, massive talc-chlorite-actinolite schist: subhedral actinolite crystals and talc lamellae included in a fine-grained chlorite-rich groundmass.*

Plate 23 - *Ongombo deposit, borehole no. OGB 153A: staurolite-bearing quartz-biotite-muscovite-chlorite schist in the hangingwall next to the ore zone.*

Plate 24 - *Ongombo deposit, borehole no. OGB 153A: biotite selvedge zone showing the coarse biotite groundmass, subhedral staurolite grains, coarse apatite crystals and part of pyrite "augen".*

Plate 25 - *Ongombo deposit, borehole no. OGB 153A: plagioclase-rich biotite schist facies within the ore zone.*

Plate 26 - *Ongombo deposit, borehole no. OGB 153A, sulphide-bearing magnetite quartzite: embayed intergrowth between recrystallized pyrite and magnetite. Chalcopyrite occurs as interstitial patches and inclusions within pyrite and magnetite.*

Plate 27 - *Ongombo deposit, borehole no. OGB 153A, semi-massive sulphide facies: annealed pyrite aggregate with interstitial chalcopyrite and inclusions of galena and chalcopyrite.*

Plate 28 - *Ongombo deposit, borehole no. OGB 153A, semi-massive sulphide facies: cracked, sub-hedral pyrite grains with inclusions of chalcopyrite + pyrrhotite, and pyrrhotite remobilized along cracks.*

INTRODUCTION

The purpose of this study is to examine the geological, mineralogical and geochemical characteristics of metamorphosed and deformed sediment-hosted volcanogenic exhalative mineralization and associated alteration. The mineralization is represented by three Besshi-type sulphide deposits, Ongeama, Ongombo and Matchless West Extension, in the eastern sector of the Matchless Amphibolite Belt, Damara Orogen, Namibia.

Information was obtained from the regional geological framework of the Matchless Belt (Part A), detailed mapping, core logging and sampling of mineralization, alteration and country rocks (Part B), microscope examination of thin and polished sections (Part C), and geochemical analyses (Part D). This information was used with the following purposes:

a) gain a better understanding of the characteristics and nature of the mineralization hosted by the Matchless Belt;

b) evaluate the effects of regional metamorphism and deformation on the mineralogy and geochemistry of mineralization and associated hydrothermal alteration;

c) obtain some guidelines and principles applicable to exploration for similar mineralization in a metamorphosed terrane.

PART A

REGIONAL GEOLOGICAL FRAMEWORK

1 GEOLOGICAL AND STRUCTURAL EVOLUTION OF THE DAMARA OROGEN

The Damara Orogen represents a part of the Pan African orogenic network dissecting Africa (Fig. 1a). The Damara Orogen (Fig. 1b) consists of a NE-trending 400 km-wide intracontinental branch, which occupies most of Central and Northern Namibia, and of a NNW-SSE-trending, 150 km-wide coastal branch, whose southern extension is represented by the Gariep Belt. The intracontinental and coastal branches define a three-armed orogenic junction. This triple junction separates the overriding Congo Craton from the Kalahari Craton, and, along its intracontinental branch, it probably is connected to the Pan African Katanga Belt in Zambia across Botswana (Martin and Porada, 1977).

A brief account of the geology and the structure of the Damara Orogen, with special reference to the intracontinental branch and, within this, to the Southern Zone, is given below.

The main geological and tectonic features of the Damara Orogen were developed during middle-late Proterozoic to early Palaeozoic times. The nature and distribution of lithologies in the Damara sequence indicate their deposition in an extensional environment. The tensional regime induced the opening of the proto-South Atlantic Ocean along the coastal branch, whereas the intracontinental arm of the triple junction evolved in an aborted rift (Tankard et al., 1982).

The complex evolution of the intracontinental branch may have involved continental rifting followed by convergence and continental collision (Miller, 1983a). During Karoo-post Karoo times, new extensional tectonism developed coincident with the Gondwana breakup and resulted in the separation of Africa from South America.

According to Mason (1981), the early tectonic history of the Damara Orogen followed trends established by an earlier, Irumide rift system, the Koras-Sinclair-Ghanzi (KSG) Rift (after Borg, 1988) (Fig. 2a). Both KSG and Damaran rift systems might represent the results of a continuous tectonic process related to southward plate migration over

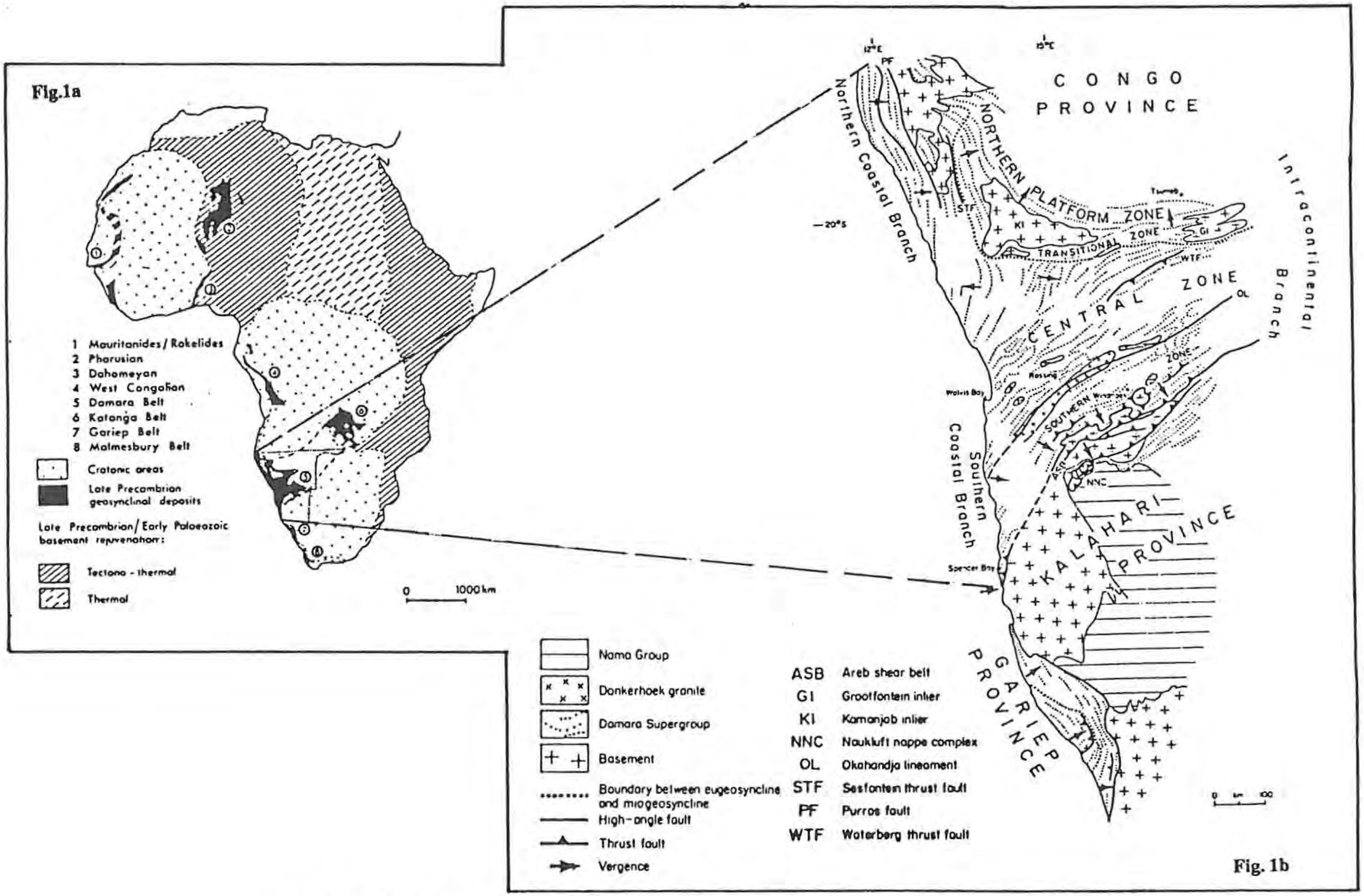

Fig. 1 - a) Pan African belts and areas of thermal and tectono-thermal rejuvenation during the Pan African event (Porada, 1983). b) Schematic tectonic map of the Damara Orogen, Namibia, showing tectonic zones (modified after Tankard et al., 1982).

Fig.2a

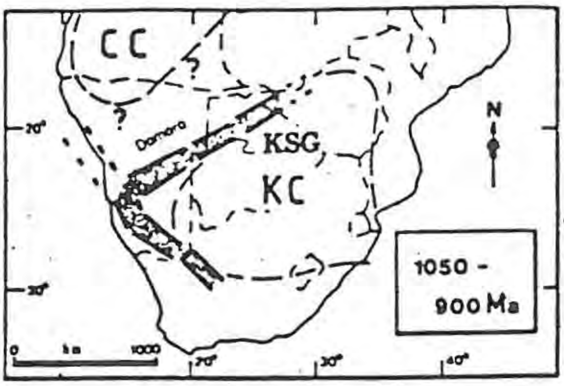

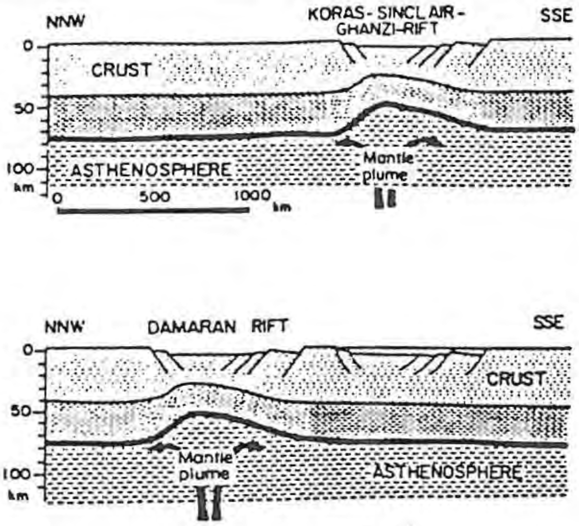

Fig. 2b

Fig. 2 - a) Sketch with the position of the Koras-Sinclair-Ghanzi rift (KSG; stippled) relative to the Damaran rift (CC=Congo Craton; KC=Kalahari Craton); b) schematic sketch of the evolution of the KSG rift and the early Damaran rift due to plate migration southwards over a mantle plume (Borg, 1988).

Fig.3

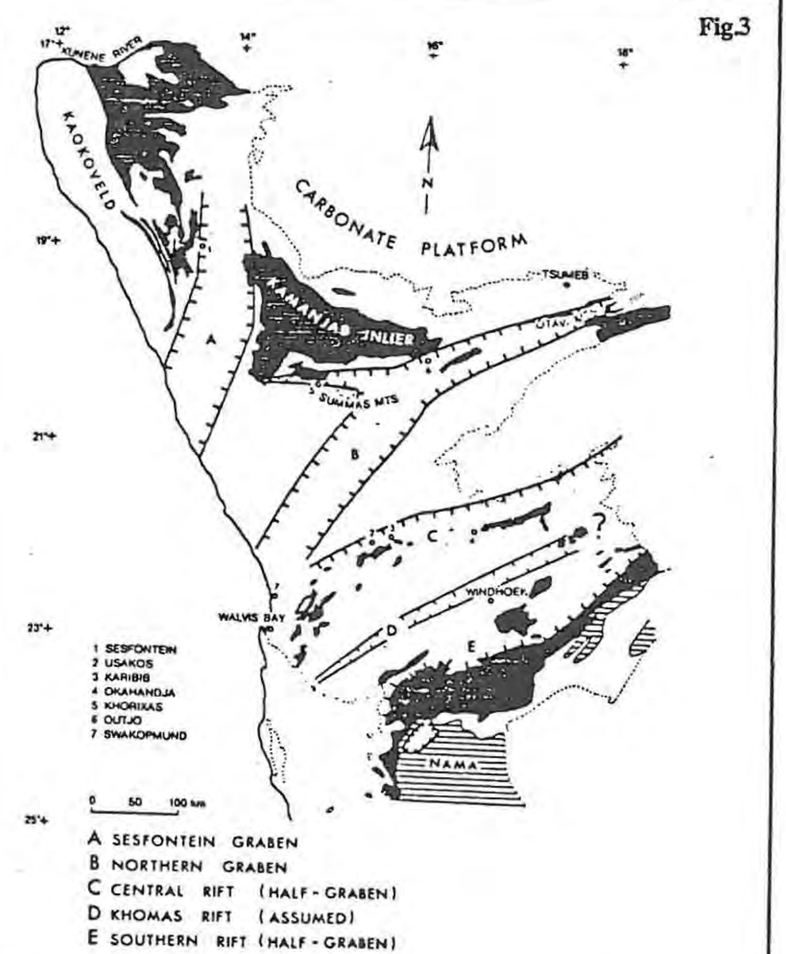

Fig. 3 - Supposed position of rift systems during the early geosynclinal development of the Damara Orogen (modified after Porada, 1983).

a stationary mantle plume (Fig. 2b).

The intracontinental belt is commonly divided into zones (i.e. Northern, Central, Southern and Southern Marginal zones) on the basis of geological, structural and metamorphic features. A simplified stratigraphy of the volcano-sedimentary Damara sequence across the belt is given in Table I. Briefly, an early rifting phase, represented by the volcano-sedimentary Nosib Group, is followed by the development of a carbonate shelf facies (Otavi Group) in the north, and a "eugeosynclinal" facies (Swakop Group) in the central and southern parts of the belt. Rifting is believed to have occurred in three main, approximately parallel NE-trending graben basins (B, C and D in Fig. 3) (Miller, 1983a; Porada, 1985). A shift of the rifting activity from north toward south is envisaged by Porada (1985). Of the three basins, only the southernmost, the Khomas Trough in the Southern Zone, experienced the most intense rifting process. In the Southern and Southern Marginal Zones several amphibolite units with transitional-within-plate to mid-ocean ridge basalt , or MORB, affinities reflect this process (Finnemore, 1978; Miller, 1983b). The latter amphibolite units are represented by the narrow and linear NE-striking Matchless Amphibolite Belt (see below). Important flysch sedimentation in the northern and southern rift basins is represented by the Kuiseb Formation, attaining a thickness of up to 10000m in the Khomas Trough. This formation includes pelagic sediments and interbedded continentally-derived terrigenous and carbonate-rich (marly) material deposited from turbidity currents (Miller et al., 1983). The carbonate component of the Kuiseb Formation is believed to have been partly derived from deep-sea debris fans (Tinkas turbidites) originating from the carbonate platform (Karibib Formation; see Table I) along the northern margin of the Khomas Trough (Fig. 4). On the basis of geophysical investigations, the Khomas Trough does not persist into the sand-covered extension of the Damara Belt into Botswana (Pirajno and Jacob, 1984).

Convergence and continental collision are responsible for polyphase deformation, metamorphism and, in the Central Zone, emplacement of

NORTH

GROUP	SUBGROUP	FORMATION	LITHOLOGY (MAX. THICKNESS)
MULDEN		OWAMBO	Shale, marl, siltstone, sandstone (1000 m)
MULDEN		KOMBAT	Shale dolomite lenses
MULDEN		TSCHUDI	Quartzite, conglomerate, arkose, argillite (3000 m)
UNCONFORMITY IN NW			
OTAVI	TSUMEB	HUTTENBERG	Dolomite with chert shale, limestone, stromatolites, oolites (900 m)
OTAVI	TSUMEB	ELANDSHOEK	Dolomite with chert stromatolites (1100 m)
OTAVI	TSUMEB	MAIEBERG	Dolomite, limestone, slump breccia (950 m)
OTAVI	TSUMEB	CHUOS	Mixtite, dolomite, limestone, sandstone, itabirite, oolite chert (700 m)
OTAVI	LOCAL DISCORDANCE		
OTAVI	ABENAB	AUROS	Dolomite, limestone, marl, shale (450 m) stromatolites
OTAVI	ABENAB	GAUSS	Dolomite, limestone, oolitic chert, sandstone (750 m)
OTAVI	ABENAB	BERG AUKAS	Dolomite, limestone, stromatolites, arkose, greywacke (525 m)
LOCAL DISCORDANCE			
NOSIB		VARIANTO	Mixtite, tuff, itabirite
NOSIB		ASKEVOLD · NAAUWPOORT	Rhyolite, tuff, agglomerate, andesite, epidosite, bostonite (6000 m)
NOSIB		NABIS	Quartzite, arkose, conglomerate

CENTRE

GROUP	SUBGROUP	FORMATION	LITHOLOGY (MAX. THICKNESS)
SWAKOP	KHOMAS	KUISEB	Quartz-biotite schist, biotite-garnet-cordierite schist, amphibole schist, quartzite, marble, calcsilicate rock (3000 m)
SWAKOP	KHOMAS	KARIBIB	Marble, biotite schist, quartz schist, calcsilicate rock (700 m)
SWAKOP	KHOMAS	CHUOS	Mixtite, marble, quartzite (700 m)
SWAKOP	LOCAL DISCORDANCE		
SWAKOP	UGAB	RÖSSING	Marble, quartzite, conglomerate, biotite schist, biotite-hornblende schist, calcsilicate rock (700 m)
LOCAL DISCORDANCE			
NOSIB		KHAN	Calcsilicate rock, amphibole-pyroxene gneiss and quartzite (1100 m)
NOSIB		ETUSIS	Quartzite, arkose, conglomerate schist, rhyolite (3500 m)

SOUTH

GROUP	SUBGROUP	FORMATION	LITHOLOGY (MAX. THICKNESS)
NAMA GROUP PARTIALLY ?			
SWAKOP	KHOMAS	KUISEB	Biotite schist, biotite quartzite, graphitic schist, calcsilicate rock, amphibolite (matchless member) (10000 m)
SWAKOP	KHOMAS	AUAS	Quartzite, schist, marble, amphibolite, itabirite (1800 m)
SWAKOP	KHOMAS	CHUOS	Pebbles schist, mixtite, quartzite, schist, itabirite, amphibolite, calcsilicate rock (1650 m)
SWAKOP	KUDIS	BLAUKRANS	Graphite schist, quartzite, quartz-mica schist, conglomerate, itabirite (1700 m)
SWAKOP	KUDIS	? HAKOS	Quartzite schist (2000 m)
SWAKOP	KUDIS	CORONA	Dolomite schist, conglomerate (400 m)
LOCAL DISCORDANCE			
NOSIB		DURUCHAUS	Phyllite, quartzite, conglomerate, limestone (5000 m)
NOSIB		KAMTSAS	Quartzite, arkose, conglomerate (6700 m)

Table I - Simplified lithostratigraphy of the Damara sequence (Porada, 1983).

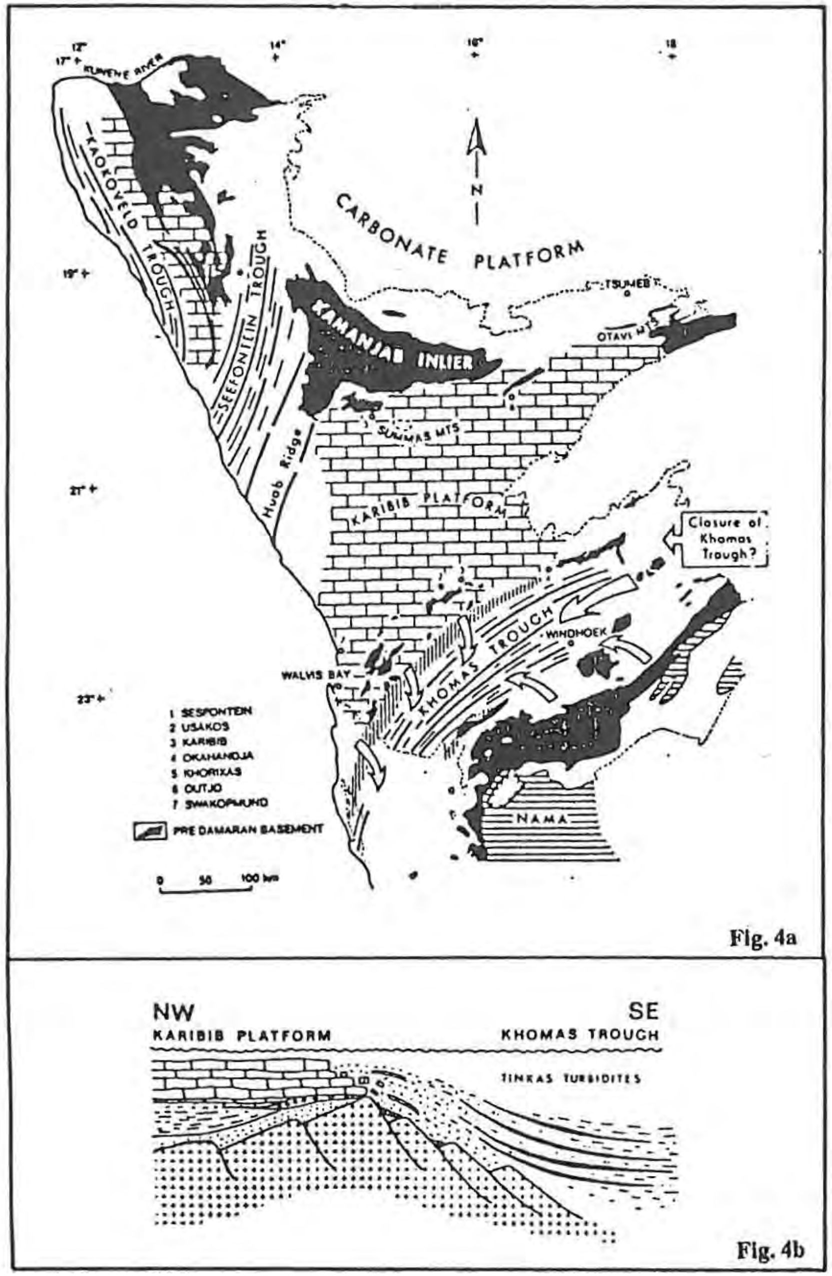

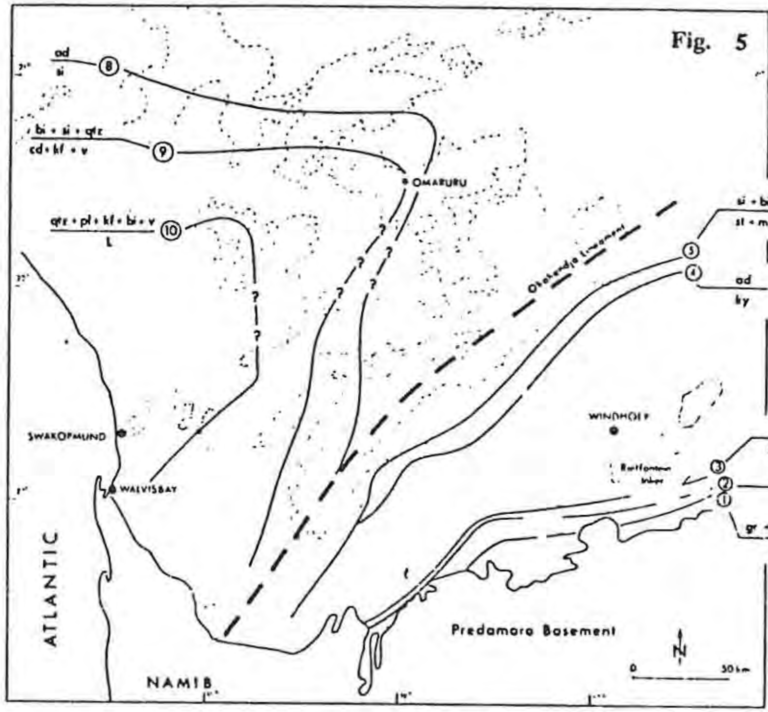

Fig. 4 - a) Palaeo-geographic map of the Damara geosyncline showing the Karibib platform and the Khomas Trough at the time of deposition of the Tinkas turbidite sequence; b) hypothetical NW-SE section from the Karibib platform to the Khomas trough, showing the deposition of the Tinkas turbidites (Porada, 1985).

Fig. 5 - Reaction isograds in pelitic rocks in the Damara Orogen (Hoernes and Hoffer, 1979). Abbreviations: *chl*, chlorite; *ms*, muscovite; *qtz*, quartz; *an(pl)*, anorthite component of plagioclase; *pl*, plagioclase; *gr*, garnet; *ky*, kyanite; *ad*, andalusite; *si*, sillimanite; *cd*, cordierite; *kf*, K-feldspar; *L*, liquid; *v*, vapor.

voluminous, almost exclusively S-type, collision-related granitoid intrusives (Pitcher, 1982; Miller, 1983a).

In general, two main deformation phases, D_1 and D_2, and a less intense D_3 phase are responsible for the structural grain of the belt. Each deformation phase was accompanied by emplacement of granitic rocks. Different deformation styles characterize the central and southern parts of the belt. The Okahandja Lineament is an important tectonic boundary between the Central and Southern Zone (Downing and Coward, 1981). In contrast with the dome-and basin tectonic style induced by granitic intrusions in the Central Zone, structures in the Southern Zone are linear: they are upright close to the Okahandja Lineament, become less steep and southeast-vergent to the south, and culminate in intense southeastward thrusting of cover and pre-Damaran basement in the Southern Marginal Zone. Tight to isoclinal folding and intense axial-plane transposition characterize the tectonic style of the Southern Zone. Depleted-mantle, Alpine-type serpentinite bodies (Barnes, 1983) were emplaced along thrust planes into both the pre-Damaran basement inliers and the Damara sequence of the Southern Zone.

The distribution of the metamorphic reaction-isograds within the belt (Fig. 5) (Miller, 1981) shows progressive increase of temperature from the margins towards the centre of the belt, and the development of anatexis in the Swakopmund area (Central Zone). This may represent the original location of the triple point. High pressure-low temperature conditions are recorded in the Southern and Southern Marginal Zones (Kasch, 1983; Miller, 1983a). Metamorphic assemblages in the Central and Southern Zone indicate two main thermal peaks, which were contemporaneous and posterior to the main deformation phase (D_2).

Post-Pan African extensional tectonics developed mostly by reactivation of Damaran trends. Faulting occurred along main NE-trending and along NNW- and NW-trending lineaments, the latter parallel to the opening of the South Atlantic Ocean. Bimodal fissure volcanism and intrusion of dolerite dike swarms and alkaline-peralkaline rocks characterize the Karoo-post Karoo intraplate magmatic activity (Eales et al., 1984).

2 THE MATCHLESS AMPHIBOLITE BELT AND ITS SIGNIFICANCE IN THE GEODYNAMIC EVOLUTION OF THE DAMARA OROGEN

The Matchless Amphibolite Belt consists of a NE-trending, approximately 350 km-long and up to 3 km-wide, linear belt of mafic rocks (Matchless Member), included in the sedimentary fill of the Khomas Trough (Fig. 6). This belt shows evidence of folding at its western end, and it disappears beneath the Kalahari sand cover to the east. In the lower half of the Kuiseb Formation, the Matchless Member occurs as numerous layers, lenses and bands of medium- to fine-grained amphibolite and chlorite-amphibole schist enveloped in the metasediments. Structures interpreted as deformed pillows in fine-grained amphibolite units suggest the presence of original basaltic lava flows. Nevertheless, the formation of pillow structures is not diagnostic only of extrusive basalts, because similar structures can form along the prograding front of basaltic sills intruding wet basinal sediments (Yagi, 1969). Lenticular pods of metagabbro, locally with basal ultramafic differentiates, locally show foliated margins and almost massive cores. These features are suggestive of structural emplacement. Several Alpine-type serpentinite bodies (see above) are associated with the Matchless Member in the eastern sector of the belt.

The chemistry of the Matchless amphibolites suggests a general affinity with MORB-type tholeiites (Finnemore, 1974, 1978; Miller, 1983b; Schmidt and Wedepohl, 1983), although meaningful variations at a regional scale are detectable (Breitkopf and Maiden, 1988; see below).

The evolution of the Damara Orogen is still the object of debate. The interpretation of the features of the Matchless Belt is one of the factors constraining the formulation of models for the geodynamic evolution of the Damara Orogen. Existing geodynamic models are divided into two groups by Martin (1983), with the assuption of a mechanism of

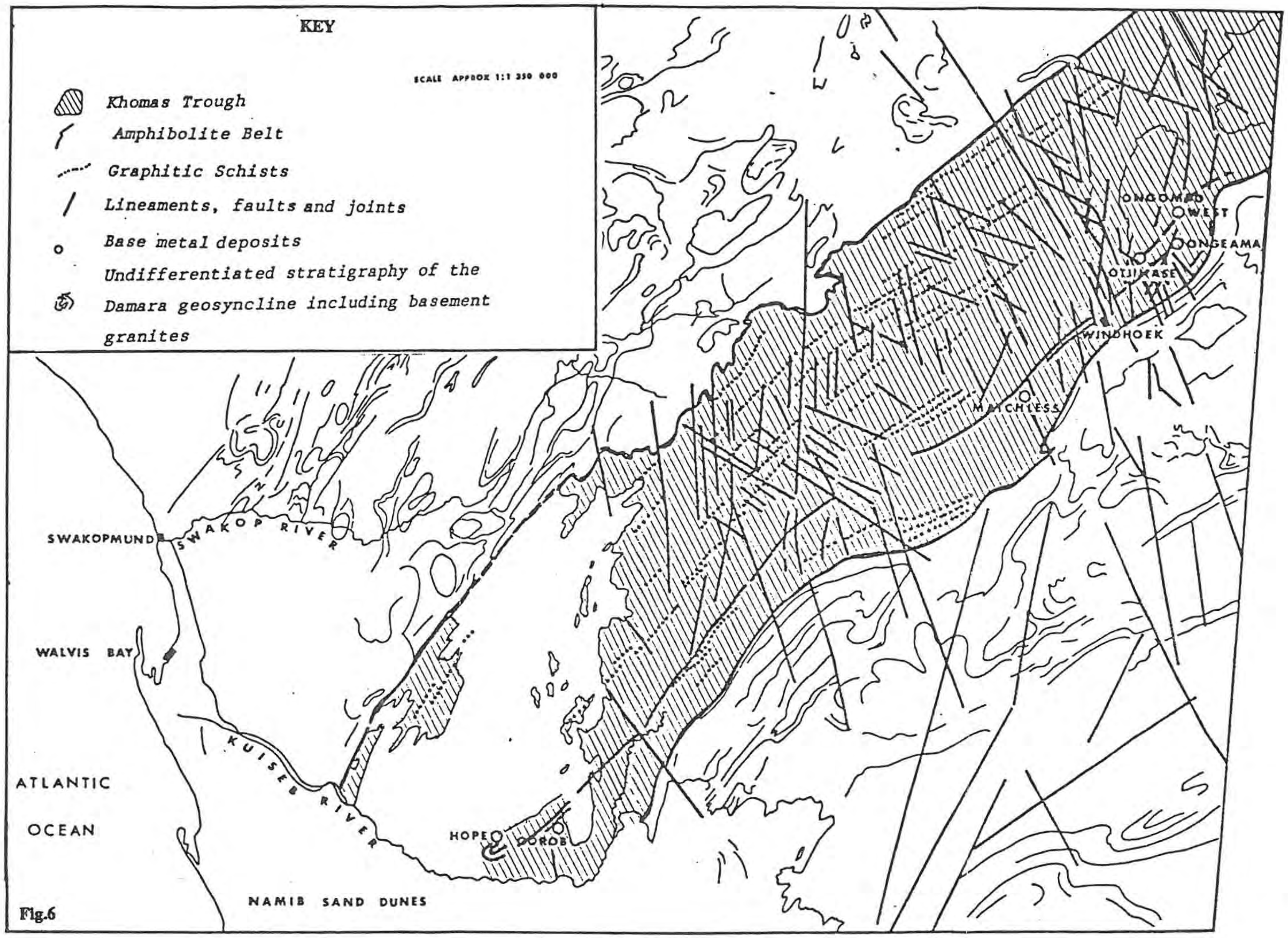

Fig.6

Fig. 6 - Interpretation of the ERTS mosaic of the central portion of the Damara geosyncline, in Central Namibia, showing the Khomas Trough, and some of the base-metal occurrences in relation to the Matchless Amphibolite Belt (Viljoen et al., 1975).

subduction (either continental or oceanic) as a common denominator (for details see Martin, 1983, and references therein):

a) continental collision models ("aulacogen" and "delamination" models);

b) oceanic crust subduction models (subduction of a wide or narrow ocean). In this group the very recent models by Hoffmann (1990) and Kukla & Stanistreet (1990) may be included, although these consider the formation of the Kuiseb schists as subduction-related clastic trench sedimentation and the emplacement of the Matchless amphibolites within an accretionary prism during subduction.

The first group of models denies the opening and subsequent closure of an oceanic basin, and, consequently, the origin of the Matchless Belt from oceanic crust. This denial is based on several factors, among which are the lack of a recognizable ophiolite sequence, the small volume of the mafic rocks in the Matchless Belt, the absence of volcanic and/or plutonic rocks typical of magmatic arcs over a subduction zone (I-type; Pitcher, 1982), and the involvement of basement inliers in all the major structural zones of the orogen.

These factors strongly affect the validity of the second group of models, which however take into account the mid-ocean-ridge-type geochemistry of the Matchless amphibolites, the tectonic emplacement of the serpentinites in that part of the orogenic belt, and the existence of major thrust sheets and nappe structures along the southern margin of the belt. According to Martin (1983), the formation of a narrow oceanic basin (1000 km wide; Miller, 1983b) and the involvement of stike-slip shear movements (Downing and Coward, 1981) appear to be interesting alternatives to the wide-ocean subduction model.

Smalley's (1988) and Breitkopf and Maiden's (1988) models for the formation of the Matchless Belt take into account the last two mentioned factors. Crustal thinning is believed to have occurred with local formation of a spreading centre in a subbasin, the sediment-

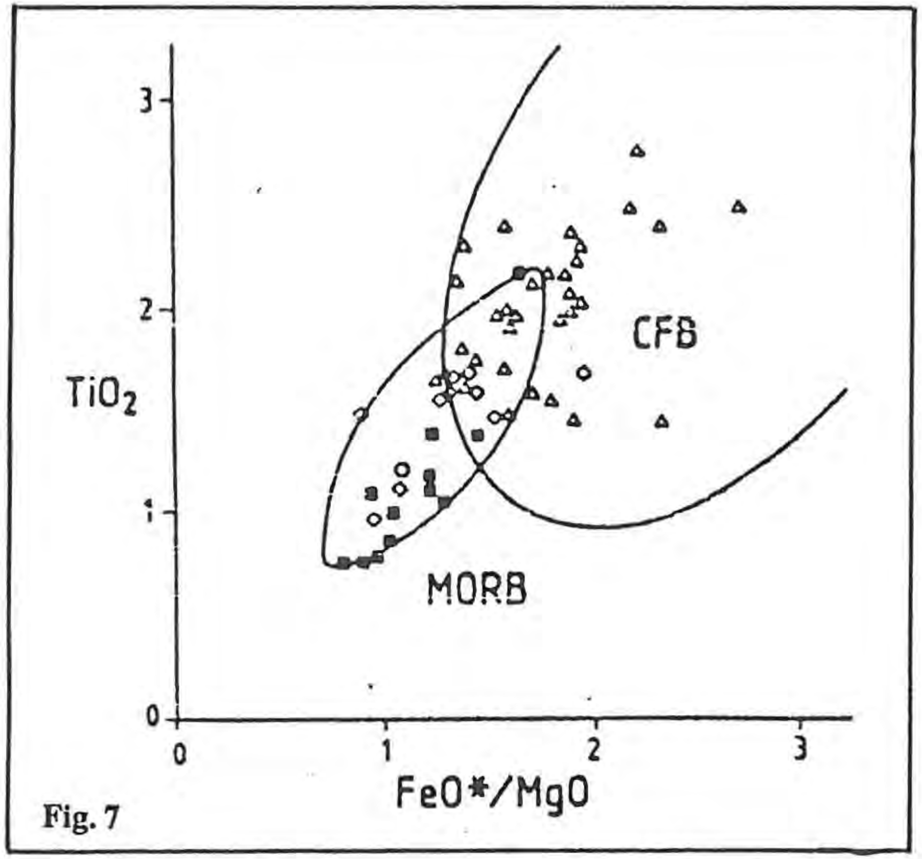

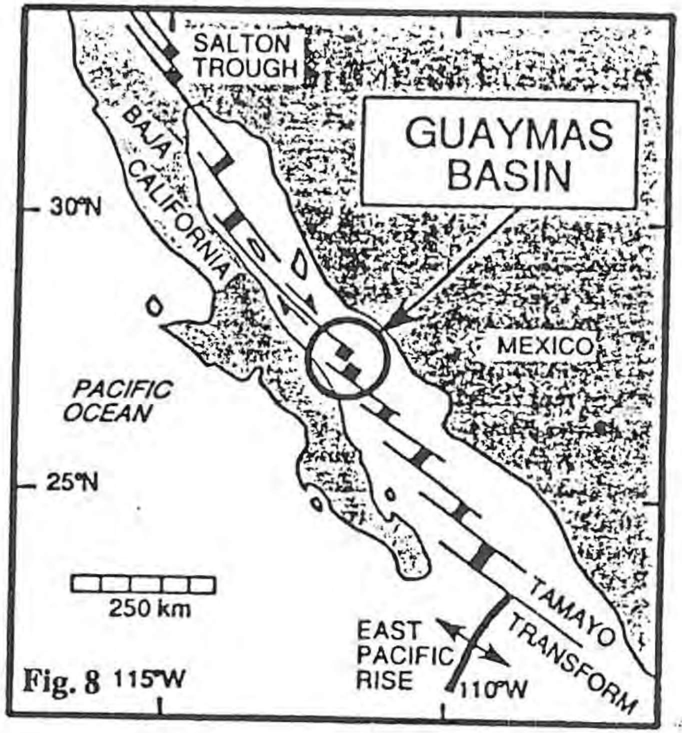

Fig. 8 - Map of the Gulf of California, showing the location of the Guaymas Basin (Peter and Scott, 1988).

Fig. 7 - Plot of TiO_2 versus FeO_{tot}/MgO. MORB=mid-ocean ridge basalt; CFB=continental floor basalt; triangles=Matchless Belt, western part; diamonds=Matchless Belt, central part; filled squares=Matchless Belt, eastern part (Breitkopf and Maiden, 1988).

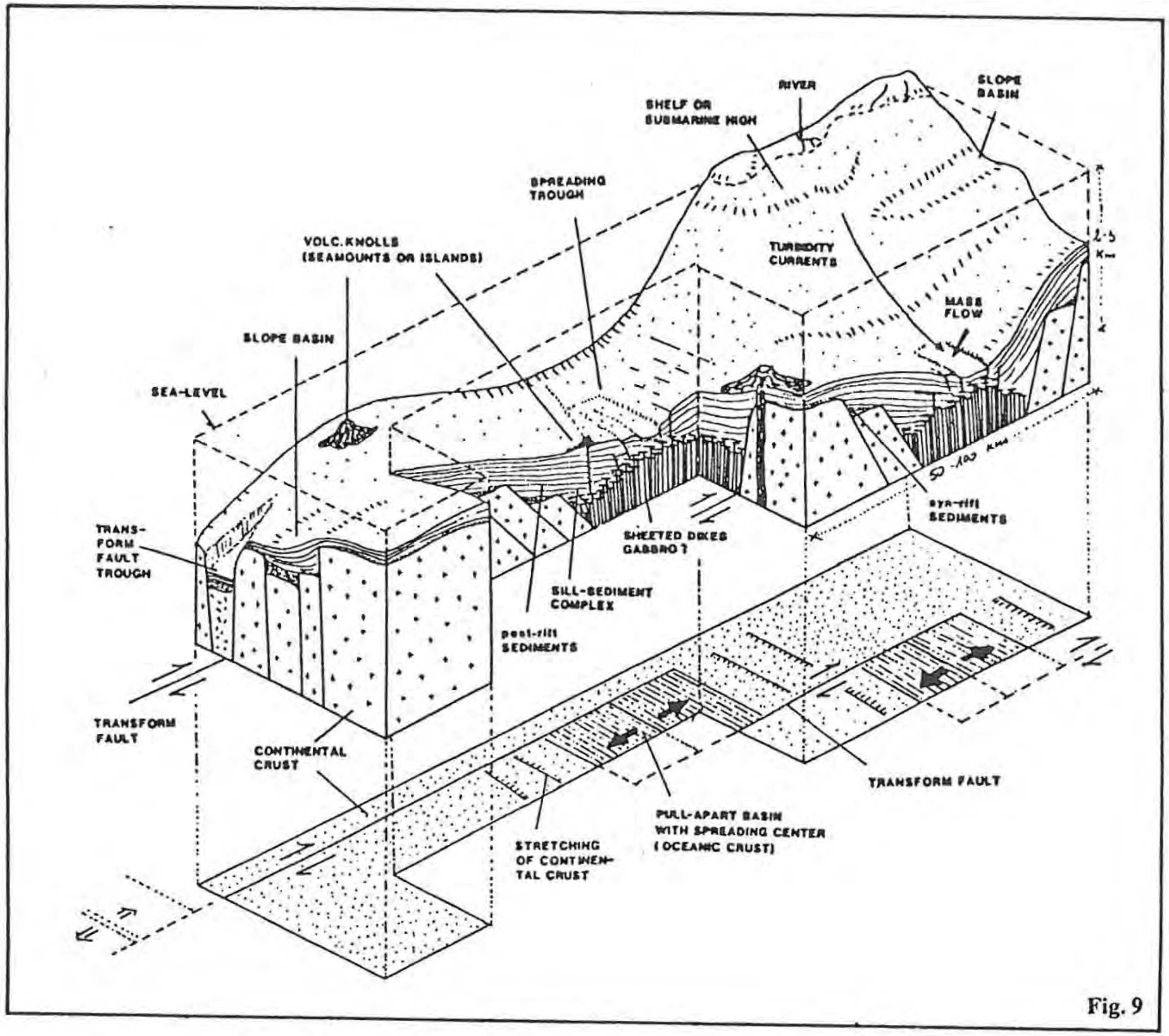

Fig. 9

Fig. 9 - Simplified block diagram and plan view of Guaymas Basin-type pull-apart basins in stage of early drifting with formation of sill-sediment complexes in spreading troughs (Einsele et al., 1980).

filled Matchless Trough (Smalley, 1988). This subbasin, along the axis of the Khomas Trough, would have originated as a pull-apart basin by simple crustal stretching and superimposed strike-slip shear movements (Breitkopf and Maiden, 1988).

A point of note is that geochemical variations along the axis of the Matchless Belt suggest that most crustal thinning , and eventual spreading, may have occurred in the eastern sector, where amphibolites with oceanic-ridge-type tholeiitic geochemical signature are present (Fig. 7). Geochemical data, however, indicate that a tectonic setting similar to that of fully developed ocean spreading centres is improbable. In the west, amphibolites with geochemical affinities to within-plate basalts suggest the original presence of thin continental crust (Breitkopf and Maiden, 1987, 1988).

The development of the Matchless Trough is comparable with that of modern counterparts, such as the Guaymas Basin (Gulf of California) (Fig. 8) (Einsele et al., 1980). The proximity to the continent determines a sedimentation rate approaching or surpassing the spreading rate. A similar situation The seismically activated sedimentary filling of the basin (turbidites) would generally preclude the extrusion of magma at the sediment-water interface and induce the intrusion of basaltic sheets within the soft, wet sediments. A particular stratigraphy of the oceanic crust is obtained with the formation of a transitional zone, i.e.,a sill-sediment complex, between the overlying youngest sediments and the sheeted dike complex at depth (Fig. 9) (Einsele et al., 1980).

3 SULPHIDE MINERALIZATION AND GEOLOGY IN THE EASTERN SECTOR OF THE MATCHLESS AMPHIBOLITE BELT

Along its length, the Matchless Amphibolite Belt hosts several volcanogenic-exhalative, stratiform and strata-bound cupriferous sulphide deposits (Fig. 6), which display common features throughout the belt. These deposits range in size from 0.3 to 16 millions tons of ore averaging 2% Cu (Smalley, 1988; Breitkopf and Maiden, 1988). Details on the main deposits of the belt are found in Killick (1983) and Breitkopf and Maiden (1988) (Gorob), Adamson and Teichmann (1986) and Klemd et al. (1987) (Matchless), Goldberg (1976) and Thomson (1989) (Otjihase).

These deposits consist of massive to semi-massive mineralization, in which predominant pyrite and/or pyrrhotite are accompanied by subordinate chalcopyrite. In addition to Cu, the mineralization can carry variable amounts of Zn, Co, Ag, Au and Mo. Layers of exhalative oxide-silicate facies iron formation (Fox, 1984) are associated with the mineralization, which is typically capped by these layers. The sulphide bodies are hosted in the metaturbiditic Kuiseb schists and are closely associated with the amphibolites. Irregular schist bands and lenses mineralogically distinct from the normal Kuiseb schists and commonly spatially related to the mineralization are considered to represent original hydrothermally altered sediments.

During the orogenesis, the sulphide bodies were deformed into isolated or closely stacked pencil- or ruler-shaped shoots, and arranged according to the regional structural grain. The plunge of the ore bodies is variable at a regional scale according to an undulating pattern (Fig. 10).

The Matchless Belt ore deposits are considered to be examples of Besshi-type mineralization according to the definition given by Fox (1984), i.e., subaqueous exhalative mineralization formed in epicratonic rift environments and resulting from hydrothermal convection developing in the subjacent mafic volcanic-clastic sedimentary piles. Besshi-type mineralization occupies an intermediate position in a rift-related metallogenic spectrum, whose end-members

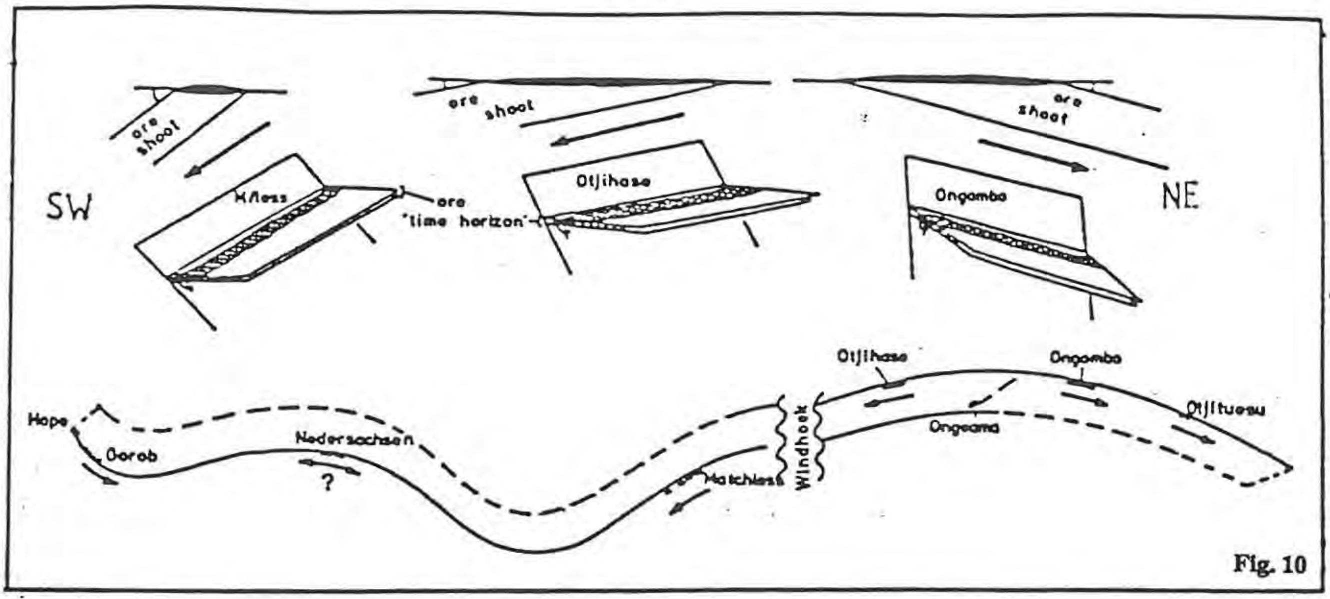

Fig. 10 - Schematic sketch of the regional undulating plunge of the mineralized bodies along the Matchless Belt (Smalley, 1988).

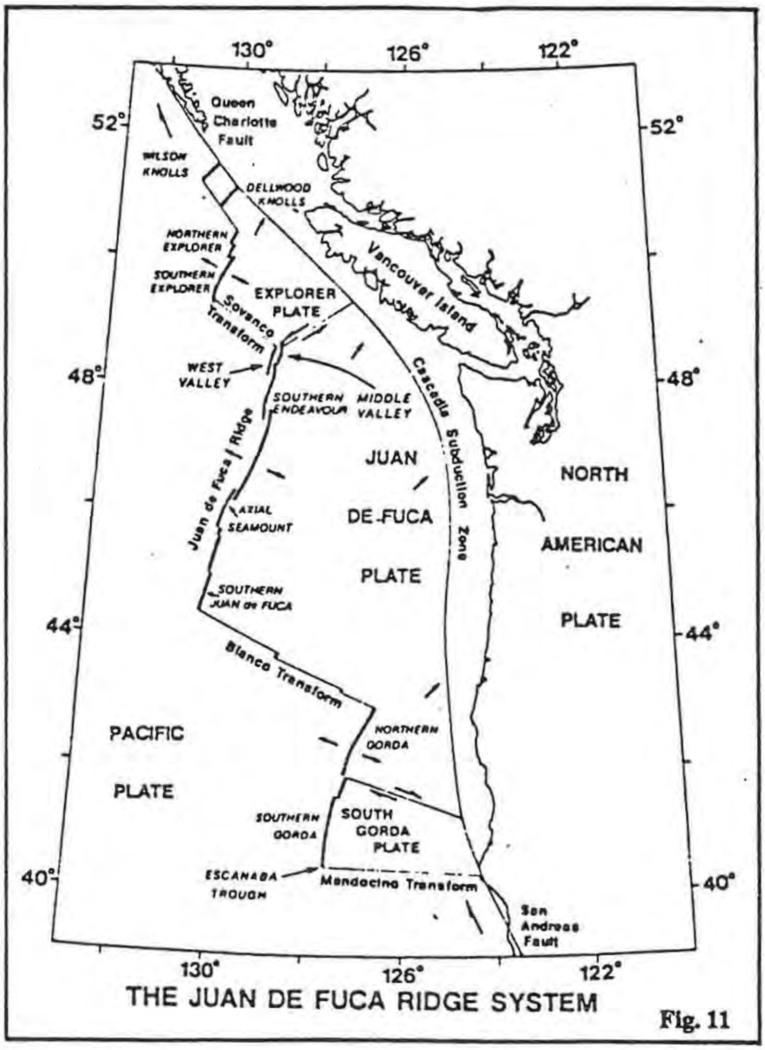

Fig. 11 - Generalized tectonic map of the northern Pacific plate boundaries and the location of the Escanaba Trough (Kappel and Franklin, 1989).

are sedimentary-exhalative- and Cyprus-type deposits. The rate and degree of crustal extension is the discriminating genetic factor for the types of mineralization between the end members. Apart from the type-locality in Japan (Kanehira and Tatsumi, 1970), other examples of Besshi-type mineralization are those in the Blue Ridge Belt (Virginia, USA) (Gair and Slack, 1984), in the Norwegian Caledonides (Fox, 1984 and references therein), and the modern sulphide mounds in the Guaymas Basin and in the Escanaba Trough (Lonsdale and Becker, 1985; Kappel and Franklin, 1989) (Fig. 11).

The size of the sulphide deposits along the Matchless Belt seems to correlate positively with the assumed occurrence of oceanic crust towards the east. In fact, the eastern sector, or Windhoek sector , of the Matchless Belt (where the study areas are located; Fig. 12) hosts the economically significant mineralization: i.e. the largest deposits, at the Matchless Mine (recently closed), at the Otjihase Mine (currently operating), and other minor deposits currently at the prospect stage.

Accounts of the geological and tectonic features of the eastern sector of the Matchless Belt are given by Viljoen et al. (1975) and Smalley (1988). ERTS imagery of this sector of the belt (see interpretation in Fig. 6) illustrates the superposition on the NE-oriented, Damaran regional trends by dominantly NNW-SSE later fault systems. Some of these faults displace the amphibolite belt in the region to the east of Windhoek to produce an "en echelon" pattern (Fig. 12). A number of less evident, older fault zones (wrench or thrust faults) occur, their traces being almost parallel to the regional trends. An example, in Fig. 13, is the wrench fault with sinistral lateral movement along the Otjihase River and extending between the Ongeama and Otjihase gossans (Viljoen et al., 1975).

Two structural features are of particular interest in the eastern sector of the Matchless Belt (Smalley, 1988):

a) the so-called Colvania Horizon, a cataclastic/mylonitic band (fault/shear zone or thrust), acutely convergent with the

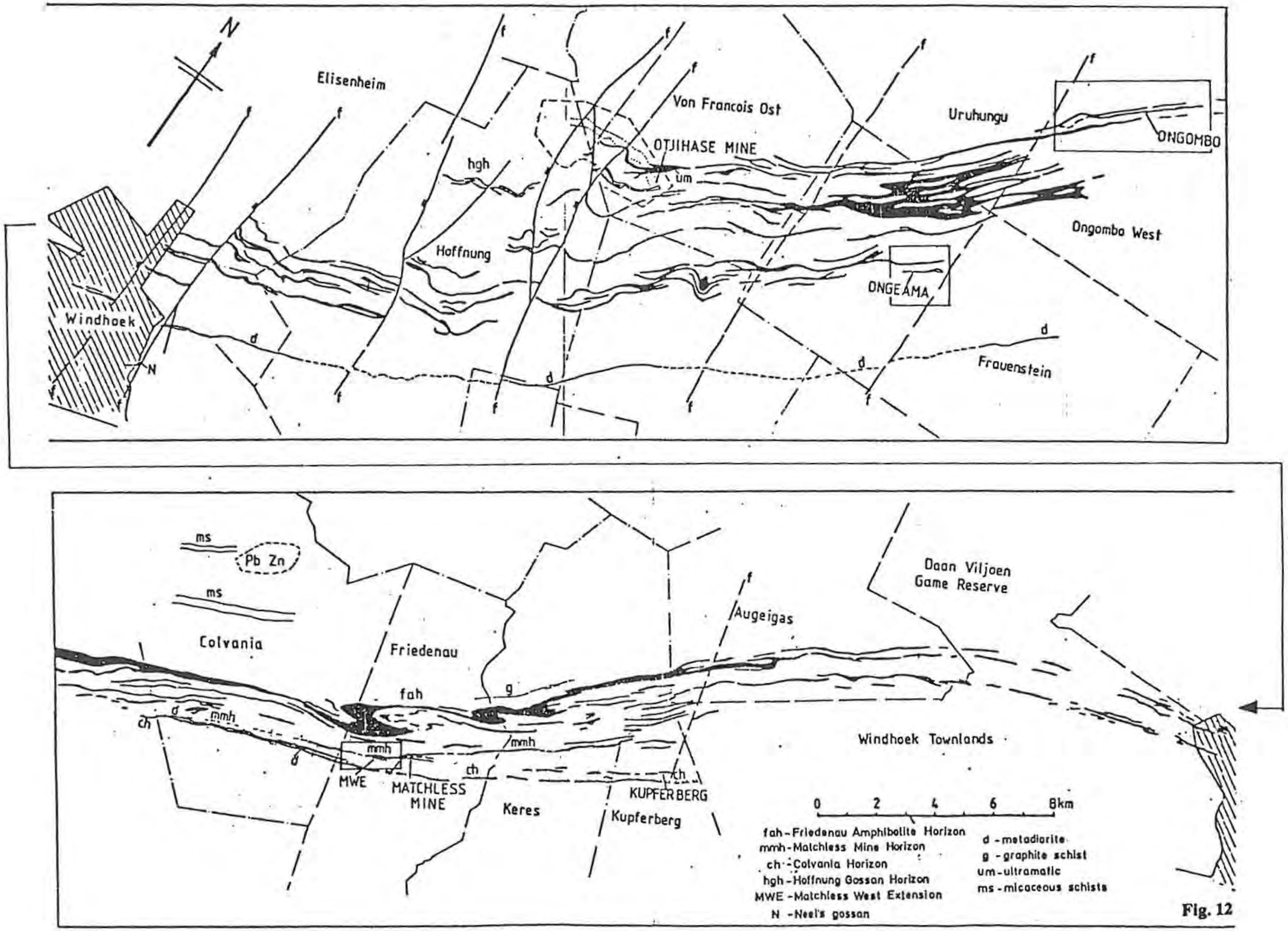

Fig. 12 - Simplified regional map showing the distribution of the main geological features of the eastern sector (Windhoek sector) of the Matchless Belt (modif. after Smalley, 1988). Study areas are outlined.

southernmost, structurally lowest amphibolite horizons. It extends both west and east of Windhoek, over a distance of 50 km (Fig. 11). Towards the east it is characterized by the presence of elongated bodies of magnetic metadiorite ;

b) the linear narrow zone of discontinuous serpentinite bodies, developed east of Windhoek and near the Otjihase Mine, and lying above the structurally uppermost amphibolite band (Fig. 12 and 22).

These features delimit the sequence of amphibolites northwards and southwards, respectively. West of Windhoek , the sequence includes two main bands of metalava, i.e., the structurally lower Matchless Mine Horizon Amphibolite and the overlying Friedenau Amphibolite Horizon (Smalley, 1988). A more complicated stratigraphy characterizes the sector east of Windhoek, in the Otjihase-Ongeama area. In spite of the dominant MORB character of the amphibolites in this sector of the belt (see above), geochemical variations across the amphibolite sequence west of Windhoek reflect an upward transition from within-plate (in the lower Matchless Mine Horizon Amphibolite) to incipient ocean spreading conditions (in the Friedenau Amphibolite) (Fig. 14).

The assessment of these geochemical variations is a significant tool in defining the polarity of the sequence in the deformed Matchless Belt, in which reliable and continuous markers are lacking. On the basis of the amphibolite geochemistry and of characteristics in the local mineralization, Smalley (1988, 1990) claims that the sequence in the western Windhoek sector is the right way up. An opposite interpretation is reported by Klemd et al. (1989). The present author's opinion is given in Part E. In the eastern Windhoek sector, in the Ongeama-Ongombo area, the sequence appears to be overturned (Hoffmann, 1976; Hallworth, 1989).

The Colvania Horizon and the ultramafic band are regarded by Smalley (1988) as the original southern and northern boundary graben faults, respectively, delimiting the Matchless Trough. Magmatic and exhalative activity is believed to have occurred only along the actively dominant side of the graben (i.e. the southern fault in the west, and the northern fault east of Windhoek). The mineralized bodies, in fact,

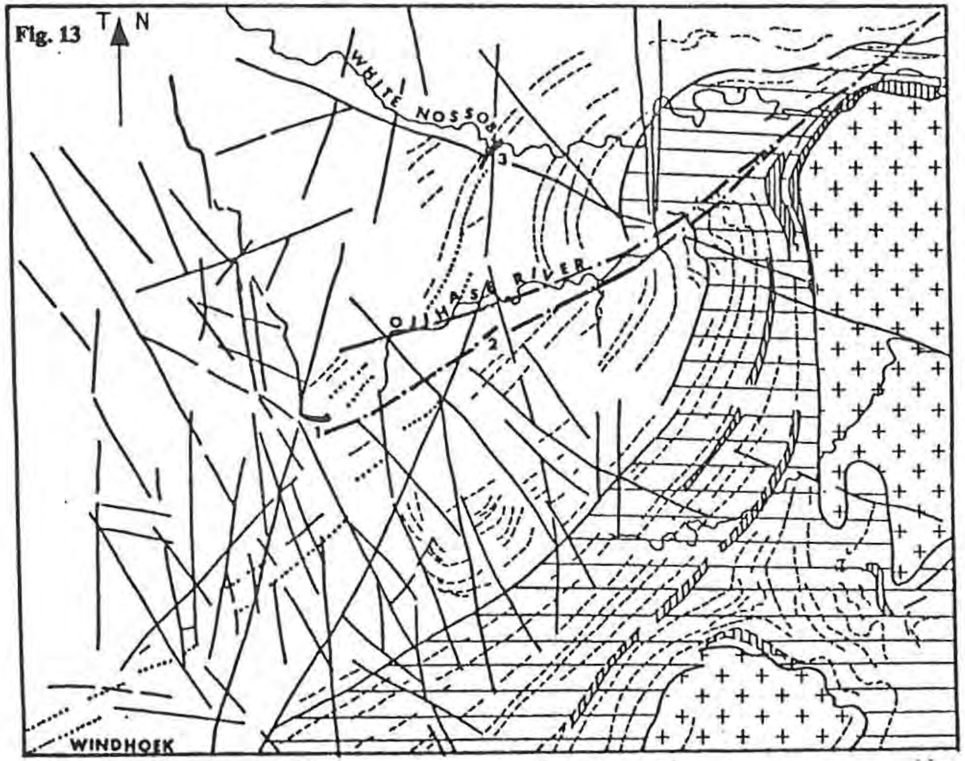

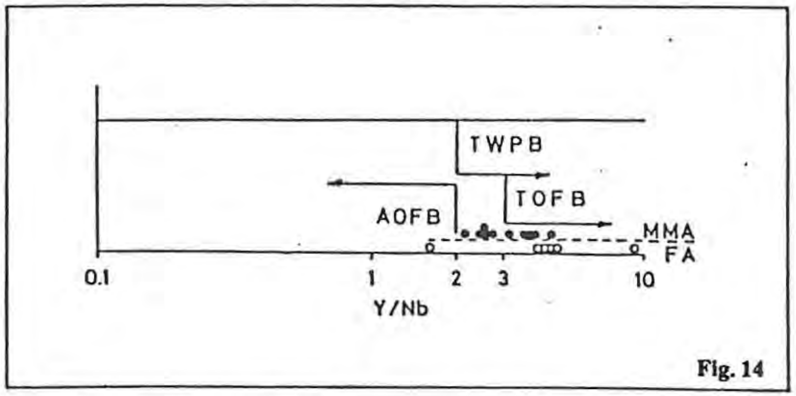

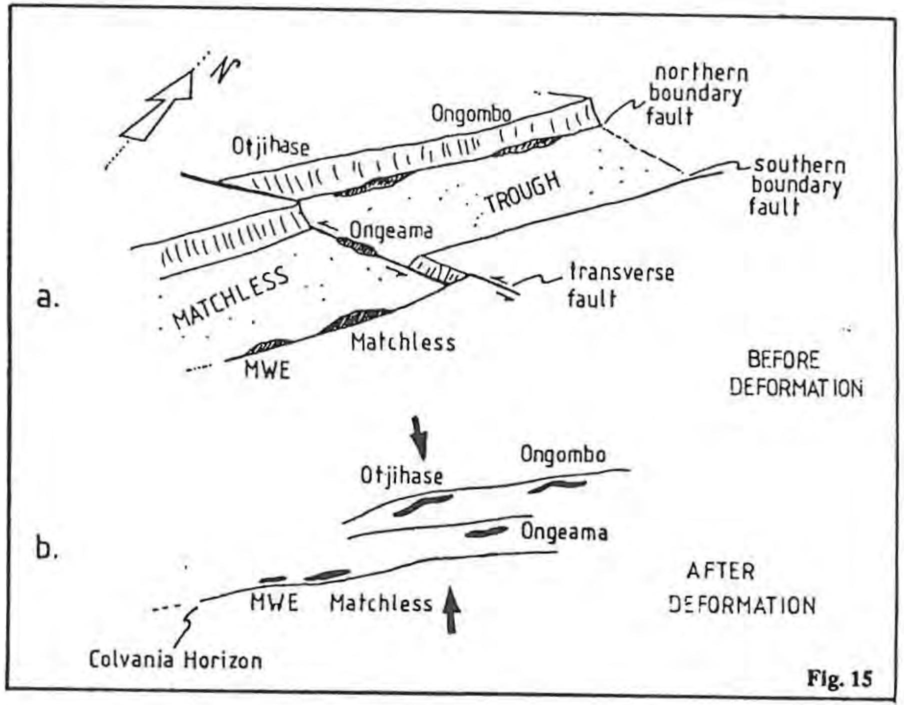

Fig. 13 - Composite geological and structural map from ERTS imagery of the area around the Otjihase deposit, eastern Windhoek sector, Matchless Belt (scale approx. 1:300000). Blank=Kuiseb Fm.; dot rows=amphibolite bands; horizontal lines=Auas Fm.; crosses=basement granites; 1=Otjihase gossan; 2=Ongeama gossan; 3=Ongombo gossan (Viljoen et al., 1975).

Fig. 14 - Y/Nb ratios for the Matchless Mine Horizon Amphibolite (MMA) and Friedenau Amphibolite (FA). TWPB=tholeiitic within-plate basalt; TOFB=tholeiitic ocean floor basalt; AOFB=alkalic ocean floor basalt (modif. after Smalley, 1988).

Fig. 15 - Schematic sketch with the assumed original location of the sulphide bodies relative to the graben-boundary and transverse (transform ?) faults before (a) and after deformation (b), according to Smalley (1988).

occur next to these assumed major graben faults. Certain overlap and additional magmatic-exhalative activity along transverse faults is thought to have contributed to the stratigraphy in the Otjihase-Ongeama area (Fig. 15) (Smalley, 1988), although in this area Viljoen et al. (1975) envisage a duplication of the amphibolite belt by thrust faulting (see above).

PART B

GEOLOGY OF THE MINERALIZATION AND COUNTRY ROCKS AT ONGEAMA, ONGOMBO AND MATCHLESS WEST EXTENSION

1. INTRODUCTION

In this chapter an account is given of the geological setting of the sulphide bodies at the Ongeama and Ongombo Prospects, and Matchless West Extension, in the Windhoek sector of the Matchless Belt (for location see Fig. 12). Geological information was gained from previous and current investigations by mining companies, and from field work by the present author, between November 1989 and February 1990.

The study of the sulphide bodies involved mapping, systematic lithogeochemical sampling of the weathered surface exposures of the mineralization, and detailed examination of drillcores. At Ongombo and Matchless West Extension maps of the outcrops were already available. In these areas, therefore, the task of the author has been the re-examination, as critically as possible, of the previous observations, concentrating on particular features related to the mineralization.

With regard to the sulphide deposits examined, additional areas, including specific facies (magnetite-rich schists, ultramafic schists) were also included for sampling purposes.

Note: in the text the abbreviations "h/w" and "f/w" are used for "hangingwall" and "footwall", respectively.

2. MINERALIZATION AT THE ONGEAMA AND ONGOMBO PROSPECTS

Ongeama and Ongombo are two copper prospects situated on the farms Ongeama and Ongombo Ost/West, about 20 and 30 km NE of Windhoek, respectively. They are currently held under prospecting grant 1623 (Ongeama claims and Hoffnung Grant) by Gold Fields Namibia. The two farms have a gently undulating topography and are traversed by the Otjihase and White Nossob Rivers, respectively. These rivers are dry for most of the year. Outcrops are often concealed by sand cover, soil and vegetation (thorn bushes and grass).

2.1 Brief review of previous and current investigations

The first geological investigations in the Ongeama and Ongombo areas were carried out by B&O Minerals in the period 1971-1973, when the copper mineralization of the two stratiform sulphide bodies was outlined by drilling. Moderate metal grades, limited distribution of ore-grade mineralization, and subeconomic tonnage did not encourage further investigation.

In February 1974, Johannesburg Consolidated Investments (J.C.I.) undertook airborne magnetic and electro-magnetic surveys, at the scale 1:50000, over the sector of the Matchless Belt between Otijhase and Ongombo. This survey resulted in the identification of a number of well defined magnetic anomalies and conductors. In November 1975, a new prospecting programme was commenced in order to define the controls on the distribution of ore-grade mineralization. This programme included surface mapping, detailed examination of diamond drill cores, soil geochemistry and geophysics, as well as revision of previous data. Additional information on the geological setting and the geometry of the sulphide bodies at depth was obtained by drilling.

Soil geochemistry confirmed the presence of anomalous metal concentrations in the geochemical profile along the strike of the well exposed gossan at Ongeama. At Ongombo erratic exposures of outcrops influenced the quality of response. Nevertheless, an almost continuous profile of metal distribution along strike indicating a minimum strike length with detectable mineralization of about 4700m, was established. Geophysical prospecting in both areas involved a ground magnetic survey and a Turam electromagnetic (EM) survey.

Results of these surveys indicated a strong anomaly over the gossan outcrop at Ongeama, due to the presence of magnetite quartzite and magnetite in the surrounding schists. At Ongombo, erratic anomalies were obtained by ground magnetics, whereas the Turam EM survey yielded more precise responses and indicated a moderate anomaly in the eastern part of the ore body.

Hoffmann's report (1976) comments on the results of the JCI's prospecting. The results for Ongeama were assessed as follows: "limited potential for viable ore ... for any significant distance in depth". At Ongombo, although limited potential was expected, further drilling was advised by Hoffmann in order to understand the nature of the mineralization and to verify its possible extent in

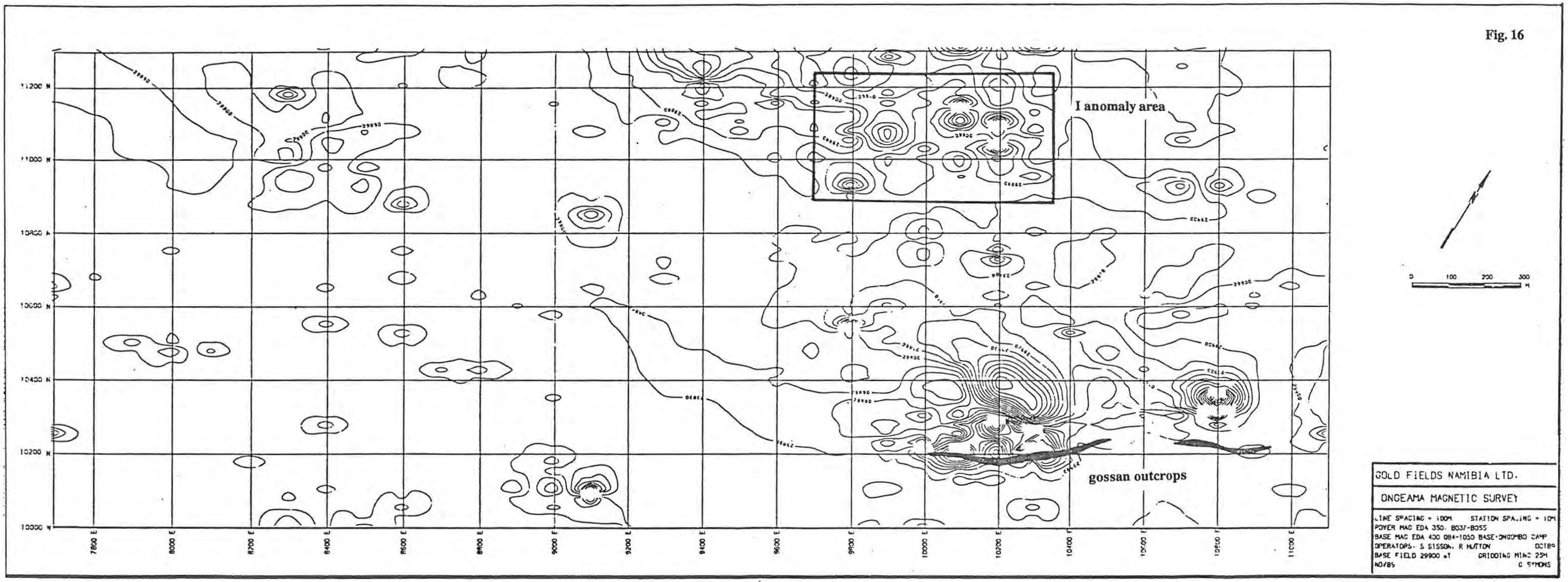

Fig. 16 - Ongeama Prospect: schematic sketch-map of the magnetic anomalies (ground magnetic survey, Gold Fields Namibia Ltd., 1989). The location of the gossan outcrops and of the "I anomaly" area (in the frame) is given.

depth.

In 1980, the Ongeama and Ongombo claims were taken over by Tsumeb Corporation Limited (TCL). TCL was subsequently incorporated into Gold Fields Namibia Ltd, which is the current holder of the grants.

In order to carry out mapping and geophysical surveys (ground magnetics and electromagnetic powerage, EMP), grids were established in both claims. Magnetic (Fig. 16) and time-domain EM surveys were completed in 1989 at Ongeama, outlining an elongated shoot at depth.

At Ongombo the EM survey outlined three trends or conductors, extending downplunge from the gossan. These correspond to two major conductors, and a secondary, eastward plunging ruler-shaped conductor (ore shoots) (see Fig. 18).

At Ongombo geological mapping was carried out by Schneeweiss (TCL) in 1984 and by McCormick from Natal University in 1988. The Gold Fields crew completed mapping in both claims in 1989. At Ongombo mapping was carried out in conjunction with a new drilling programme.

The geological data obtained by the author were integrated with information from previous work.

2.2 THE ONGEAMA PROSPECT

2.2.1 Geological setting

During this study the weathered outcrops of the sulphide mineralization (gossan) at the Ongeama Prospect were geologically mapped and sampled (see section 5.1 below) at the scale 1:1000 over an area of 1200m x 150m. The limits of this area were chosen according to the existing grid established by Gold Fields Namibia in 1989 and utilized during the mapping project by Hallworth (1989).

Mapping was carried out by the author along 20m-spaced traverses and limited to exposure of the ore zone and the enclosing schists. Details of the geological setting of the Ongeama area are mostly derived from Hallworth (1989) and Hoffmann (1976) and, in part, from the author's observations. A more detailed description of the gossan exposure is given in section 2.2.2 below.

The mineralization is exposed over a strike length of 915 m (Plan 1 in Appendix A). It consists of two discrete sinuous gossanous bands, which are here indicated as "major" and "minor" outcrops. Their strike length is 600m and 315m respectively, and their maximum width is about 20m. An estimate of the maximum thickness of the ore zone is approximately 2m in the centre of the major outcrop (Hoffmann, 1976). The gap offsetting the two gossan outcrops is roughly 200m wide.

The mineralization is conformable with the schists. Accordingly, the strike is from 050^{o} to 078^{o}, with dips varying between 15^{o} and 20^{o} to the north. The plunge of the ore body at 7^{o}-8^{o} is towards WSW.

The gossan is exposed on a shallow slope on which it stands out as a ridge in places. Only gossan and quartz float occur downslope, where outcrops are concealed by sand from a tributary of the Otjihase River. Country rocks surrounding the gossan outcrop are mainly upslope and in the dry river bed.

Hallworth (1989) mapped the geology of the area, including the gossan outcrop and the extension at depth SW of the shoot, as indicated by the magnetic survey.

The country rocks predominantly consist of Kuiseb metapelites and intercalated metapsammitic horizons, with transitional facies between the two rock types. Metapelites are represented by well foliated, planar to contorted, light-grey to greenish, garnetiferous muscovite-bearing biotite-chlorite-quartz schist and chlorite-biotite-quartz schist. The schists often contain quartz pods, boudins ("sweat-outs") and veins of metamorphic segregation. The metapsammitic intercalations consist of a fine-grained massive to slightly foliated, light-grey garnetiferous quartz-biotite schists. The metapsammites locally include centimetre- to decimetre-thick layers made up of coarse-grained amphibole-bearing calc-silicate rock. Hallworth's mapping showed the impossibility of mapping the different schist facies as distinct units, because of their lenticular and interdigitating character. Graphitic schists occur as thin and discontinuous pods in the structural h/w of the major gossan outcrop (see Plan 1).

Amphibolites do not occur in the area mapped by the author. They outcrop, however, to the NW and SW, in the h/w of the mineralization. Amphibolites occur as three finely foliated metalava horizons associated with coarse-grained, sheared lenticular metagabbro plugs and metadolerite sills, in Hallworth's area and in its southwestward extension (not indicated in Fig. 17). The attitude of the mafic rocks is conformable with that of the enclosing schists.

The schists enclosing the mineralization display planar to wavy D_2-related S_2-cleavage planes and remnants of the folded D_1-related S_1 foliation. A D_3-related E-W- to NW-SE-trending crenulation cleavage is visible in the foliation planes of schists and metalavas. Late, barren crosscutting quartz veins strike 010^o to 082^o . The orientation of the veins is conformable with fracture and joint patterns observed in the gossanous schists in the h/w of the major gossan outcrop (see section 2.2.3 and Plan 1). The sinuous, lenticular and strongly elongate shape of the mineralization appears to be the result of stretching and boudinaging induced by the D_2 deformation. According to Hoffmann (1976), thickness variations of the ore shoot at depth are the result of an *en-echelon* arrangement of several thick lenses down the plunge. A D_2-related lineation, generated by the main deformation phase and typically indicating the plunge of the deformed sulphide body, is observed in the magnetite quartzite outcrop. The trend of this lineation varies from 111^o to 099^o , and suggests the occurrence of deformation induced by a sinistral shear movement.

There is geological and geophysical evidence for faulting at Ongeama. A general, simplified tectonic sketch from Hallworth (1989) (Fig 17) indicates several major lineaments, with strikes varying from N-S to E-W to ENE-WSW. Hallworth indicates a major 100^o-striking dextral shear as the cause of the offset in the gossan outcrops (the large "bull quartz" vein outcrop at the grid reference 10660 E/ 10252 N; Plan 1). In the western portion of the major outcrop, an E-W-striking dextral shear fault may be the cause of the drag deformation recorded in the gossan (Plan 1). At the eastern end of the minor outcrop a N-S-trending lineament extending through the Otjihase River is possibly responsible for the abrupt interruption of the

Fig. 17 - Ongeama Prospect: simplified geological-structural sketch-map with the position of the main air-photo lineaments, fault trends and amphibolite outcrops (hatched). Blank areas indicate sub-outcrops of Kuiseb schists (modified after Hallworth, 1989).

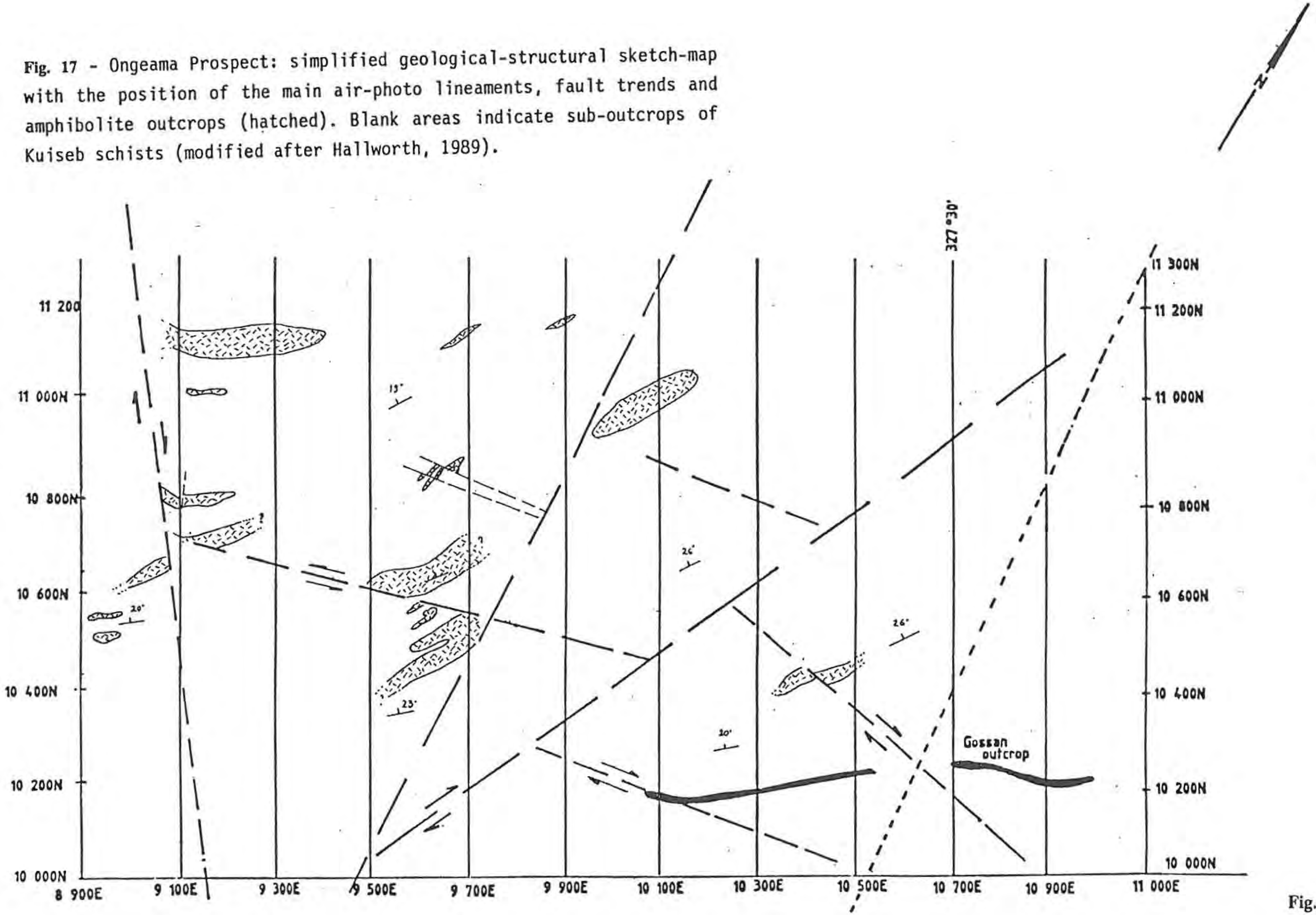

Fig. 17

mineralization towards E.

No evidence of major folding is recorded in the gossan or in the enclosing schists.

The overturning of the stratigraphic sequence at Ongeama was initially inferred from the arrangement of the different facies of the mineralized system (D.H. Corbett,1989, pers. comm.), assuming that magnetite quartzite is typically located above a sulphide body. The present position of the magnetite quartzite is at the structural f/w of the sulphide body (see sect. 2.2.2).

A detailed description of the Ongeama mineralization revealed by drill cores is reported by Hoffmann (1976). Here a brief account of it is given.

The mineralization extends downplunge for a distance of at least 1650m (vertical depth of 230m) and with a maximum width of 500m. The ore shoot at depth consists of a single, well-defined zone. A small subsidiary mineralized lens occurs above the middle portion of the shoot. The styles of mineralization vary from unevenly disseminated to streaky, sub-massive and massive. Sulphides are represented by pyrite, pyrrhotite, chalcopyrite and sphalerite, with the last two being minor constituents. The best mineralization is hosted in quartz-chlorite-garnet-magnetite schists and subordinate magnetite quartzite. The contact with the barren wall rocks is gradational along the margins of the shoot, but abrupt at the h/w and f/w. Pyrite forms a considerable proportion of the coarse-grained, massive to semimassive ore associated with the stratigraphically higher/structurally lower magnetite quartzite. Disseminated and banded chalcopyrite and pyrrhotite largely occur in the structurally higher schists, where pyrite becomes subordinate.

2.2.2 The gossan exposure

The two limonite-rich gossan outcrops (major and minor), represented in Plan 1, pinch and swell along strike and gradually thin towards the ends.

The ore zone is represented by quartz-bearing gossan derived from massive sulphide mineralization (hereafter indicated as "massive sulphide gossan"), and magnetite quartzite. A gossan facies derived from amphibole-rich semi-massive mineralization (hereafter indicated as "semi-massive amphibole-rich gossan") is well developed in the centre of the major outcrop. Only in the major gossan outcrop is the ore zone overlain by an irregular band of gossanous magnetite-bearing chlorite and muscovite schists.

Ferruginous schists occur as lenses within the ore zone and in the h/w. The lithofacies of the ore zone are similar in the two separate gossan outcrops, although the gossan in the major outcrop displays a more complex rock association. An account of the distribution of the gossan facies and of their nature is given below.

The minor outcrop consists of a weathered massive sulphide lens in the east, which grades into a poorly exposed magnetite quartzite band towards the west. Non-magnetic ferruginous schists only occur along a shallow trench in the E in the h/w of the massive lens. Deformation is probably responsible for the repetition of the magnetite quartzite band in the f/w.

The major outcrop consists of a well developed pinch-and-swell structured gossan after a massive sulphide layer. This layer is underlain by a magnetite quartzite layer, and overlain by a band of magnetite-bearing schists (Plate 1). The magnetic schist band is best developed in the central part of the outcrop, whereas towards the margins only non-magnetic ferruginous schists are present.

The transition from magnetite quartzite to massive sulphide gossan is either gradational or due to tectonic interleaving. The blocky, banded magnetite quartzite is best developed in the eastern-central sector of the exposure, whereas in the west it crops out very discontinuously . The massive sulphide gossan facies shows considerable thickening at both ends and towards the centre of the sulphide body. A peculiarity of the central portion of the gossan is the lateral transition to a semimassive amphibole-rich quartz-poor gossan facies. This facies occurs in association with the maximum thickness of the magnetite-rich gossanous schists in the h/w of the sulphide body. Late mobilization of the mineralization is manifested by sulphide infilling of crosscutting metamorphogenic quartz veinlets.

The gap between the two gossan outcrops is mostly barren, with minor evidence of mineralization emerging from an isolated trench (grid reference 10720E; Plan 1).

The massive sulphide gossan consists of mainly massive siliceous Fe-hydroxide-rich bands which alternate with rusty quartzitic and/or thin phyllitic lenses. The limonitic bands may contain massive brownish limonitic jasper, crumbly or cellular siliceous limonite portions, or brown to black concretionary limonite crusts. Fine-grained crystalline quartz, of thin network texture, appears to be a common groundmass for the mineralization. In the cellular portions well preserved round and cubic boxwork structures after pyrite can be observed. Delicate ladder-like boxwork structures after chalcopyrite are less common. Pyrrhotite replicas were recognized only under the microscope (see Section 3.1.1 Part C). Magnetic massive sulphide gossan is rather common in the western central part of the major outcrop, although it may also occur elsewhere.

The semimassive amphibole-rich gossan facies is a slightly banded, relatively porous quartz-poor rock type. It consists of a fine network of yellowish fibrous anthophyllite aggregates (Andrew, 1980, and this study). Ladder-like boxwork structures are locally observed within the interstitial weathered sulphide patches. The transition from siliceous to amphibole-rich gossan is gradational. Isolated small amphibole-rich lenses are also noted in other parts of the massive gossan and magnetite quartzite, in both gossan outcrops. Lenses of ferruginous schist occur associated with the anthophyllite-enriched sector in the major outcrop (grid coordinates 10260E/10197N). This schist facies consists of a magnetic, strongly micaceous, schistose rock type, in which the mica-rich groundmass hosts limonitic boxwork probably pseudomorphing garnet-like porphyroblasts.

Magnetite quartzite is a banded, rusty, chlorite-bearing quartzite, containing fine- to coarse-grained magnetite-rich and non-magnetic gossanous bands. Banding, thought to be the result of metamorphism, is mostly planar, although minor slump-like structures can also be observed (Plate 2). Cellular spongy and ladder-like boxworks probably after pyrite and chalcopyrite, respectively, occur in patches not totally invaded by massive or concretionary limonite. Cubic cavities remain after coarse euhedral pyrite grains.

2.2.3 The magnetic hanging wall schists

Detailed mapping carried out by the author outlined the distribution of the magnetite-bearing, gossanous chlorite and muscovite schist band in the structural h/w of the major gossan outcrop (Plates 1 and 3).

The strike of the magnetic schists compares well with that of the country rocks. Nevertheless, the h/w magnetic schists define a transverse, elongated zone of chlorite enrichment, and a continous muscovite-rich band parallel to the strike of the gossan outcrop (Plan 1). The transverse chlorite-rich zone converges with the sulphide body at an angle of about 20^{o}.

Both chlorite and muscovite schists contain abundant coarse disseminated magnetite and are quartz-rich. The deep bluish-green chlorite-rich schists in the axial zone are pockmarked by unusually coarse-grained garnet and honey-brown staurolite porphyroblasts. The latter occur also as centimetre-scale clusters rimming quartz boudins. The magnetic muscovite-quartz schists have a mottled appearance imparted by the numerous and coarse euhedral magnetite crystals. The magnetic schists are moderately gossanous, due to the original presence of small streaks, lenses and disseminations of sulphides. This schist type laterally grades into a fine-grained non-magnetic ferruginous sericite schist, similar to the phyllitic intercalations within the massive gossan. The transition from one rock type to the other can be either abrupt, gradational or characterized by tectonic interleaving.

2.3 THE ONGOMBO PROSPECT

2.3.1 General geological setting

In the Ongombo Ost/West farm areas sulphide mineralization crops out as a gossanous magnetite quartzite for a total strike length of 4,9 km (Fig 18). The estimated thickness of the mineralization at the surface is in the range of 1 to 2 m.

The mineralization crops out almost continuously from the White Nossob River (Plate 4) towards the SW. East of the river it is found mainly as suboutcrops beneath the sand cover. The gossan outcrop is thickest in the central western portion, and thins towards both ends. It strikes NE-SW (average 039°) with a shallow (15°-20°) NW dip. As at Ongeama, the attitude of the mineralized body is conformable with the regional trend of the enclosing Kuiseb schists. However, the plunge of the ore shoot, as shown by the EMP trends, is towards the NE (Fig. 18). Statistical evaluation of strike readings of the D_2-related lineation in the magnetite quartzite outcrops confirm the EMP trends (Schneeweiss, 1984).

Outcrops in the area around the ore zone (Fig. 18) are poorly exposed. The subdued surface expression of the ore-hosting schists prevents the recognition of any sign of alteration related to the mineralization. Only the more resistant mafic rocks crop out locally in the gently sloping to flat-lying topography of the area.

Previous geological mapping indicated the presence of two main bands of amphibolites positioned above and below the ore body and intercalated within the metasediments. Amphibolites occur as thin, medium-grained, sheet-like bodies in the metasediments, and as coarse-grained boudinaged, lens-shaped metagabbro bodies with sheared margins. Metalava layers do not outcrop. As at Ongeama, the bulk of the stratigraphic sequence is represented by metapelites and metapsammites of the Kuiseb Formation. The Ongombo metapelites are generally garnetiferous and staurolite-rich, unlike the staurolite-

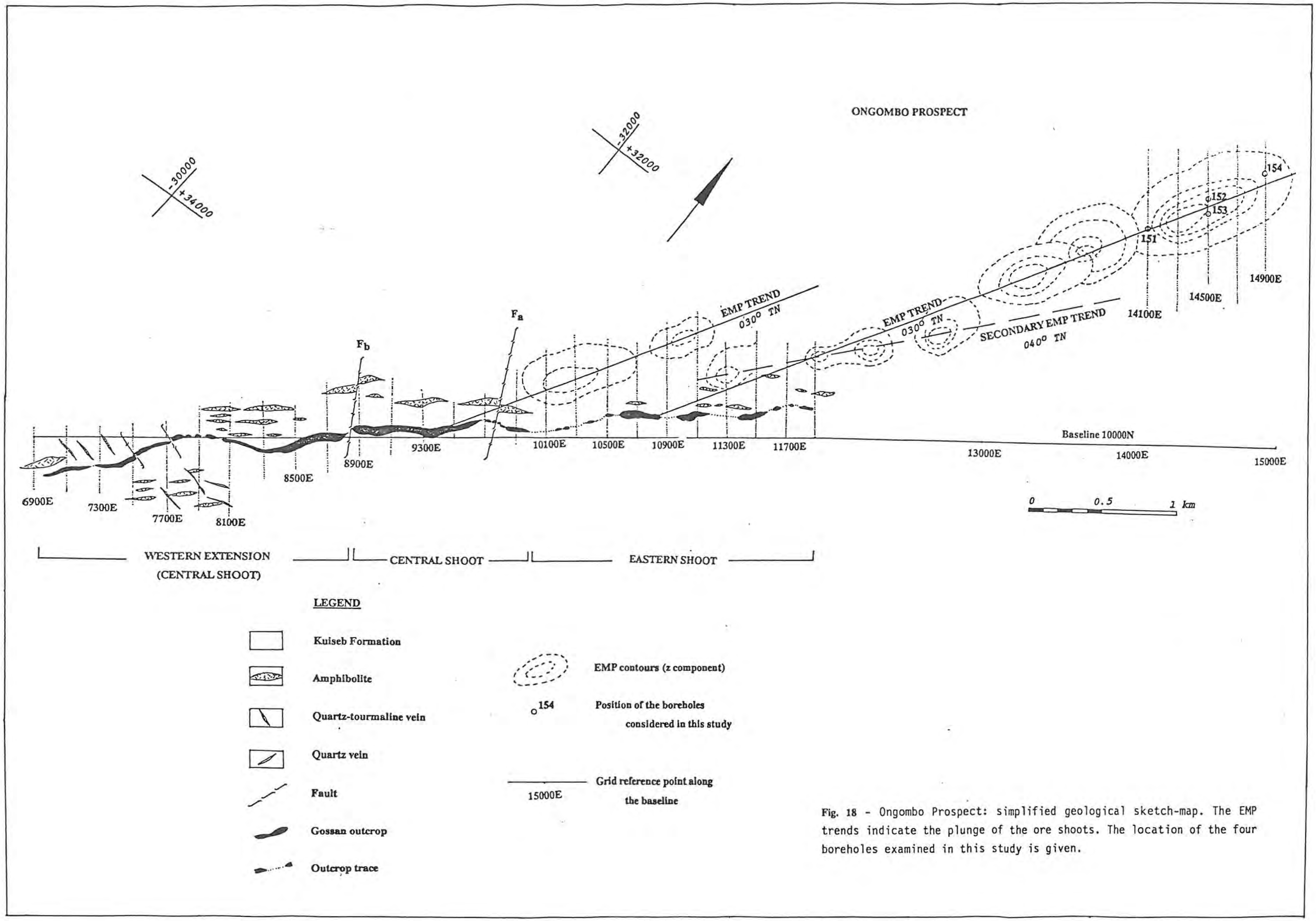

Fig. 18 - Ongombo Prospect: simplified geological sketch-map. The EMP trends indicate the plunge of the ore shoots. The location of the four boreholes examined in this study is given.

devoid country rocks at Ongeama.

The style of deformation at Ongombo is similar to that observed in the Ongeama area. Minor fold structures are preserved in coarse metagabbro outcrops and occasionally in banded magnetite quartzite. Faulting is revealed by moderate displacement in the gossan outcrop and in the amphibolite zones (Fig. 18). Late veining is widespread throughout the gossan and in the country rocks. Two crosscutting vein sets are recognized by McCormick (1988): WNW-ESE-trending banded tourmalinite veins and ENE-WSW-trending quartz veins. Tourmalinite veins are well developed towards the western end of the gossan outcrop. Tectonic stretching during the main phase of deformation is considered to be responsible for the variations in thickness of the quartzitic sulphide body, which behaved as a rigid and competent unit.

2.3.2 The gossan exposure

The surface exposure of the Ongombo mineralization does not show the complexity shown by the main gossan outcrop at Ongeama.

The Ongombo gossan consists of a moderately gossanous, locally chloritic, banded magnetite quartzite. Subordinate non-magnetic gossanous schists are unevenly intercalated as thin lenses and bands within this magnetic quartzite. In the deeply leached outcrop, copper oxide staining is only confined to the excellent exposure along the White Nossob River and to two other small outcrops (grid reference: 11740E/10225N and 7920E/10000N) (Fig. 18). In general the magnetite quartzite is coarse- to medium-grained, with a sugary texture. Magnetite is clustered in bands or finely disseminated in the granular quartz matrix.

Weathered sulphide mineralization occurs:

a) as disseminations, bands, lenses and stringers along the whole strike extension of the magnetite quartzite;

b) as disseminations in the schists;

c) as impregnations in discordant, fine-grained amphibole-rich patches (possibly anthophyllite);

d) as remobilised, semimassive quartz-vein infillings.

In Fig. 18 three main sectors of the gossan have been highlighted. They correspond to the surface intersection of the two main EMP trends which coincide with the two major downplunging ore shoots. From E to W, the three sectors are the Eastern Shoot, the Central Shoot and the western extension of the Central Shoot. This subdivision of the gossan was devised (see Section 5.1 below) in order to record possible significant changes in the areas approaching the intersection of the shoots with the surface. The evaluation of the lithologic changes along the strike of the mineralized outcrop is dependent on the conditions of the exposure. In general, the approach to the zone of intersection of the EMP trends with the surface is characterized by an increase in the proportion of sulphides within magnetite quartzite and crosscutting quartz veins. This is particularly evident in the better exposed central-western portion of the gossan, towards the Central Shoot. This is less evident towards east due to the poorer outcrop conditions. The two thicker portions of the Central Shoot outcrop coincide with a relative increase in the gossanous sulphide content. An interesting feature in the outcrop of the central-western sector, is the presence of irregular amphibole-rich patches. These patches start to be abundant from within the Central Shoot exposure towards its western extension. The amphibole-rich patches show a fibrous-radiating texture and are similar to those at Ongeama. Amphibole enrichment was observed neither in the Eastern Shoot exposure nor in the corresponding cores examined.

2.3.3 The ore zone and the enclosing schists in drill cores

Drill cores of a total length of approximately 240m were examined in detail in order to examine the relationships between the mineralization and enclosing schists, and to study the mineralization in unweathered samples. The drill cores studied are part of a drilling programme by Gold Fields Namibia, currently exploring the Eastern Shoot.

In the cores, lithologic changes (chloritization and magnetite dissemination) were recognised within the schists overlying the ore zone. These changes were originally interpreted as representing a zone of ore-related hydrothermal alteration (D.H. Corbett, pers. comm., 1989). The overturning of the sequence was inferred from the position of this chloritic alteration zone in the structural h/w of the mineralization. A complication to this preliminary assumption is provided by the presence of mafic units near the ore zone in the h/w. Therefore, one of the aims of the detailed study of cores was to find ways of discriminating between possible contact metasomatism related to the mafic intrusions and ore-related hydrothermal alteration.

Appendix B shows the logs of the four boreholes examined (Nos. OGB 151A, OGB 152A, OGB 153A and OGB 154A). These boreholes were re-logged from the position of the first appearance of chloritization downwards for about 45m. The first appearance of chloritization coincides with the first occurrence of the mafic units in the sequence. Several metres of schists in the immediate f/w of the mineralized intersection, down to the end of the hole, were considered as examples of unaltered schists. The f/w schists also include magnetite-bearing metapsammitic layers apparently not directly related to the mineralization. In these layers magnetite occurs as small grains, generally less than 0.5 mm in size.

The h/w schist sequence (see Appendix B and Appendix J) consists of alternating, planar to contorted, metapelitic staurolite-bearing and garnetiferous quartz-biotite-muscovite-chlorite schist and massive metapsammitic, locally garnetiferous quartz-biotite schist. In the detailed logs in Appendix J, the two schist end-members and intermediate schist types are schematically indicated by symbols. These symbols are commonly used during the current drilling programme to indicate schematically the proportion of phyllosilicates.

The mafic units occur as few-cm- to 3-m-thick intercalations. Augen-textured feldspathic amphibolite characterizes the thickest intercalations. Coarse-grained, spotted chlorite-actinolite-biotite schist layers are well developed along the h/w margins of the amphibolite horizons. They can attain a thickness of approximately 80 cm and are in sharp contact with the underlying mafic unit. They commonly occur as an asymmetrically developed margin to the mafic units. Narrow layers of chlorite enrichment within the amphibolite units appear to be related to localized shearing. Thin chlorite-actinolite-bearing bands are often intercalated with quartz-rich sediments in well defined horizons. The numerous mafic layers occurring in the h/w schist sequence can be grouped into two main bands separated by a 15m- to 25 m-thick schist sequence.

The chloritization observed in the schists is detectable as a weak, but perceivable change in colour towards a green hue in the usual light grey quartzites and phyllites. This change is more evident in the vicinity of both thin and thick mafic units, although it can also be observed elsewhere. The intensity of the chloritization is variable. Where most intense, it can be accompanied by disseminations of magnetite and locally of minute sulphide specks. The magnetite grains have an average size of 1 mm and rarely exceed 4 mm. In general, no increase in magnetite is observedin the immediate h/w contact of the ore zone, although magnetite enrichment is locally found proximal to the ore zone.

Garnet irregularly decreases in abundance in the h/w rocks towards the ore zone. This irregular garnet decrease appears to be accompanied by a concomitant staurolite enrichment.

The simplified stratigraphy of the ore zone is schematically represented in Fig. 19.

The ore zone is delimited by well-developed bands of coarse-grained brownish staurolite-rich biotite schists, or "biotite selvedges". These selvedges contain finely to coarsely disseminated lens-shaped sulphide grains (mostly pyrite) (see Plate 25). Within the ore zone

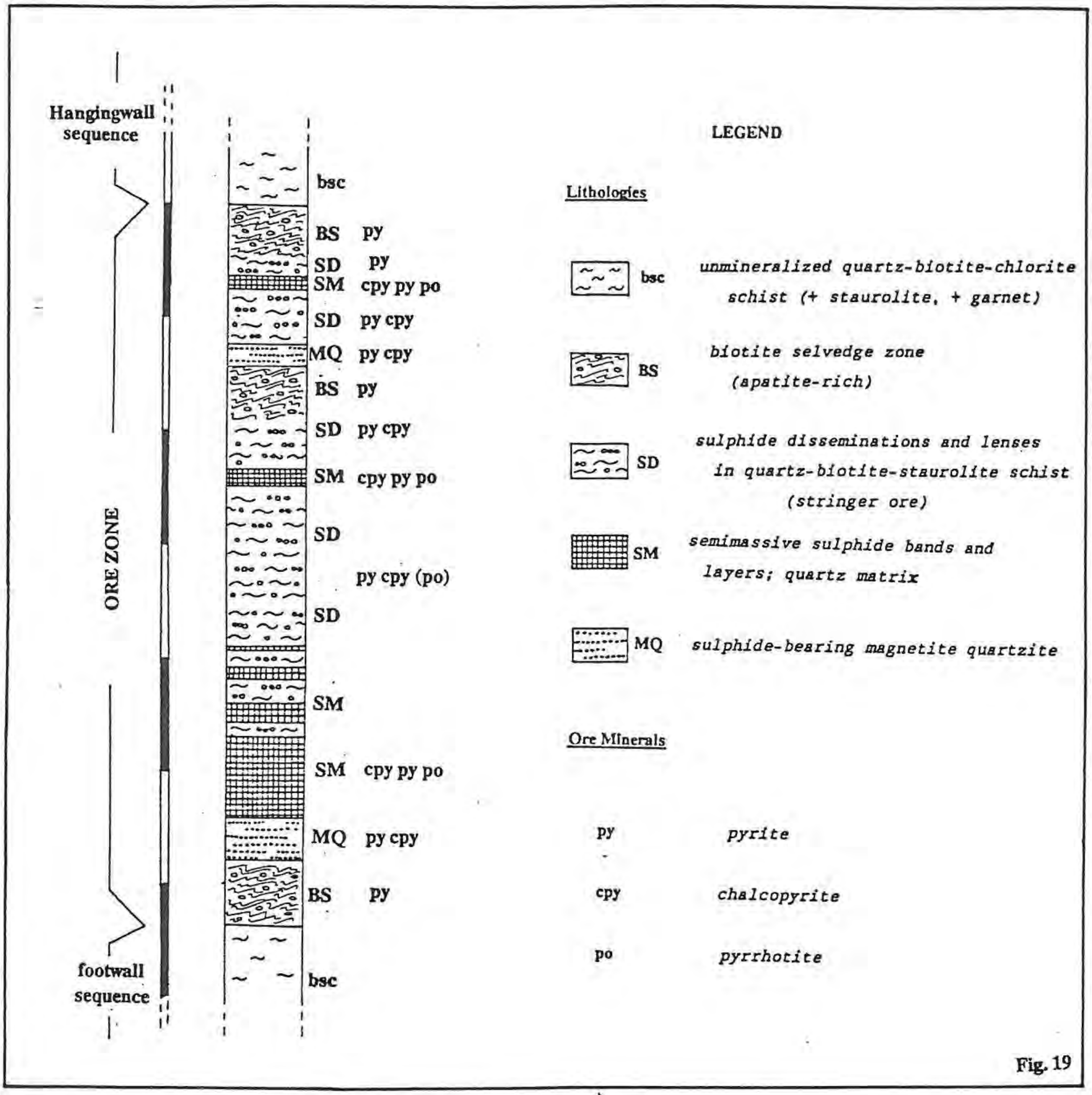

Fig. 19 - Schematic stratigraphy of the "ore zone" at Ongombo, in the thickest mineralized intersections (boreholes No. OGB 151A and OGB 153A). In the column zones of remobilized ore in veins are not indicated. Details of the hangingwall and footwall sequence are in the logs in Appendix B.

the mineralization occurs as disseminated, streaky, banded and locally semimassive coarse granular sulphide aggregates (pyrite + chalcopyrite and minor pyrrhotite) in both non-magnetic and magnetite-bearing quartzitic groundmass. Semimassive mineralized bands are intercalated with barren biotite- and staurolite-rich schists. In the schists sulphides occur in quartz lenses and streaks, and subordinately as disseminations. Remobilized ore in quartz veins and boudins occurs as semimassive sulphide blebs and patches, which commonly consist predominantly of chalcopyrite. Laminated magnetite quartzite, with disseminated and semimassive mineralized bands, occurs as two or more, thin, decimetre-thick units separated by zones of weaker mineralization. The lowest part of the ore zone is generally characterized by a poorly mineralized magnetite quartzite layer, up to 1 m thick, separated from the barren f/w schists by a biotite selvedge zone.

3 MATCHLESS WEST EXTENSION: SURFACE GEOLOGY OF THE MINERALIZATION

The Matchless West Extension sulphide deposit is situated about 25 km SW of Windhoek in proximity to the Matchless Mine. Both deposits are hosted in a schist sequence included between the "Colvania Horizon" and the mafic rocks of the Matchless Mine Horizon (Fig. 12 and 20) (see also Section 3 Part A).

Matchless West Extension is a small sulphide body with a maximum strike extension of about 240m. It is conformable with the enclosing schists which dip between 38^{o} and 64^{o}. Resistant rocks such as quartzite crop out as ridges, whereas pits expose part of the mineralized body in places. The deposit was mapped in detail, at a scale 1:500, by T. Smalley in 1984 under contract to Tsumeb Corporation Limited (TCL). That mapping was part of an exploration programme which covered the area between the deposit and the Colvania Horizon. This programme also included geophysical (electro-magnetic) surveys.

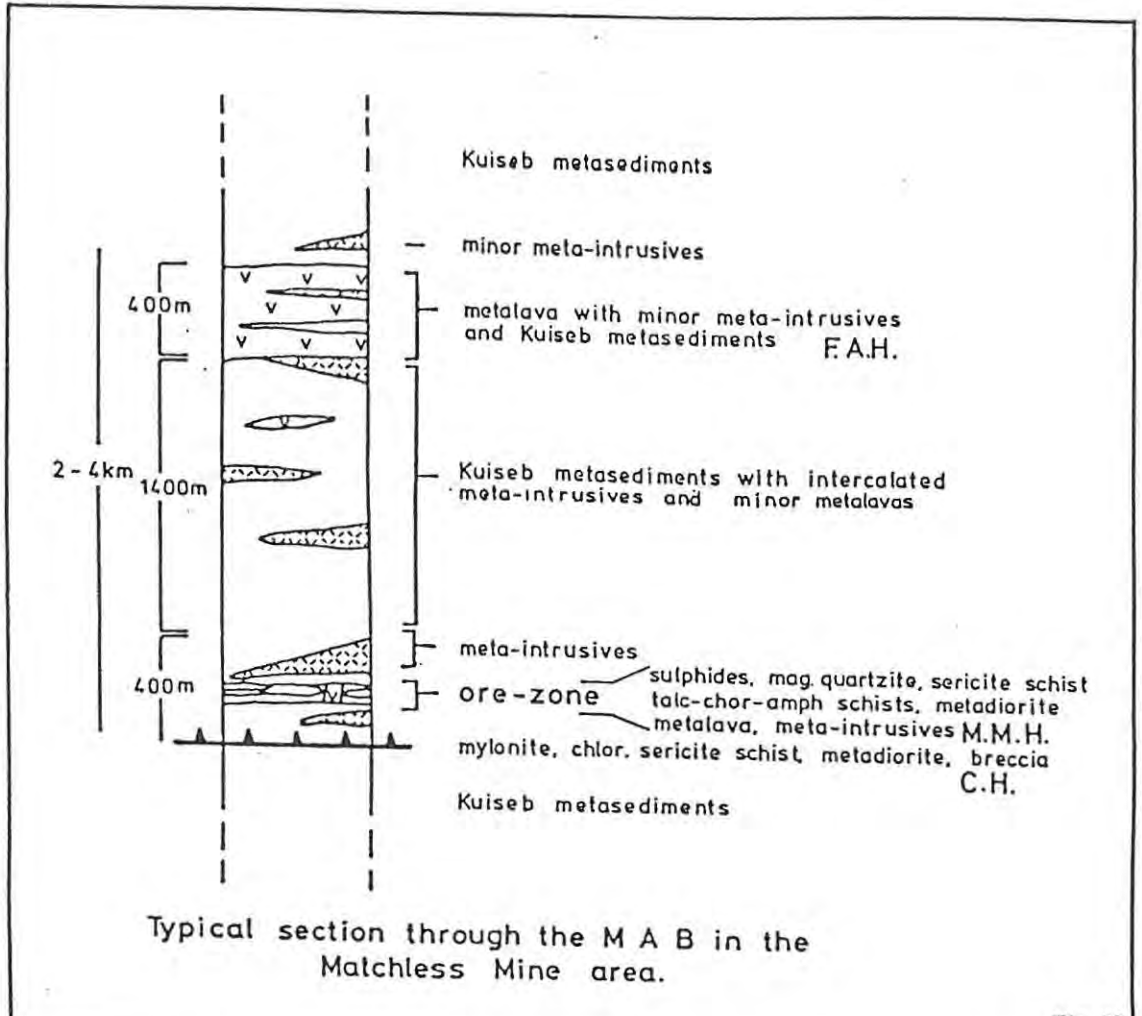

Fig. 20

Fig. 20 - Stratigraphic section of the Matchless Belt in the Matchless Mine area, showing the position of the Colvania Horizon (CH), the Matchless Mine Horizon amphibolite (MMH) and the Friedenau Amphibolite Horizon (FAH) (Smalley, 1988).

The map shown in Fig. 21 is a slightly modified version of Smalley's map. The latter was mainly used as a reference for the sampling of the deposit carried out by the present author.

The surface geology of the deposit is characterized by remarkable lateral lithological changes from E to W. Gossanous sericite schists (sericite zone) are well developed in the eastern sector of the area. These schists contain abundant fine-grained pyrite as disseminations or thin stringers parallel to the foliation. Sericite schists occur along most of the f/w of the mineralized body. In the eastern sector a distinct symmetrical zonation is observed in the exposure of the sericite zone. A fine-grained sugary-textured quartzitic facies (sericite quartzite) defines an elongated axial portion orientated at an angle of 12^{o} relative to the strike of the mineralized body. This transverse band is symmetrically bordered by a more schistose, sericite-rich, locally chlorite-bearing facies. The sericite zone is overlain by a poorly exposed porous massive gossan in the east, and by a well developed gossanous, sulphide-rich magnetite quartzite band in the centre. The transition between these two lithologies appears to be gradational. The massive gossan displays a quartz-rich fine-grained groundmass, but it locally contains clots of minute phyllosilicate-like material. Unlike Ongeama and Ongombo, the magnetite quartzite has a very fine-grained quartz-rich matrix, in which small magnetite grains are distributed as dust-like disseminations and as well defined bands.

Talc- and actinolite-bearing schists occur as bands and lenses in the central sector. Locally, in this sector, they appear to be finely intercalated with quartzitic material or in direct contact with the gossanous sericite schists. The best development of talc- and actinolite-bearing schists is in the western sector, where a thick zone of these rocks is situated between two magnetite quartzite layers. This composite ultramafic layer consists of alternating, almost monomineralic, decimetre- to metre-thick, schistose to massive bands, in which either actinolite or talc is the dominant component. The weathering of rhombic carbonate porphyroblasts, commonly hosted in the talc-rich facies, leaves pitted rock surfaces. The gossanous

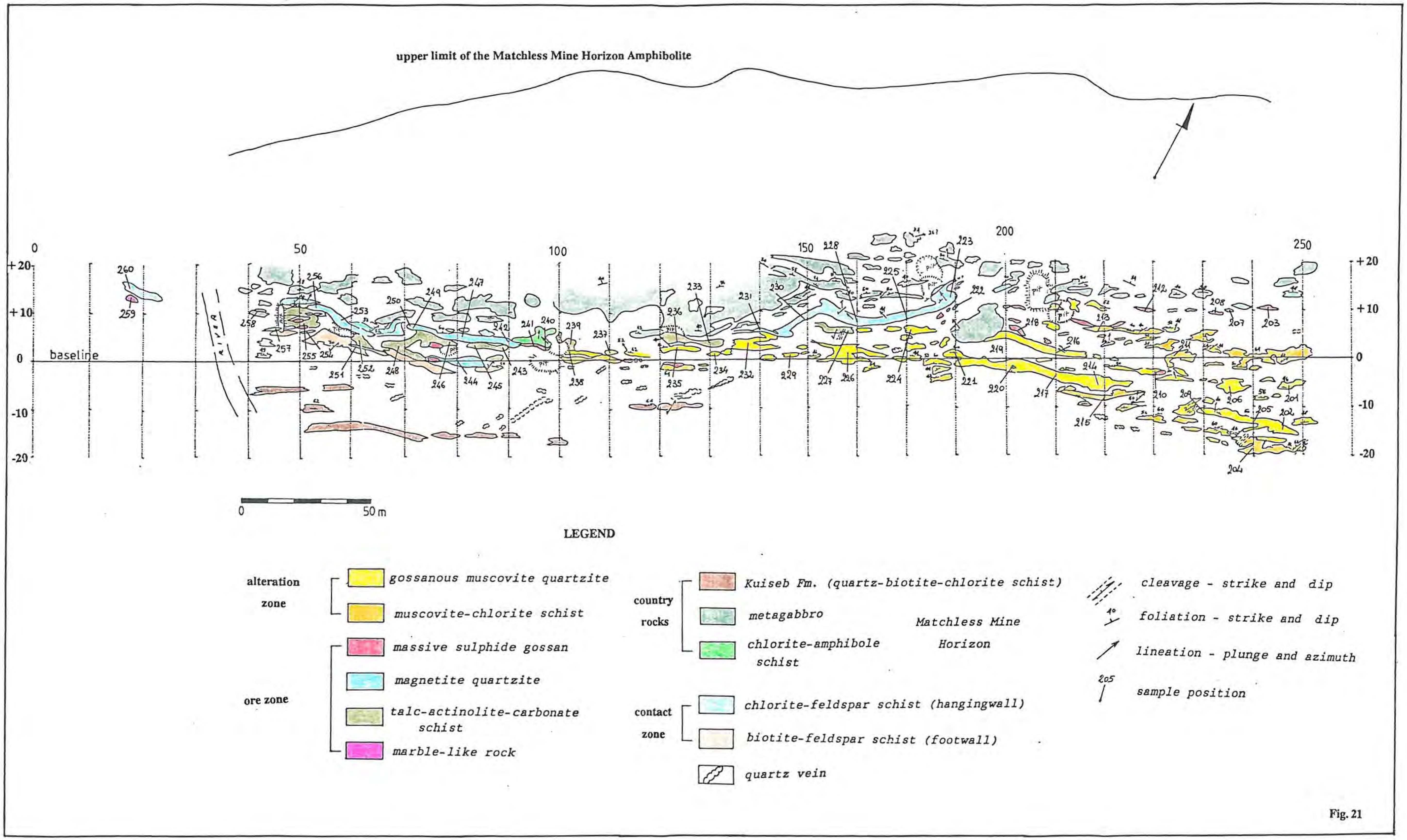

Fig. 21 - Geological sketch-map of the Matchless West Extension sulphide deposit (modified after Smalley, TCL, 1984).

appearance of these ultramafic units is due to copper staining and intercalations of weathered sulphide-rich quartzitic bands. The spatial association of these rock types with magnetite quartzite suggests an exhalative origin (see Section 3.2.3. Part C).

The two magnetite quartzite layers, including the ultramafic band in the western sector, display different characteristics. The stratigraphically lower layer is massive, poorly banded, very dark due to the exceptional abundance of finely disseminated magnetite, and it often contains malachite-stained, limonitized sulphide streaks. A faint compositional layering is suggested by these gossanous streaks, by the localized denser magnetite concentrations and by the presence of thin amphibole-bearing lenses. Local black staining and crusts suggest Mn-enrichments. The upper magnetite quartzite layer is distinctly non-gossanous and well banded. The thin amphibole-rich lenses rapidly decrease towards the h/w.

Beyond the river on the western side a white marble-like rock, with scarce disseminated pyrite, occurs next to the gossanous magnetite quartzite exposure.

Wall rocks are represented by garnetiferous quartz-biotite schists of the Kuiseb Formation in the f/w, and by massive to sheared amphibolites (metagabbro) and chlorite-amphibole schists in the h/w.

An outstanding deformation-related feature observed by T. Smalley (1989, pers. comm.) is the development of an "ore cusp", or sulphide injection structure in the central-eastern portion of the exposure (see Fig. 21). The cause may have been competency contrast between the sulphide mineralization, the overlying rigid metagabbro and the underlying quartz-sericite schists, during the main deformation phase (D_2). Similar cuspate ore-wall rock interfaces were observed also at the Matchless Mine (Maiden et al., 1986), where they are responsible for localized thickening of the ore zone. The later, less severe, D_3 deformation phase induced only small-scale crenulation cleavage in the finely laminated quartz-sericite schists.

4 THE SAMPLING PROGRAMME

A detailed and systematic lithogeochemical sampling programme was carried out by the author on mineralized and barren outcrops and on cores in the areas of study. A total of 487 samples was collected and submitted for chemical analysis. Appendix C contains a list of the samples, their location and the rock type.

4.1 Sampling procedure on the mineralization

At Ongeama, the gossan exposure has been systematically sampled along a 20m-spaced grid. This grid was also used for geological mapping and was based on the existing 50m-spaced grid established by Gold Fields. Composite chip samples, with the approximate weight of 1 kg, were collected at lithological changes considered significant on the scale of the mapping. Due to poor outcrops, samples of barren schists had to be collected outside the area studied, but, nevertheless, within the main grid.

At Matchless West Extension sampling was carried out along a 10m-spaced grid. The new grid was superimposed on an earlier grid established by TCL in the early 80's.

At Ongombo the sampling of the 4.7km-long mineralized outcrop was organized in a different way. The assumed zones of intersection of the EMP trends (i.e., ore shoots) with the surface were defined. Within these zones, samples were collected every 20m, whereas, in the remaining portions, samples were collected every 50m. One or two samples only were collected for small, isolated outcrops along strike. The sampling was done according to the existing grid established by Gold Fields Namibia (Fig. 18).

Drillcores examined from the Ongombo drilling programme (borehole No. OGB 151A, OGB 152A, OGB 153A and OGB 154A), were sampled from approximately 16-20 m in the h/w, across the "ore zone", to 6-10m in the f/w. The whole core was sampled, except in the "ore zone". In this portion the core was quartered and only one quarter sampled.

4.2 Sampling of the "I anomaly" area at Ongeama

At Ongeama the "I anomaly" is located approximately 800m NW of the gossan outcrop (Fig. 16). The "I anomaly" is an area characterized by a positive magnetic anomaly in the form of clustered peaks. In the field these magnetic peaks were found to coincide with metapsammitic, and subordinate calc-silicate, units containing fine-grained disseminated magnetite grains. Only in one case (sample OG 138, grid ref. 9905E/11058N) does coarse-grained magnetite occur in a few cm-thick chlorite-rich selvedge wrapping around a quartz pod or vein.

Samples have been collected from each area corresponding to a positive peak. According to what was observed in the south-easterly gossan exposure, the sampling of the "I anomaly" was done in order to check whether these magnetite disseminations might be associated with an ore-forming hydrothermal system. However, no positive evidence of hydrothermal alteration was observed in the field. Mafic rocks (metagabbros and chlorite-amphibole schists) are present towards the northwestern boundary of the "I anomaly" area.

Comments on the trace element content of the "I anomaly" samples are given in section 2.5 Part D.

4.3 Sampling of ultramafic rocks

Two ultramafic bodies outcropping in the Eastern Windhoek sector of the Matchless Belt were sampled. In section 4 Part D, the geochemistry of these bodies is compared with that of the ultramafic schists in the ore zone at Matchless West Extension and with that of the chlorite-actinolite margins of the metagabbroic horizons in the Ongombo cores.

The ultramafic bodies sampled are located NNE and WNW of the Otjihase Mine, in the Van Francois Ost 60 and Elisenheim 68 farm areas (for location see Fig. 22 and 12). The ultramafic outcrop at Elisenheim Farm was previously studied by Finnemore (1974). The ultramafic bodies considered belong to the group of Damaran Alpine-type serpentinites studied by Barnes (1983).

These ultramafic bodies consist essentially of talc- and actinolite-rich lithologies, crenulated to massive talc-carbonate schists with varying amounts of chlorite and magnetite and coarse actinolite-

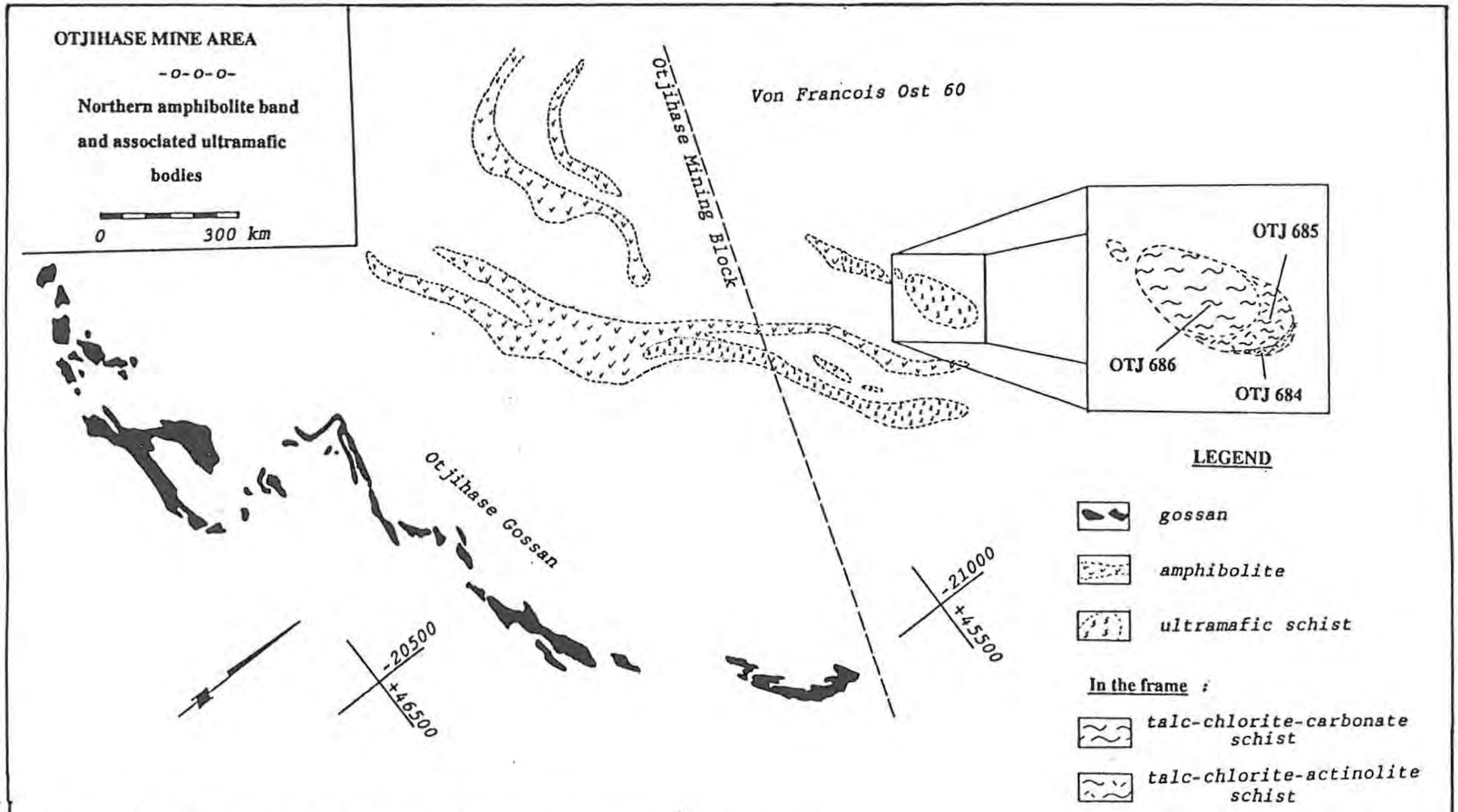

Fig. 22 - Schematic sketch-map of part of the northern amphibolite band and associated ultramafic bodies in the east of the Otjihase Mine (Von Francois Ost 60 farm area). In the frame the lithological zonation in the ultramafic outcrop is indicated.

chlorite schists. In the Van Francois Ost outcrop, the actinolite-chlorite schists occur as a peripheral band around a talc-carbonate magnetite-rich core (Fig. 22). Such concentric zonation is similar to that reported by Sanford (1982) for the metasomatic reaction zones developed at the contacts between ultramafic bodies and country rocks in greenschist- to amphibolite-facies metamorphism.

5 DISCUSSION

The most significant result of the detailed work at Ongeama and at Matchless West Extension is the recognition of some schist facies, which are exclusively associated with the mineralization, and quite distinct from the country rocks. Based on field relationships, it is the opinion of the present author that these schist facies suggest the occurrence of pre-metamorphic ore-related hydrothermal alteration zones. The discordant nature of the lithologic changes characterizing the schists within the assumed alteration zones, does not appear to be the result of deformation and/or metamorphism. The distribution of the rock types reflects the geometry of typical pipe-like alteration zones associated with volcanogenic sulphide deposits. In the alteration pipe, facies changes may occur both laterally and vertically.

At Ongeama the magnetite-staurolite-garnet-bearing chlorite schist facies may represent the metamorphism of an aluminous and chloritic axial zone of an alteration pipe. The occurrence of abundant staurolite is an indication of the Fe-rich environment. The associated, marginal magnetic muscovite schist band seems to correspond to an outer sericitic envelope. Sulphides in fine disseminations and small lenses in the altered schists can be interpreted as an original disseminated and stringer-type mineralization developed along the hydrothermal fluid conduit. The outcrops of these schist facies, compared to the more subdued exposures of the country rocks, may, in fact, reflect an original silicification along the pipe. The outermost non-magnetic ferruginous schists may represent the product of the interaction of waning ore-forming fluids with the sediments. An alternative interpretation is that these gossanous schists may be the metamorphosed equivalent of chemical precipitates (i.e. montmorillonite-kaolinite, silica gel and sulphides) deposited as a hydrothermal apron on the sea-floor contemporaneously with the massive mineralization (McLeod and Stanton, 1984).

The position of the assumed alteration pipe in the h/w of the mineralization at Ongeama suggests the overturning of the stratigraphic sequence. The attitude of the pipe is similar to the plunge direction of the ore shoot, as indicated by the corresponding magnetic anomaly (Fig. 16), and by the lineation in the magnetite quartzite outcrops (Plan 1). A sinistral shear movement is inferred from the flattening undergone by the pipe (Fig. 23).

Similar considerations can be made for Matchless West Extension. On the basis of field observations, the author agrees with Smalley's (1990) opinion that the sericite zone in the f/w of the mineralized horizon may represent the metamorphosed equivalent of an original alteration pipe-like zone (Fig. 24). This discordant alteration pipe consists essentially of a quartz-sericite-pyrite alteration assemblage. The symmetric lateral zonation, from the silicified axis to the more mica-rich margins, is not obliterated by deformation and metamorphism. A sinistral shear deformation is evident also at Matchless West Extension, as it is at Ongeama. The presence of this unusual lithological association in the f/w of the mineralized body should imply that the ore-hosting sequence is the right way up. Additional field evidence confirming the above statement can be seen in the two magnetite quartzite horizons in the western sector of the outcrop. In these two horizons, the gradually upward decreasing sulphide abundance seems to reflect the normal transition from an underlying sulphide-richer portion of the mineralization to an overlying sulphide-poor oxide cap, as observed in similar, undeformed volcanogenic sulphide deposits (Lydon, 1988).

The distribution patterns of trace elements along the alteration pipes at Ongeama and Matchless West Extension provide further data on the

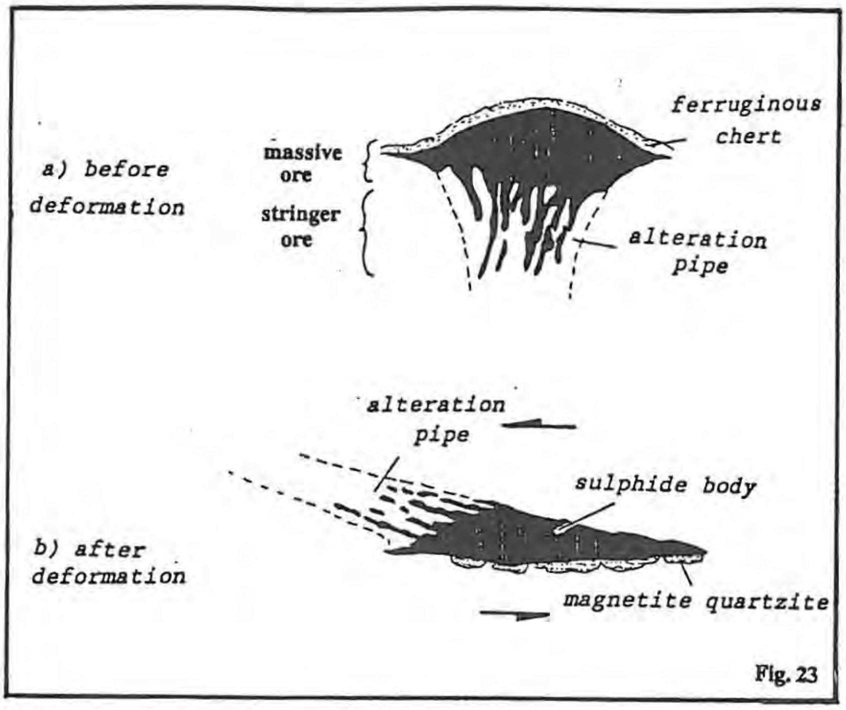

Fig. 23 - Reconstruction of the possible original mineralized system at Ongeama (a) on the basis of its present attitude (b) (modified after Sangster and Scott, 1976).

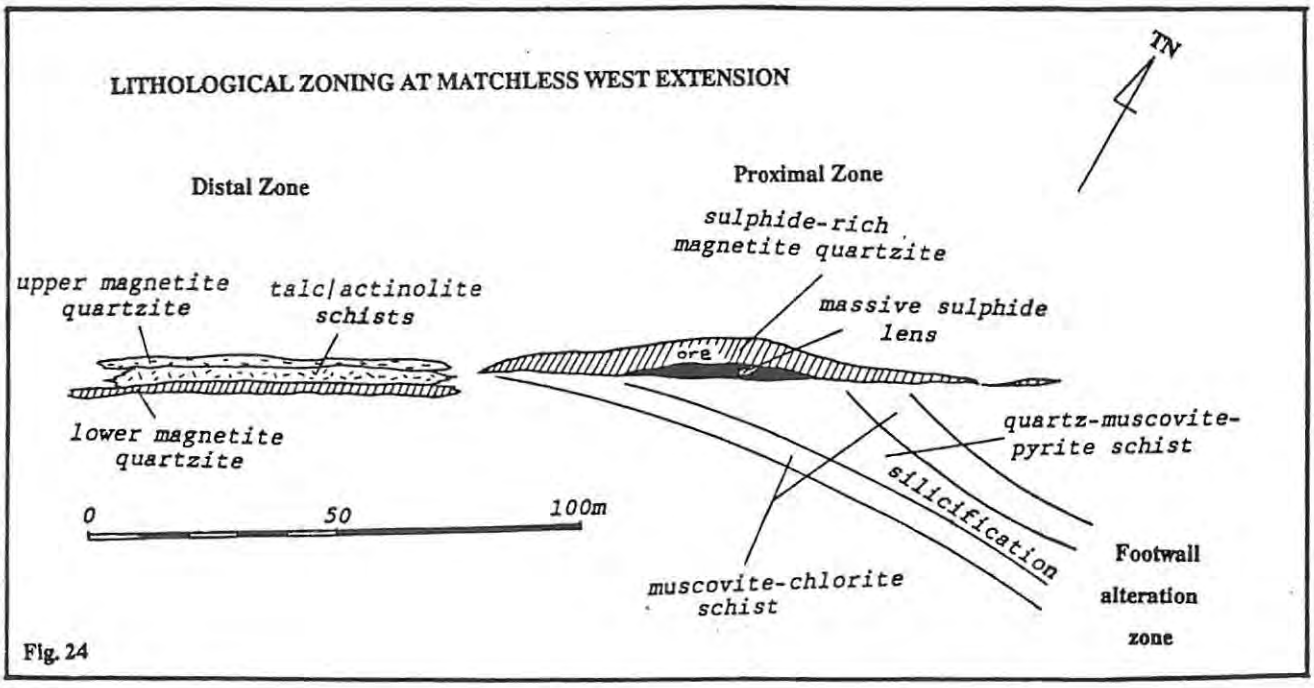

Fig. 24 - Schematic plan with the lithological zoning at Matchless West Extension (modified after Smalley, 1988).

nature of these pipe-like features (see Part D).

A further confirmation of the hydrothermal nature of these lithologic associations is provided by their greatest development in correspondence to significant facies changes of the mineralized body. For example, at Ongeama the intersection between the assumed alteration pipe and the sulphide body is characterized by the development of the amphibole-rich facies within the massive sulphide portion. At Matchless West Extension the top of the alteration pipe coincides with the occurrence of a richly mineralized portion of the ore horizon, which, in the field, is represented by massive sulphide gossan and gossanous, sulphide-rich magnetite quartzite.

The above considerations cannot be extended to Ongombo with certainty at this stage. The areally localized lithological changes (e.g. amphibole enrichment), observed in the gossan, may be a primary feature of ore deposition, and may suggest the position of a possible alteration pipe. However, they cannot be related to any rock association suggestive of hydrothermal alteration in the field because of insufficient outcrop.

The association of amphibole and sulphide enrichment with the thickening of the mineralized body in the Central Shoot may, alternatively, be interpreted as a deformation-related feature. As a matter of fact, the inflection of that part of the outcrop is considered by Hoffmann (1976) to have been induced by a major monoclinal fold structure. This feature stands out from the minor structural undulations present throughout the gossan outcrop (Fig. 18).

In the Ongombo cores, chloritization is the only major (although weak) lithologic change in the h/w schists. Magnetite disseminations are not evenly distributed. Chloritization can be seen at distances exceeding 40m from the ore zone and coincident with the first occurrence of mafic units in the drill cores. In consideration of the extent of deformation, this distance appears to be excessive for the chloritization to be considered as a product of hydrothermal alteration related to the ore zone. Moreover, no significant chlorite increase or change is observed in proximity of the ore zone. However, visual observation alone of the cores is not sufficient to evaluate the obliterating effects of metamorphism on hydrothermally altered schists, or to discriminate the effects of ore-forming fluids, and of sill intrusions into the sediments. A discussion about the significance of the chloritization in the cores at Ongombo is, therefore, reported at the end of the next chapter, in which details of the mineralogical and textural characters of mineralization and related alteration are discussed.

PART C

PETROLOGY OF MINERALIZED AND BARREN ROCKS

1. INTRODUCTION

The mineralogical and textural features of the metamorphosed volcano-sedimentary sequence, of the enclosed mineralized bodies and of the associated zones of pre-metamorphic hydrothermal alteration in the areas of study are described and discussed in this chapter.

A list of the thin and polished sections examined and relative locations is given in Appendix D.

2. PETROLOGY OF THE COUNTRY ROCKS

2.1 Petrology of the metasedimentary Kuiseb Formation and of the intercalated mafic rocks of the Matchless Member

2.1.1 Schists of the Kuiseb formation

In the area of study the bulk of the Kuiseb Formation is represented by strongly micaceous metapelitic schists and subordinate metapsammitic, quartzitic schists with locally associated "calc-silicate" intercalations. Gradations between the two main schist types are observed both on the scale of the hand specimen and thin section.

The main mineralogical components of the metapelites (OG 755, 756 and sections from OGB 153A) are biotite, chlorite, muscovite, quartz, plagioclase (oligoclase), staurolite and garnet. Epidote (clinozoisite), apatite, opaque minerals, zircon and tourmaline occur as common accessories. Variations in the relative abundance of biotite and chlorite result in the occurrence of more biotitic or more chloritic facies. The minerals are arranged in alternating granoblastic quartz-plagioclase-rich microlithons and lepidoblastic cleavage stripes, in which the fine- to medium-grained accessories are variably distributed.

Biotite occurs in two distinct associations:

a) a chlorite-biotite association, intergrown with muscovite in the cleavage planes, is characteristic of greenschist facies metamorphism (Winkler, 1979) and occurs as well oriented fibro-lamellar aggregates which define the foliation;

b) a staurolite-biotite association, which probably derives from the breakdown of chlorite in the presence of muscovite at the boundary between greenschist and lower amphibolite facies metamorphism (Winkler, op. cit.). Such association is characterized by lenticular aggregates of biotite and euhedral staurolite porphyroblasts grown discordant to the foliation. Biotite-staurolite layers alternate with the chlorite-biotite laminae, indicating the development of prograde metamorphic reaction in a "lit par lit" fashion.

Poikiloblastic garnet porphyroblasts are generally associated with staurolite and may display an atoll-like growth pattern. Muscovite lamellae often rim staurolite grains.

Retrograde metamorphic replacement of biotite by chlorite is common and can be recognized by preserved biotite inclusions in poikilitic sulphide blebs growing on chlorite plates (OG 756).

In the area of study the metamorphic paragenesis in the metapelites is comparable with that characterizing the staurolite + chlorite + biotite zone recognized by Hoffer (1983) in the phyllites just W and S of Windhoek. Hoffer estimates the temperature and pressure conditions for the biotite + staurolite association at 590°C and 5 kb. In the metapelites, as well as in the other rock types examined, a pronounced metamorphic recrystallization is indicated by the granoblastic polygonal texture of the quartz aggregates.

In the thin sections examined at least two metamorphic foliations, S_{0-1} and S_2, and a D_3-related crenulation are recognized. The tight isoclinal D_2-related folding of the S_1 foliation is shown by the disposition of mica flakes and tabular opaque minerals along fold hinges. Layers with remnant fold structures, as pod-like fold closures, alternate with layers with a composite S_0-S_1-S_2 foliation. In these layers a strong tectonic transposition of the folded S_1 has been enhanced by the further tightening of folding. Quartz boudins are syntectonic to S_2. The D_3-related crenulation is shown by local gentle to narrow folding and kink banding in the S_2-oriented micaceous laminae. The common helicitic texture, defined by the rectilinear to sygmoidal and spiralled disposition of the inclusions, indicates the syn-late timing of the garnet nucleation relative to the S_2-generating deformation phase. The euhedral staurolite and associated biotite porphyroblasts growing along S_2 are not deformed. The arrangement of the inclusions in staurolite parallel to S_2 suggests a static blastesis and consequently the development of the metamorphic peak (lower amphibolite facies) after the D_2 deformation phase.

The metapsammites (OG 693 and sections from OGB 153A) are fine-grained quartzitic schists with poor to indistinct compositional layering. Their mineral assemblage consists of quartz, plagioclase, biotite, epidote, apatite, opaques and zircon. Garnet occurs locally. Short biotite lamellae grow both isolated and in discontinuous laminae in the granoblastic quartzose groundmass. They impart the slight foliation to the rock type. A single foliation is recognizable. Retrograde metamorphic chlorite replaces biotite.

The calc-silicate layers (OG 757) essentially consist of a mica-free hornblende-epidote-rich, plagioclase-bearing quartzite with a distinctive grano-porphyroblastic texture. The poikiloblastic porphyroblasts of greeny-blue hornblende are mostly arranged parallel, locally transgressive, to the foliation. Inclusions consist of coarse-grained subhedral epidote and quartz and plagioclase from the groundmass. The assemblage might be suggestive of an indirect contribution from mafic volcanic activity.

2.1.2 Magnetite-bearing schists

A few sections from magnetite-bearing schist units have been examined in order to characterize the mode of occurrence of the magnetite disseminations in the sequence, and to verify its possible association with ore-related hydrothermal activity. The schists occur both in the f/w and in the h/w of the ore zone at Ongombo.

The selected sections represent four different modes of magnetite occurrence, namely:

a) apparently not related to hydrothermal alteration, i.e. distant from the ore zone or in the f/w of the same (OG 688);

b) in the relative vicinity of (sulphide-magnetite-bearing) quartz veins but not proximal to the ore zone (OG 689A, 690);

c) in the h/w of the ore zone, within a maximum distance of 50-60 m from the ore zone itself, and spatially related to thin to coarse mafic units (OG 692A-B, 697 and 699);

d) in the immediate vicinity of the ore zone (within a few m in the h/w) although close to mafic units (sections from core OGB 153A).

Schist types containing disseminated magnetite are represented by both quartz- and mica-rich facies. The euhedral magnetite crystals or aggregates mostly cross-cut the foliation, and only locally (OG 688) deform the surrounding micaceous laminae during growth. The grain size of the crystals varies from less than 1 mm to 1.5 mm. Magnetite is coarser in the occurrences c) and d).

Fine-grained massive quartz-biotite schists seem to be more frequently carriers of disseminated magnetite away from the ore zone or from the mafic rocks. In these schists magnetite occurs in modes a) and b) described above. No remarkable mineralogical change distinguishes the schists of these sections from those devoid of magnetite (see section 2.1.1 above). The only distinguishing feature is the moderately poikiloblastic nature of some magnetite grains in the schists intersected by quartz veins, and the partial chloritization of biotite (in OG 690). The former indicates progressive grain growth, while the latter might merely be related to retrograde metamorphism.

Disseminations of magnetite in proximity to mafic units (occurrence c)) generally occur in both chlorite-rich metapsammitic and metapelitic schist facies (OG 682B, 697, 699), and together with sieve-textured actinolite porphyroblasts. The latter are frequently conformable with the foliation and possibly indicate the proximity of mafic units (OG 682A-B). Minute sulphide blebs are disseminated.

In parts of the h/w schists above the ore zone (core OGB 153A) (occurrence d), magnetite can be fairly abundant, and it occurs as isolated or clustered grains in moderately chloritized quartz-biotite schists.

2.1.3 Mafic rocks and their relationship to the enclosing schists

Metalavas (MAB 261, 264, OTJ 682 and OG 135) are characterized by a fine to very fine-grained and finely foliated fabric. A fine-grained fibrous aggregate of acicular, pale-green to bluish actinolite with nematoblastic texture is intergrown, or alternates, with minor granoblastic, fine-grained plagioclase-quartz lenticular aggregates. The zoned plagioclase grains are oligoclase in composition. Chlorite is either not present or, if so, only in minimal quantities as remnant flakes. Prismatic to tabular, fine- to coarse-grained clinozoisite/epidote is a common constituent. It occurs as regular disseminations in the amphibole-rich groundmass; as coarse-grained knot-like aggregates; in crosscutting contorted and boudinaged monomineralic veinlets (MAB 261). Apatite is a common and rather abundant accessory, together with sphene. Rutile is the Ti-bearing phase in OTJ 682.

The foliation is commonly planar. Wavy foliation wraps around epidote knots (MAB 261) and particularly around lensoidal, stretched nodules consisting of coarse quartz, epidote and amphibole. Such centimetre-scale nodular features, observed in OTJ 682, occur in the Otjihase metalava horizon, where structures interpreted as deformed pillows are found. The nodules are characterized by a pronounced grain size increase, by increase in the quartz content, by the chaotic arrangement of the few amphiboles and by dissemination of sulphide blebs.

The mineralogy of the examined metagabbroic horizons from Ongombo is only slightly different from that observed in the metalavas outcropping SW of Ongombo.

The main components are hornblende and plagioclase (andesine), with minor quartz, biotite, chlorite, apatite and epidote. The colour and shape of the hornblende crystals suggest that this mineral might be intermediate towards an actinolite composition. The minerals are arranged in medium-grained grano-nematoblastic aggregates which have undergone intense shearing. Tabular ilmenite, sulphide blebs and locally abundant magnetite (OG 700) are disseminated in the groundmass. The characteristic spotted, augen-like appearance of this rock type is imparted by the flattened granular plagioclase aggregates. Plagioclase grains are poikiloblastic, zoned and rarely twinned.

The mineral assemblage observed in the metamorphosed mafic rocks of the Matchless Member in the areas of study compares well with that marking the greenschist-amphibolite metamorphic facies boundary (Moody et al., 1983). This boundary is characterized by:

a) the growth of low-Al, -Ti and -Na amphibole (actinolite or actinolitic hornblende) coupled with a decrease in the amount of chlorite present as main constituent in the greenschist assemblage;

b) change in the plagioclase composition from albite- to anorthite-richer;

c) breakdown of sphene and formation of ilmenite;

d) changing composition of the coexisting ilmenite-magnetite-rutile assemblage with increasing temperature.

These changes are temperature- (Fig. 25) and f_{O2}-dependent. The pressure conditions attained during these changes are indicated by the occurrence of staurolite in the metapelites.

Although a single observation is not sufficient, the mineral assemblage in the Ongombo amphibolites seems to point to a slightly higher metamorphic grade than in the Ongeama and Matchless Mine area. This is, however, against the regional trend of increasing metamorphic grade towards the WSW, as reported by Miller (1983) for the Damara

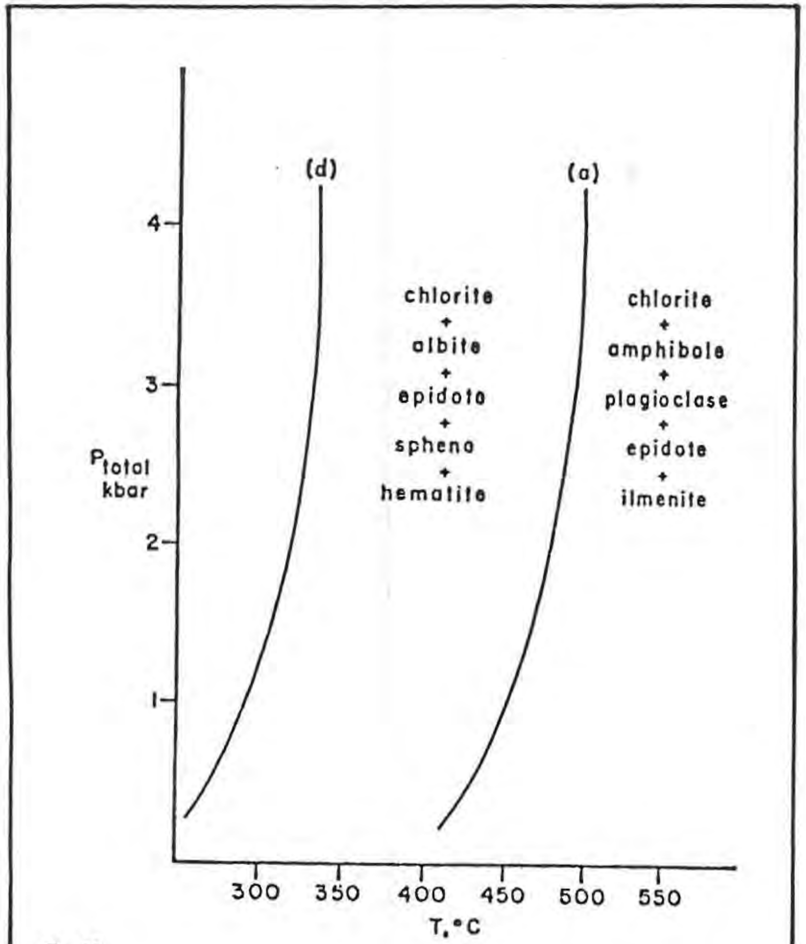

Fig. 25

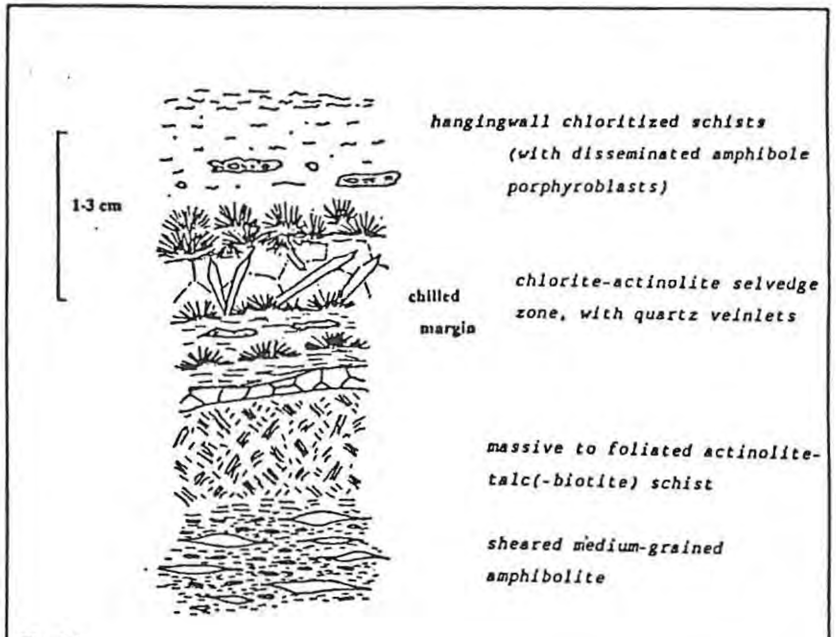

Fig. 26

Fig. 25 - Metamorphic mineral assemblages, as functions of total fluid pressure and temperature, in greenstones at the transition greenschist-amphibolite grade. Curve (a) marks the chlorite-decreasing amphibole-increasing boundary and sphene-out boundary; curve (d) marks the epidote-in boundary (modified after Moody et al., 1983).

Fig. 26 - Sketch illustrating the mineralogical zonation in the hangingwall margins of the amphibolite units in the drillcores from Ongombo.

Orogen.

The h/w margins of the meta-sills (OG 695, 712) consist of coarse, foliated to massive, talc- and carbonate-bearing actinolite schists. Abundant talc fibres, biotite and/or chlorite plates and very little quartz are interstitial to the actinolite-rich groundmass. Carbonate (calcite?) is in finely granular aggregates, locally replacing amphiboles along the cleavage planes. Disseminated, medium-grained rutile is common.

A rapid increase in the mica content and a concomitant decrease of the amphibole mark the transition to the chilled margin of the sill. This chilled margin is characterized by foliated, compact fibro-lamellar aggregates of coarse-grained chlorite and/or biotite with very subordinate interstitial quartz. Biotite often overgrows chlorite. Rutile, isolated or in clusters, and apatite can be unusually abundant. Coalescing coarse chlorite in radiating and fan-like aggregates, accompanied by euhedral actinolite porphyroblasts, give way to a well developed chlorite-actinolite selvedge zone along the margin of the sill. Elongated prismatic actinolite crystals freely grow within quartz veins, parallel to the chloritic sill margin (OG 694, 695). Fig. 26 illustrates the mineralogical and textural changes from amphibolite across the ultramafic layer to the chilled margin and the schists at the contact. The presence of coarse-grained chlorite and the growth of the chlorite "fans" suggest activity of aqueous fluid as a result of the interaction between wet sediments and the intrusive mafic sill.

The schists at the contact with the mafic units (OG 692A-B, 694, 696, 697, 698 and 699) record several mineralogical changes:

a) a general decrease in biotite, an increase in the abundance of chlorite and an increase in its grain size. This might mean an original chloritization of the sediments, preserved during metamorphism. This feature is evident in OG 692A-B and 694;

b) dissemination of sulphides, as fine- to medium-grained anhedral blebs and flattened aggregates, and medium-grained euhedral magnetite (OG 692A-B, 697, 699);

c) increase of abundance and grain size of apatite and, locally, of rutile (OG 694 and 695);

d) coarsening of the quartzose groundmass;

e) local dissemination of pale green actinolite porphyroblasts parallel to the foliation (OG 682A-B).

Poikiloblastic, often epidote-rich green-blue hornblende porphyroblast enrichment, occurs in the quartzitic schists at the contact with mafic units (OG 689A-B). Because of their similarity to calc-silicate lenses far from mafic units, these may not be related to the effect of the mafic sill intrusion. They probably represent a calc-silicate metapsammitic facies.

3 PETROLOGY OF THE MINERALIZATION AND ASSOCIATED ALTERATION

Because of the lack of unweathered samples, microscopic studies of the ore zone at Ongeama were limited to a qualitative evaluation of the gossan textures by means of thin and polished sections.

In Matchless West Extension attention is focussed on aspects of the alteration zone and of the well developed magnetite quartzite and talc-actinolite-carbonate facies. The latter are mineralogically compared with samples of Damaran serpentinites.

The nature and texture of the Ongombo "ore zone" and enclosing schists will be considered in this Section; in this case, the term "ore zone " is the name given to the sulphide-bearing portion of the sequence, inclusive of the alteration zone.

3.1 The Ongeama sulphide deposit

3.1.1 The gossan

The petrology of the three main facies recognized in the gossan exposure at Ongeama (i.e. massive sulphide gossan, amphibole-rich semimassive gossan and magnetite quartzite) and of the ferruginous schist pockets associated with the amphibole-rich gossan facies, is discussed in this Section.

The strongly leached character of the surface gossan is such that no residual sulphide grain is preserved within the existing boxwork structures. Therefore, replica textures, when not obliterated by massive or concretionary exotic limonite, have been tentatively interpreted according to the criteria established by Blanchard (1966) and Blaine and Andrew (1977), and with the aid of Hoffmann's description of the mineralization in cores (see also Sect. 2.2.1 Part B).

Limonite is the main constituent of the porous massive sulphide gossan facies (OG 15, 38 and 47A-B). Quartz occurs as recrystallized, coarse- to medium-grained aggregates, probably representing the groundmass of the mineralization. Muscovite, fibrous amphibole (anthophyllite) and fragmentary garnet occur as occasional accessories, isolated in limonite crusts. A faint banding is only recognizable in OG 15, where few mm-wide porous limonite bands irregularly grade to limonite-impregnated quartz-rich layers. When present (OG 47A-B), the tiny fibrous anthophyllite aggregates occur within the quartz groundmass or along the boundaries between the former and the limonitic spongy patches.

Different Fe-hydroxide species are distinguished by their different colour and reflectivity in thin and polished sections, respectively. The term "limonite" is here used as a general name for Fe-hydroxides.

In thin section, dark brown-blackish limonite corresponds to the "autochtonous" product of weathering of the sulphides, whereas the reddish limonite clearly shows its exotic nature. Brown limonite constitutes areas of preserved boxwork textures and compact, rounded remnants of clustered sulphide grains. Limonite pseudomorphs after sulphides are surrounded by exotic concretionary limonite. These limonite crusts also coat fractures and form large colloform patches in which every previous structure is obliterated.

The brown limonite-bearing portions are dominated by a thin- to thick-walled sponge-like texture containing recognizable sulphide replicas. Thin-walled limonitic "sponges" consist of medium-grained round to elongate cells reflecting the granular nature of the recrystallized ore. Progressive thickening of the cell walls frequently occurs by precipitation of brown and of late reddish limonite. Square boxwork replaces pyrite grains (Plate 5). Within the thin-walled cellular portions the fine-grained limonite crusts which often coat the inner walls of the cells, suggest pyrrhotite-derived textures (see Blanchard, 1966). By contrast, smooth-walled cells are more indicative of pyrite. Limonite boxwork faithfully mimics concentric shrinkage cracks, typical of bird's eye weathering of pyrrhotite in OG 38 and 47B (Plate 6). In these sections delicate ladder-like patterns consisting of thicker longitudinal walls and thinner transversal septa, which might be chalcopyrite replicas, can be seen (Plate 5).

The amphibole-bearing semimassive gossan facies(in OG 63) is a porous rock type deficient in quartz. Anthophyllite and limonite are the only constituents. Anthophyllite occurs in densely clustered rosettes and variably oriented fibrous aggregates, which give way to a network-like pattern. The amphibole aggregates are impregnated with reddish limonite along cleavage and transverse cracks (Plate 7 and 8). In places where the amphiboles were dissolved during weathering, a delicate and elongate ladder-like boxwork similar to that after chalcopyrite, and a cellular texture with minute rhombic cells are observed. Round blackish limonite patches probably replace original sulphides. Occasional cubic cells are possibly after pyrite. As in the massive gossan, cells coated with limonite crusts probably replace pyrrhotite grains.

In the magnetite quartzite (OG 17, 19A-B), the recrystallized granular quartz groundmass contains patches and lenticular aggregates of fine-grained euhedral magnetite which form a discontinuous banding at the scale of the thin section. Gossanous sulphide patches and limonitized anthophyllite aggregates are contained in the groundmass. Coarse actinolite is occasionally present in the anthophyllite aggregates. Magnetite grains are mostly unweathered, but are sometimes surrounded by crusts of exotic limonite. Cellular gossan is probably indicative of pyrite.

The ferruginous schist (OG 64A-B) associated with the semimassive amphibole-rich gossan facies is composed of yellowish mica, magnetite and limonite. The strongly schistose fabric is caused by the dominant lamellar, lepidoblastic micaceous groundmass, which shows evidence of folding. Where the limonite staining is minimal, the mica lamellae are slightly but distinctly pleochroic from pale yellowish to pale brown, and their interference colors are similar to that of biotite. Although the identity of this mica cannot be clearly established under the microscope, it does resemble phlogopite mica. Magnetite occurs as abundant medium to coarse-grained crystals, either isolated or more often in clusters, which seem to replace the micaceous groundmass. An unknown mineral occurs in places. This mineral is fractured. It forms roughly round grains, including few mica flakes, and is strictly associated with magnetite clusters. Black limonite films penetrate its fractures. The optical properties of this mineral, i.e. high relief, transparent color with greenish tinge, isotropy, might be indicative of a garnet or a spinel. In places a faint double set of almost perpendicular cleavage suggests a spinel: either the Mg-Fe-bearing pleonaste or the Zn-bearing gahnite (Plate 9).

3.1.2 The hangingwall schists

In this section the petrology of the unusual schists in the h/w of the Ongeama sulphide body is described from the central part of the outcrop towards the margins.

The chloritic schists in the axial portion of the discordant pipe-like feature described in Section 2.2.3 (OG 77A-B-C), show a markedly foliated fabric and a distinctive porphyroblastic texture. The mineral assemblage includes quartz, chlorite, garnet, chloritoid, staurolite, magnetite and limonite. Quartz and chlorite form the schistose groundmass. The groundmass shows two foliations: one is planar to crenulated S_2 and the other is a tightly folded S_1.

Both prismatic staurolite and tabular pale blue-violet chloritoid occur as coarse skeletal porphyroblasts. They locally display characteristic penetration and polysynthetic twinning, respectively. They are often associated with chlorite and carry disseminations of tiny sulphide blebs. The growth of staurolite seems to occur at the expense of chloritoid. Lamellar chlorite aggregates appear to form a reaction rim between staurolite and chloritoid. They are considered as a localized and incipient retrograde metamorphic breakdown of chloritoid. Chloritoid is also found in contact with both garnet and staurolite (Plate 10) or overgrown by garnet alone. Garnet (almandine) occurs as coarse, partially limonitized skeletal porphyroblasts, whose S_2-synkinematic growth is indicated by the helicitic spiralled texture (Plate 11).

Magnetite occurs as porphyroblastic aggregates of coarse subhedral grains. The generation of magnetite may be ascribed to the reaction (Deer et al., 1982):

$$\{\text{chloritoid} + \text{qtz} + O_2\} = \{\text{staur} + \text{almand} + \text{magnetite} + H_2O\}$$

Fig. 27 illustrates the relationships between staurolite and chloritoid at the transition between upper greenschist and lower amphibolite facies metamorphism in moderate to high pressure conditions.

The reaction

$$\{\text{Al-silicate (pyrophyllite or kaolinite)} + \text{Fe-rich chlorite}\} = \{\text{chloritoid} + \text{qtz}\}$$

is considered responsible for the first appearance of chloritoid in metapelites under conditions approximating the greenschist facies (Winkler, 1979). Chloritoid is also formed through the reaction

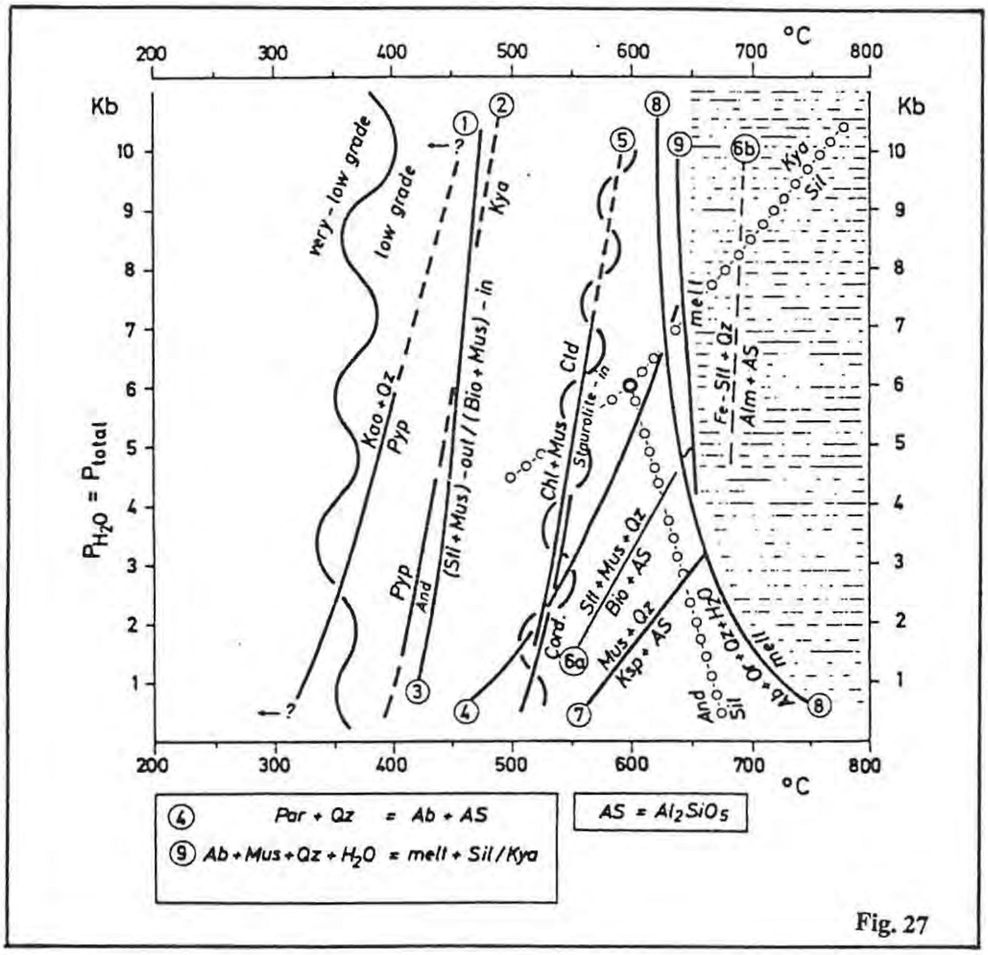

Fig. 27 - Metamorphic reactions in pelitic rocks as function of total pressure and temperature (Winkler, 1979). Note: curve (5) marks the chloritoid-out-staurolite-in boundary.

{Fe-oxide + Fe-rich chlorite} = {chloritoid + magnetite + quartz},

which might also be responsible for an initial nucleation of magnetite. Chloritoid formation has also been related to zones of shearing stress (Deer et al., 1982).

The rusty, spotted magnetite-muscovite schist (OG 62) occurs as a sheath to the axial chlorite zone. This schist (Plate 12) consists of abundant quartz, muscovite, magnetite, staurolite, garnet and minor chlorite. The rusty appearance is due to limonite derived from weathering of disseminated sulphides. Garnet is limonitized along cracks. Muscovite laminae define the planar to wavy S_2 foliation, where syn-kinematic skeletal staurolite and flattened garnet are grown. Magnetite porphyroblasts crosscut the foliation. Chlorite is present in some weathered lamellae isolated in the quartzose groundmass or interleaved with muscovite.

The transition from the chloritic axial zone to the muscovite sheath, as described in Sect. 2.2.3 Part B, is more obvious in the field. Nevertheless, on the scale of the thin section (OG 78) it can be noticed as an increase of the chlorite content within the muscovite laminae.

The non-magnetic ferruginous schists in the peripheral portion of the muscovite zone are strongly gossanous and show a very simple mineralogy. They consist of a grano-lepidoblastic aggregate of quartz and muscovite with disseminated, weathered sulphide blebs, and accessory tourmaline. Dark brown limonite replaces sulphides and impregnates the groundmass, whereas reddish limonite concretions encrust fractures and cavities.

3.2 The Matchless West Extension sulphide body

The petrological study of the Matchless West Extension was mainly focussed on the alteration and exhalite lithologies. Only one thin section of gossan material was examined.

3.2.1 Gossan and alteration zone

Section MWE 207 represents a talc-rich facies of the porous massive gossan outcropping just above the alteration pipe. Talc occurs in a band within the thin section. It occurs as fibrous-flaky aggregates and coarse bent lamellae, which grow on a coarse, irregularly granular quartzose groundmass (Plate 13). Brown limonite impregnates the talc and quartz aggregates, and forms coarse, irregular thick-walled sponge-like and massive patches, where boxwork structures are no longer preserved. An unknown secondary mineral occurs as concretionary and botryoidal crusts. It is colourless, with moderate relief and isotropic.

The marginal facies of the alteration pipe is characterized by a finely foliated muscovite-chlorite schist (MWE 204). Muscovite and chlorite occur as parallel lamellar bands, locally associated with phlogopite lamellae. Coarse muscovite plates locally replace chlorite aggregates, and they may belong to a second generation of muscovite. Tiny sulphide blebs and prismatic rutile are present as disseminations.

The mineralogy of the axial part of the alteration pipe is fairly simple. It consists of variable proportions of quartz, muscovite, limonitized pyrite and accessory tourmaline (MWE 205, 217, 219) (Photo 14). Pyrite is disseminated as tiny cubic weathered crystals in the schistose grano-lepidoblastic quartz and muscovite groundmass. Limonite impregnates quartz and mica as thin films and curiously also as very dense disseminations of black and red spherulites (MWE 205).

The foliation is planar to crenulated. Complex kink-banding in the micas is visible in some sections, where the quartzose laminae also show evidence of strain. A new foliation, well displayed in hand specimens, is formed by recrystallization of mica plates along a cleavage plane inclined approximately 30^{o} relative to the old foliation.

3.2.2 Exhalites

The exhalites at Matchless West Extension include at least two rock types: magnetite quartzite and ultramafic schists. In the field the two rock types appear to grade into one another. Two samples were examined from this transition zone.

Sections of MWE 241A-B and MWE 253 represent the two different magnetite quartzite layers characterizing the western portion of the outcrop (see Sect. 3 Part B).

The upper magnetite quartzite band (Plate 15) is massive, well banded and non-gossanous. It contains exclusively quartz, magnetite and baryte. Euhedral fine- to medium-grained magnetite is densely clustered in bands in the recrystallized quartz matrix. Medium- to fine-grained, round to amoeboidal baryte grains occur both as interstitial material in the quartz groundmass and as inclusions in quartz grains.

The gossanous, lower magnetite quartzite band (Plate 16) is characterized by a remarkable increase in magnetite, that almost obliterates the banding. Quartz, magnetite and baryte are accompanied by actinolite and subordinate limonite and malachite. Actinolite is in coarse-grained poikiloblastic prismatic porphyroblasts containing inclusions of quartz and magnetite.They are grouped in lenses parallel to the banding. Baryte blebs, irregular patches of weathered sulphides and encrusting emerald-green malachite aggregates are commonly associated with the actinolite-rich bands.

The ultramafic schists display the following fabrics:

a) strongly foliated, especially in some talc-rich facies, as in MWE 246B, and in the actinolite schist in MWE 245B;

b) massive, as in the monomineralic actinolitite in MWE 239 or in the talc-phlogopite schist in MWE 246A (Plates 17 and 18);

c) porphyroblastic, particularly where carbonate porphyroblasts occur, as in MWE 245A.

The foliated actinolite schists (MWE 245B) are essentially monomineralic, being composed of a medium- to coarse-grained nematoblastic actinolite aggregate. Phlogopite and interstitial talc and quartz are rare.

The massive "actinolitite" is outstanding for its coarse grain size. The interstices of this amphibole-rich, felted aggregate are occupied by fine-grained granular yellow-greenish patches of an unknown secondary mineral, limonite and rare quartz grains.

The massive fibrous talc schist in MWE 246A consists of an irregular talc-phlogopite aggregate developing on a granular quartz-rich matrix (Plates 17 and 18). Totally limonitized, post-tectonic carbonate porphyroblasts overprint the talc-phlogopite-quartz groundmass.

Sections MWE 236 and MWE 245A illustrate the transition from "ultramafic" to quartzite exhalite facies. In MWE 236 the nematoblastic actinolite schist interfingers with a baryte-bearing quartzitic facies (Plate 19). The coarse baryte grains are intergrown with quartz and are in normal contact with the actinolite crystals. No evidence of disequilibrium between the two minerals is observed. In MWE 245A a foliated talc-actinolite-carbonate schist passes to a gossanous quartz-actinolite-baryte-rich facies. The transition occurs by means of rapid decrease in talc and concurrent increase in amphiboles and quartz. The quartz-actinolite-baryte facies is distinctly banded and shows a grano-nematoblastic texture. The coarse-grained actinolite bands are gossanous and are associated with abundant coarse-grained baryte aggregates (Plate 20).

The carbonate-rich rock, initially identified as a marble associated with the exhalative layer (see section 3, Part B), may in fact not be part of it. The marble-like rock type outcropping at the grid reference 17/+3.5 (Fig. 21) is interpreted as the result of a hydrothermal pervasive carbonatic alteration replacing a baryte-bearing quartzite facies. From field observations, the replaced muscovite-bearing quartzite facies is probably part of the nearby outcropping magnetite quartzite. Calcite forms a granular aggregate, whose irregular texture is not comparable with that characterizing true marbles (Spry, 1969; Bard, 1980). There is no sign of deformation in the carbonates. Where the replacement is incipient, a sieve-like texture of the carbonate patches is noted. Amoeboidal baryte grains are associated with quartz in the groundmass. At advanced stages of replacement both baryte and quartz blebs are isolated in the carbonate groundmass.

3.2.3 Comparison between the ultramafic schists at Matchless West Extension and the Alpine-type Damaran ultramafic rocks

Thin sections cut from the ultramafic body outcropping near Otjihase Mine (see sect. 5.3 Part B) were also examined.

These rocks are represented by coarse-grained actinolite-chlorite schists (OTJ 684), talc-chlorite-actinolite schists (OTJ 685) and magnetite-bearing talc-chlorite-carbonate schists (OTJ 686A-B). The fabric varies from massive to coarsely foliated.

Mixed talc and chlorite form a fine-grained felt-like groundmass (Plate 22). This groundmass hosts isolated or clustered actinolite porphyroblasts and disseminated magnetite grains. Rhombic cavities are remainders of carbonate porphyroblasts. In the foliated actinolite schists in OTJ 684 euhedral actinolite porphyroblasts are included in a coarse, rutile-bearing fibro-lamellar chlorite matrix. Chlorite laths are grown both in parallel and in fan-like aggregates in the intergranular spaces. Comb-like texture of the chlorite aggregates is often seen between close actinolite crystals.

The mineralogy of these Damaran ultramafic rocks and that of the ultramafic schists of assumed exhalative origin are very similar in their main components (i.e., talc and actinolite). However, some differences can be observed, namely:

a) in the serpentinites quartz is basically absent, whereas it can be an important constituent in some of the exhalative schists examined (e.g., the quartz-rich groundmass in the talc-phlogopite schist in MWE 246A);

b) the unusual association of actinolite - quartz - baryte in the exhalative schists;

c) the absence of magnetite, a common product of serpentinization of igneous ultramafics, in the exhalative schists;

d) the layered distribution of the different facies of the ultramafic schists at Matchless West Extension (e.g., talc-rich, actinolite-rich) is probably a primary depositional feature;

e) the interfingering of the exhalative ultramafic schists with mineralized quartzite facies is observed even at the scale of the thin section.

The association of talc flakes with the quartz-rich massive gossan proximal to the alteration zone can be interpreted as an indication of the genetic link of talc, or premetamorphic Mg-rich precursors (sepiolite or palygorskite; McLeod and Stanton, 1984), with the ore-forming hydrothermal system. Actinolite is observed as a primary mineral associated with mineralization in the present-day Atlantis II Deep in the Red Sea (Zierenberg and Shanks, 1983, 1988). The mineral is considered as an indirect input of volcanism contemporary with the mineralizing event.

3.3 The Ongombo sulphide body

A detailed account of the "ore zone" and enclosing schists from drillcore is given below; only limited work has been carried out on gossan material.

3.3.1 The amphibole-rich facies of the Ongombo Gossan

Attention has been focussed on the portion of the outcrop characterized by the discordant gossanous amphibole-rich patches. These features were not observed in the cores (see Sect. 2.3.3 Part B).

In the gossan exposure, the magnetite quartzite proximal to the amphibole-rich patches (OG 192A) is pockmarked by weathered sulphide aggregates and by discontinuous amphibole-rich gossanous bands. These features are very similar to those observed at Ongeama. Flaky talc aggregates are disseminated both in the amphibole-rich patches and in the quartz matrix.

The discordant amphibole-rich pockets (OG 192B, 196, 281) are preserved only as fine-grained limonite replicas of the fibrous amphibole aggregates. By analogy with what was observed at Ongeama, it is believed that the amphibole in this facies was probably anthophyllite. Large massive black and colloform exotic limonite patches possibly correspond to weathered sulphides. Coarse poikilitic, prismatic plagioclase crystals form radiating aggregates within the gossanous portion in OG 281. They contain the acicular traces of dissolved amphibole inclusions. These plagioclase aggregates may be equivalent to the zones of plagioclase enrichment observed within the ore zone in the core OGB 153A (see below).

3.3.2 The "ore zone" and the enclosing schists in drill cores

A series of 40 thin sections has been obtained from the ore-hosting sequence in the OGB 153A borehole (Eastern Shoot). The total length of core portion examined is 12,5 m. A schematic log is reported in Appendix E.

The aims of this detailed examination are :

a) to verify the existence of an alteration-related mineral association in the h/w schists in approaching the "ore zone";

b) to discriminate between ore-related alteration, if any, and contact metasomatism in the schists enclosing the metasills;

c) to distinguish the different styles of mineralization within the "ore zone".

The h/w schist sequence consists of alternating metapelitic and metapsammitic schist units and includes a metamorphosed gabbroic sill. The main mineral constituents of the metasediments are quartz, plagioclase (oligoclase), biotite and chlorite. Accessory epidote, apatite, tabular ilmenite and subordinate disseminated sulphides are constantly present. Abundant zircon imparts a mottled appearance to the host biotite. The occurrence of muscovite, staurolite and garnet is restricted to mica-rich layers. Plagioclase can be fairly abundant and occurs either finely intergrown with quartz or in coarser flattened poikiloblastic lenses associated with the mica layers. Sieve-textured amphibole, epidote and minor calcite distinguish a calc-silicate-bearing layer.

The distribution of chlorite varies from one layer to the other, but considerable chlorite enrichment is observed towards the margins of the metamorphosed sill intrusion. Part of the chlorite appears to be a product of retrograde metamorphism.

Chlorite, however, is not commonly found in the plagioclase-rich schists between the "ore zone" and the mafic sill. These schists contain abundant biotite and muscovite, associated with staurolite and garnet. Tourmaline can be relatively common in the muscovite aggregates rimming staurolite grains.

There is no outstanding magnetite dissemination in approaching the "ore zone". Magnetite does occur, with disseminated sulphides, in the chloritized schists and "calc-silicates" in the structural h/w of the mafic unit (OG 710A-B) and in the vicinity of a thin amphibole-enriched layer of probable volcanic origin (OG 706).

A comparison between the h/w schists and unaltered schists away from the "ore zone" and those in the f/w, highlights the few differences between these three groups of schists. The only variations (e.g. chloritization, magnetite dissemination), of possible hydrothermal origin, are confined to the aureoles of the intrusive mafic units.

An important feature that distinguishes the schists within the "ore zone" from those of the h/w and f/w, is the colour of biotite. This biotite displays a marked colour change from dark greenish (Plate 23) to reddish-brown in the sharp contact from either h/w and f/w to the "ore zone", thereby defining a selvedge zone approximately 1 cm-thick (Plate 24). This reddish-brown biotite also constitutes a major component along the entire vertical development of the "ore zone" (sections OG 718-751). The only exception is represented by a minor intercalation of unaltered quartz-biotite schist (OG 731), containing dark brown-greenish biotite. This intercalation may result from tectonic interleaving.

Quartz, biotite, plagioclase (oligoclase) and staurolite are the most abundant silicate minerals within the "ore zone". Chlorite is scarce, and it becomes significant only in the lowest part of the "ore zone". Accessory fine- to coarse-grained apatite is present in remarkable amounts. Tabular ilmenite is disseminated along the schistosity planes.

The sharp contact from the unaltered schists to the "ore zone" is mineralogically defined by the development of the coarse biotite-rich selvedge zone, mentioned earlier. This selvedge zone is characterized by compact biotite bands with disseminated coarse- to fine-grained staurolite, coarse apatite and poikiloblastic flattened sulphide grains (pyrite "augen") (Plate 24).

The "ore zone" is approximately 6 m-thick. Below the biotite selvedge zone, the "ore zone" can be ideally subdivided in two sections, each defined by a magnetite quartzite band.

The first section, 1.5 m-thick, is characterized by coarse plagioclase-rich, staurolite-bearing biotite quartz schists. The schists contain densely disseminated sulphide-rich centimetre-sized quartz lenses. These lenses thicken downwards. Sulphides are only subordinately disseminated in the schists. Such arrangement is suggestive of a deformed stringer system passing to a zone of poorly developed semimassive mineralization. The first section ends with a 40 cm-thick magnetite quartzite layer, in which the mineralization is recrystallized in semimassive bands. Sulphides are partially remobilized along metamorphogenic quartz veins rimmed by coarse plagioclase and chlorite.

In the second portion of the "ore zone", up to 20 cm-thick chlorite-bearing quartzite layers contain well developed coarse semimassive sulphide mineralization. A second, poorly mineralized magnetite quartzite occurs at the structural f/w of the "ore zone" (OG 743, m 367.83-368.29). The semimassive-ore facies represents the main style of mineralization in this second section of the "ore zone". A remarkable feature of the second section is the increase in the plagioclase content within schist bands included between richly mineralized quartzite horizons (e.g., OG 732 and 735). In these schist layers deformed biotite aggregates are included in a coarse-grained poikiloblastic plagioclase groundmass (Plate 25). The plagioclase (oligoclase) is zoned, locally twinned and often sericitized. The abundance of plagioclase in these layers may be a primary feature. It may reflect the metamorphic recrystallization of original authigenic albite(?)-rich sedimentary layers. The plagioclase enrichment in the sediments might have been induced by the ore-related hydrothermal activity.

The transition from the lower magnetite quartzite horizon (OG 749) to the f/w schist package is marked by the occurrence of a moderately chloritized biotite selvedge zone carrying flattened sulphide lenses. An unusual pod-like, coarse-grained poikilitic plagioclase aggregate marks the lower contact of the "ore zone" (OG 752). It contains coarse to very coarse euhedral apatite crystals (up to 6 mm in diameter) rimmed by reddish biotite and muscovite laths. In the hand specimen the color of the apatite is pale green.

The passage to the dark brown biotite-bearing f/w schists is sharp.

3.3.3 The sulphide mineralization

The sulphide mineralization from core OGB 153A (Eastern Shoot) is characterized by the following styles, namely:

a) coarse disseminated sulphides in biotite schist (OG 720B, 744, 750);

b) semimassive ore in magnetite-devoid quartz-rich bands (OG 718, 722, 729, 733, 735, 737, 741);

c) disseminated in magnetite quartzite (OG 724, 747, 748);

d) partly remobilized ore along S_2-syntectonic quartz veins (OG 723, 726).

The ore assemblages characterizing these styles of mineralization are the following:

1) in biotite schists, dominant pyrite with subordinate chalcopyrite and pyrrhotite as sulphide species; ubiquitous ilmenite and occasional magnetite as oxide species;

2) in the semimassive ore, pyrite, chalcopyrite and pyrrhotite are the main components, with subordinate sphalerite. Only chalcopyrite, pyrrhotite and sphalerite occur in OG 729. Magnetite is accessory in OG 718 and 733. Galena is in minimal amounts in OG 718 and 741;

3) in magnetite quartzite, magnetite is accompanied by variable amounts of chalcopyrite and pyrite, subordinate pyrrhotite and accessory galena; sulphides are concentrated in bands;

4) in the remobilized ore, chalcopyrite, pyrite, pyrrhotite and minor

sphalerite are the sole components.

A characteristic of the pyrite in this mineralization is a slight but perceivable anisotropy. Two main generations of pyrite can be distinguished: the first generation is represented by early porphyroblasts deformed into "augen" (Plate 24) and by recrystallized aggregates; the later generation includes undeformed cubic porphyroblasts.

Magnetite, chalcopyrite, pyrrhotite and galena display the usual optical characters. Marmatitic sphalerite occurs as typical tiny star-shaped and drop-like exsolutions in chalcopyrite, whereas globular chalcopyrite blebs are exsolved in the rare coarser sphalerite patches. Star-shaped sphalerite exsolutions are typical of high-temperature chalcopyrite (Ramdohr, 1980). Their presence may be related to the high temperatures of recrystallization undergone by the sulphide mineralization during lower amphibolite facies metamorphism. Pyrrhotite is mostly associated with chalcopyrite, where it occurs as small amoeboidal blebs and anhedral fractured patches. Tabular ilmenite crystals display characteristic lamellar hematite exolutions. The crystals occur parallel to the S_2 foliation of the hosting schists and are locally clustered and recrystallized in the hinges of microfolds. Ilmenite locally contains elongated chalcopyrite inclusions incorporated during growth.

Pyrite and magnetite crystals commonly show inclusions of ore and gangue minerals: chalcopyrite, pyrrhotite and galena, and quartz, apatite and mica, respectively (Plate 26). Galena is only observed in inclusions, alone or associated with chalcopyrite (Plate 27).

Regional dynamo-thermal metamorphism, in the form of temperature increase and directed pressure, is responsible for an overall coarsening of the grain size, recrystallization and reorganization of the initial paragenesis through deformation. This is reflected in the general texture of the mineralized layers. These layers are, in fact, characterized by the development of coarse-grained idioblastic to flattened pyrite grains (Plate 26) and annealed aggregates (Plate 27) over a chalcopyrite- and pyrrhotite-rich recrystallized matrix (Plate

30). A similar texture is seen where magnetite is abundant, although magnetite does not show evidence of plastic deformation as pyrite does (see below).

The chalcopyrite-pyrrhotite matrix around the pyrite augen is intensely strained; this is clearly visible in the pyrrhotite, which shows a noticeable wavy extinction.

Experimental studies on sulphide deformation with increasing temperature and confining pressure (Kelly and Clark, 1975; Cox et al., 1981; McClay and Ellis, 1983) show (Fig. 28):

a) a change from brittle to moderately ductile rheological behavior in pyrite in metamorphic grades higher than greenschist facies and at low strain rates;

b) the overall greater ductility of chalcopyrite and sphalerite than pyrite in the different geological conditions;

c) the rapid strength loss of pyrrhotite with increasing temperature.

The formation of pyrite "augen" is thereby referred to a pressure solution strain mechanism active during D_2. The ductility contrast among sulphides results in the inclusion of harder pyrite grains in a matrix of softer ore minerals. The resulting texture does not reflect the original relationship among the components. Grain growth and annealing must have occurred between the D_2 and D_3 phases. A late, brittle deformation manifested in fractured pyrite porphyroblasts is referred to the D_3 deformation phase by Klemd et al. (1987). The open fractures in pyrite are filled by softer matrix material, i.e. pyrrhotite and chalcopyrite (Plate 28).

In the biotite schists, other possible effects of deformation on pyrite may also be seen in the recrystallization of fine-grained, thin pyrite lenses ("ribbon pyrite" in Klemd et al., 1987) arranged in *en-echelon* patterns within the deformed micaceous laminae. The ribbon pyrite develops along the borders of subhedral pyrite grains, on the side of the grains parallel to the foliation. These structures are

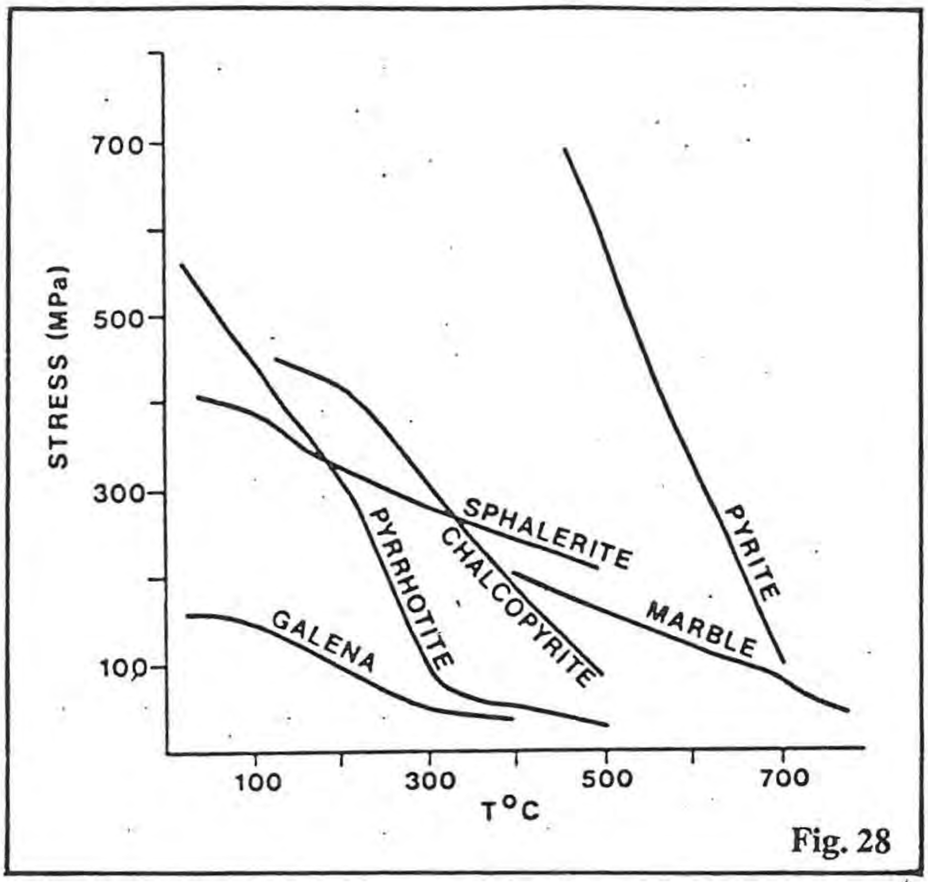

Fig. 28 - Comparison of strengths of pyrite, chalcopyrite, pyrrhotite, sphalerite and galena at a constant 1 kb confining pressure (Cox et al., 1981).

confined to limited portions of the schists, and probably indicate the action of slow plastic deformation (creep) induced by shear stress. Coarsely recrystallized pyrite and magnetite generally show a strong tendency to idiomorphism and to development of crystal faces. Where both pyrite and magnetite occur in remarkable amounts, as in the magnetite quartzite in OG 747, the contemporaneous recrystallization of the two minerals leads to the formation of interference textures, with mutual inclusion and development of atoll-like, embayed aggregates (Plate 26).

4. DISCUSSION

Petrological studies of country rocks and of the alteration zones have provided evidence of important mineralogical changes, which, at least in some cases, are confirmed by field observations. The scheme in Fig. 29 reports the main mineralogical characters observed in the alteration zones.

In spite of the postulated common genetic mechanism for these sulphide bodies (see Part A) and of the relatively short distance between them, the mineralogy of the alteration zones is variable. For example, at Ongeama the alteration pipe consists of a chlorite core and a sericitic envelope, whereas at Matchless West Extension the pipe consists of a quartz-sericitic core and a poorly developed chloritic margin (see also Sect. 3 Part B). Nevertheless, the chemical environment inferred from the alteration mineral assemblages is essentially similar. This appears to be especially true for Ongeama and Matchless West Extension, where the alteration pipes are better defined both in shape and relationship with the mineralization.

The occurrence of chloritoid, staurolite, garnet, magnetite and chlorite at Ongeama, and the dense pyrite dissemination in the sericitic quartzite at Matchless West Extension, reflect conditions of high Fe/Mg ratio, high Al and low alkali (Na, Ca and K) along the axis of the alteration pipe. Although devoid of plagioclase, both alteration zones are highly enriched in quartz, due to extensive

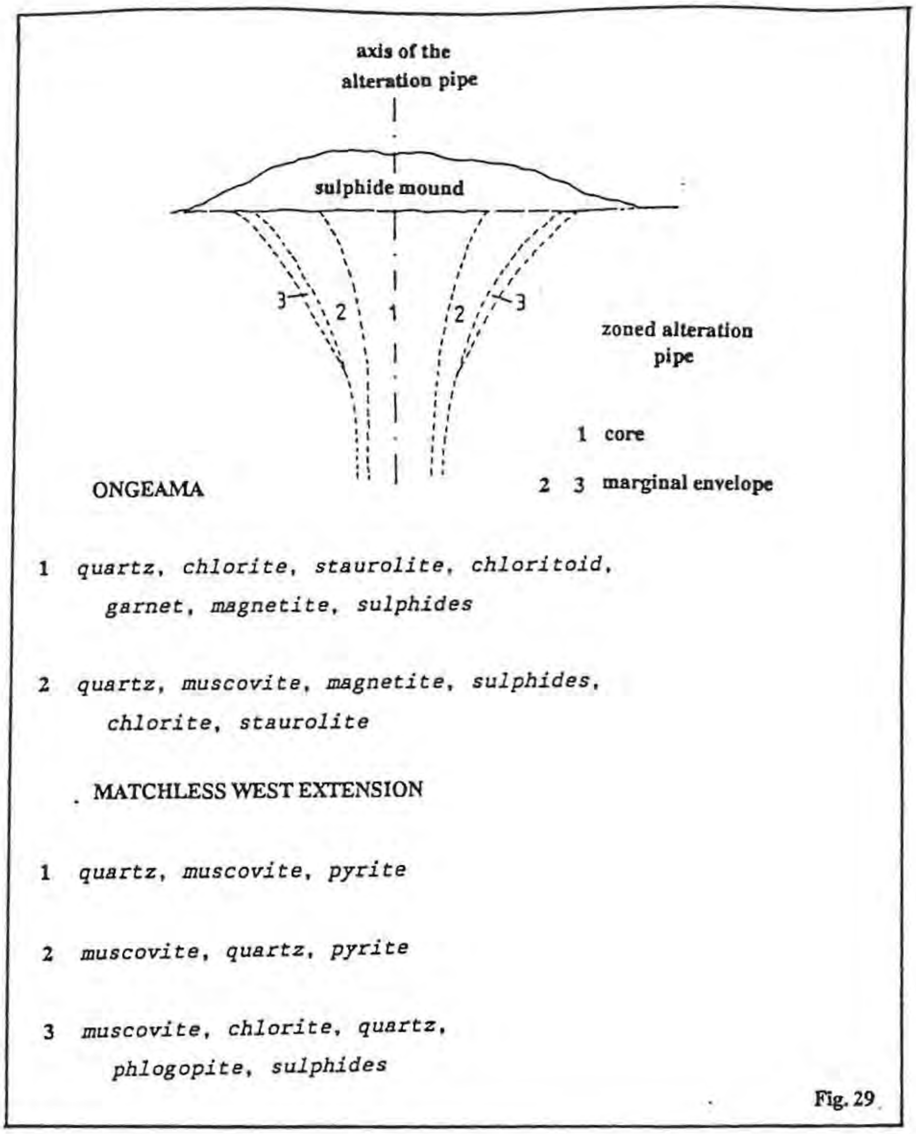

Fig. 29 - Scheme of the mineralogical zonation within the alteration zones at Ongeama and Matchless West Extension. The zonation is referred to a generalized scheme of zoned alteration pipe. The minerals are listed according to decreasing abundance.

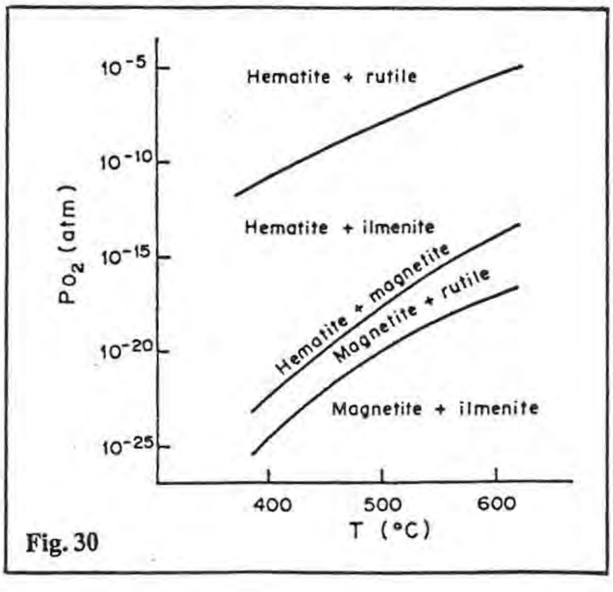

Fig. 30 - Theoretical stability fields for the systems Fe_3O_4-TiO_2-$FeTiO_3$-Fe_2O_3 as function of oxygen pressure and between 400° and 600°C (Stanton, 1972).

silicification.

At Matchless West Extension the marginal zone of phlogopite-bearing muscovite-chlorite schists may correspond to an overlap between the sericite zone and a marginal Mg-enriched zone. The occurrence of sporadic phlogopite may be also interpreted as marking a late and marginal domain of potassic alteration. According to Costa et al. (1983), this limited potassic alteration would be induced by late hydrolysis of mica in the outer regions of the mineralizing system, hence supply of K to the fluids, and breakdown of alteration-related chlorite.

The presence of anthophyllite and talc in the ore proximal to the assumed discharge vent at Ongeama and Matchless West Extension, respectively, is suggestive of major Mg enrichment external to the alteration pipe. Mg, however, is further enriched in the talc- and actinolite-bearing exhalites at Matchless West Extension. Mg enrichment in positions proximal to the discharge vent is reported for both ancient and present-day sub-seafloor deposits (e.g., Guaymas Basin) (Costa et al., 1983; Aggarwal and Nesbitt, 1984; Lonsdale et al., 1980). By analogy with what was observed at Ongeama and Matchless West Extension, the anthophyllite and talc enrichment of the gossanous central-western portion of the Central Shoot (Ongombo) could be considered as indicating proximity to a main discharge site. The absence of these minerals in the Eastern Shoot mineralization may be, on the other hand, interpreted as a "distal" feature.

Sulphide disseminations and lenses, which, on weathering, impart the gossanous aspect to the schists within the alteration pipes, may be interpreted as the result of deformation and metamorphism of a "stringer"-type mineralization. "Stringer" mineralization was formed within the fracture network, which acted as fluid channelways, along the alteration pipe.

In spite of the higher metamorphic grade, the mineralogy of the alteration zone at Gorob, as reported by Haussinger and Okrusch (1990) seems to reflect the same trends of major element variations as those inferred for Ongeama and Matchless West Extension.

At Ongombo, chloritization and magnetite and sulphide dissemination in the schists above the ore zone, although irregularly distributed, are spatially associated with the mafic sills. This suggests that the enrichment in chlorite, magnetite and sulphides is probably the result of contact metasomatism induced by the intrusion of basaltic sills into wet unconsolidated sediments, and not to ore deposition. It is, therefore, concluded that there are at least two separate events: one related to contact metasomatism and the other to the action of ore-forming fluids. This separation is reflected also by the trace-element distribution in the ore-hosting sequence (see Sect. 2.3.2 Part D).

Klemd et al. (1987, 1989) attribute similar chlorite- and magnetite-enriched schists in the h/w of the ore zone at Matchless Mine to the effects of an ore fluid system. Their interpretation, however, is possibly incorrect, if the observations above are taken into account.

Studies of the drill core from Ongombo suggest that the change in colour of biotite, among other factors, is considered a fundamental indicator of the interaction of the ore-bearing fluids and the schists. The abrupt colour change of biotite both in the h/w and f/w of the "ore zone", and the deformed nature of the "smeared" pyrite augen disseminations within the marginal biotite "selvedge zones", are suggestive of tectonic deformation. The strain would be largely concentrated along the margins of the sulphide-bearing horizon.

Assumed remnants of sheared f/w stringer zones are observed also in ancient deformed mineral deposits similar to those associated with the Matchless Belt (e.g., Hoy et al., 1984).

The mineralogical and textural features of the Ongombo ore zone indicate a fairly well defined vertical lithological zonation. The reconstruction of this vertical zonation, after eliminating the effects of deformation, is as follows:

a) h/w "stringer"-feeder zone;

b) siliceous ore zone containing semimassive sulphides in lenses and layers;

c) f/w sulphide-bearing magnetite quartzite.

The inverted polarity of the sequence given above is confirmed by the inverted zonation observed in the mafic sills, in which ultramafic differentiates occur in the h/w.

The gangue mineralogy of the Ongombo "ore zone" is somewhat different from that of Ongeama and Matchless West Extension. At Ongombo the gangue is characterized by the almost total lack of chlorite, abundance of zircon-bearing biotite and staurolite, less pronounced silicification, and unusual abundances of plagioclase and of apatite. Phosphorus enrichment is also reported by Haussinger and Okrusch (1990) at Gorob. The presence of plagioclase, however, does not appear to be restricted to the Eastern Shoot, as the mineral also occurs in the anthophyllite-rich zones of the western Central Shoot (see Sect. 3.3.1 above). It is worth noting that in studies of iron formations in the Southern Marginal Zone of the Damara Orogen, Breitkopf and Maiden (1986) and Breitkopf (1988) have found high abundances of apatite, plagioclase and amphibole. These authors consider these minerals as evidence for the volcano-exhalative origin of the mineralization.

Unusual mineralogical associations, similar to those described in this study for the "ore zone" at Ongombo, were also noted by Gair and Slack (1982), in relation to the Appalachian Besshi-type sulphide deposits of the Gossan Lead District (Blue Ridge Belt, Virginia, USA). The two authors report, in fact, the occurrence of almost monomineralic biotite schists, with high content of fluoro-apatite and zircons, and of plagioclase-rich rocks alternating with bands of massive mineralization. The origin of these rocks is attributed by the authors to the action of ore-related metasomatizing fluids.

At Ongombo, the absolute prevalence of biotite and staurolite over chlorite might be simply a result of metamorphic conditions. The abundance of highly degradable minerals within the "ore zone" is possibly the reason of the lack of surface expression of lithofacies other than the resistant magnetite quartzite.

It is clear from the petrological work carried out that mineralogical changes are important in the attempt to define an alteration zone. These changes can be discerned in spite of the obliterating effects of regional metamorphism and deformation.

Magnetite disseminations (e.g., in the "I" anomaly area north of the Ongeama gossan and in the Ongombo cores), unless associated with other important mineralogical changes in the host rocks, are not to be considered "a priori" as pathfinders to the mineralization.

During metamorphism, oxides can undergo pronounced chemical and less notable physical modifications. The latter occur by simple coarsening and crystal face development (Stanton, 1972). Chemical modifications during metamorphism largely depend on f_{O2} (Fig 30). Therefore, the occurrence of magnetite in barren metapsammitic horizons of the Kuiseb Formation can be interpreted as:

a) recrystallization of detrital magnetite grains;

b) metamorphism of moderately hematite-rich metapsammitic horizons.

Magnetite occurs as disseminations also in "calc-silicate" layers within the metapsammitic horizons. The "calc-silicate"-bearing metapsammites in the Kuiseb Formation appear to be correlated with the north-westerly calcareous Tinkas turbidites, developed from the Karibib carbonate platform (Porada and Wittig, 1983; see Sect. 1 Part A). In view of this possible connection between the metapsammites in the Kuiseb Formation and the Tinkas turbidites, the presence of magnetite disseminations in the former may be interpreted as the result of metamorphic breakdown of siderite (James, 1955), or may represent an indirect, detrital contribution of the mafic volcanism characterizing the the north-westerly Karibib platform (Miller, 1983b).

The preservation of alteration zones, well defined in shape and mineralogy, in spite of deformation and metamorphism, confirms Stanton's (1982) opinion that stratiform ores and their envelopes are striking examples of compositional inhomogeneity that metamorphism has not been able to homogenize. This appears to be the result of the restriction of metamorphic diffusion to minute distances and of the consequent lack of attainment of metamorphic equilibrium even in very small domains (e.g., single grain).

The alteration zones studied contain contrasting greenschist- and amphibolite-facies mineral assemblages (e.g., chlorite-staurolite at Ongeama), or display mineral associations of apparent slightly higher grade than the enclosing schists (e.g., the chlorite-poor biotite-staurolite schists in the "ore zone" at Ongombo). In Stanton's view, these restricted anomalies can be attributed to primary precursor patterns, depending on the interplay between hydrothermal fluids, seawater and sediments along the channelways, rather than to localized variations in metamorphic grade.

PART D

GEOCHEMISTRY OF MINERALIZATION, ALTERATION ZONES AND COUNTRY ROCKS

1. INTRODUCTION

The 487 samples collected during the field work were submitted to chemical analysis.

A suite of 22 elements was selected for analysis: Cu, Pb, Zn, Co, Ni, Ag, Au, Mn, Cr, V, Ti, Ba, Mo, Zr, Nb, Y, Rb, Sr, Sn, W, As and Bi. Concentrations of the first nine elements, from Cu to Cr, were determined by means of atomic absorption spectrometry (AAS), and the balance by X-ray fluorescence (XRF) analysis. These analyses were carried out at Scientific Services Ltd. in Windhoek and Cape Town. Results and detection limits are given in Appendix E, Tables 1 to 18. Selected samples of altered and unaltered schists and ultramafic rocks were analyzed for major elements by XRF analysis. Fusion discs and powder pellets were analyzed by means of a Philips 1410 XRF spectrometer at Rhodes University (Table 9). A number of selected elements was used to construct element distribution profiles, contour maps and diagrams.

Anomalous major- and trace-element distribution characterizes present-day hydrothermal mineralizing systems in the oceanic environment and well-studied ancient equivalents. Therefore, one of the aims of this study is to verify whether similar distribution patterns exist or are still preserved in the metamorphosed and deformed deposits at Ongeama, Matchless West Extension and Ongombo.

2 GEOCHEMISTRY OF SULPHIDE BODIES AND ASSOCIATED ALTERATION ZONES

2.1 Geochemical trends at Ongeama: trace element distribution

The geochemical data from the weathered mineralization and associated alteration zone at Ongeama (table 2, Appendix E) were used to construct element distribution profiles. In the evaluation of each profile, the average content of a given element in barren schists has been taken into account, and shown as a reference line.

Appendices F and G include the geochemical profiles along strike for the minor and major gossan band, respectively. The different rock types are indicated by symbols. Each rock type is characterized by a distinct range of element concentration. However, within the same rock type, variations can occur in space and can represent, in some cases, a well defined zonation.

The two gossan bands are considered separately because of their differences in lithological complexity and geochemical character.

The **minor gossan outcrop** consists of three rock types: massive gossan, magnetite quartzite and subordinate non-magnetic ferruginous muscovite schists (see Part B for details).

In general, the massive gossan in this outcrop appears to be relatively more enriched in Cu (up to 0.73 %), subordinately in Mn and Ba and Ti, and depleted in Pb, Zn, Ag, V, Rb, Sr, Zr, Sn and As.

Magnetite quartzite is enriched in Pb (up to 0.19 %) and, to a lesser extent, in Zn (up to 471 ppm), Mn (1164 ppm) and Sn (110 ppm). Although the massive gossan locally contains high Au values (on average 455 ppb Au), the average Au content in the magnetite quartzite is higher (698 ppb Au). Magnetite quartzite is slightly enriched in Ag relative to the other two rock types.

The ferruginous schists show the highest Ba (up to 503 ppm), Ti (up to 0.84 %), V (up to 224 ppm) and Zr (up to 148 ppm) contents, and moderate enrichment in Zn, Pb and Sn. They are depleted in the other elements.

Lateral variations of the most significant elements (i.e. Cu, Zn, Pb, Ag, Au, Ba and Mn) are observed. Detailed profiles for all the elements considered are contained in Appendix G-a. A general increase towards the western end of the outcrop is shown by most of the elements considered (Fig. 31a-e).

In particular:

- The Cu distribution outlines a clear zonation with westward increase within the massive gossan. This trend is not shown in the adjacent magnetite quartzite. The Cu increase in the massive gossan

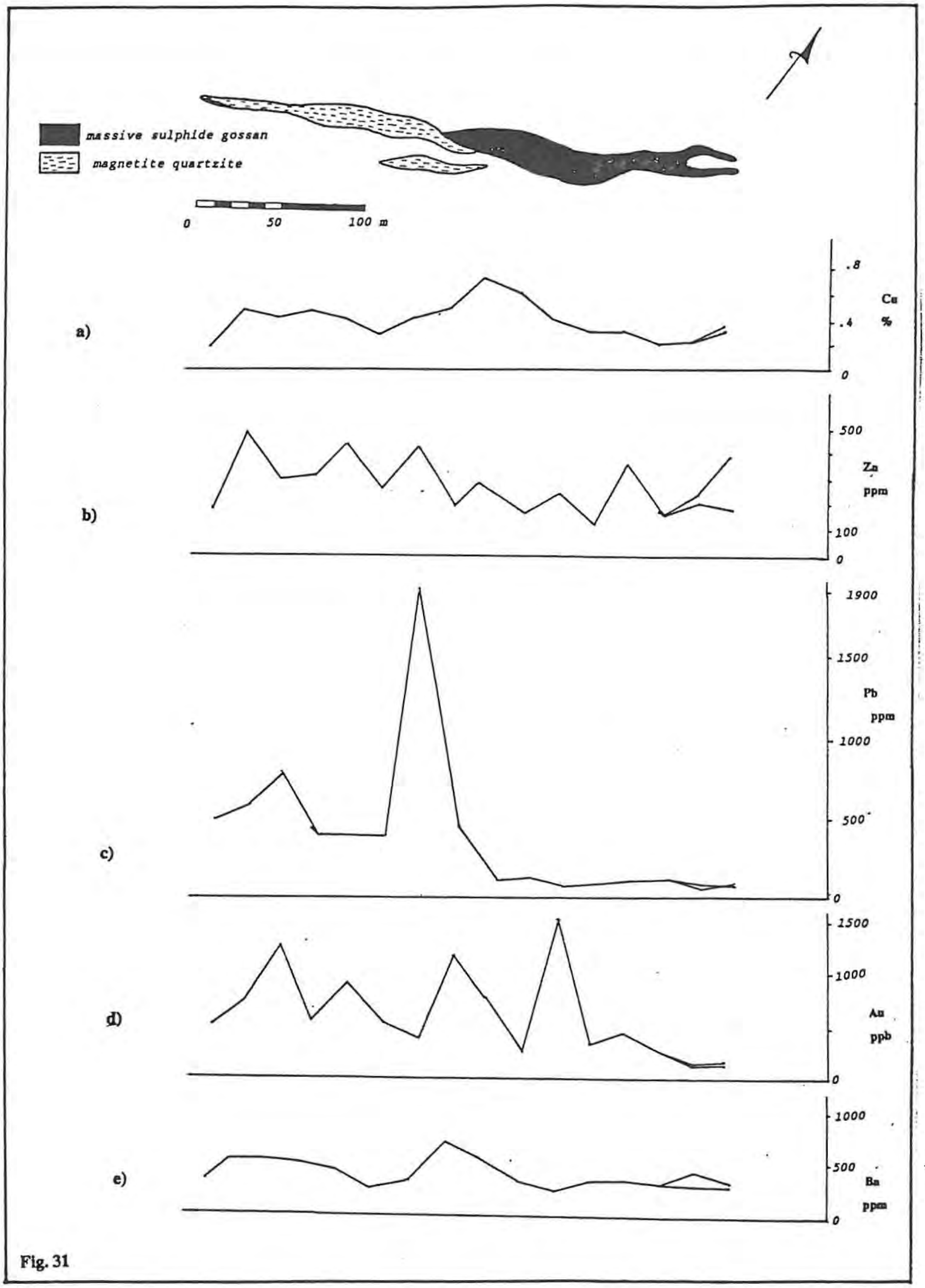

Fig. 31a-e - Ongeama Prospect, minor gossan outcrop: geochemical profiles for Cu, Zn, Pb, Au and Ba along strike.

outcrop correlates with its thickening. It may be either a primary feature or it may be related to deformation. However, a similar distribution for Ti, which is typically considered as an immobile element (Finlow-Bates and Stumpfl, 1981), would suggest that it is a primary feature.

- Zn displays a general increase westward, from massive gossan to magnetite quartzite, although within each facies the values are irregularly distributed.

- The Pb distribution shows a prominent, isolated peak (0.19 % Pb) next to the boundary between magnetite quartzite and massive gossan and proximal to the Cu-enriched portion of the outcrop. This isolated peak notwithstanding, a general westward increase is observed.

- Au exhibits a gross westward increase within the massive gossan. In the latter, Au enrichment appears to coincide with the thickening of this horizon. In the magnetite quartzite the average content is slightly higher (see above) but with no apparent regular distribution trend. In the massive gossan isolated peaks may correspond to late remobilization of mineralization in veins.

- Ba is clearly enriched in the centre of the massive gossan outcrop next to the boundary with magnetite quartzite. The Ba profiles for these two rock types are similar. Sr peaks (not shown in the figure) coincide with Ba highs.

It is worthy to note that, in general, the small massive gossan lens situated at the western end of the magnetite quartzite band displays the highest element concentrations (see profiles in Appendix F).

For the **major gossan outcrop** (profiles in Appendix G), the five rock types considered in this section are: siliceous gossan (MS), amphibole-rich semimassive gossan (AS), magnetite quartzite (MQ), non-magnetic ferruginous schists (FS), magnetic muscovite schists (MM) and magnetic chlorite schists (CS) (see section 2.2.2 Part B for details).

MS, AS and MQ ("ore zone") are enriched in Cu, Zn, Pb, Ag, Au, Mn and, subordinately, Ti and Sn relative to the "alteration" rocks (FS, MM and CS), which are enriched in Ba and, subordinately, in Sr, Rb, As, Zr, Ti, V, Ni and Cr.

In the major gossan outcrop, the most important feature is the increasing trend of some elements towards the centre of the sulphide body, i.e. towards the portion of the outcrop characterized by the AS facies (Fig. 32a-h) .

The main points of note are:

- The Cu distribution clearly reflects this trend of progressive centreward increase, with the highest value in the AS facies, close to the intersection with the assumed alteration pipe.

- The Au distribution is characterized by numerous, isolated peaks (up to 4870 ppb). The position of these peaks shows an apparent increase towards the periphery, and depletion in the central Cu-rich portion. However, this trend may be more apparent than real. It is reasoned that, if the lateral peaks are ignored, as they may be related to local remobilization, then a normal centreward increase is observed.

- Zn is highest in the MS portion surrounding the AS core, whereas a relatively flat profile characterizes the marginal portion of the outcrop.

- Mn shows a flat profile in the E, but peaks towards the centre: the major peaks correspond to the thickening of MS and to the occurrence of AS in that position. A similar pattern is shown in MQ. Overall higher Mn contents are recorded in the western portion of the MS outcrop.

- The Pb profile in the MS is relatively flat, with isolated peaks. A slight enrichment occurs in AS and persists towards W. The Pb concentration is highest in MQ. In this facies Pb shows a prominent enrichment next to the alteration pipe (up to 0.22 %).

- Ti shows a distribution pattern with an isolated peak in the AS facies with relative enrichment in MS towards the margins.

- the Ba and V distribution exhibits a limited enrichment within the AS facies.

- As is enriched in the central MS portion but it also shows an increase to the E both in MS and MQ facies. Sn (not shown in Fig. 32) exhibits a countinuous profile only in MQ.

In the profiles shown in Appendix G,elements which are preferentially concentrated in the "alteration" rock types (CS, MM, FS) (i.e. Ba, Sr, Zr, As, Rb, Ti, V, Ni and Cr) suggest a lateral zonation with increasing values from the periphery towards the axial zone. Zonation along the pipe is further illustrated in section 2.3 below).

The following trends are noteworthy:

- Ba is highly concentrated in the MM facies and progressively increases towards the chloritic pipe, in which the Ba distribution is more irregular (Fig. 32g). The affinity of Sr and Ba is reflected in their similar distribution trends.

- Zr is highest in the chloritic pipe and slightly depleted in MMS and FS towards the margins.

- As (Fig. 32h) and Bi are exclusively concentrated along the axial zone.

- the flat distribution profile for Ti (Fig. 32f): higher Ti contents occur in the eastern portion of the outcrop. In proximity to the pipe a decrease of the Ti content in MM and CS is coincident with the Ti peak in the AS facies.

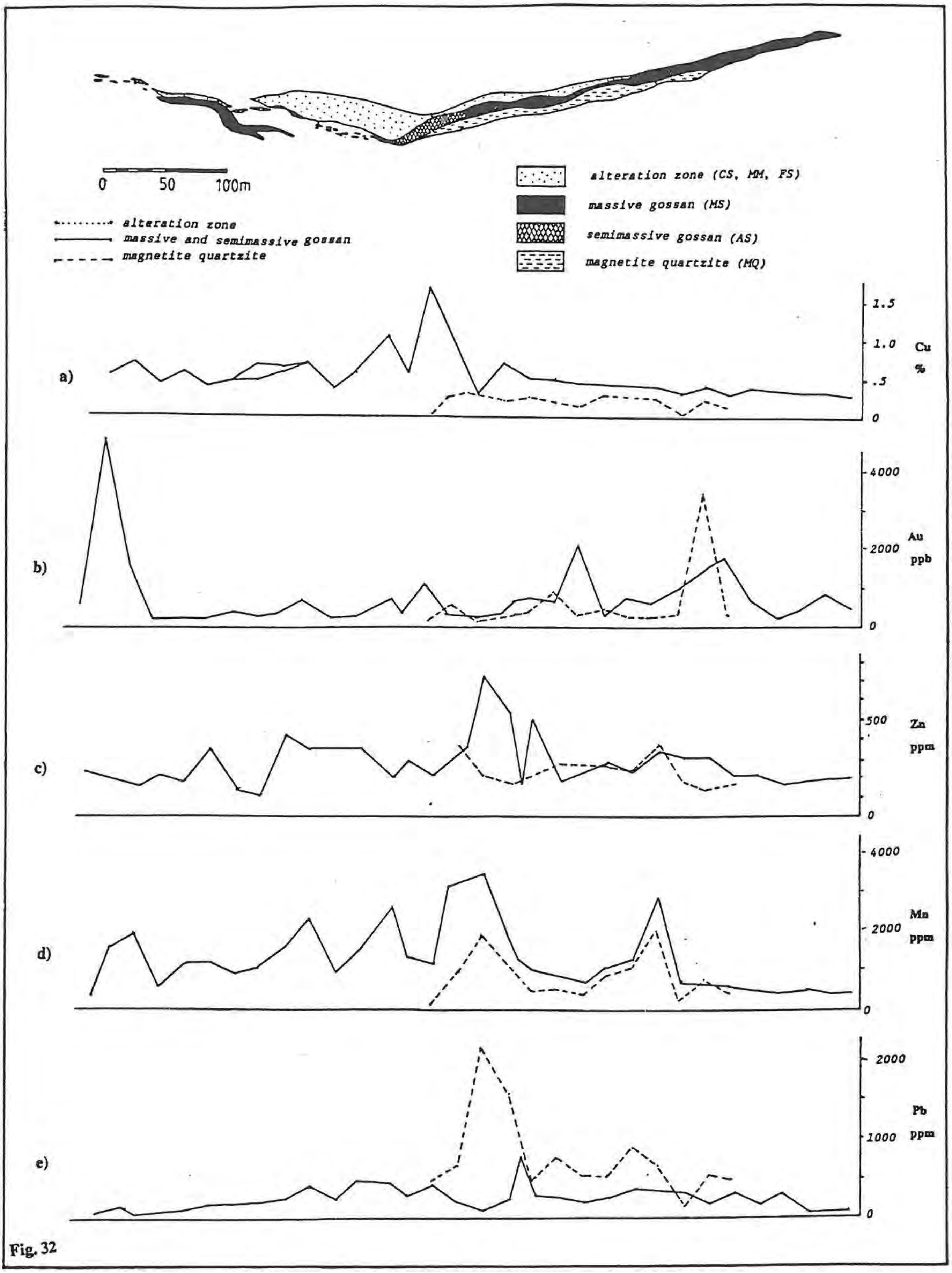

Fig. 32a-h - Ongeama Prospect, major gossan outcrop: geochemical profiles for Cu, Au, Zn, Mn, Pb, Ti, Ba and As along strike.

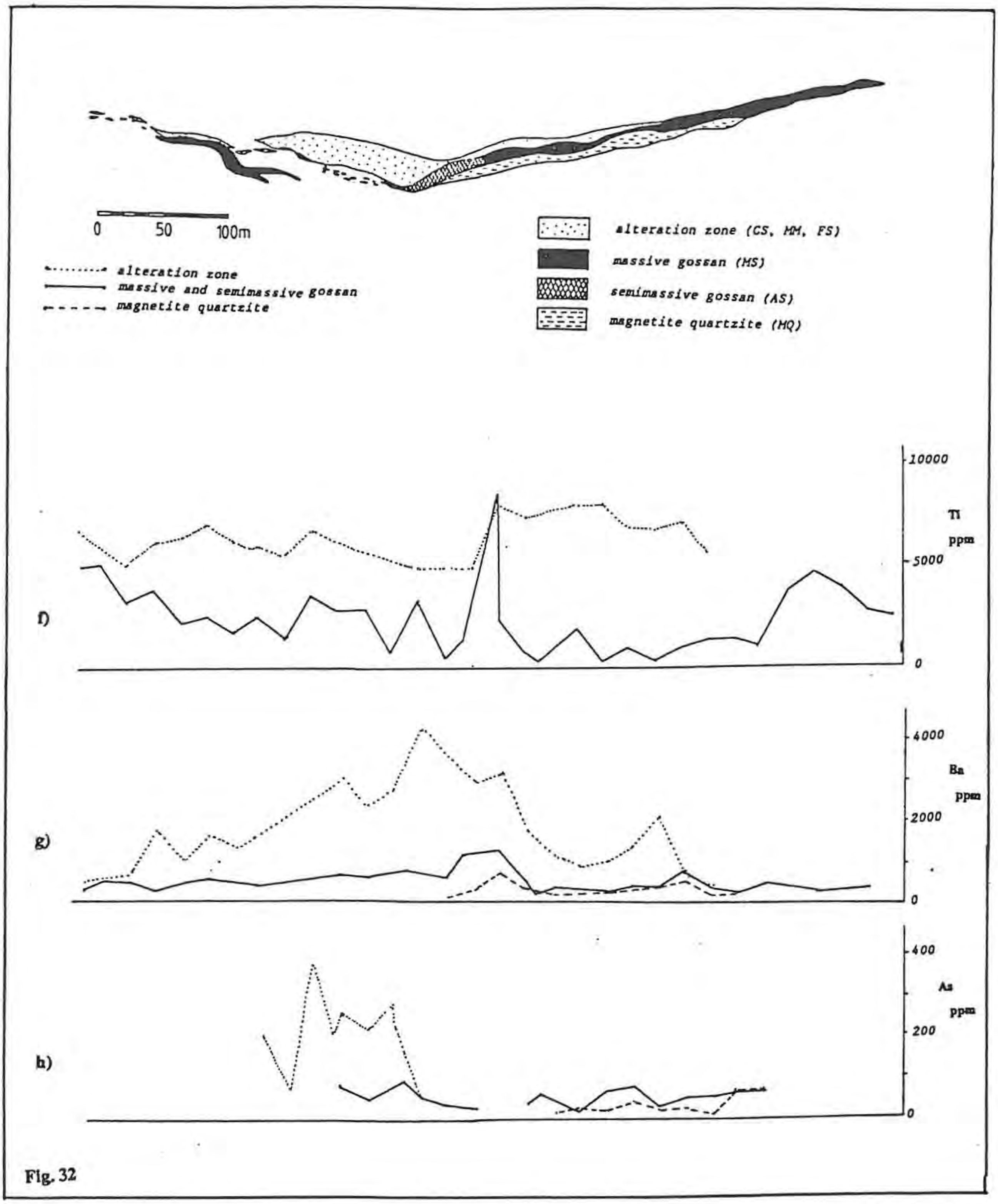

Fig. 32

Fig. 32 - See previous page.

- Cr and Ni are slightly enriched in the MM and CS of the axial zone; Cr appears to increase in the CS closer to the intersection with the mineralized horizon.

A comparison between the schists within the alteration pipe and the unaltered country rocks highlights different distribution trends of the elements.

The altered schists are remarkably enriched in Cu, Au and Ba, and moderately in Sn, As, Bi, Cr and Co relative to the country rocks. The schists in the pipe are also strongly depleted in Rb, and, to a lesser extent, in Sr and Ni. The Zr, Ti, Zn, Pb, Ag concentrations in the country rocks compare fairly well with those in the alteration pipe.

Tectonic disturbances (e.g. faults, quartz veins) in the outcrop are outlined by the coincidence of either highs or lows in the trace element distribution. For example, in the eastern sector of the outcrop, probable late ore remobilization is suggested by coincident Au and Ag peaks in both MS and MQ facies. In the western sector (grid ref. 10060 E in Plan 1 Appendix A), the prominent fault, causing the drag-like deformation in the gossan, is indicated by enrichment of Zr in MS and Cr in MM, and by depletion for Ba in MM and Zn and Pb in MS.

In comparing the trace element distribution patterns between the two distinct gossan bands, several differences exist. It is noted that Zn, Au, Ag, Mn and Sr show opposing concentration in the MQ and MS facies of the two gossan bands. In the minor gossan outcrop these elements are enriched in the MQ, whereas in the major outcrop they are enriched in the MS facies.

2.2 Geochemical trends at Matchless West Extension: trace element distribution

The trace element distribution trends for the Matchless West Extension mineralization are represented as contour maps in Appendix H. Threshold values for the contour maps were obtained by means of construction of histograms. Elements were grouped as follows:

a) Cu + Zn + Pb + Ba + Mn representing a volcano-exhalative association;
b) Ni + Co representing an association in sulphide deposits related to mafic volcanism;
c) Ti + V + Cr representing elements related to mafic magmatism;
d) Au + Ag;
e) Sn + W + Mo + Bi, elements of crustal affinity,
f) Rb, Sr and Zr, lithophile elements.

In this section the six rock types considered are: gossanous pyrite-rich muscovite-quartz schist of the axial zone of the alteration pipe (QMP schist), marginal muscovite-chlorite schist (MC schist), massive gossan (MS), magnetite quartzite (MQ), talc-actinolite schists (TA schists) and marble-like rock (MB).

The mineralized body is depleted in Ti, Zr and Rb. The concentrations of Ti, Zr, Au, Ag, Sn, W, Mo and Bi in the altered schists are comparable with those in the barren country rocks. Cu, Zn, Pb and Ba are enriched, whereas Mn, V, Ni, Co, Rb and Sr are slightly depleted, in the alteration zone relative to barren country rocks (see Tables 3 and 6, Appendix E).

Within the ore system, Cu, Zn, Pb, Ba and Au best show a well defined increasing trend from the alteration pipe to the overlying mineralized body (Fig. 33a-f).

The following features are observed:

- The main Cu enrichment is recorded proximal to the alteration pipe, with MS containing up to 8.49% Cu. Notable "distal" Cu enrichment occurs in the TA schists (up to 3.56% Cu). In the MQ Cu does not exceed 0.7%.

- Zn and Pb are enriched in a more distal position compared with the Cu distribution pattern. However, a remarkable, "proximal" Zn increase is recorded in the eastern portion of the MS outcrop, where Zn attains concentrations of up to 0.30%. High Zn values occur in the TA schists (up to 0.87% Zn) and, to a lesser extent, in the enclosing MQ units. A Zn peak marks the MB outcrop. The Pb distribution pattern shows a more gradual enrichment compared with Zn towards the margins of the mineralized body. MS to the east and MQ above the alteration pipe show isolated Pb peaks (up to 0.37% Pb in MQ). In the western, distal portion of the outcrop the highest Pb contents are recorded in MQ and, subordinately, in TA. Within the upper MQ layer, the f/w, amphibole-richer, and the h/w, amphibole-poorer, portions of the layer, show a drop in the Pb content from the base to the top (from 1.54% to 315 ppm Pb).

- The degree of Ba enrichment in the Matchless West Extension gossan is noteworthy if compared with Ongeama. Lower Ba contents are recorded in the f/w QMP schists and in the eastern portion of the MS outcrop. The highest Ba enrichment is found within the central portion of the outcrop, in MS, in MQ (up to 5.4% and 4.42% Ba, respectively) and in ultramafic schists intercalated with quartzitic or phyllitic material (up to 7.24% Ba). Further Ba enrichment is observed in the distal MQ outcrop, with contents of up to 4.94% Ba in the lower MQ horizon. As expected, the Sr distribution reflects in part the Ba enrichment within the central and western sectors of the outcrop.

- A gradual Au increase occurs in the transition zone between alteration pipe and overlying massive gossan (up to 749 ppb Au). A minor, distal Au enrichment is irregularly shown in MQ and in associated gossanous TA schists.

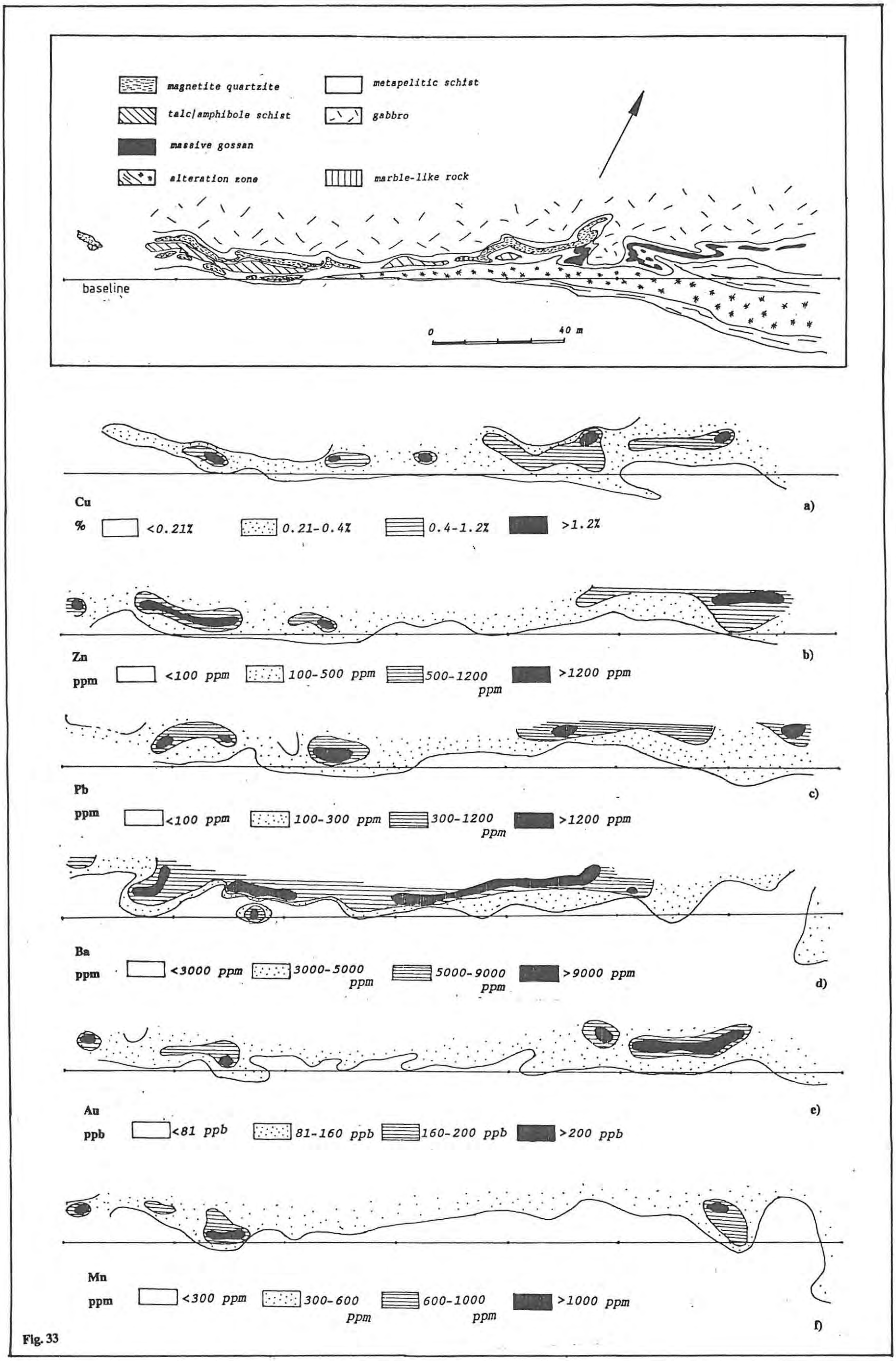

Fig. 33a-f - Schematic contour maps illustrating the element distribution within the mineralized system at Matchless West Extension (reference sketch-map modified after Smalley, 1990).

- Mn is significantly concentrated in the western distal sector of the outcrop and only enriched to a limited extent in a proximal position in MS. This element is irregularly distributed in MQ and TA schists (up to 1843 ppm Mn), but the highest peak is recorded in MB (2385 ppm Mn).

- Sn, Mo, Bi and W show well defined trends . Mo is mainly enriched proximal to the alteration pipe (up to 219 ppm Mo in MS), whereas Sn, W and Bi are concentrated in intermediate and distal positions. Peaks in the Bi concentration are observed in the actinolite schists and in MQ.

An account of the trace-element zonation recorded in the alteration pipe at Matchless West Extension is given in Section 2.3 below.

2.3 Major element distribution in the alteration pipes at Ongeama and Matchless West Extension

Tables 10, 11 and 12 in Appendix E compare the major-element contents of selected samples from the alteration pipes at Ongeama and Matchless West Extension with unaltered country rocks.

Attention is drawn to the following features:

- an outstanding Fe enrichment (on average 24% Fe_2O_3, but locally exceeding 60%) characterizes the schists in the alteration zones relative to unaltered schists. The Fe content appears to increase towards the margins of the pipes;

- Ca, Na and K are remarkably depleted, and locally below detection, in both alteration pipes;

- Al_2O_3 is relatively depleted in the alteration zones, in favour of an Fe_2O_3 and/or SiO_2 enrichment. However, the two alteration pipes display a contrasting distribution of these oxides. In the pipe at Ongeama the axial zone appears, in fact, to be more aluminous than the margins, whereas at Matchless West Extension the axis of the pipe is almost totally silicified (in excess of 90% SiO_2);

- at Ongeama, Mg is mostly immobile along the axis of the pipe, and considerably depleted at the margins. The element displays an opposite distribution at Matchless West Extension.

2.4 Geochemical zoning within the alteration pipes at Ongeama and Matchless West Extension

The alteration pipes associated with the Ongeama and Matchless West Extension sulphide deposits were subdivided into a number of sectors along their axial and lateral extensions (Fig 34 and 35).

The average content for each element was calculated in each sector (Tables 13 and 14; Appendix E). These averages were plotted against distance (expressed as progressive numbers of the sectors) in diagrams. The purpose was to verify the existence of possible trace element zonation within the alteration zones. The trends observed at Ongeama are illustrated in Fig. 36 and those of Matchless West Extension in Fig. 37.

At Ongeama (Fig. 36a-i) only one half of the muscovite-rich sheath (which is developed along the eastern portion of the ore body and the least tectonically disturbed) was considered. It is assumed that lateral variations in the element distribution are symmetric relative to the axial zone.

Most of the elements show regular variations within the alteration zone. The results can be summarized as follows:

- The distribution of Zn, Ba, Sr, Cr and Sn show an axial zonation , with values increasing from sector VII to sector IV. This zonation is remarkable for Ba and Zn and less pronounced for Sn and Sr. Outside the axial zone the distribution of these elements varies irregularly.

- Cu, Co, Au and Rb display a lateral zonation with values

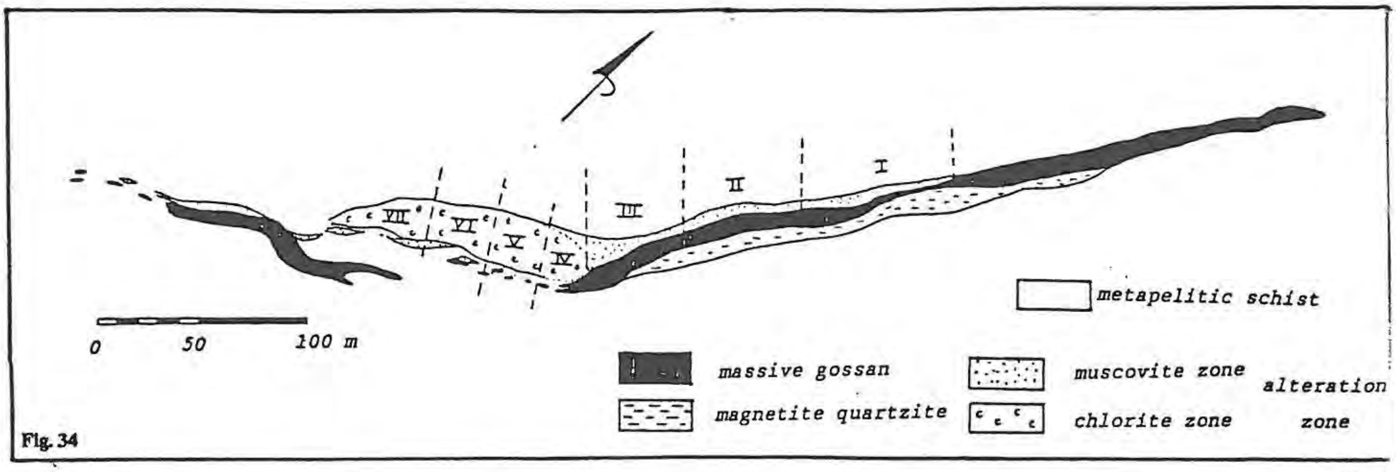

Fig. 34 - Ongeama Prospect: subdivision of the outcrop of the alteration zone into sectors.

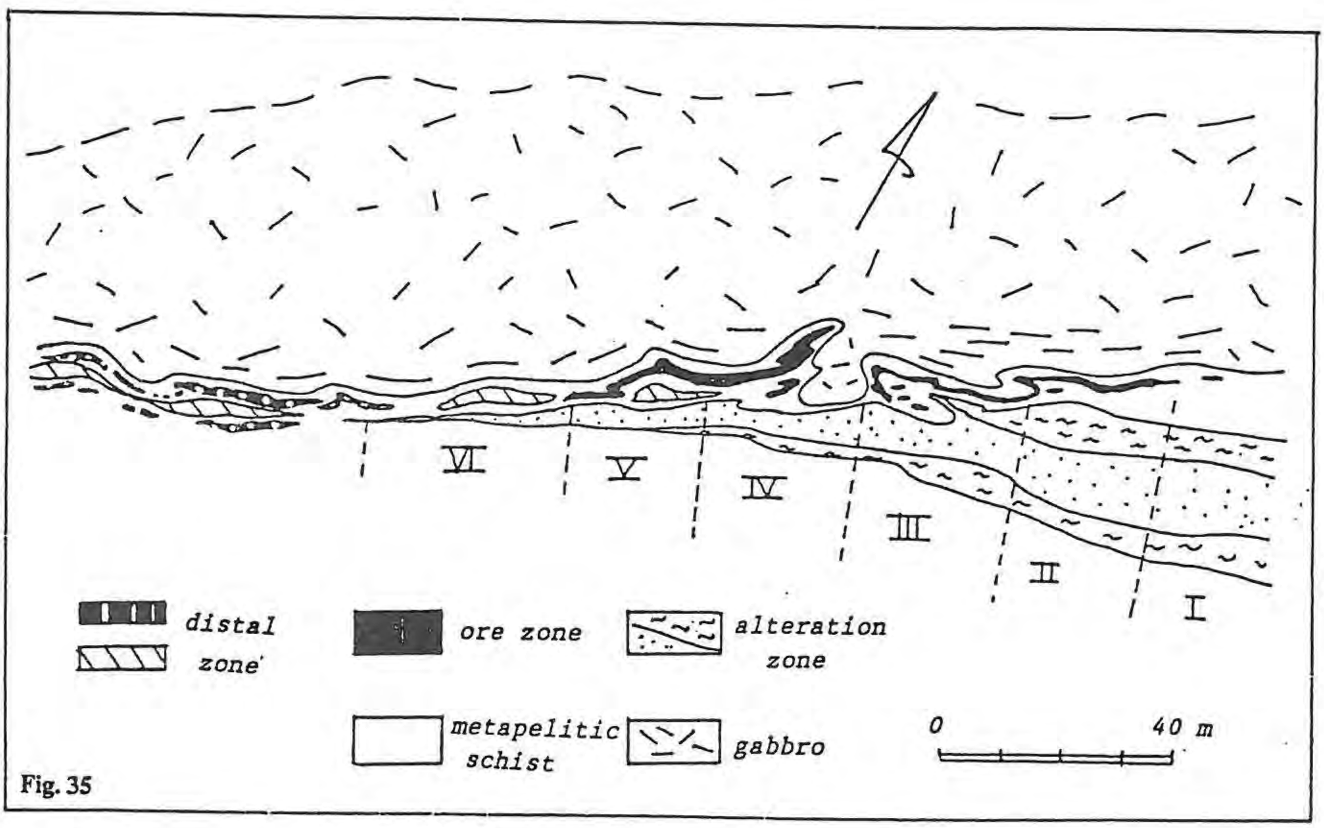

Fig. 35 - Matchless West Extension deposit: subdivision of the outcrop of the alteration zone into sectors (sketch-map modified after Smalley, 1990).

ONGEAMA....

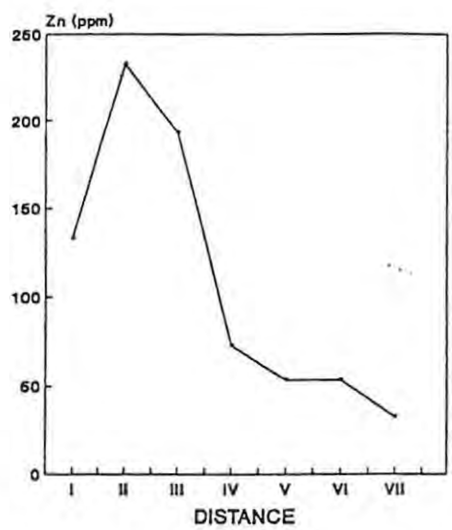

b)

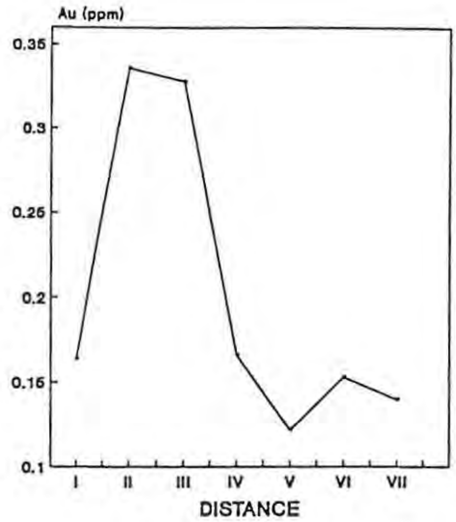

a)

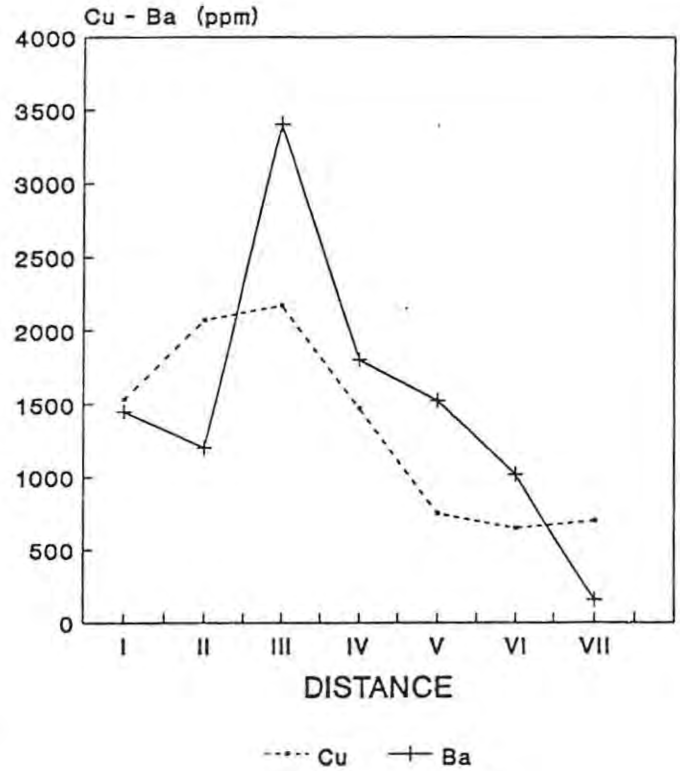

c)

Fig. 36a-i - Ongeama Prospect: trace element zoning within the alteration pipe. Roman numbers along the X axis (distance) correspond to the subdivision in sectors of the alteration zone, as shown in Fig. 34. Element concentration for each sector is obtained by averaging the values of the samples included in the sector.

ONGEAMA

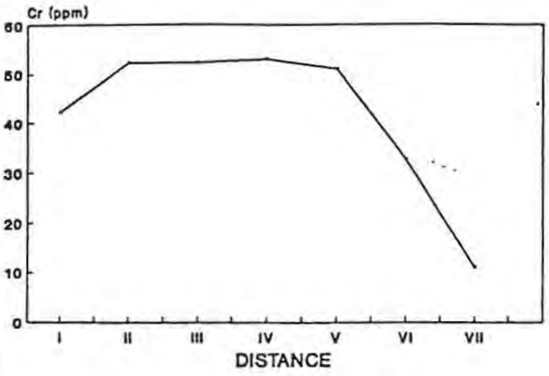

e)

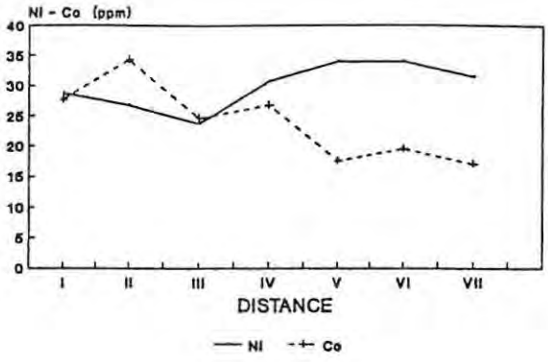

d)

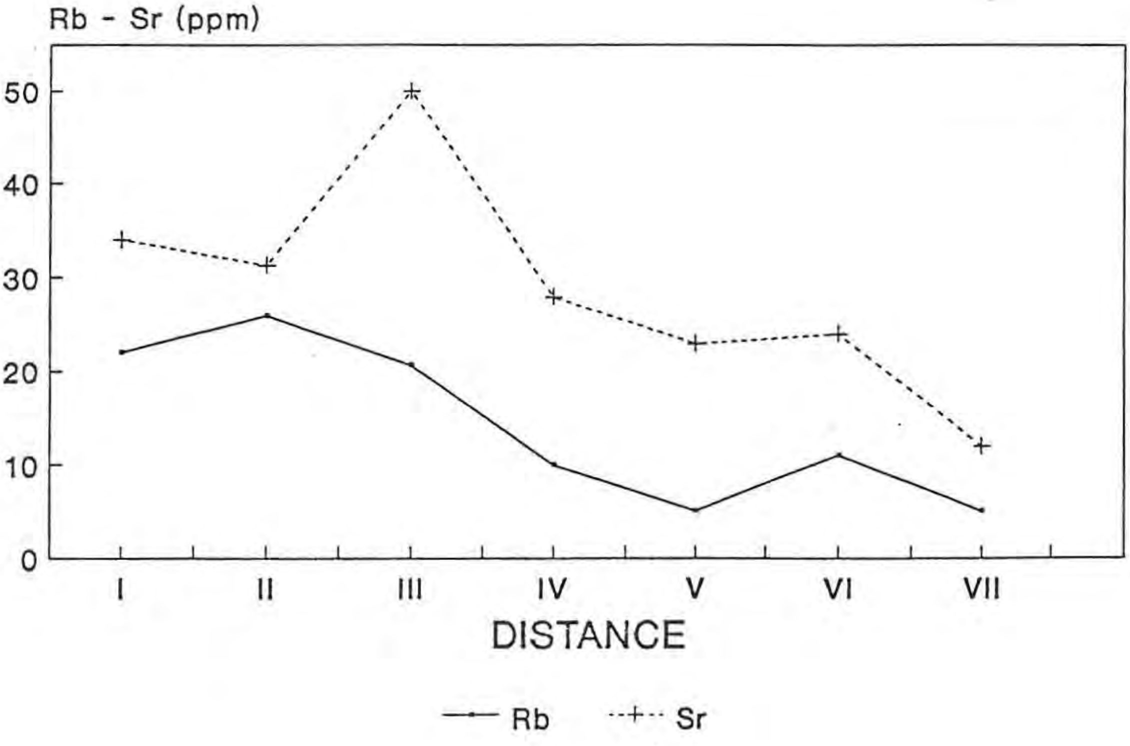

f)

Fig. 36a-i - See previous page.

ONGEAMA

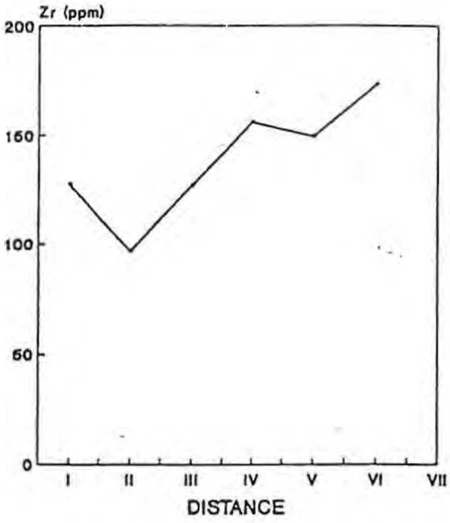

h)

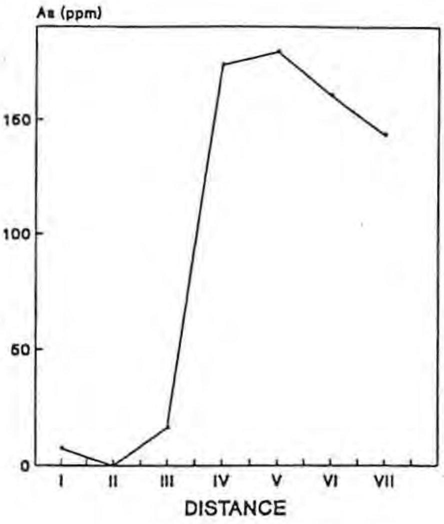

g)

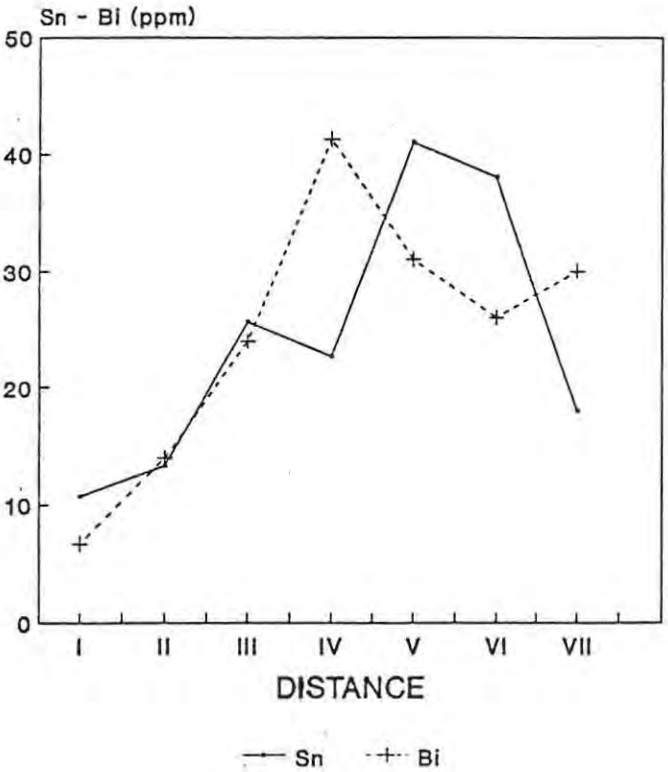

i)

Fig. 36a-i - See previous pages.

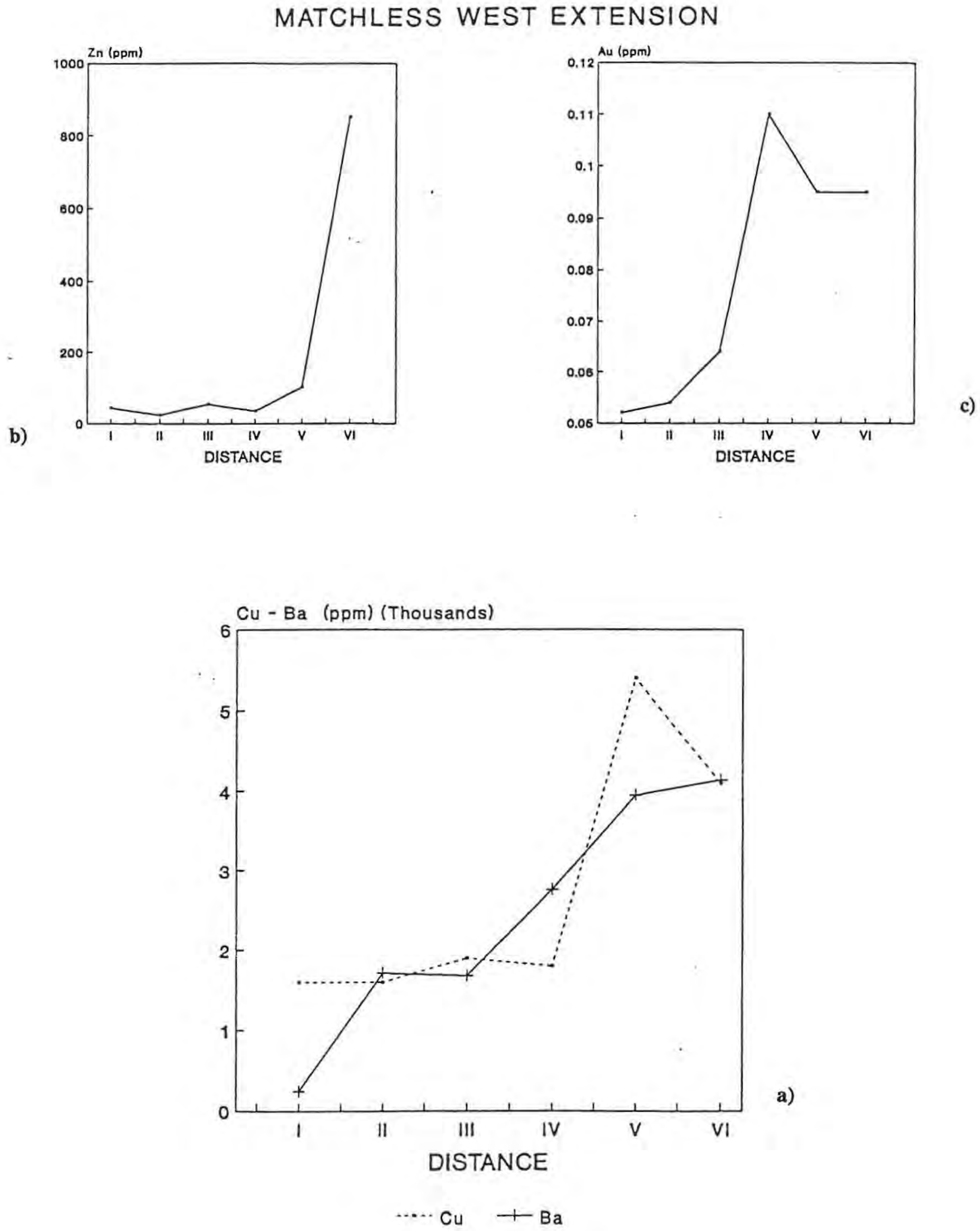

Fig. 37a-c - Matchless West Extension deposit: trace element zoning within the alteration pipe. Roman numbers along the X axis (distance) correspond to the subdivision in sectors of the alteration zone, as reported in Fig. 35. Element concentration for each sector is obtained by averaging the values of the samples included in the sector.

MATCHLESS WEST EXTENSION

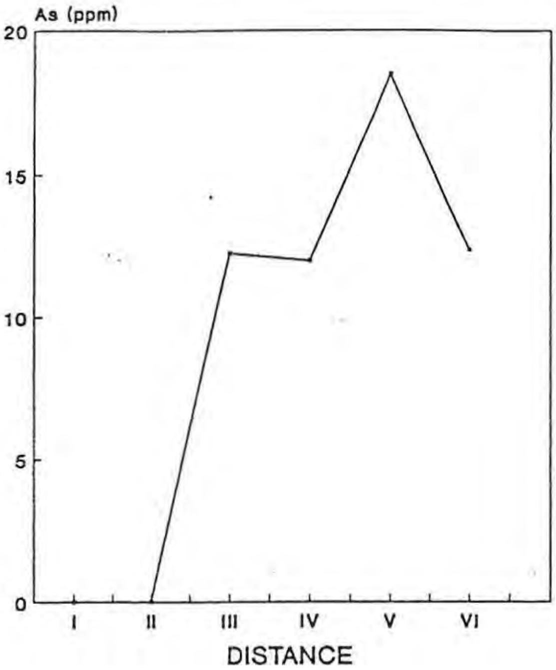

d)

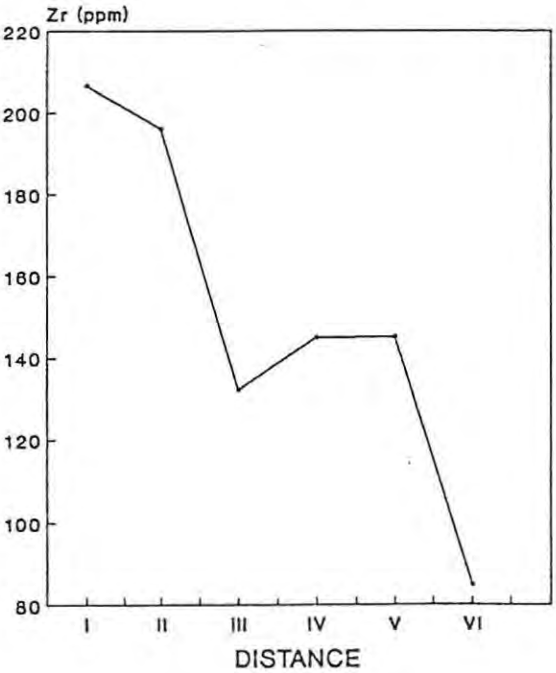

e)

Fig. 37a-e - See previous page.

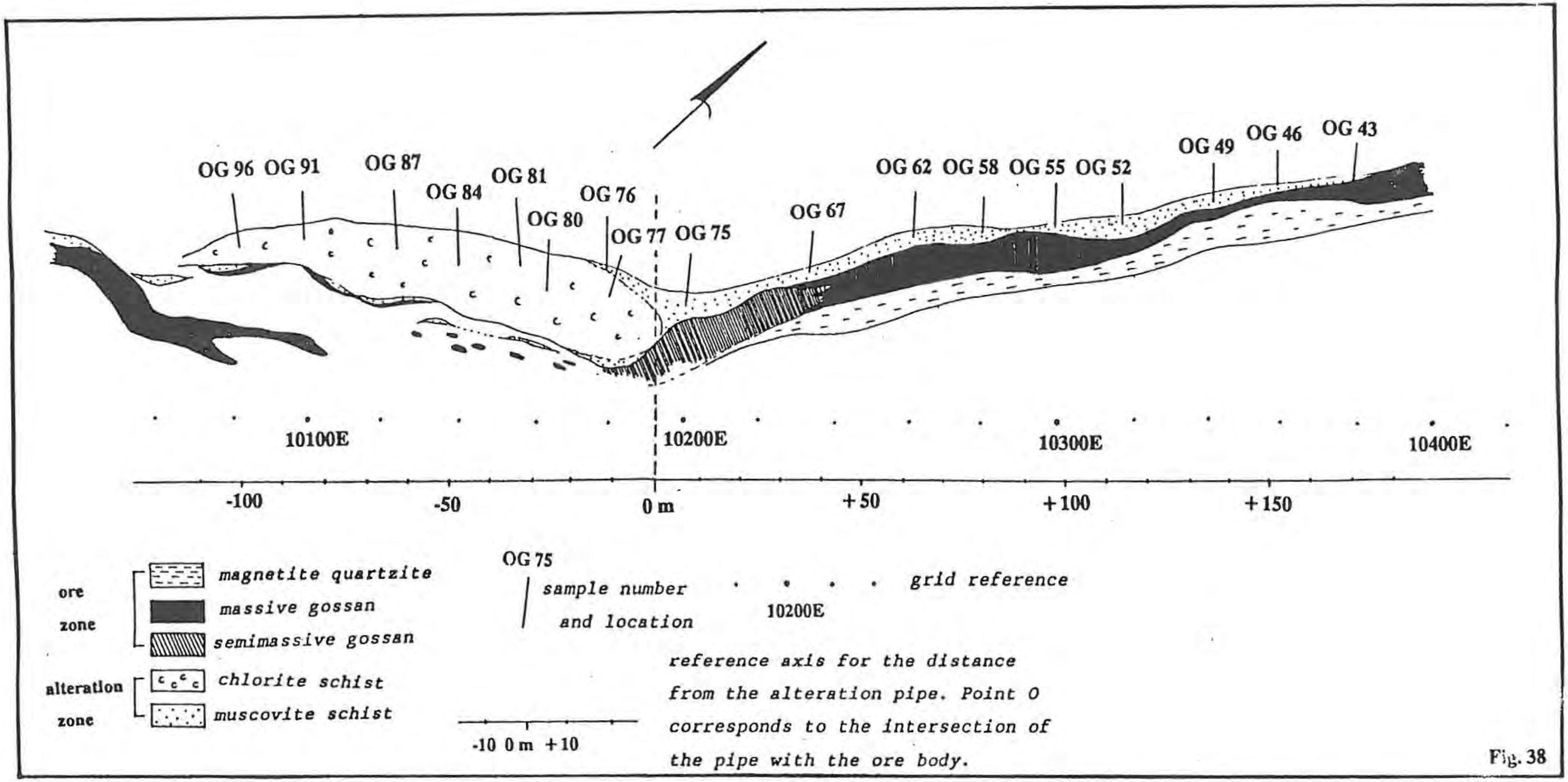

Fig. 38 - Ongeama Prospect: scheme of the position of the samples in the alteration zone. The surface geology of the central sector of the major gossan outcrop is schematically shown.

ONGEAMA

a)

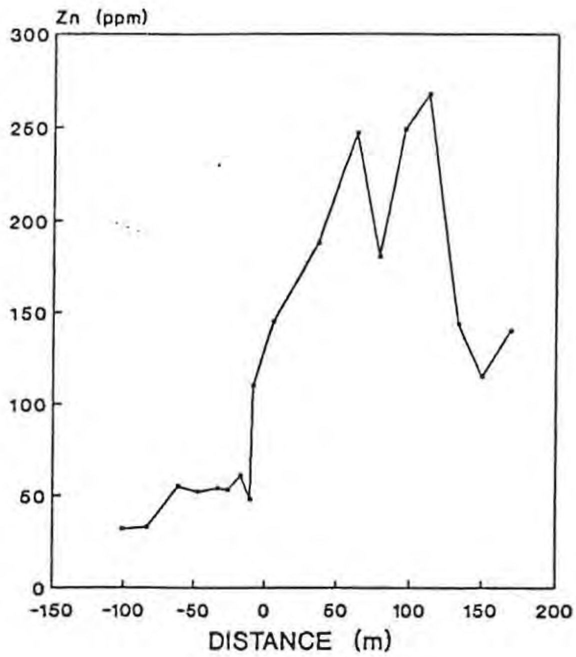

b)

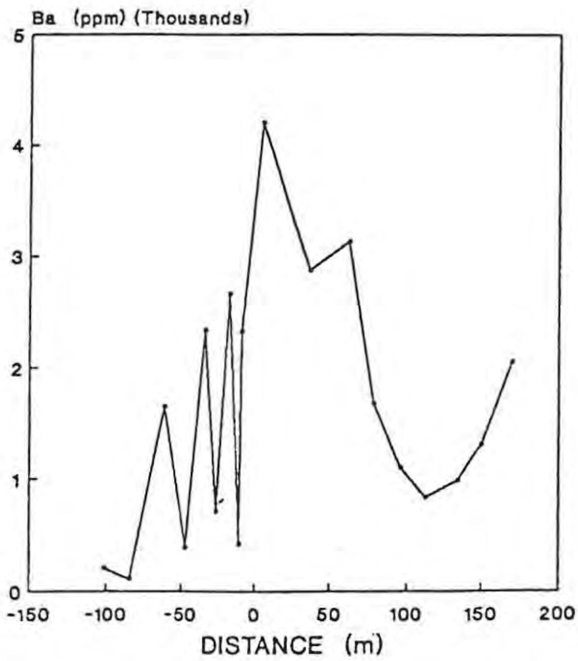

Fig. 39a-b - Ongeama Prospect: zoning of Zn and Ba within the alteration pipe. Concentration values of all the samples along the pipe are plotted. Along the X axis, distance is considered from a 0 metre reference point, which corresponds to the intersection between the alteration pipe and the sulphide body.

increasing from the axial zone towards the margins, in the muscovite-rich envelope. Along the axial zone the concentration of these elements is fairly constant, except for Rb, which displays variations within the same range of concentration.

- Zr, As, Bi and Ni exhibit a lateral zonation with concentrations increasing from the margins to the core. This trend is particularly well displayed by the Zr and As profiles. In the latter a remarkable difference in the As content distinguishes the chloritic pipe from the muscovite-bearing envelope.

Two profiles for the Zn and Ba distribution were obtained by plotting values of each sample (see Fig. 38 for sample location) instead of averages (Table 15, Appendix E). This procedure was used in order to test the validity of the method. The results (Fig. 39a-b) match the trends previously assessed for these elements by using averages.

At Matchless West Extension only Cu, Zn, Ba, Au, Zn and As define a clear zonation within the alteration pipe (Fig. 37a-e). In particular, Cu, Ba, Au, As and Zn define an axial zoning with upward and lateral increase, whereas Zr contents increase with depth along the pipe. The Ba distribution shows the most regular profile, whereas the Zn and Cu contents record an abrupt increase in the marginal part of the alteration zone, i.e. towards the west.

2.5 Geochemical trends at Ongombo

2.5.1 Trace element distribution in the gossan exposure

The profiles in Appendix I represent the trace element distribution along strike in the gossan exposure at Ongombo. The irregularity and the complexity of these profiles are due to uneven sample density.

The most clearly discernible trends are as follows (Fig. 40):

- important Cu, Zn, Mn, Ni and Co enrichment is confined to the

Central Shoot and to its western extension. This seems to be especially the case for the localized distribution of Ni and Co. In this sector of the outcrop, Co has concentrations exceeding 500 ppm. Bischoff et al. (1983) report similar high Co contents in the Galapagos Rift;

- Ba shows remarkable enrichments on both ends of the outcrop;

- V and Ti display a slight, overall increase west of the fault along the White Nossob River (F_a);

- the two major faults are indicated by the position of peaks for Ba and Cu; peaks of Mn, Ni and Co outline the F_b fault.

In particular, it is noted that:

- The Cu content in the Ongombo Gossan is lower than that recorded in the magnetite quartzite of the other two deposits examined. In fact, the Cu distribution at Ongombo is characterized by peaks greater than 1000 ppm above a background of 200-400 ppm. The main Cu enrichment occurs in proximity of the major western fault (fb) westwards. In that sector the gossan outcrop is affected by conspicuous veining and is characterized by the presence of the amphibole-rich patches. One of the highest values (0.32% Cu) coincides with a sample representative of one of these amphibole-rich pockets. The western extension of the Central Shoot appears to be the Cu-richest portion of the outcrop, with an average Cu content of approximately 1092 ppm Cu. The East Shoot has an average of 329 ppm Cu.

- In the irregular Ba profile, two main zones of enrichment are distinguished:

a) to the east, high Ba contents (up to 5221 ppm) characterize the outcrop close to the intersection of the Eastern Shoot EMP trend with surface;

b) at the western end of the mineralized outcrop Ba displays a

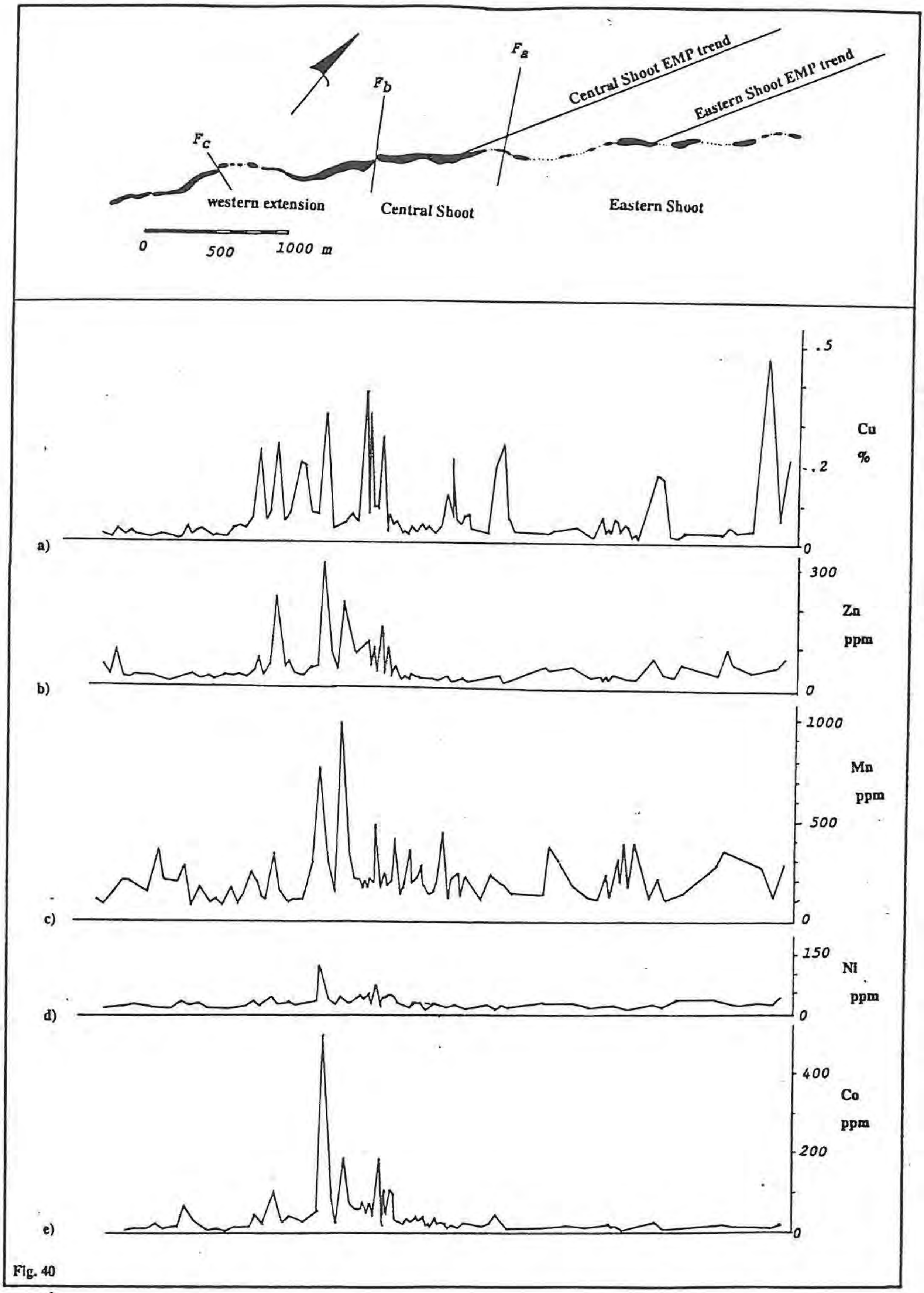

Fig. 40a-h - Ongombo Prospect: geochemical profiles for Cu, Zn, Mn, Ni, Co, Ba, Ti and V along the strike of the gossan outcrop. (F_a, F_b, and F_c correspond to faults)

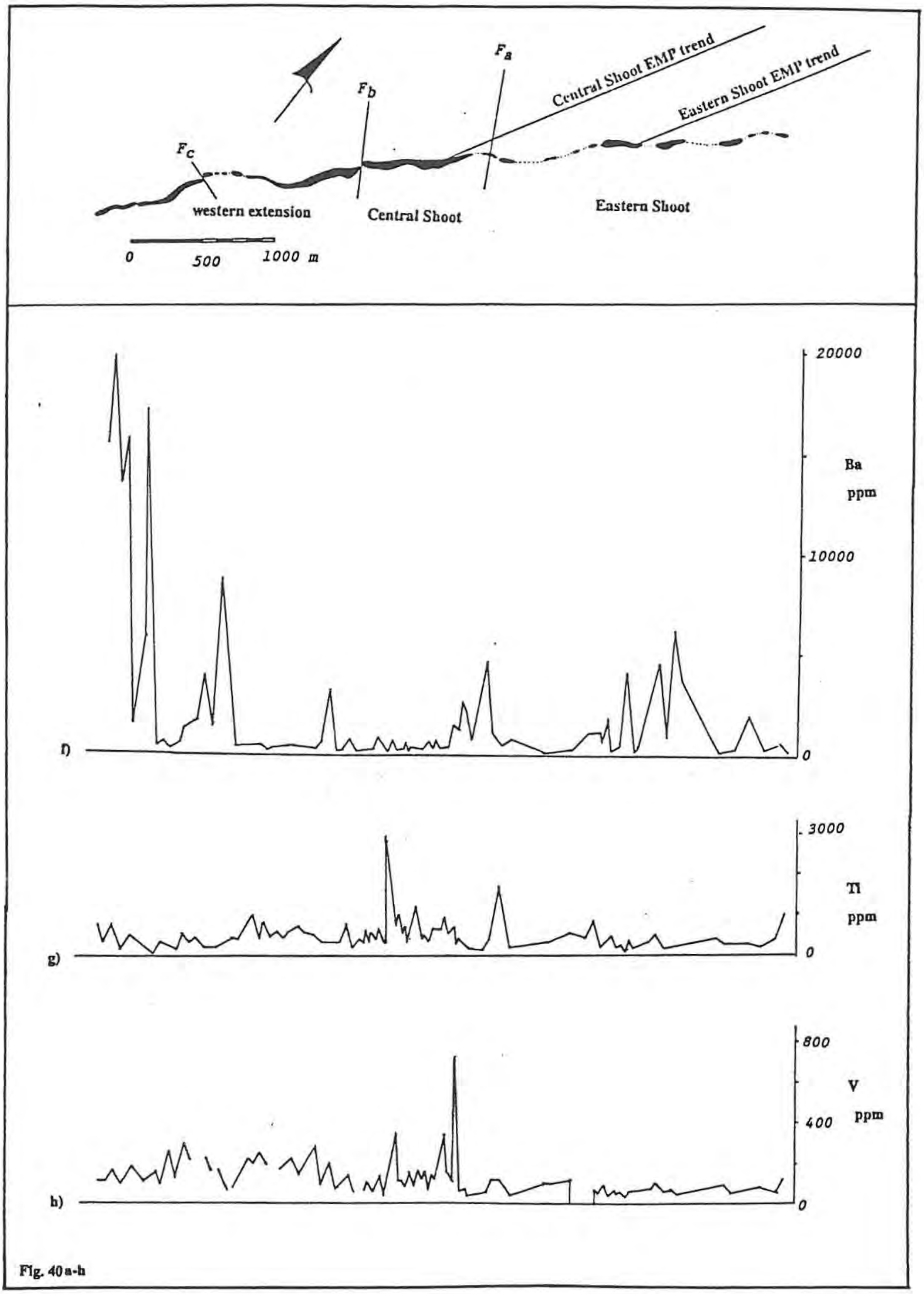

Fig. 40a-h - See previous page.

series of peaks (from 4127 ppm up to 1.98% Ba). These localized high Ba anomalies appear to be related to faulting (e.g. the 4127 ppm peak of the F_C fault). The two main faults bordering the Central Shoot sector are outlined by Ba peaks. However, it is also possible that a primary Ba enrichment may have occurred in the margins of the mineralized body.

- The Pb profile (not shown in Fig. 40) shows a variable distribution with contents not exceeding 158 ppm. Only at the western end of the outcrop is there Pb enrichment.

- Au displays a relatively smooth profile (not shown in Fig. 40). Apart from small-scale variations within the range of the general average (163 ppb Au), peaks occur in correspondence with, and close to, the Eastern Shoot-surface intersection.

- Sn, Zr, W, Bi, Sr and Mo show a "broken" profile (not shown in Fig. 40). The first five elements are enriched in the western end of the outcrop. Sr shows some outstanding peaks (up to 364 ppm Sr), probably reflecting the Ba enrichment.

2.5.2 Trace element distribution in drillcores

Vertical profiles of the trace-element distribution in the drillcores OGB 151A, OGB 153A and OGB 154A from Ongombo are represented in Appendices J and K (see also Tables 5 and 6, Appendix E).

As reported in Part B and Part C, the metapelitic schists in the h/w of the ore zone are intercalated with mafic units of probable intrusive origin. Zones of chloritization and of sulphide- and/or magnetite dissemination appear to be spatially related to these mafic units. In the f/w, the unaltered schists locally carry fine disseminations of sulphides and/or magnetite, as well as remobilized ore in quartz veins.

From the examination of the geochemical profiles along the drillcores, the first point of note is that, on the whole, there is only a slight difference in the element distribution between the schists in the h/w and in the f/w of the ore zone. The peaks occurring in the h/w profiles coincide either with important lithological changes, i.e. from metapelitic schist to mafic unit, or with local sulphide and magnetite disseminations.

No significant trend of either enrichment or depletion **in the h/w sequence towards the ore zone** is discernible (see profiles in Appendix J and Fig. 41).

The following remarks are made:

- Cu, Zn and Pb peaks commonly coincide with zones of sulphide disseminations in the h/w schists. Cu and/or Zn peaks, of variable extent, characterize mafic and ultramafic units, although in correspondence with thin chlorite-amphibole schists (in OG 154) only a relative Zn and Pb enrichment is observed.

- Au is in isolated, small peaks, occasionally coinciding with Cu, with quartz veins and sulphide disseminations.

- Ni shows conspicuous enrichments in the mafic units and especially in their h/w ultramafic margin. Ni and Co peaks locally match, although Co is locally enriched in magnetite- and sulphide-bearing schist layers.

- The V and Ti distribution is mainly controlled by the distribution of mafic rocks.

- The Cr values in the barren f/w schists in the Ongombo drill cores are remarkably higher than those in the barren schists at Ongeama (compare Tables 5 and 7, Appendix E). Cr peaks correspond to mafic-ultramafic units. Within these units differentiation is shown by the gradual variation in the Cr content. An inverted zonation for Cr is observed, e.g., in the mafic layers in the drill core OGB 153A. Within these mafic units, the highest Cr values coincide with the occurrence of the actinolite-chlorite-talc-rich h/w margins. The observed Cr distribution reflects, and further confirms, the overturning of the stratigraphic sequence, previously inferred on petrological grounds.

- The Mn distribution shows extreme variations. Prominent peaks occur in magnetite-bearing schist horizons, whereas low contents characterize some of the mafic units. The thickest mafic units show slight Mn enrichments towards the f/w (e.g. OGB 154A).

- Ba exhibits an irregular distribution, with values below 750 ppm in the h/w. A trend of Ba depletion in the h/w schists relative to the f/w schists is also observed. This trend is opposite to the Mn trend. In the h/w, major Ba lows correspond to the mafic-ultramafic units. An abrupt increase in the Ba content is observed in OGB 153A in schists directly overlying the ore zone, although magnetite- and sulphide-bearing schists proximal to the ore zone do not generally show Ba enrichment. Ba peaks in the f/w only locally coincide with fine sulphide disseminations at the margins of late quartz veins (OGB 151A).

- The Rb and Sr distribution profiles are sympathetic, although Rb forms remarkable lows over mafic units. The Sr and Ba distributions are not entirely sympathetic. Because of its affinity for K, Rb depletion is indicative of K-feldspar-poor lithologies such as amphibolites. Beside Ba, Sr has affinity for Ca (Wedepohl, 1969). In amphibolites Sr abundance may be related to the Ca content in plagioclase and/or in calcic amphiboles (e.g. hornblende). In OGB 151A, Rb is depleted in the schists included between two mafic units above the ore zone. This depletion trend is followed to a lesser extent also by Sr, and is concomitant with some of the irregularities in the distribution of other elements (e.g. Ni, Pb, Zn, Mn, Ba).

- The irregular Zr profile displays depletion in coincidence with mafic units. Zr peaks match Rb and Ba peaks. Zr and Y profiles are more irregular in the h/w than in the f/w schists.

- Nb, Mo, Sn, Bi and As show "broken" profiles with some isolated

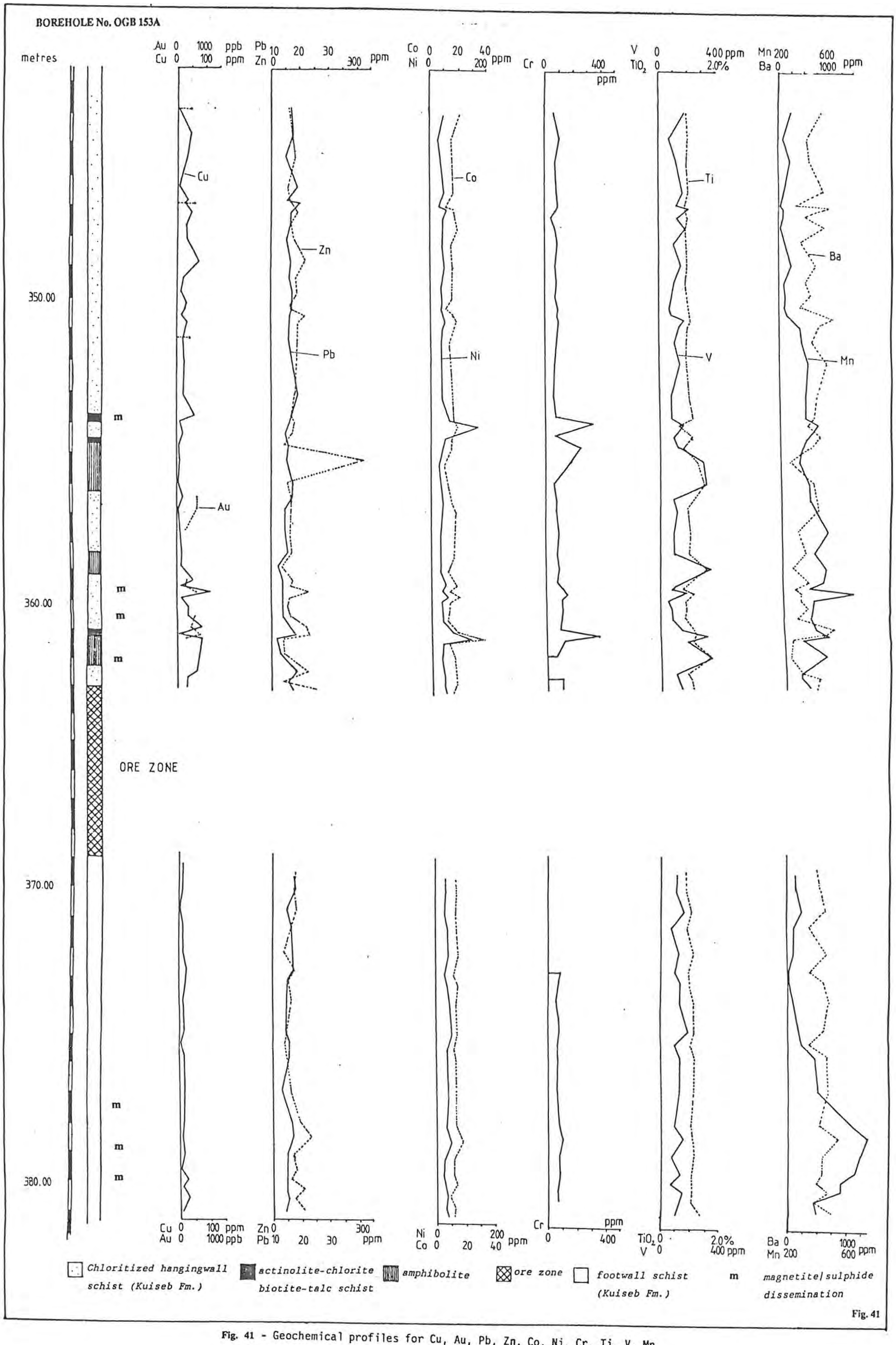

Fig. 41 - Geochemical profiles for Cu, Au, Pb, Zn, Co, Ni, Cr, Ti, V, Mn and Ba in the hangingwall and footwall sequence enclosing the ore zone at Ongombo (borehole No. OGB 153A).

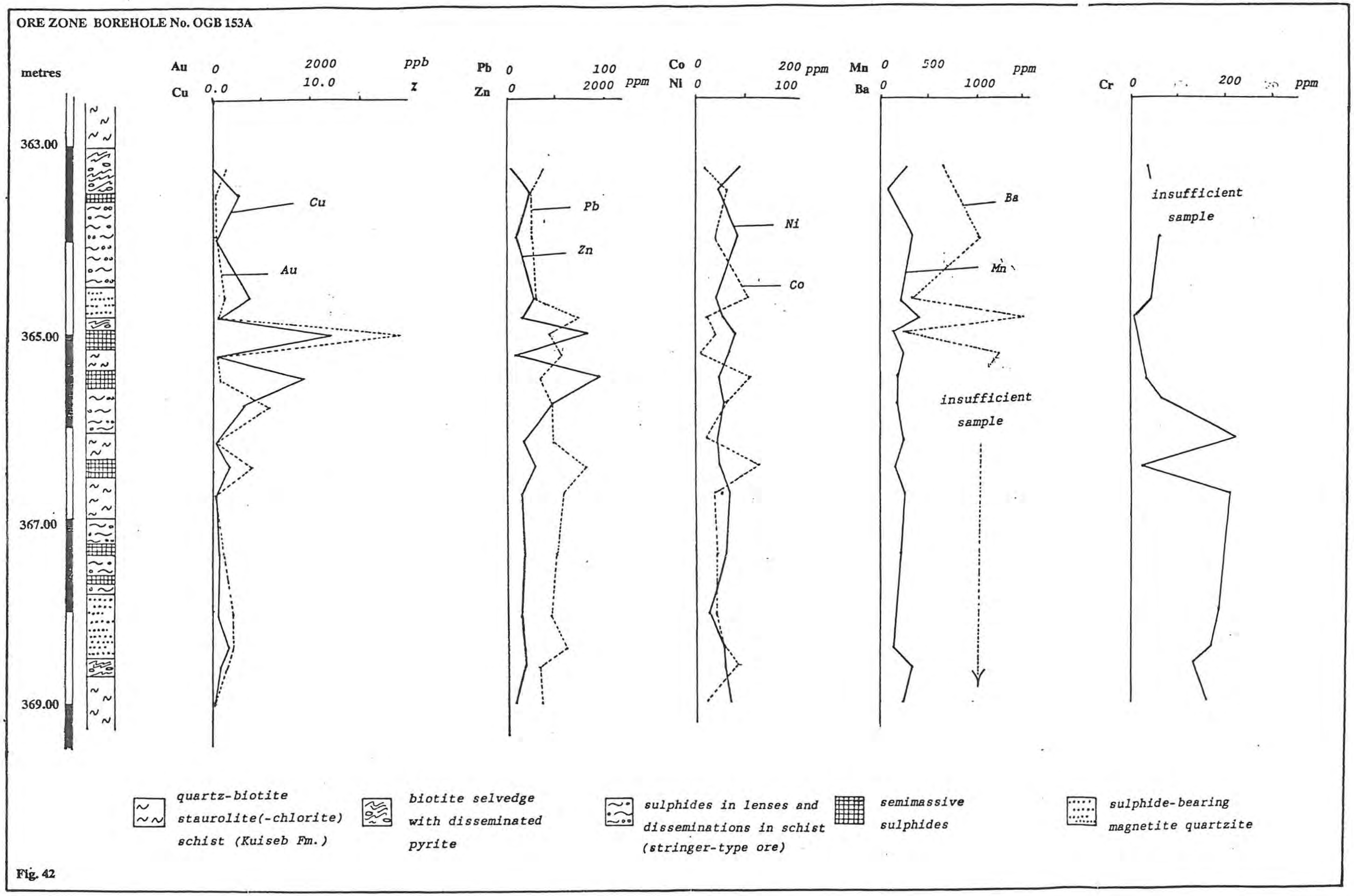

Fig. 42 - Geochemical profiles for Cu, Au, Pb, Zn, Co, Ni, Cr, Mn and Ba in the ore zone at Ongombo (borehole No. OGB 153A).

values. Bi, Mo and Sn peaks are locally observed in magnetite- and sulphide-bearing schist horizons.

With regard to the **ore zone**, the following observations can be made (Fig. 42 and Appendix K):

- as expected ,the ore zone is characterized by a remarkable Cu enrichment relative to the enclosing schists. Major peaks (11.75% Cu) are associated with layers of semimassive sulphide mineralization and with the upper magnetite quartzite horizon;

- Au (up to 3.78 ppm Au) and Ag peaks commonly match Cu highs in semimassive mineralization ; Ag is slightly enriched in MQ.

- the Zn profile sympathetically follows the Cu distribution, whereas Pb shows a flat profile with a few minor peaks;

- the Ba concentration in the ore zone is distinctly higher than that in the enclosing schists. Within the ore zone, Ba increases towards the bottom of the ore zone. Ba peaks correspond to schist horizons containing disseminated and stringer-type mineralization;

- Cr shows a variable distribution: peaks with over 100 ppm characterize either magnetite quartzite or disseminated mineralization in schists and in biotite selvedges;

- Zr, Rb and Sr (not represented in Fig. 42) are remarkably depleted within the ore zone relative to the wall rocks.

2.6 Alteration index as a tool for the evaluation of hydrothermal alteration

In order to evaluate the geochemical changes occurring in the ore-hosting metapelites during premetamorphic hydrothermal alteration, Haussinger and Okrusch (1990) propose the calculation of an "alteration index". This index is defined as the ratio between the sum of enriched elements and the sum of the enriched plus depleted elements in a rock.

The alteration index, calculated for both major and trace elements, is plotted against an index representing the elements immobile during metamorphism and alteration (Ti and Zr; Finlow-Bates and Stumpfl, 1981). Altered and unaltered lithologies define two different fields in the diagram, i.e. an upper field for altered schists and a lower field for unaltered schists. Fig. 43, for example, shows the result of the application of Haussinger and Okrusch's alteration index to the Gorob sulphide deposit. These authors recommend this method as a mine-scale exploration tool in order to locate a buried ore body in drill cores.

In the present study, the alteration indices for major and for trace elements were used for the purpose of comparing the chloritized h/w schists in the Ongombo drill cores and the magnetite-bearing schists from the "I anomaly" at Ongeama, with the assumed altered schists at Ongeama and Matchless West Extension (Tables 16a-g, Appendix E).

Haussinger and Okrusch's alteration index for major elements, I_{major}, is defined as:

$$I_{major} = \frac{Fe_2O_3tot + MgO + MnO}{(Fe_2O_3tot + MgO + MnO) + (CaO + K_2O + Na_2O)},$$

the alteration index for trace elements, I_{trace}, as

$$I_{trace} = \frac{Cu + Zn + Pb + Ba}{(Cu + Zn + Pb + Ba) + (Rb + Sr)}$$

and TZ as

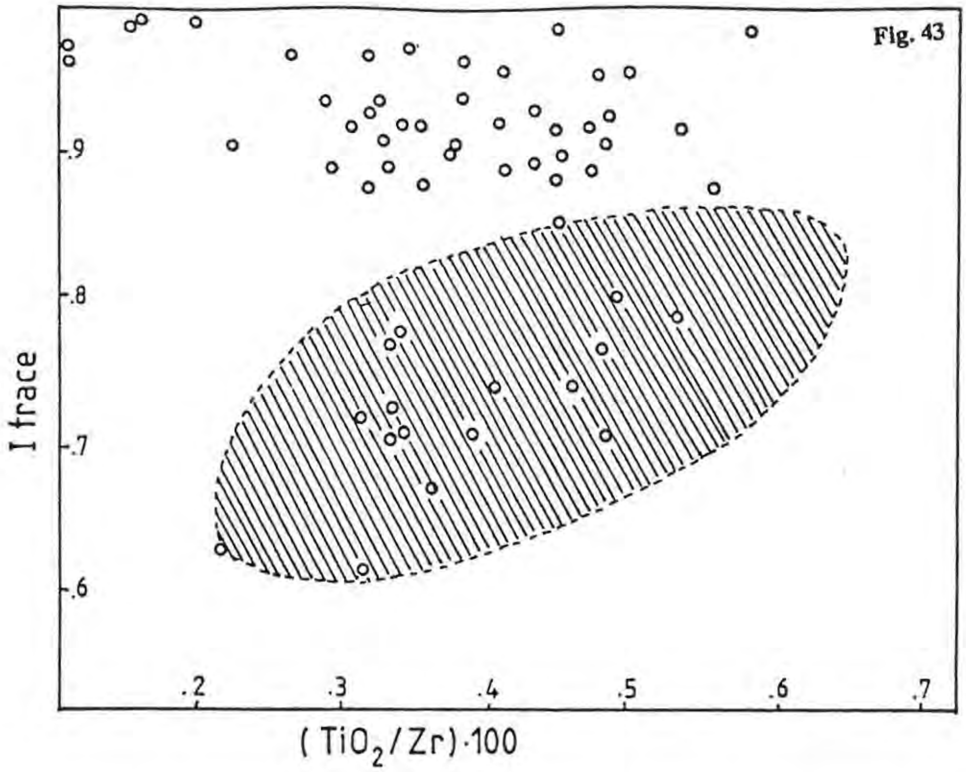

Fig. 43 - Alteration index for trace elements against TZ index for the alteration zone at Gorob (modified after Haussinger and Okrusch, 1990). The dashed field includes smples of unmineralized schists from the Kuiseb Formation.

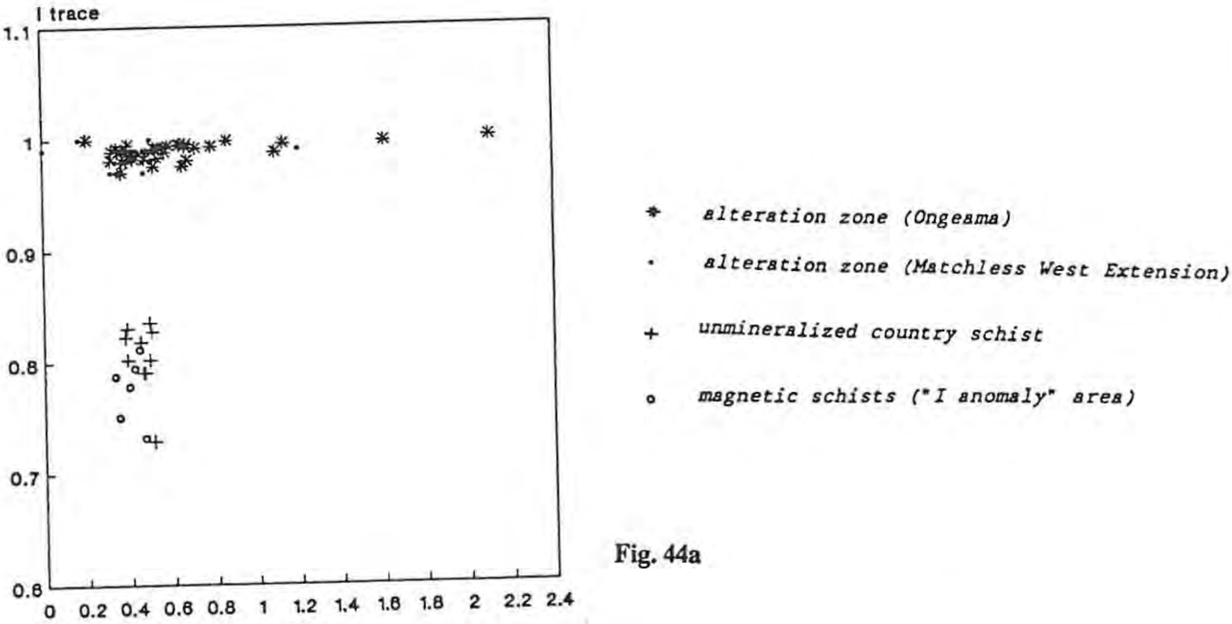

Fig. 44a

Fig. 44a-c - Discrimination between unmineralized schists and hydrothermally altered schists associated with mineralization (alteration zone) by means of Haussinger and Okrusch's (1990) alteration index for trace and major elements (see text for details). a) I^{trace} vs. TZ index diagram for schists from alteration pipes and unmineralized country schists. b) I^{trace} vs. TZ index for schists from alteration pipes and schists from the ore-hosting sequence at Ongombo. c) I^{major} vs. TZ index for schists from alteration pipes and unmineralized country schists.

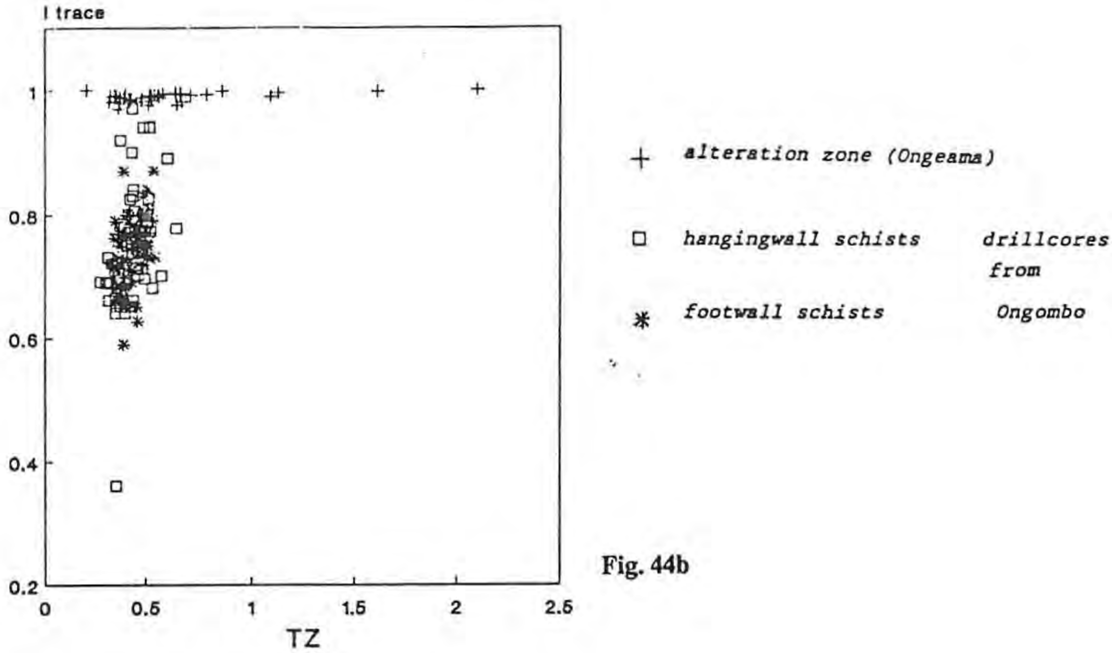

Fig. 44b

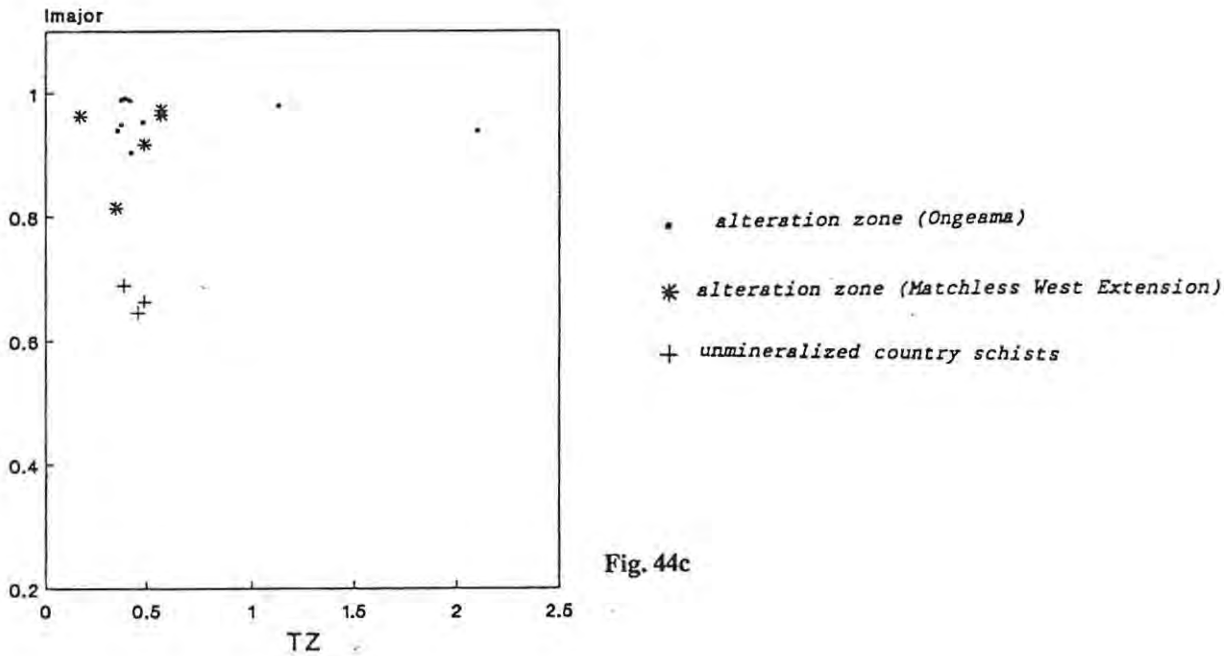

Fig. 44c

Fig. 44a-c - See previous page.

$$TZ = \frac{TiO_2}{Zr} \times 100$$

Results are illustrated in Fig. 44a-c. It is further observed that:

- samples from the assumed alteration zones of Ongeama and Matchless West Extension plot in a field characterized by both I_{major} and I_{trace} values greater than 0.9 (Fig. 44a-c);

- magnetic schists from the "I anomaly" plot within the field defined by I_{major} and I_{trace} values less than 0.7 and 0.9, respectively, and occupied by the Ongeama barren schists (Fig. 44a and 44c).

- samples from the chloritized h/w schists in the Ongombo drill cores plot in the lower I_{trace}-TZ field, in which both the f/w schists and the barren schists from Ongeama are included (Fig. 44b). Some samples from these h/w schists plot in a position intermediate between the two main fields. Some of these samples represent schist units containing magnetite and sulphide disseminations either related to mafic units or isolated (see the corresponding profiles in Fig. 41). In the immediate h/w of the ore zone , only some drill core samples (from OGB 154A) show I_{trace} index values comparable with those in altered schists (see Table 16g, Appendix E). In those core samples Ba enrichment is recorded.

3 ULTRAMAFIC EXHALITES AND IGNEOUS ULTRAMAFIC ROCKS: A COMPARISON

Tables 3, 5, 17 and 18 (Appendix E) contain trace- and major-element abundances of the ultramafic schists from Matchless West Extension, the ultramafic bodies outcropping near Otjihase and, in part, of the ultramafic differentiates in the mafic units at Ongombo (see sections 3 and 4.3 Part B and section 3.32 Part C for details).

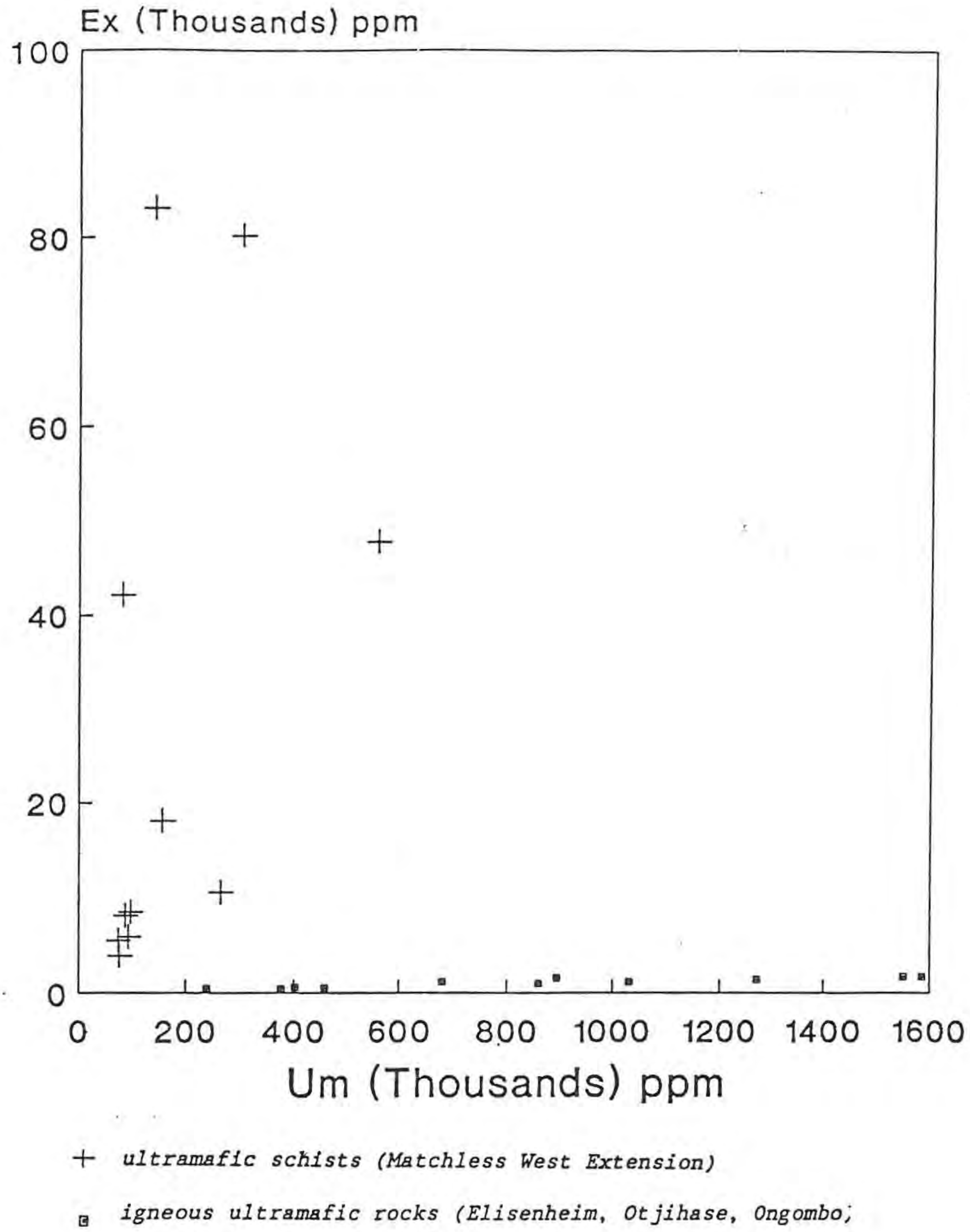

Fig. 45 - Comparison between ultramafic schists associated with the Matchless West Extension sulphide deposit, and igneous ultramafic rocks by means of the "Ex" and "Um" indexes (see text for details).

A comparison between the major-element geochemistry of the exhalative ultramafic schists, from Matchless West Extension, and the Damaran ultramafic bodies (data in Table 18, Appendix E, and in Finnemore, 1974, and Barnes, 1983), highlights the fact that the major-element contents are quite similar in the two rock categories.

Outstanding differences are shown, on the other hand, in the trace-element geochemistry of these two ultramafic rock types. Therefore, two groups of trace elements were selected (Table 19, Appendix E) in order to discriminate between the assumed exhalative ultramafic schists and ultramafic rocks of igneous derivation.

The first group of elements includes Cr, Ni and Co. These elements were chosen because of their typical association with mantle-derived material (Henderson, 1982). The second group of elements includes Ba, Cu, Zn and Pb, which are considered as discriminators for an exhalative environment. For each sample the indexes "Um" and "Ex" are defined by the sum of the (Cr + Ni + Co) and of the (Ba + Cu + Zn + Pb) contents, respectively.

In Fig. 45, two distinct distributions are obtained. The ultramafic exhalites plot within a field defined by high Ex and low Um values. This field is separated from the high Um-low Ex field including the igneous ultramafic rocks.

The geochemical separation between these two rock groups is considered significant for discriminating the exhalative, and not igneous, nature of the ultramafic schists at Matchless West Extension.

DISCUSSION

Geochemical results discussed in this chapter document the existence of well-defined trends of element distribution within the mineralized outcrops at Ongeama, Matchless West Extension and Ongombo. It is pointed out that the presence of geochemical zoning at Ongeama was not recognized by previous lithogeochemical sampling (Andrew, 1984).

The presence of element zoning along the alteration pipe at Ongeama and Matchless West Extension is meaningful because:

a) together with field observations and petrological study, it is proof of the hydrothermal origin of these pipe-like features;

b) the presence of an alteration pipe aids in the interpretation of the element zoning within the mineralization in terms of proximal and distal facies.

In the three mineralized bodies studied, large-scale zoning exhibits some common features.

- Cu primarily, and, to a variable extent, Zn, Au and Mn, are typically enriched close to the alteration pipes in both the Ongeama and Matchless West Extension gossans. The similar Cu + Zn + Mn distribution, together with the coincident, and localized, Ni and Co enrichment in the western extension of the Central Shoot suggest proximity to the source of the ore-bearing fluids. The association of these metals with the amphibole-rich ore facies at both Ongeama and Ongombo, may be more than just a coincidence.

- In the three orebodies studied, Pb, Ag, Ba, Sn and, to some extent, Zn and Au, represent the elements concentrated in a "distal" position (e.g. exhalites).

Fig. 46 schematically shows these trends.

However, it is noted that there are some minor differences, namely:

- at Matchless West Extension and Ongombo, "distal" enrichment of W and Bi is observed (see Appendices H and I). However, at Ongombo, the occurrence of Bi, W, together with Sn and Pb highs at the western end of the gossan suggests the affiliation of these metals to late tourmalinite veins, which are common and well developed in that part of the outcrop.

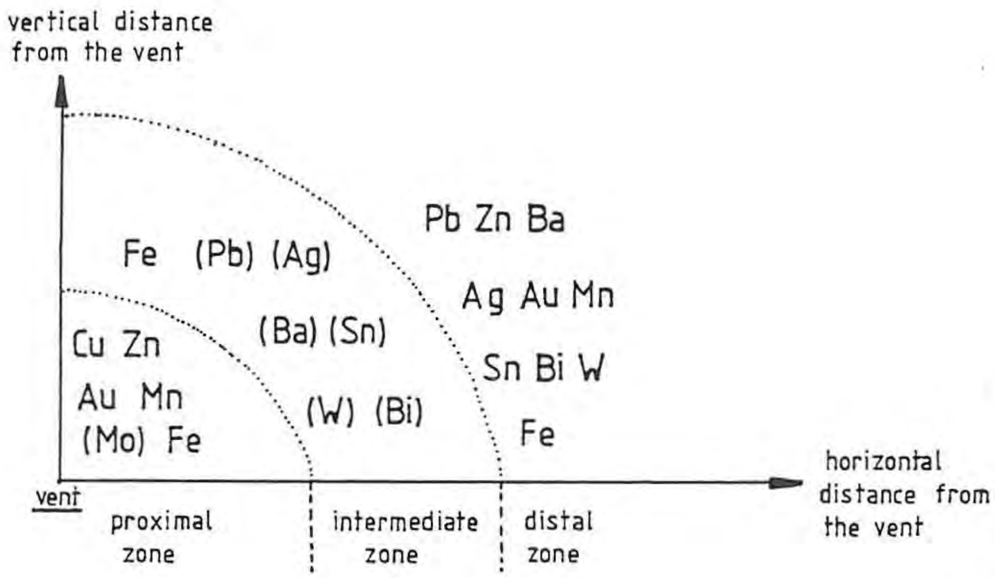

Fig. 46

Fig. 46 - Schematic representation of the trace element distribution within the mineralization in relation to the vertical and horizontal distance from the vent. Elements in brackets are enriched to a limited extent in the corresponding zone.

- only the Matchless West Extension deposit exhibits an unusual Cu enrichment in ultramafic exhalites and in a distal position relative to the alteration pipe (Fig. 33 and Appendix H). This feature may be interpreted in three different ways, namely:

a) in consideration of the moderate to high mobility of Cu in an oxidizing environment, such as is found in semi-arid climates (Rose et al., 1979), one possible explanation may be the deposition of secondary Cu-sulphides and/or oxides from migrating groundwater;

b) high Cu content (up to 0.7%) is recorded in present-day exhalative talc deposits in the Guaymas Basin (Lonsdale et al., 1980). Modern Mg-rich deposits are typically formed proximal to the hydrothermal vents (Lonsdale et al., 1980, and references therein; McLeod and Stanton, 1984). This would imply that the Mg and Cu enrichment in the westerly "distal" ultramafic schists at Matchless West Extension may, in fact, correspond to an additional small vent subsidiary to the main vent in the east (Smalley, 1990, pers. comm.);

c) the third possibility takes into account the actual position of the Cu-rich ultramafic beds within the mineralized horizon at Matchless West Extension (see Fig. 21). This may be the result of tectonic remobilization of ductile, talc-rich material, proximal to the vent, along planar discontinuities (e.g. compositional layering in the magnetite quartzite) during deformation.

Residual enrichment of weathering-resistant baryte, unaffected by the acidic environment of sulphide oxidation, accounts for the anomalous Ba contents within the mineralized bodies considered. Baryte is a common residual mineral in the Matchless Belt gossans (Andrew, 1984). Although concentrated in exhalites, Ba also displays a strong positive correlation with the alteration zones. In fact, the hydrothermally altered schists are characterized by significant Ba contents relative to the unaltered country rocks. In the major gossan outcrop at Ongeama, Ba is more enriched in the h/w altered schists than in the ore zone. In the Ongombo drillcores, Ba peaks characterize the disseminated sulphide-bearing red biotite schists, and progressive increase in the Ba content is also detected in the schists immediately above the ore zone in borehole OGB 154A (see Fig. 41 and 42).

In the hydrothermally altered host rocks of Cyprus-type mineralization, Ba is believed to be incorporated into hydrothermal sericite and illite in substitution for K (Herzig, 1986, 1988). Ba-bearing micas are included in the gangue mineralogy of metamorphosed sediment-hosted mafic volcanic-related sulphide deposits of the Broken Hill-type (Plimer, 1986). The presence of Ba in the mineralized system suggests a strong similarity of the ore-forming fluids to fluids responsible for modern Cu-Zn deposits in oceanic environments (Lonsdale and Becker, 1985; Peter and Scott, 1988; Koski et al., 1988; Kappel and Franklin, 1989). Ba is probably derived either from leaching of mafic rocks and consequent breakdown of a Ba-bearing phase (plagioclase with intermediate anorthite content; Herzig, 1986), or from seawater sulphate (Lydon, 1988).

There is, in general, a fair degree of concurrence between the results of this study and those from the previous investigations (Hoffmann, 1976; Andrew, 1984). Agreement is found on the position of the main anomalous zones within the mineralized outcrops and on the main trends of metal distribution. However, a few minor discrepancies are also observed. They are:

- the overlap between the Cu and Ag distribution observed by Hoffmann (1976) and Andrew (1984) is not recorded in the geochemical profiles of the gossans. The sympathetic relationship between these two metals is, nevertheless, noticeable in the unweathered mineralization (Ongombo drillcores), where Ag could be lattice-bound to chalcopyrite. A similar primary association is observed at Otjihase (Goldberg, 1976);

- no significant Co distribution was detected at Ongeama during the present study.

According to Andrew (1980, 1984) the composition of the sulphide ore and the progressive geochemical changes during supergene alteration have a fundamental influence on the ultimate composition of the corresponding gossan. The ratio of pyrite and/or pyrrhotite versus matrix sulphides (e.g., chalcopyrite, sphalerite) in massive ore is proportional to the acid production during oxidation, to leaching and consequent dispersion of metals in groundwater. Insufficient acid buffering dependent on a chemically inert gangue, such as quartzite, further promotes metal dispersion. However, where sulphides are less abundant, e.g. in disseminated to semi-massive mineralization, at Ongeama and Ongombo, and in other deposits in the Matchless Belt, acid leaching can be less pronounced and higher concentrations of trace metals are retained in the corresponding gossan. This may be a reason for the preservation of well defined zoning in the deposits examined.

Hydrous Mn oxides compete with Fe-hydroxides for trace metal ions amenable to adsorption (Rose et al., 1979). Significant association of Mn with Zn and Cu in both "proximal" and "distal" positions may be, in fact, of secondary origin, as this association does not occur in unweathered ore. The significant Cu-Zn association, probably due to the exsolution of sphalerite in chalcopyrite and viceversa (see Section 3.3.3 Part C), may be enhanced during gossan formation by co-precipitation of the two metals with Fe- and Mn-hydroxides.

In spite of metamorphism and deformation, the geochemical zoning revealed in this study is comparable with that observed in ancient and present-day seafloor volcanogenic polymetallic sulphide deposits. In these deposits, a high-temperature Cu(-Zn)-rich core typically grades into lower-temperature Zn-Pb-Ba-rich margins (Bischoff et al., 1983; Hoy et al., 1984; Peter and Scott, 1988; Embley et al., 1988; Barrett et al., 1988; Lydon, 1988). In currently forming sulphide deposits, the development of metal zoning appears to be a gradual process. Zoning is dependent on redox potential and temperature variations, and, partly, on selective remobilization of metal ions during the interaction of high-temperature solutions with massive sulphides previously deposited (Janecky and Shanks, 1988).

In the deposits considered in this study, the pronounced lateral zonation of elements and the high metal values in either the central or thicker portion of the mineralized bodies are probably due to an original depositional configuration. Although the patterns of zoning may also be the result of deformation, the coincidence of the zonation patterns observed with the development of unusual rock types, previously referred to as alteration zone, cannot be explained by simple tectonic deformation.

The occurrence of Au enrichment in either "proximal", high-temperature ore facies (massive sulphide ore) or in "distal", lower-temperature ore facies (exhalite), as seen in the major and minor gossan outcrop at Ongeama respectively, is believed to be a function of the different chemistry of the ore-bearing fluids (Hannington and Scott, 1988). Au is deposited from a bisulphide complex in pyritic Zn-Pb-Ba-Ag-SiO_2 assemblages at lower temperatures (less than 300°C), at high oxygen and sulphur activity and near-neutral pH. At temperatures higher than 300°, the metal is deposited from chloride complexes in sulphur-poorer, Cu-rich assemblages, characteristic of low-pH, high-salinity fluids. Therefore, the Au increase in the magnetite quartzite, the concomitant overall Ag enrichment in the minor gossan outcrop relative to the major gossan (see Section 2.1 above for details), suggests that the former could be the surface expression of a well defined mineralizing system. This mineralizing system may be distinct from that represented by the major gossan outcrop, which is characterized by a different fluid chemistry.

The differences in the geochemistry of the schists within the assumed alteration zones, compared with the country rocks, and the existence of lateral and axial zoning of elements within the discordant alteration pipes, can be considered as definitive evidence of a hydrothermal origin of the latter. The elements involved in the zoning are Cu, Zn, Ba, Au, As, Zr, Ni, Co, Cr, Rb, Sr, Sn and Bi (see Sect. 2.4 above and Fig. 47). The alteration pipes at both Ongeama and Matchless West Extension are characterized by Rb and Sr depletion relative to the country-rock schists. Because of the affinities of Rb with K and Sr with Ca and Ba (Wedepohl, 1969), Rb and Sr variations may monitor variations in alkalis in rocks. In the alteration pipes examined, the Rb and Sr depletion significantly coincides with the

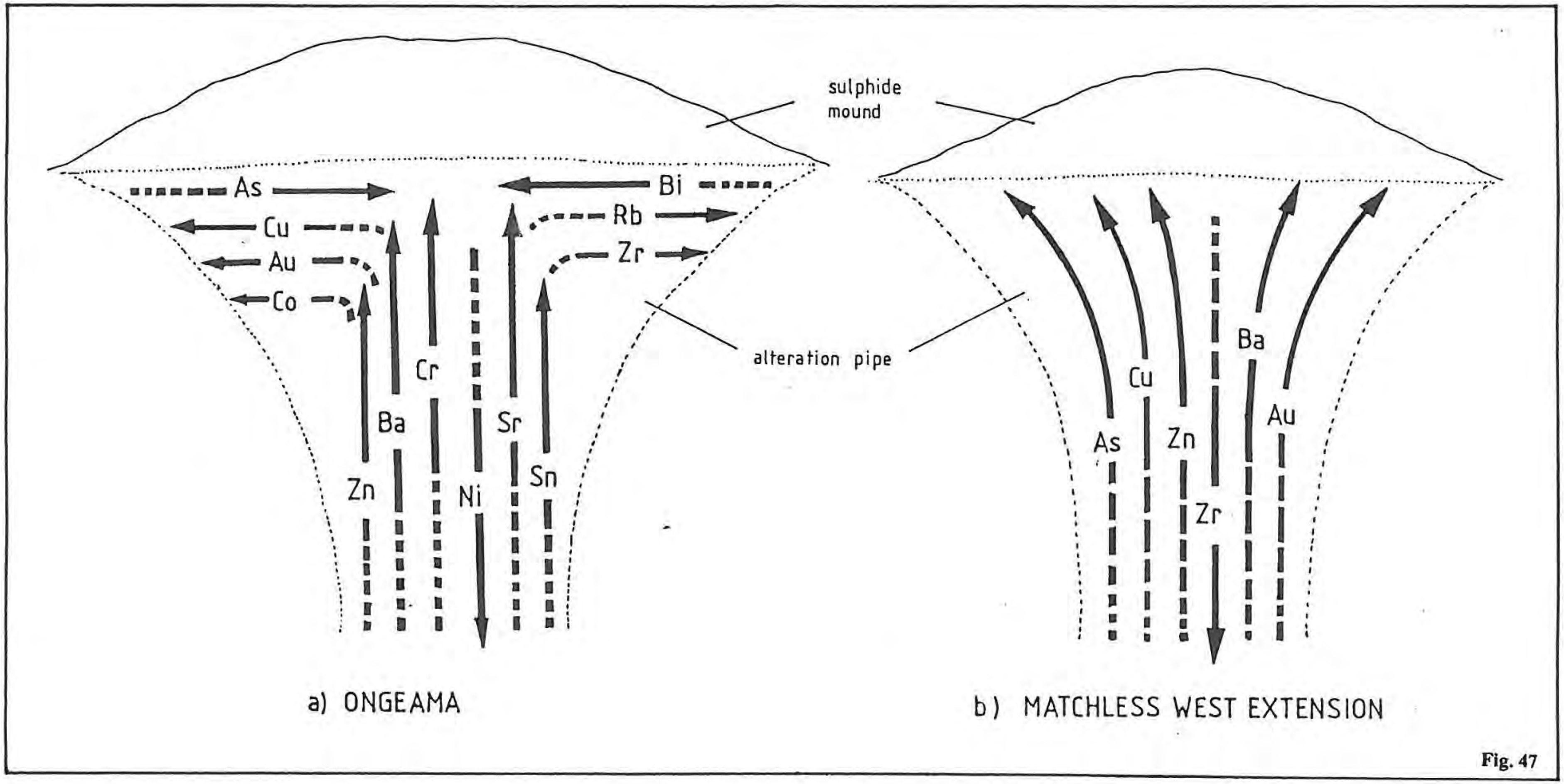

Fig. 47 - Scheme of the geochemical zonation within the alteration pipe at Ongeama (a) and Matchless West Extension (b). Arrows indicate the direction of increasing abundance of the corresponding elements.

alakali depletion and the absence of plagioclase and, at Ongeama, with the occurrence of chloritoid. The latter is an index mineral for a low-alkali chemical environment (Deer et al., 1982). Alkali depletion along hydrothermal alteration pipes is due to hydrolysis of rock-forming minerals by means of interaction between high-temperature acidic solutions and wall rocks. This is a common feature in volcanogenic sulphide deposits. The lesser Sr depletion, relative to Rb, recorded at Ongeama and the type of Sr distribution observed at Matchless West Extension suggest a limited association of Sr also with Ba.

The alteration index, proposed by Haussinger and Okrusch (1990) as a discriminator between altered and unaltered turbidite schists, was tested in this study on the alteration zones at Ongeama and Matchless West Extension. It is concluded that the use of this index is effective. With this assumption, the diagrams obtained for the h/w chloritized schists in the Ongombo drillcores (Fig. 44b) further indicate that the chloritization, and the subordinate magnetite + sulphide disseminations, are not caused by ore-related hydrothermal alteration. Given the spatial association of chloritization with the mafic intercalations in the h/w schist sequence, it is contended that these modifications originate from contact metasomatic processes induced by sheet-like mafic intrusions in H_2O-rich deep-sea sediments. The values of the alteration index suggest that also the magnetite-bearing schists from the "I anomaly" (Fig. 44a and 44c) do not correspond to any ore-related hydrothermal alteration.

Apart from the alteration index, the use of base metals and Ba, together with Cr and Ni, is also effective in discriminating between different ultramafic rock types and in revealing the exhalative nature of the ultramafic schists at Matchless West Extension.

PART E

CONCLUSIONS

1 GENERAL DISCUSSION

The aims of this study were to:

a) evaluate the effects of metamorphism and the significance of mineralogical changes in both mineralization and wall rocks;

b) interpret the mineralogical changes and related geochemical patterns in the mineralization and wall rocks;

c) attempt and relate these patterns to an original geochemical signature using examples from similar present-day sulphide deposits.

Sulphide mineralization in the Matchless Amphibolite Belt is generally attributed to a Besshi-type genetic model according to Fox's (1984) definition (e.g. Breitkopf and Maiden, 1988). In the belt, mineralization consists of sediment-hosted cupriferous iron sulphide deposits, associated with mafic rocks, and containing primarily pyrrhotite and/or pyrite, chalcopyrite and sphalerite. This mineralization is thought to have formed within a narrow, oceanic basin, the Matchless Trough, in which abundant terrigenous sediments accumulated. The present-day Guaymas Basin (Gulf of California) may be a modern example of this tectonic setting (Lonsdale and Becker, 1985) (see Fig. 8 for location).

The main features observed in the sulphide deposits at Ongeama, Matchless West Extension and, only in part, Ongombo, can be summarized as follows:

a) the presence of a discordant, pipe-like feature in the schists enclosing the mineralized horizon. This discordant feature is distinct from the country rocks, and is characterized by mineralogical and metal zoning. This feature is interpreted as an originally typical, inverted cone-shaped footwall alteration pipe;

- the presence of massive to semi-massive sulphide mineralization rich in silica, but characterized by Mg-rich minerals (talc, anthophyllite) and high Fe, Cu and Zn contents in its original high-temperature portion adjacent to the assumed alteration pipe (syn-discharge deposit; Bonatti, 1983);

- the presence of a Pb-Zn-Ba-enriched ferruginous siliceous cap consisting of metamorphosed chemical oxide sediments, locally interlayered with sulphide lenses (post-discharge deposit; Bonatti, 1983).

The results of this study indicate that the sulphide deposits at Ongeama, Matchless West Extension and Ongombo originated as sulphide mounds. A good example is afforded by the small sulphide body at Matchless West Extension, in which a sulphide mound configuration is suggested by:

1) the rapid lateral zonation in rock types;

2) the development of the massive sulphide portion above the vent;

3) the peripheral location of oxidized chemical sediments.

The formation of this deposit was probably due to a very short-lived hydrothermal system (see below).

At Ongeama and Ongombo the evidence for sulphide mounds is less compelling. The elongated nature of the mineralization in these two sites, and, especially at Ongeama, the development of an elongated massive sulphide lens in the basal portion of the ore zone, overlain by an almost continous exhalite horizon, may indicate that these two deposits formed from density-stratified brine-pools. However, this hypothesis may not be feasible. There is some geochemical evidence that the eastern sector of the original Matchless Trough, where Ongeama and Ongombo are situated, was in fact characterized by a fast spreading rate, and that conditions of full ocean opening were approached (Breitkopf and Maiden, 1988). Apart from considerations of fluid density, a fast spreading rate would not allow the formation of long-lived topographic depressions within which brines can pond over a lengthy period.

At Ongeama, the occurrence of specific ore rock types (i.e. the porous cupriferous anthophyllite-bearing semimassive facies) which only occur proximal to the vent, is suggestive of a mound-like zone. A more sustained, and probably episodic hydrothermal activity, compared to that at Matchless West Extension, would have been responsible for the lateral accretion of the sulphide body by means of:

a) lateral accumulation of massive sulphide detritus resulting from the disaggregation of inactive chimneys;
b) leaking of ore-bearing fluids through the relatively porous structure of the accreting sulphide mound.

The overall banded nature of the massive-sulphide ore and the common occurrence of phyllitic lenses in it suggest an original roughly bedded, clastic detrital ore deposition at the sides of the mound (sulphide talus).

Similar considerations may be applicable to the Ongombo deposit, if the anthophyllite and corresponding metal enrichment in the western extension of the Central Shoot are regarded as indicative of proximity to a discharge vent.

The extremely elongate lens-like shape of the Ongeama and Ongombo deposits is interpreted to be the result of tectonic stretching. This, coupled with metamorphic recrystallization, may be responsible for the textural homogenization of the mineralization.

Based on the geological, mineralogical and geochemical characteristics discussed in this study, a general model that may account for the formation of these sulphide deposits, is represented in Fig. 48.

The model shown in Fig. 48 considers the interaction between fracture zones and the basaltic sill-sediment complex (Einsele et al., 1980; Einsele, 1985). According to this model, the effect of sills intruding soft sediments results in a strong decrease in porosity, contact metamorphism ("baking" of the enclosing sediments), decomposition of organic matter and expulsion of metal-enriched, hot pore-fluids. Three distinct, but superimposed, hydrothermal circulation systems can be considered (Einsele et al., 1980; Lonsdale and Becker, 1985):

a) short-lived expulsion of pore water, as a result of the intrusion of shallow mafic sills;

b) a more sustained and important deep-seated circulation, probably due to a cooling magma chamber: this circulation discharges at high temperature through fractures in the overlying sills;

c) slowly recharging hydrothermal convection within the sediments overlying the shallows sills, possibly driven by heating from still-hot intrusions.

The main recharge to the system would occur along major rift-bounding faults. The discharge is necessarily focussed along faults or fracture zones which intersect the otherwise impermeable cap of mafic sills, and along which also the sedimentary cover is more permeable. Lonsdale and Becker (1985) noticed that in present-day, heavily sedimented oceanic basins, mineralization overlies zones of high permeability (faults) in the igneous rocks, and is not formed because the fluids rise along faults in the superficial sediments.

One possible source for ore-bearing solutions is seawater modified and enriched with metals by reaction with basaltic rocks at water/rock ratios between 16 and 22 (Reed, 1983). The other possible source for metals is magmatic. This is shown by the enrichment of volcanogenic

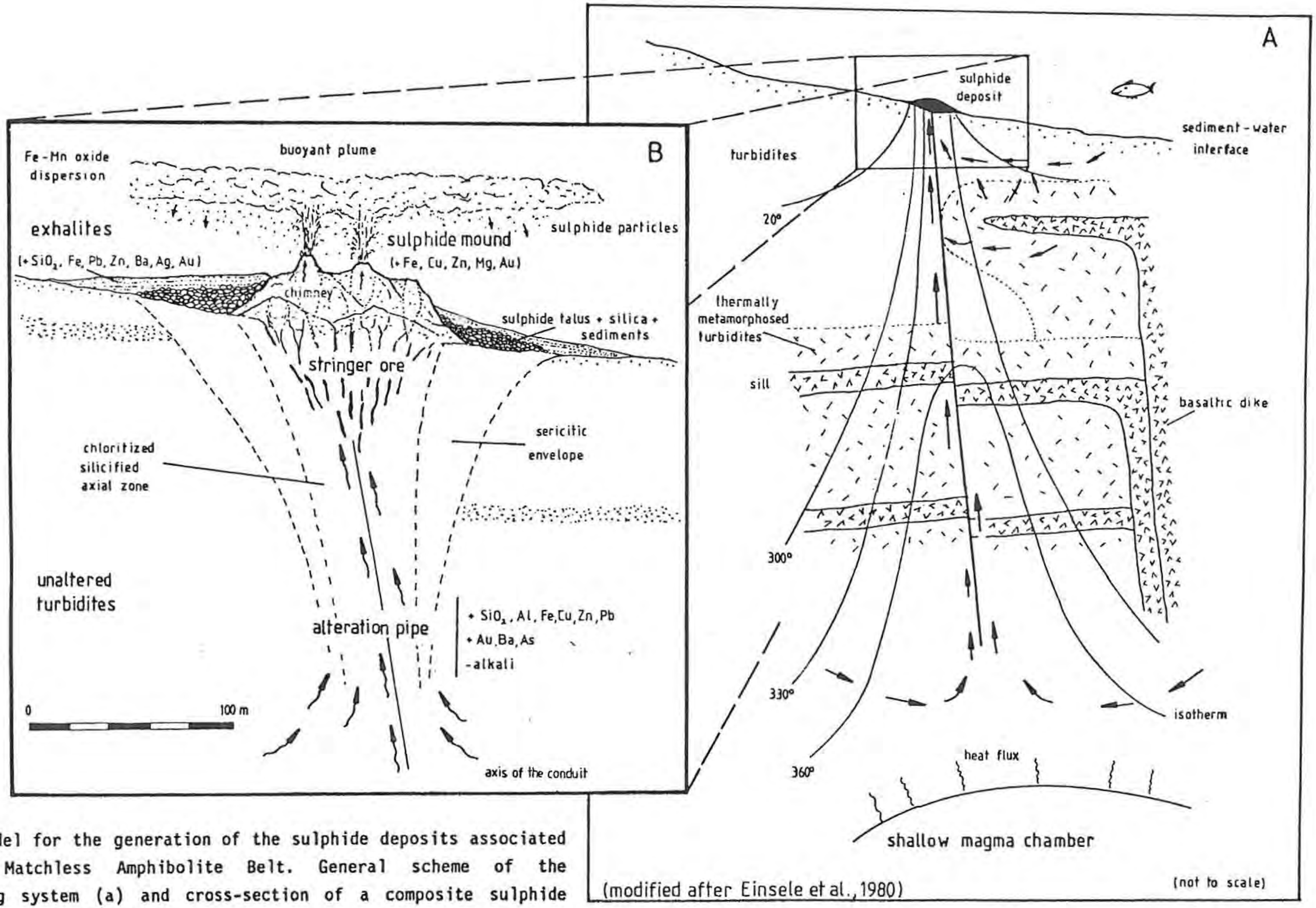

Fig. 48 - Model for the generation of the sulphide deposits associated with the Matchless Amphibolite Belt. General scheme of the mineralizing system (a) and cross-section of a composite sulphide mound (e.g., Ongeama) (b).

helium (^3He) in the bottom waters next to discharge sites in the Guaymas Basin (Lupton, 1979). Sulphur-isotope analyses of the Otjihase mineralization (chalcopyrite and pyrite) give $\delta^{34}S$ values ranging from +7.9‰ to +9.4‰ (Pirajno, pers. comm., 1990). On the basis of a sulphur-isotope research programme being conducted by F. Pirajno (Rhodes University) and J. Kinnaird and A. Fallick (St. Andrews University, Scotland) on different types of sulphide-bearing mineralization in Namibia, it appears that the above values for Otjihase may be interpreted as mixing between magmatic sulphur ($\delta^{34}S$ from -2‰ to +5‰) and seawater-derived sulphur ($\delta^{34}S$ approximately +20‰).

The Cu-Zn-rich sulphide accumulations were formed at the sediment-water interface by short-lived to sustained discharge of hot (150-350^{o}C) metal-bearing fluids. Evidence of episodic hydrothermal activity may be seen in the alternation of sulphide mineralization with magnetite quartzite observed at Ongombo (see Part B and C). Boiling probably did not occur because of the high hydrostatic pressure at the seafloor (Plimer, 1981). Although it is established that metamorphic desulphurization can turn pyrite into pyrrhotite, the metamorphic grade here is rather low for this to have happened (McDonald, 1967). The interaction between ore-bearing fluids and reducing organic matter may account for an original pyrrhotite-rich nature of the mineralization. Organic matter, as hydrothermal petroleum condensates associated with mineralization, occurs at the discharge sites in the Guaymas Basin and in the Escanaba Trough (Simoneit and Lonsdale, 1982; Von Damm et al., 1985; Koski et al., 1988). Graphitic schists relatively proximal to the mineralization at Ongeama (Hoffmann, 1976) and at Otjihase (Thomson, 1989) may have had the same origin.

A rapid and short-lived discharge is inferred for the sulphide deposits at Matchless West Extension. This is suggested by the size of the deposit, and the strong talc enrichment. According to Lonsdale et al. (1980), rapid, unidirectional and focussed fluid motion along the hydrothermal conduit can explain the preservation of high Mg concentrations in the discharged fluid. In recirculating hydrothermal systems Mg can be partly extracted at depth by rock alteration reactions. Costa et al. (1983) explained similar talc enrichments at Mattagami as being caused by turbulent mixing of hot saline fluids with Mg-rich seawater.

Along the fluid conduit, where steep thermal gradients are encountered, ion exchange reactions between metal-bearing solutions and wall rocks would cause a variable degree of hydrothermal alteration with intensity decreasing with distance from the conduit. Silicification, addition of metals (Fe, Cu, Zn, Pb, Ba, etc.) and depletion in alkalis due to hydrolysis of rock-forming minerals, are the main characteristics of the alteration zone.

The exhalative activity probably developed in conjunction with an active magmatic phase, as observed in present-day oceanic environments (Einsele et al., 1980; Kappel and Franklin, 1989).

A metamorphosed equivalent of sill-sediment complex associated with the mineralization is well preserved in the eastern Windhoek sector of the Matchless Belt. Ongeama and Ongombo, for example, display a sequence of mafic and metaturbidite rocks in their structural hangingwall (i.e. stratigraphic footwall).

Evidence revealed in this study indicates that the sequence at Matchless West Extension, and at Matchless Mine is the right way up. this indicates that a thick volcano-sedimentary pile is present only in the hangingwall of the mineralization (see Fig. 12). Although exhalative activity might have preceded the magmatic activity (Smalley, 1990, unpubl.), thrusting along the Colvania Horizon might have been responsible for the slicing-off of an original sill-sediment complex in the footwall of the sulphide deposits. This appears to be confirmed by the width of the Matchless Amphibolite Belt in the western Windhoek sector (where Matchless West Extension and Matchless Mine are situated), which is less than that in the Eastern Windhoek Sector (where Ongeama, Ongombo and Otjihase occur).

2 IMPLICATIONS FOR EXPLORATION

During metamorphism, the mineralization and associated hydrothermal alteration behaved as a closed system, i.e. their components experienced very limited chemical diffusion. This favoured the preservation of the main original features and of the zoned element distribution, as outlined in this study. Therefore, important implications for exploration are that some of the characteristics of hydrothermal alteration zones, even if overprinted by metamorphism and disrupted by tectonism, may still be recognized.

In the case of exploration for blind volcanogenic mineralization in metamorphic terranes, the detection of hydrothermal alteration is fundamental in indicating the proximity to the mineralization during follow-up operations. The alteration zone is characterized by both mineralogical and geochemical variations with respect to the country rocks. Although mineralogical changes can be easily detectable during detailed mapping, this study has shown that, in some cases, the original pre-metamorphic hydrothermal alteration can be recognized by means of subtle changes (e.g. the change in colour of biotite under the microscope, as at Ongombo). The geochemical variations detected are comparable to the general geochemical patterns observed in modern and ancient volcanogenic mineralized systems.

It is emphasized that a combination of mineralogical and geochemical factors is required to distinguish successfully between ore-related alteration and alteration-like features induced by other processes, not related to ore-formation.

The careful evaluation of selected geochemical data and the use of alteration indices are useful and effective exploration tools. These help in determinating the potential for mineralization.

In metamorphosed terranes, where deformation has modified most of the original sedimentary and volcanic structures, and where reliable markers are rare, the determination of the stratigraphic position of the alteration zone relative to the mineralization is of foremost importance for the interpretation of the structure and the way up of the strata in the explored area.

REFERENCES

ADAMSON R.G., TEICHMAN R.F.H. (1986) - The Matchless cupreous pyrite deposit, South West Africa/Namibia. In: Anhaeusser C.R., Maske S. (Eds.) "Mineral deposits of Southern Africa", Geol. Soc. S. Afr., Vol. II, 1755-1760.

AGGARWAL P.K., NESBITT B.E. (1984) - Geology and geochemistry of the Chu Chua massive sulphide deposit, British Columbia. Econ. Geol., 79, 813-825.

ANDREW R.L. (1980) - Supergene alteration and gossan textures of base-metal ores in Southern Africa. Minerals Sci. Engng., v.12, n.4, 193-215.

ANDREW R.L. (1984) - The geochemistry of selected base-metal gossans, Southern Africa. J. Geochem. Expl., 22, 161-192.

BARD J.P. (1980) - Microtextures des roches magmatiques et metamorphiques. Masson, 192 pp..

BARNES S.-J. (1983) - Pan-African serpentinites in central South West Africa/Namibia and the chemical classification of serpentinites. Geol. Soc. S. Afr. Spec. Publ., 11, 147-155.

BARRETT T.J., WARES R.P., FOX J.S. (1988) - Two-stage hydrothermal formation of a Lower Proterozoic sediment-hosted massive sulphide deposit, Northern Labrador Trough, Quebec. Can. Miner., 26, 871-888.

BISCHOFF J.L., ROSENBAUER R.J., ARUSCAVAGE P.J., BAEDECKER P.A., CROCK J.G. (1983) - Seafloor massive sulphide deposits from 21°N, East Pacific Rise, Juan da Fuca Ridge and Galapagos Rift: bulk chemical composition and economic implications. Econ. Geol., 78, 1711-1720.

BLAIN C.F., ANDREW R.L. (1977) - Sulphide weathering and the evaluation of gossans in mineral exploration. Minerals Sci. Engng., v.9, n.3, 119-150.

BLANCHARD R. (1968) - Interpretation of leached outcrops. Bull. 66, Nevada Bureau of Mines, 196 pp..

BONATTI E. (1983) - Hydrothermal metal deposits from the oceanic rifts: a classification. In: Rona P.A., Bostrom K., Lambier L., Smith K.J.jr. (Eds.) "Hydrothermal processes at seafloor spreading centers. Plenum Press, 796 pp..

BORG G. (1988) - The Koras-Sinclair-Ganzi rift in Southern Africa. Volcanism, sedimentation, age relationships and geophysical signature of a late-middle Proterozoic rift system. Prec. Res., 38, 75-90.

BREITKOPF J.H. (1988) - Iron formations related to mafic volcanism and ensialic rifting in the Southern Marginal Zone of the Damara Orogen, Namibia. Prec. Res., 38 , 111-130.

BREITKOPF J.H., MAIDEN K.J. (1986) - A volcanogenic exhalative iron formation in the Southern Marginal Zone of the Damara Orogen. Communs. Geol. Surv. SW Africa/Namibia, 2, 131-143.

BREITKOPF J.M., MAIDEN K.J. (1987) - Geochemical patterns of metabasites in the southern part of the Damara Orogen, South West Africa/Namibia: applicability to the recognition of tectonic environment. Geol. Soc. London Spec. Publ., 33, 355-361.

BREITKOPF J.M., MAIDEN K.J. (1988) - Tectonic setting of the Matchless Belt pyritic copper deposits, Namibia. Econ. Geol., 83, 710-723.

COSTA U.R., BARNETT R.L., KERRICH R. (1983) - The Matagami Lake Mine Archean Zn-Cu sulphide deposit, Quebec: hydrothermal coprecipitation of talc and sulphides in a sea-floor brine pool - evidence from geochemistry, $^{18}O/^{16}O$ and mineral chemistry. Econ. Geol., 78, 1144-1203.

COX S.F., ETHERIDGE M.A., HOBBS B.E. (1981) -The experimental ductile deformation of polycrystalline and single crystal pyrite. Econ. Geol., 76, 2105-2117.

DEER W.A., HOWIE R.A., ZUSSMANN J. (1982) - Rock-forming minerals. Vol. 1A - Orthosilicates. 2nd edition, Longman, 919 pp.

DOWNING K.N., COWARD M.P. (1981) - The Okahandja Lineament and its significance for the Damaran tectonics in Namibia. Geologische Rundschau, Band 70, 972-1000.

EALES H.V., MARSH J.S., COX K.G. (1984) - The Karoo igneous province: an introduction. Geol. Soc. S. Afr. Spec. Publ., 13, 1-26.

EINSELE G., GIEKES J.M., CURRAY J., MOORE D.G., AGUAYO E., KASTNER M., KALTS K., LYLE M., MATOBA Y., MOLINA-CRUZ A., NIEMTZ J., RUEDA J., SAUNDERS A., SCHRADER H., SIMONEIT B., VAQUIER V. (1980) - Intrusion of basaltic sills into highly porous sediments, and resulting hydrothermal activity. Nature, 283, 441-445.

EINSELE G. (1985) - Basaltic sill-sediment complexes in young spreading centres: genesis and significance. Geology, 13, 249-252.

EMBLEY R.W., JONASSON I.R., PERFIT J.M., TIVEY M.A., MALAHOFF A., SMITH M.F., FRANCIS T.J.G. (1988) - Submersible investigation of an extinct hydrothermal system on the Galapagos Ridge: sulphide mounds, stockwork zone and differentiated lavas. Can. Miner., 26, 517-539.

FINNEMORE S.H. (1974) - Geology of the Elisenheim area, Windhoek district, South West Africa, with special reference to the Matchless Amphibolite Belt. Unpubl. B.Sc.(Hons) thesis, Rhodes University, Grahamstown, 72 pp..

FINLOW-BATES T., STUMPFL E.F. (1981) - The behaviour of the so-called immobile elements in hydrothermally altered rocks associated with volcanogenic submarine-exhalative ore deposits. Miner. Deposita, 16, 319-328.

FINNEMORE S.H. (1978) - The geochemistry and origin of the Matchless Amphibolite Belt, Windhoek district, South West Africa. In: Verwoerd W.J. (Ed.) "Mineralization in metamorphic terranes", Geocongress 75, Stellenbosch, Geol. Soc. S. Afr., J.L. van Schaik Ltd., Pretoria, 433-447.

FOX J.S. (1984) - Besshi-type volcanogenic sulphide deposits - a review. CIM Bulletin, v.77, n.864, 57-68.

GAIR J.E., SLACK J.F. (1984) - Deformation, geochemistry and origin of massive sulphide deposits, Gossan Lead District, Virginia. Econ. Geol., 79, 1483-1520.

GOLDBERG I. (1976) - A preliminary account of the Otjihase copper deposit, South West Africa. Econ. Geol., 71, 384-390.

HALLWORTH B.A. (1989) - A report on the detailed mapping carried out at the Ongeama prospect, north-east of Windhoek, Namibia. Unpubl. M.Sc. project, Gold Fields Namibia-Camborne School of Mines, Cornwall, Great Britain.

HANNINGTON M.D., SCOTT S.D. (1988) - Gold mineralization in volcanogenic massive sulphide deposits: modern and ancient. Bicentennial Gold 88, Melbourne, May 1988, 353-358.

HAUSSINGER H., OKRUSCH M. (1990) - Petrology and geochemistry of metasediments hosting massive sulphide lenses at Gorob, Damara Orogen, Namibia. Abstr. Geocongress 90, Geol. Soc. S.Afr., Cape Town, 435-438.

HENDERSON P. (1982) - Inorganic geochemistry. Pergamon Press, 353 pp..

HERZIG P.M. (1986) - Barium in seafloor hydrothermal processes and its significance for exploration of Cyprus sulphide deposits. In:

Gallagher m.j., Ixer r.a., Neary C.r., Prichard H.M. (Eds.) "Metallogeny in basic and ultrabasic rocks", IMM, London, 499-506.

HERZIG P.M. (1988) - A mineralogical, geochemical and thermal profile through the Agrokipia "B" hydrothermal sulphide deposit, Troodos Ophiolite Complex, Cyprus. In: Friedrich G.H., Herzig P.M. (Eds.) "Base metal sulphide deposits", Springer Verlag, 182-215.

HOFFMANN K.H. (1976) - Re-examination of the Ongombo and Ongeama prospect, South West Africa. J.C.I. Exploration Research Unit - Rep. no. 16 (unpubl. report), 33 pp.

HOFFMANN K.H. (1990) - Sedimentary depositional history of the Damara Belt related to continental breakup, passive to active margin transition and foreland basin development. Abstr. Geocongress 90, Cape Town, 2-6- July 1990, 250-253.

HOY T., GIBSON G., BERG N.W. (1984) - Copper-zinc deposits associated with basic volcanism, Goldstream area, south-eastern British Columbia. Econ. Geol., 79, 789-814.

JAMES H.L. (1955) -Zones of regional metamorphism in the Precambrian of Northern Michigan. Bull. Geol. Soc. America, 66, 1455-1488.

JANECKY D.R., SHANKS W.C. III (1988) - Computational modeling of chemical and sulphur isotopic reaction processes in seafloor hydrothermal systems: chimneys, massive sulphides, and subjacent alteration zones. Can. Miner., 26, 805-825.

KANEHIRA K., TATSUMI T. (1970) - Bedded cupriferous iron sulphide deposits in Japan, a review. In: Tatsumi T. (Ed.) "Volcanism and ore genesis", Tokyo Univ. Press, 55-76.

KAPPEL E.S., FRANKLIN J.M. (1989) - Relationships between geologic development of ridge crests and sulphide deposits in the north-east Pacific Ocean. Econ. Geol., 84, 485-505.

KASCH K.W. (1983) - Regional P-T variations in the Damara Orogen with particular reference to early high-pressure metamorphism along the southern margin. Geol. Soc. S. Afr. Spec. Publ., 11, 243-253.

KELLY W.C., CLARK B.R. (1975) - Sulphide deformation studies: III. Experimental deformation of chalcopyrite to 2,000 bars and 500°C. Econ. Geol., 70, 431-453.

KILLICK A.M. (1983) - Sulphide mineralization at Gorob and its genetic relationship to the Matchless Member, Damara Sequence, SWA/Namibia. Geol. Soc. S.Afr. Spec. Publ., 11, 381-384.

KLEMD R., MAIDEN K.J., OKRUSCH M. (1987) - The Matchless copper deposit, South West Africa/Namibia: a deformed and metamorphosed massive sulphide deposit. Econ. Geol., 82, 587-599.

KLEMD R., MAIDEN K.J., OKRUSCH M., RICHTER P. (1989) - Geochemistry of the Matchless metamorphosed massive sulphide deposit, South West Africa/Namibia: wall rock alteration during submarine ore-forming processes. Econ. Geol., 84, 603-617.

KOSKI R.A., SHANKS W.C. III, BOHRSON W.A., OSCARSON R.L. (1988) - The composition of massive sulphide deposits from the sediment-covered floor of the Escanaba Trough, Gorda Ridge: implication for depositional processes. Can. Min., 26, 655-673.

KUKLA P.A., STANISTREET I.G. (1990) - Tectonic setting of the Late Proterozoic Khomas Hochland accretionary prism of the Damara Orogen, Central Namibia. Econ. Geol., Res. Unit, Inf. Circul., n.220, Wits University, Johannesburg.

LONSDALE P.F., BECKER K. (1985) - Hydrothermal plumes, hot springs and conductive heat flow in the Southern Trough of Guaymas Basin. Can. Miner., 26, 211-225.

LONSDALE P.F., BISCHOFF J.L., BURNS V.M., KASTNER M., SWEENEY R.E. (1980) - A high-temperature hydrothermal deposit on the seabed at a Gulf of California spreading center. Earth Plan. Sci. Lett., 49, 8-20.

LUPTON J.E. (1979) - Helium-3 in the Guaymas Basin: evidence for injection of mantle volatiles in the Gulf of California. J. Geophys. Res., 84, 7446-7452.

LYDON J.W. (1988) - Ore deposit models #14 - Volcanogenic massive sulphide deposits. Part 2: genetic models. Geosci. Canada, 15, 43-65.

MAIDEN K.J., CHICHIMBA L.R., SMALLEY T.J. (1986) - Cuspate ore-wallrock interfaces, piercement structures and the localization of some sulphide ores in deformed sulphide deposits. Econ. Geol., 81, 1464-1472.

MARTIN H. (1983) - Alternative geodynamic models for the Damara Orogeny. A critical discussion. In: Martin H., Eder F.W. (Eds.) "Intracontinental Fold Belts", Springer Verlag, 913 pp..

MARTIN H., PORADA H. (1977) - The intracratonic branch of the Damara Orogen in South West Africa. I. Discussion of geodynamic models. II. Discussion of relationships with the Pan African Mobile Belt system. Precambrian Res., 5, 311-338 and 339-357.

MASON R. (1981) - The Irumide Cycle. In: Hunter D.R. (Ed.) "Precambrian of the southern hemisphere". Developments in Precambrian Geology. Elsevier, 2, 669-675.

McCLAY K.R., ELLIS P.G. (1983) -Deformation and recrystallization of pyrite. Miner. Mag., 47, 527-538.

McLEOD R.L., STANTON R.L. (1984) - Phyllosilicates and associated minerals in some Palaeozoic stratiform sulphide deposits of Southern Australia. Econ. Geol., 79, 1-22.

MILLER R.McG. (1981) - Geology of the Damara Belt. Damara Excursion Guidebook. Geol. Soc. S. Afr., Geocongress 81, 115 pp..

MILLER R.McG. (1983a) - The Pan-African Damara Orogen of South West Africa/Namibia. Geol. Soc. S. Afr. Spec. Publ., 11, 431-515.

MILLER R.,McG. (1983b) - Tectonic implications of the contrasting geochemistry of the Damaran mafic volcanic rocks, South West Africa/Namibia. Geol. Soc. S. Afr. Spec. Publ., 11,115-138.

MILLER R.McG., BARNES S.-J., BALKWILL G. (1983) - Possible active margin deposits within the Southern Damara Orogen: the Kuiseb Formation between Okahandja and Windhoek. Spec. Publ. Geol. Soc. S. Afr., 11, 73-88.

MOODY J.B., MEYER D., JENKINS J.E. (1983) - Experimental characterization of the greenschist/amphibolite boundary in mafic systems. Am. Journ. Sci., 283, 48-92.

PETER J.M., SCOTT S.D. (1988) - Mineralogy, composition and fluid-inclusion microthermometry of seafloor hydrothermal deposits in the Southern Trough of Guaymas Basin, Gulf of California. Can. Min., 26, 567-587.

PITCHER W.S. (1982) - Granite type and tectonic environment. In: Hsu K.J. (Ed.) "Mountain building processes", Academic Press, 19-40.

PLIMER I.R. (1981) - Water depth - a critical factor for exhalative ore deposits. B.M.R. Journ. Australas. Geol. Geophys., 6, 293-300.

PLIMER I.R. (1986) - Sediment-hosted exhalative Pb-Zn deposits - products of contrasting ensialic rifting. Trans. Geol. Soc. S. Afr., 89, 57-73.

PORADA H. (1983) - Geodynamic model for the geosynclinal development of the Damara Orogen, Namibia, South West Africa. In: Martin H., Eder

F.W. (Eds.) "Intracontinental Fold Belts", Springer Verlag, 503-541.

PORADA H. (1985) - Stratigraphy and facies in the upper Proterozoic Damara Orogen, Namibia, based on a geodynamic model. Prec. Res., 29, 235-264.

PORADA H., WITTIG R. (1983) - Turbidites and their significance for the geosynclinal evolution of the Damaran Orogen, South West Africa/Namibia. Geol. Soc. S. Afr. Spec. Publ., 11, 21-36.

RAMDOHR P. (1980) - The ore minerals and their intergrowths. 2nd edition, Pergamon Press, 1205 pp..

REED M.H. (1983) - Seawater-basalt reaction and origin of greenstones and related ore deposits. Econ. Geol., 78, 466-485.

RICHARDS H.G., CANN J.R., JENSENIUS J. (1989) - Mineralogical zonation and metasomatism of the alteration pipes of Cyprus sulphide deposits. Econ. Geol., 84, 91-115.

ROSE A.W., HAWKES H.E., WEBB J.S. (1979) - Geochemistry in mineral exploration. 2nd Edition. Academic Press, 657 pp..

SANFORD R.F. (1982) - Growth of ultramafic reaction zones in greenschist to amphibolite facies metamorphism. Am. Journ. Sci., 282, 543-616.

SANGSTER D.F., SCOTT S.D. (1976) - Precambrian, strata-bound, massive Cu-Zn-Pb sulphide ores of North America. In: Wolf K.H. (Ed.) "Handbook of strata-bound and stratiform ore deposits. Vol.6, 129-222.

SCHIMDT A., WEDEPOHL K.H. (1983) - Chemical composition and genetic relations of the Matchless Amphibolite (Damara Orogenic Belt). Spec. Publ. Geol. Soc. S. Afr., 11, 139-145.

SIMONEIT B.R.T., LONSDALE P. (1982) - Hydrothermal petroleum in mineralized mounds at the seabed of Guaymas Basin - Nature, 295, 198-202.

SMALLEY T.J. (1988) - A genetic model for part of the Matchless Amphibolite Belt and its exploration significance. Abstr. Geocongress 88, Durban, Geol. Soc. S. Afr., 563-566.

SMALLEY T.J. (1990) - The Matchless West Extension cupreous pyrite deposit, Namibia: a field based study. Abstr. Geocongress 90, Cape Town, Geol. Soc. S. Afr., 514-517.

SPRY A. (1969) - Metamorphic textures. Pergamon Press, 350 pp..

STANTON R.L. (1972) - Ore petrology. McGraw-Hill, 713 pp..

STANTON R.L. (1982) - An alternative to the Barrovian interpretation ? Evidence from stratiform ores. Austral. Inst. Min. Metall., Proc. n. 282, 11-32.

TANKARD A.J., JACKSON M.P.A., ERIKSSON K.A.,HOBDAY D.K., HUNTER D.R., MINTER W.E.L. (1982) - Crustal evolution of Southern Africa: 3.8 billion years of earth history. Springer Verlag, New York, 523 pp.

THOMSON A. (1989) - The Otjihase massive sulphide deposit: a brief description. Tsumeb Corporation Limited (TCL), Otjihase Mine, unpubl. report.

VILJOEN R.P., VILJOEN M.J., GROOTENBOER J., LONGSHAW T.G. (1875) - ERTS-1 imagery: an appraisal of applications in geology and mineral exploration. Minerals Sci. Engng., 7, 132-168.

VON DAMM K.L., EDMOND J.M., MEASURES C.I., GRANT B. (1985) - Chemistry of submarine hydrothermal solutions at Guaymas Basin, Gulf of California. Geoch Cosmoc. Acta, 49, 2221-2237.

WINKLER H.G.F. (1979) - Petrogenesis of metamorphic rocks. Springer

Verlag, 348 pp..

YAGI K. (1969) - Petrology of the alkalic dolerites of the Nemuro Peninsula, Japan. In:Larsen l., Manson V., Prinz M. (Eds.) "Igneous and metamorphic geology", Geol. Soc. America, Memoir 115, 103-147.

ZIERENBERG R.A., SHANKS W.C. III (1983) - Mineralogy and geochemistry of epigenetic features in metalliferous sediments, Atlantis II Deep, Red Sea. Econ. Geol., 78, 57-72.

ZIERENBERG R.A., SHANKS W.C. III (1988) - Isotopic studies of epigenetic features in metalliferous sediments, Atlantis II Deep, Red Sea. Can. Miner., 26, 737-753.

APPENDIX A

Ongeama Prospect

Geological map of the gossan outcrop

Scala 1:1000

(in the back pocket)

APPENDIX B

Ongombo Prospect

Logs of the ore-bearing sequence in drill cores

Boreholes no. OGB 151A, OGB 152A,OGB 153A, OGB 154A

(in the back pocket)

APPENDIX C

LIST OF THE SAMPLES

Abbreviations used in the table:

QBC - quartz-biotite-chlorite schist	gossan. - gossanous
T1 - massive quartz-biotite schist	qtz - quartz
T2 - foliated quartz-biotite-muscovite-chlorite schist	chlor. - chlorite
T3 - contorted biotite-muscovite-chlorite-quartz schist	amph. - amphibole
QMP - quartz-muscovite-pyrite schist	magn. - magnetite
H/W - hangingwall (relative to the ore zone)	actin. - actinolite
F/W - footwall (relative to the ore zone)	sulph. - sulphide(s)
ES - Eastern Shoot (Ongombo)	carb. - carbonate
CS - Central Shoot (Ongombo)	epid. - epidote

ONGEAMA

----

sample no.	description	grid reference
OG 2	qtz-rich massive gossan	11060E/10240N
OG 3	qtz-rich massive gossan	11060E/10247N
OG 4	qtz-rich massive gossan	11040E/10239.5N
OG 5	qtz-rich massive gossan	11040E/10252.5N
OG 6	qtz-rich massive gossan	11020E/10241.7N
OG 7	ferruginous schist	11020E/10255N
OG 8	qtz-rich massive gossan	11000E/10245.5N
OG 9	qtz-rich massive gossan	10980E/10240.5N
OG 10	qtz-rich massive gossan	10960E/10250N
OG 11	qtz-rich massive gossan	10940E/10250N
OG 12	qtz-rich massive gossan	10920E/10255.3N
OG 13	magnetite quartzite	10900E/10240N
OG 14	magnetite quartzite	10900E/10250N
OG 15	qtz-rich massive gossan	10900E/10258.2N
OG 16	magnetite quartzite	10880E/10246N
OG 17	magnetite quartzite	10880E/10260.3N
OG 18	magnetite quartzite	10860E/10263N
OG 19	magnetite quartzite	10840E/10271N
OG 20	magnetite quartzite	10820E/10268.5N
OG 21	magnetite quartzite	10800E/10272.3N
OG 22	magnetite quartzite	10780E/10272.9N
OG 23	magnetite quartzite	10760E/10276N
OG 24	qtz-rich massive gossan	10760E/10273N
OG 25	ferruginous schist gossan	10720E/10253.3N
OG 26	qtz-rich massive gossan	10560E/10257.4N
OG 27	qtz-rich massive gossan	10540E/10244N
OG 28	qtz-rich massive gossan	10520E/10244N
OG 29	qtz-rich massive gossan	10500E/10252N
OG 30	ferruginous schist gossan	10500E/10250N
OG 31	qtz-rich massive gossan	10480E/10235.8N
OG 32	ferruginous schist gossan	10480E/10237N
OG 33	qtz-rich massive gossan	10460E/10230N
OG 34	magnetite quartzite	10460E/10232N
OG 35	qtz-rich massive gossan	10440E/10225N
OG 36	magnetite quartzite	10440E/10219N
OG 37	ferruginous schist gossan	10420E/10224N
OG 38	qtz-rich massive gossan	10420E/10220N
OG 39	magnetite quartzite	10420E/10214N
OG 40	ferruginous schist gossan	10400E/10222N
OG 41	qtz-rich massive gossan	10400E/10219N
OG 42	magnetite quartzite	10400E/10212N
OG 43	magnetic muscovite schist	10380E/10216N
OG 44	magnetite quartzite	10380E/10206N
OG 45	qtz-rich massive gossan	10380E/10212N
OG 46	magnetic muscovite schist	10360E/10213N
OG 47	qtz-rich massive gossan	10360E/10206N
OG 48	magnetite quartzite	10360E/10204N
OG 49	magnetic muscovite schist	10340E/10209N
OG 50	qtz-rich massive gossan	10340E/10205N
OG 51	magnetite quartzite	10340E/10200N
OG 52	magnetic muscovite schist	10320E/10203N
OG 53	qtz-rich massive gossan	10320E/10196.5N
OG 54	magnetite quartzite	10320E/10190N
OG 55	magnetic muscovite schist	10300E/10203N
OG 56	qtz-rich massive gossan	10300E/10194N
OG 57	magnetite quartzite	10300E/10187.5N
OG 58	magnetic muscovite schist	10280E/10201N
OG 59	qtz-rich massive gossan	10280E/10193N
OG 60	magnetite quartzite	10280E/10188N
OG 61	qtz-rich massive gossan	10277E/10197N
OG 62	magnetic muscovite schist	10260E/10201N
OG 63	semi-massive gossan	10260E/10197N
OG 64	ferruginous schist	10260E/10193N
OG 65	qtz-rich massive gossan	10260E/10199N
OG 66	magnetite quartzite	10260E/10182N
OG 67	magnetic muscovite schist	10240E/10189N
OG 68	semi-massive gossan	10240E/10182N
OG 69	magnetite quartzite	10240E/10177N
OG 70	qtz-rich massive gossan	10240E/10176N
OG 71	unmineralized QBC schist (F/W)	10240E/10168N
OG 72	semi-massive gossan	10220E/10180N
OG 73	magnetite quartzite	10220E/10172N
OG 74	qtz-rich massive gossan	10200E/10176.5N
OG 75	magnetic muscovite schist	10200E/10179N
OG 76	magnetic muscovite schist	10180E/10191N
OG 77	magnetic chlorite schists	10180E/10170N
OG 78	magnetic chlorite-muscovite schist	10180E/10166N
OG 79	semi-massive gossan	10180E/10165N
OG 80	magnetic chlorite schists	10160E/10190N
OG 81	magnetic chlorite schists	10160E/10180N
OG 82	qtz-rich massive gossan	10160E/10168N
OG 83	magnetite quartzite	10160E/10165N
OG 84	magnetic chlorite schists	10140E/10190N
OG 85	magnetic muscovite schist	10140E/10180N
OG 86	qtz-rich massive gossan	10140E/10172N
OG 87	magnetic chlorite schists	10120E/10196N
OG 88	magnetic muscovite schist	10120E/10190N
OG 89	ferruginous schist	10120E/10183N
OG 90	qtz-rich massive gossan	10120E/10181N
OG 91	magnetic chlorite schists	10100E/10202N
OG 92	magnetic muscovite schist	10100E/10198N
OG 93	magnetic muscovite schist	10100E/10193N
OG 94	qtz-rich massive gossan	10100E/10191N
OG 95	qtz-rich massive gossan	10100E/10170N
OG 96	magnetic chlorite schists	10080E/10197N
OG 97	qtz-rich massive gossan	10080E/10190N
OG 98	magnetic muscovite schist	10080E/10192N
OG 99	magnetic muscovite schist	10080E/10176N
OG 100	qtz-rich massive gossan	10080E/10172N
OG 101	magnetic muscovite schist	10060E/10192N
OG 102	qtz-rich massive gossan	10060E/10175N
OG 103	magnetite quartzite	10060E/10170N
OG 104	magnetic muscovite schist	10040E/10197N
OG 105	qtz-rich massive gossan	10040E/10194N
OG 106	magnetite quartzite	10040E/10191N
OG 107	magnetic muscovite schist	10040E/10184N
OG 108	qtz-rich massive gossan	10040E/10180N
OG 109	magnetic muscovite schist	10020E/10201N
OG 110	qtz-rich massive gossan	10020E/10196N
OG 111	magnetic muscovite schist	10000E/10202N
OG 112	qtz-rich massive gossan	10000E/10198N
OG 113	magnetic muscovite schist	9980E/10212N
OG 114	qtz-rich massive gossan	9975E/10210N
OG 115	qtz-rich massive gossan	9968E/10213N
OG 116	magnetic muscovite schist	9940E/10217N
OG 117	qtz-rich massive gossan	9940E/10213N
OG 118	qtz-rich massive gossan	9950E/10191N
OG 119	unmineralized QBC schist (H/W)	10920E/10270N
OG 120	mafic meta-lavas - upper layer	8400E/11160N
OG 121	mafic meta-lavas - upper layer	8090E/11100N
OG 122	mafic meta-lavas - central layer	8000E/10840N
OG 123	mafic meta-lavas - central layer	8180E/10860N
OG 124	mafic meta-lavas - central layer	8300E/10860N
OG 125	mafic meta-lavas - lower layer	8100E/10310N
OG 126	mafic meta-lavas - lower layer	8160E/10290N
OG 127	mafic meta-lavas - lower layer	8260E/10310N
OG 128	mafic meta-lavas - upper layer	8700E/11280N
OG 129	unmineralized QBC schist (F/W)	10700E/10164N
OG 130	unmineralized QBC schist (F/W)	10690E/10168N
OG 131	unmineralized QBC schist (F/W)	10400E/10120N
OG 132	unmineralized QBC schist (F/W)	10380E/10100N
OG 133	unmineralized QBC schist (H/W)	10360E/10300N
OG 134	unmineralized QBC schist (H/W)	10320E/10300N
OG 135	unmineralized QBC schist (H/W)	10290E/10255N
OG 136	unmineralized QBC schist (H/W)	10400E/10330N
OG 137	magnetic QB schist ("I" anomaly)	9900E/11125N
OG 138	magnetic chlorite-rich schist	9905E/11058N
OG 139	magnetic QB schist ("I" anomaly)	9909E/11030N
OG 140	magnetic QB schist ("I" anomaly)	9800E/11930N
OG 141	magnetic QB schist ("I" anomaly)	10100E/11100N
OG 142	magnetic QB schist ("I" anomaly)	10100E/11100N
OG 143	magnetic QB schist ("I" anomaly)	10100E/10150N

ONGOMBO GOSSAN

----

sample no.	description	grid reference
OG 144	magnetite quartzite	11900E/10220N
OG 145	magnetite quartzite	11820E/10220N
OG 146	magnetite quartzite	11740E/10225N
OG 147	magnetite quartzite	11650E/10200N
OG 148	magnetite quartzite	11525E/10175N
OG 149	magnetite quartzite	11475E/10175N
OG 150	magnetite quartzite	11425E/10170N
OG 151	magnetite quartzite	11100E/10150N
OG 152	magnetite quartzite	11050E/10150N
OG 153	magnetite quartzite	11000E/10135N
OG 154	magnetite quartzite	10950E/10135N
OG 155	magnetite quartzite	11150E/10150N
OG 156	magnetite quartzite (ES)	10850E/10150N
OG 157	magnetite quartzite (ES)	10830E/10150N
OG 158	magnetite quartzite (ES)	10810E/10150N
OG 159	magnetite quartzite (ES)	10790E/10150N

OG 160	magnetite quartzite (ES)	10770E/10150N
OG 161	magnetite quartzite (ES)	10750E/10160N
OG 162	magnetite quartzite (CS)	10730E/10160N
OG 163	magnetite quartzite (ES)	10710E/10160N
OG 164	magnetite quartzite (ES)	10690E/10160N
OG 165	magnetite quartzite (ES)	10670E/10160N
OG 166	magnetite quartzite (ES)	10650E/10160N
OG 167	magnetite quartzite (ES)	10630E/10170N
OG 168	magnetite quartzite (ES)	10610E/10170N
OG 169	magnetite quartzite	10525E/10175N
OG 170	magnetite quartzite	10400E/10180N
OG 171	magnetite quartzite	10250E/10170N
OG 172	magnetite quartzite	10200E/10170N
OG 173	magnetite quartzite	9960E/10040N
OG 174	magnetite quartzite	9910E/10045N
OG 175	magnetite quartzite	9860E/10060N
OG 176	magnetite quartzite	9820E/10070N
OG 177	magnetite quartzite	9770E/10100N
OG 178	magnetite quartzite (CS)	9640E/10100N
OG 179	magnetite quartzite (CS)	9620E/10095N
OG 180	magnetite quartzite (CS)	9600E/10090N
OG 181	magnetite quartzite (CS)	9580E/10085N
OG 182	magnetite quartzite (CS)	9560E/10080N
OG 183	magnetite quartzite (CS)	9540E/10075N
OG 184	magnetite quartzite (CS)	9520E/10075N
OG 185	magnetite quartzite (CS)	9500E/10070N
OG 186	magnetite quartzite (CS)	9480E/10070N
OG 187	magnetite quartzite (CS)	9460E/10065N
OG 188	magnetite quartzite (CS)	9440E/10065N
OG 189	magnetite quartzite (CS)	9420E/10060N
OG 190	magnetite quartzite (CS)	9400E/10060N
OG 191	magnetite quartzite (CS)	9380E/10055N
OG 192	magnetite quartzite (CS)	9360E/10055N
OG 193	amph.-rich magn. quartzite (CS)	9340E/10055N
OG 194	amph.-rich magn. quartzite (CS)	9320E/10050N
OG 195	magnetite quartzite (CS)	9300E/10045N
OG 196	amph.-rich magn. quartzite (CS)	9280E/10045N
OG 197	magnetite quartzite (CS)	9260E/10045N
OG 198	magnetite quartzite (CS)	9240E/10050N
OG 199	magnetite quartzite (CS)	9220E/10050N
OG 200	magnetite quartzite (CS)	9200E/10050N
OG 270	magnetite quartzite (CS)	9180E/10050N
OG 271	magnetite quartzite (CS)	9160E/10050N
OG 272	amph.-rich magn. quartzite (CS)	9140E/10050N
OG 273	amph.-rich magn. quartzite (CS)	9120E/10050N
OG 274	magnetite quartzite (CS)	9100E/10050N
OG 275	magnetite quartzite (CS)	9080E/10045N
OG 276	magnetite quartzite (CS)	9060E/10045N
OG 277	magnetite quartzite (CS)	9040E/10045N
OG 278	magnetite quartzite (CS)	9020E/10040N
OG 279	amph.-rich magn. quartzite (CS)	9000E/10040N
OG 280	magnetite quartzite (CS)	8980E/10040N
OG 281	amph.-rich magn. quartzite (CS)	8960E/10040N
OG 282	magnetite quartzite (CS)	8940E/10040N
OG 283	magnetite quartzite (CS)	8920E/10045N
OG 284	amph.-rich magn. quartzite (CS)	8900E/10050N
OG 285	amph.-rich magnetite quartzite	8850E/10020N
OG 286	amph.-rich magnetite quartzite	8800E/9980N
OG 287	amph.-rich magnetite quartzite	8750E/9980N
OG 288	magnetite quartzite	8700E/9980N
OG 289	amph.-rich magnetite quartzite	8650E/9980N
OG 290	amph.-rich magnetite quartzite	8600E/9970N
OG 291	amph.-rich magnetite quartzite	8550E/9950N
OG 292	amph.-rich magnetite quartzite	8500E/9925N
OG 293	magnetite quartzite	8450E/9900N
OG 294	magnetite quartzite	8400E/9900N
OG 295	magnetite quartzite	8350E/9900N
OG 296	amph.-rich magnetite quartzite	8300E/9900N
OG 297	magnetite quartzite	8250E/9925N
OG 298	amph.-rich magnetite quartzite	8200E/9950N
OG 299	magnetite quartzite	8150E/9970N
OG 300	amph.-rich magnetite quartzite	8100E/9970N
OG 301	magnetite quartzite	8050E/9980N
OG 302	magnetite quartzite	8000E/10000N
OG 303	magnetite quartzite	7950E/10000N
OG 304	magnetite quartzite	7920E/10000N
OG 305	magnetite quartzite	7850E/10000N
OG 306	magnetite quartzite	7800E/10000N
OG 307	magnetite quartzite	7750E/9970N
OG 308	magnetite quartzite	7700E/9950N
OG 309	amph.-rich magnetite quartzite	7650E/9940N
OG 310	amph.-rich magnetite quartzite	7600E/9920N
OG 311	magnetite quartzite	7550E/9900N
OG 312	magnetite quartzite	7500E/9830N
OG 313	magnetite quartzite	7450E/9810N
OG 314	magnetite quartzite	7400E/9800N
OG 315	magnetite quartzite	7350E/9800N
OG 316	magnetite quartzite	7250E/9800N
OG 317	magnetite quartzite	7200E/9780N
OG 318	magnetite quartzite	7150E/9780N
OG 319	magnetite quartzite	7100E/9770N
OG 320	magnetite quartzite	7050E/9740N
OG 321	magnetite quartzite	7000E/9720N

ONGOMBO - DRILLCORES
----

sample no.	description	depth (metres)
OG 322	OGB 153 A T2 T3	343.20-344.40 H/W
OG 323	OGB 153 A T1	344.40-344.79 H/W
OG 324	OGB 153 A T2	344.79-345.89 H/W
OG 325	OGB 153 A T3	345.89-346.68 H/W
OG 326	OGB 153 A T1	346.68-346.77 H/W
OG 327	OGB 153 A T2 T3	346.77-346.87 H/W
OG 328	OGB 153 A T1 T2	346.87-347.35 H/W
OG 329	OGB 153 A T3	347.35-347.60 H/W
OG 330	OGB 153 A T1 T2	347.60-348.35 H/W
OG 331	OGB 153 A T2 T3	348.35-349.14 H/W
OG 332	OGB 153 A T1 T2	349.14-349.60 H/W
OG 333	OGB 153 A T2	349.60/349.93 H/W
OG 334	OGB 153 A T3	349.93-350.27 H/W
OG 335	OGB 153 A T1 T2	350.27-350.38 H/W
OG 336	OGB 153 A T3	350.38-350.56 H/W
OG 337	OGB 153 A T2	350.56-350.92 H/W
OG 338	OGB 153 A T1 T2	350.92-351.47 H/W
OG 339	OGB 153 A T3	351.47-352.33 H/W
OG 340	OGB 153 A T2	352.33-353.65 H/W
OG 341	OGB 153 A T1	353.65-353.74 H/W
OG 342	OGB 153 A chlor. amph. schist	353.74-354.02 H/W
OG 343	OGB 153 A T1 T2	354.02-354.55 H/W
OG 344	OGB 153 A chlor. amph. schist	354.65-354.71 H/W
OG 345	OGB 153 A feldspatic amph.	354.71-355.57 H/W
OG 346	OGB 153 A chlor. amph. schist	355.57-356.30 H/W
OG 347	OGB 153 A T1 T2	356.30-356.45 H/W
OG 348	OGB 153 A T2	356.45-357.00 H/W
OG 349	OGB 153 A T1 T2	357.00-358.17 H/W
OG 350	OGB 153 A T2	358.17-358.375 H/W
OG 351	OGB 153 A chlor. amph. schist	358.375-359.18 H/W
OG 352	OGB 153 A T2	359.18-359.36 H/W
OG 353	OGB 153 A T2 (magn.)	359.36-359.53 H/W
OG 354	OGB 153 A T3	359.53-359.70 H/W
OG 355	OGB 153 A T1 T2 (magn.)	359.70-360.00 H/W
OG 356	OGB 153 A T1 T2	360.00-360.25 H/W
OG 357	OGB 153 A T2 (magn.)	360.25-360.685 H/W
OG 358	OGB 153 A T3	360.685-361.01 H.W
OG 359	OGB 153 A chlor. amph. schist	361.01-361.18 H/W
OG 360	OGB 153 A quartz vein	361.18-361.31 H/W
OG 361	OGB 153 A amphibolite	361.31-362.34 H/W
OG 362	OGB 153 A T1 T2	362.34-362.44 H/W
OG 363	OGB 153 A T2 T3	362.44-362.88 H/W
OG 364	OGB 153 A T3	362.88-363.00 H/W
OG 365	OGB 153 A T1 T2	369.27-370.26 F/W
OG 366	OGB 153 A T1	370.26-370.74 F/W
OG 367	OGB 153 A T2 T3	370.74-371.30 F/W
OG 368	OGB 153 A T3	371.30-372.36 F/W
OG 369	OGB 153 A T1	372.36-372.52 F/W
OG 370	OGB 153 A T1 T2	372.52.373.00 F/W
OG 371	OGB 153 A T3	373.00-374.00 F/W
OG 372	OGB 153 A T3	374.00-374.90 F/W
OG 373	OGB 153 A T1	374.90-375.00 F/W
OG 374	OGB 153 A T3	375.00-375.79 F/W
OG 375	OGB 153 A T2	375.79-377.50 F/W
OG 376	OGB 153 A T1 T2	377.50-377.82 F/W
OG 377	OGB 153 A T3	377.82-378.24 F/W
OG 378	OGB 153 A T1	378.24.379.00 F/W
OG 379	OGB 153 A T2 T3	379.00-379.44 F/W
OG 380	OGB 153 A T1 T2	379.44-379.60 F/W
OG 381	OGB 153 A T3	379.60-379.98 F/W
OG 382	OGB 153 A T1	379.98-380.20 F/W
OG 383	OGB 153 A T2	380.20-380.62 F/W
OG 384	OGB 151 A T2 T3	335.69-336.22 H/W
OG 385	OGB 151 A T1 T2	336.22-336.48 H/W
OG 386	OGB 151 A T2	336.48-340.39 H/W
OG 387	OGB 151 A T1 T2	340.39-340.90 H/W
OG 388	OGB 151 A T1	340.90-341.14 H/W
OG 389	OGB 151 A chlor. amph. schist	341.14-341.61 H/W
OG 390	OGB 151 A T1	341.61-342.82 H/W
OG 391	OGB 151 A T1 T2	342.82-345.67 H/W
OG 392	OGB 151 A T1	345.67-347.16 H/W
OG 393	OGB 151 A T1 (magn.)	347.16-347.20 H/W
OG 394	OGB 151 A T2	347.20-347.25 H/W
OG 395	OGB 151 A chlor. amph. schist	347.25-347.66 H/W
OG 396	OGB 151 A T2	347.66-348.23 H/W
OG 397	OGB 151 A chlor. amph. schist	348.23-348.35 H/W
OG 398	OGB 151 A T1 T2	348.35-349.55 H/W
OG 399	OGB 151 A T1	349.55-350.00 H/W
OG 400	OGB 151 A T1 T2	350.00-351.41 H/W
OG 601	OGB 151 A T2 T3	351.41-351.74 H/W
OG 602	OGB 151 A T3	351.74-351.83 H/W
OG 603	OGB 151 A T1 T2	351.83-352.27 H/W
OG 604	OGB 151 A T3	352.27-352.46 H/W
OG 605	OGB 151 A T1 T2	352.46-353.09 H/W
OG 606	OGB 151 A T3	353.09-353.56 H/W

OG 607	OGB 151 A T1 T2	353.56-354.00 H/W
OG 608	OGB 151 A chlor.-amph. schist	354.00-355.31 H/W
OG 609	OGB 151 A T1	355.31-355.38 H/W
OG 610	OGB 151 A T2 T3	355.38-355.93 H/W
OG 611	OGB 151 A T2 T3	362.66-363.05 F/W
OG 612	OGB 151 A T3	363.05-363.89 F/W
OG 613	OGB 151 A T2	363.89-364.12 F/W
OG 614	OGB 151 A T1	364.12-364.87 F/W
OG 615	OGB 151 A T2 T3	364.87-365.05 F/W
OG 616	OGB 151 A T1 T2	365.05-365.40 F/W
OG 617	OGB 151 A T3	365.40-365.82 F/W
OG 618	OGB 151 A T1	365.82-365.87 F/W
OG 619	OGB 151 A T3	365.87-367.18 F/W
OG 620	OGB 151 A T1	367.18-367.29 F/W
OG 621	OGB 151 A T3	367.29-367.63 F/W
OG 622	OGB 151 A T1 T2	367.63-368.00 F/W
OG 623	OGB 151 A T3	368.00-368.89 F/W
OG 624	OGB 151 A qtz vein + sulph.	368.63-368.73 F/W
OG 625	OGB 151 A T2	368.83-371.15 F/W
OG 626	OGB 151 A T1 T2	371.15-372.24 F/W
OG 627	OGB 151 A T2 T3	372.24-372.94 F/W
OG 628	OGB 151 A T1	372.94-373.44 F/W
OG 629	OGB 151 A T1 T2	373.44-375.32 F/W
OG 630	OGB 154 A T2	492.83-493.70 H/W
OG 631	OGB 154 A T2 T3	493.70-493.83 H/W
OG 632	OGB 154 A chlor. amph. schist	493.83-494.54 H/W
OG 632	OGB 154 A amphibolite	494.54-495.47 H/W
OG 633	OGB 154 A chlor. amph. schist	495.47-495.71 H/W
OG 634	OGB 154 A T2	495.71-496.70 H/W
OG 635	OGB 154 A T2 (magn.)	496.70-497.07 H/W
OG 636	OGB 154 A FA	497.07-497.12 H/W
OG 638	OGB 154 A T2 T3	497.12-497.68 H/W
OG 639	OGB 154 A T1	497.68-498.50 H/W
OG 640	OGB 154 A chlor.-amph. schist	498.50-498.62 H/W
OG 641	OGB 154 A T2	498.62-499.38 H/W
OG 642	OGB 154 A T2 (m)	499.38-499.56 H/W
OG 643	OGB 154 A amphibolite	499.56-501.15 H/W
OG 644	OGB 154 A amphibolite	501.15-502.64 H/W
OG 645	OGB 154 A chlor.-amph. schist + T1	502.64-502.73 H/W
OG 646	OGB 154 A T1	502.73-503.23 H/W
OG 647	OGB 154 A T2 T3	503.23-503.47 H/W
OG 648	OGB 154 A T1 T2	503.47-503.83 H/W
OG 649	OGB 154 A chlor. amph. schist	503.83-503.90 H/W
OG 650	OGB 154 A T1 T2	503.90-504.27 H/W
OG 651	OGB 154 A T2 T3	504.27-504.53 H/W
OG 652	OGB 154 A T1 T2	504.53-505.36 H/W
OG 653	OGB 154 A T2 T3	505.36-505.79 H/W
OG 654	OGB 154 A T3	505.79-506.48 H/W
OG 655	OGB 154 A T2 T3	506.48-507.40 H/W
OG 656	OGB 154 A T1 T2	507.40-507.68 H/W
OG 657	OGB 154 A T3	507.68-507.74 H/W
OG 658	OGB 154 A T1 T2	507.74-507.89 H/W
OG 659	OGB 154 A T2 T3	507.89-508.82 H/W
OG 660	OGB 154 A T2	510.21-511.00 F/W
OG 661	OGB 154 A T2 T3	511.00-511.71 F/W
OG 662	OGB 154 A T1 T2	511.71-512.04 F/W
OG 663	OGB 154 A T2 T3	512.04-512.19 F/W
OG 664	OGB 154 A T1	512.19-513.40 F/W
OG 665	OGB 154 A T2	513.40-514.49 F/W
OG 666	OGB 154 A T2 T3	514.49-515.48 F/W
OG 667	OGB 154 A T1	515.48-516.00 F/W
OG 668	OGB 154 A T2	516.00-517.18 F/W
OG 669	OGB 154 A T3	517.18-517.41 F/W
OG 670	OGB 154 A T1	517.41-517.66 F/W
OG 671	OGB 154 A T1 T2	517.66-517.91 F/W
OG 672	OGB 154 A T2 T3	517.91-518.95 F/W
OG 673	OGB 154 A T1 T2	518.95-519.29 F/W
OG 674	OGB 154 A T3	519.29-521.15 F/W

MATCHLESS WEST EXTENSION DEPOSIT

sample no.	description	grid reference
MWE 201	QMP schist	246/-5.5
MWE 202	QMP schist	246/-19
MWE 203	qtz-rich gossan	243/10
MWE 204	muscovite chlorite schist	240/-18
MWE 205	QMP schist	240/-13
MWE 206	QMP schist	235/-6
MWE 207	talc-rich gossan	235/10
MWE 208	magnetite quartzite	233/9.5
MWE 209	QMP schist	230/-11
MWE 210	QMP schist	221/-3.5
MWE 211	muscovite chlorite schist	224/1
MWE 212	qtz-rich gossan	218/10
MWE 213	qtz-rich gossan	208/6
MWE 214	QMP schist	208/-5
MWE 215	muscovite chlorite schist	210/-8
MWE 216	QMP schist	200/2.5
MWE 217	QMP schist	200/-3.5
MWE 218	qtz-rich massive gossan	192/6
MWE 219	QMP schist	190/5
MWE 220	QMP schist	191/-1
MWE 221	QMP schist	180/1
MWE 222	qtz-rich massive gossan	179/10
MWE 223	magnetite quartzite	179/12.5
MWE 224	QMP schist	171/6
MWE 225	magnetite quartzite	170/8.5
MWE 226	QMP schist	158/1
MWE 227	talc-actinolite schist	158/6
MWE 228	magnetite quartzite	160/8
MWE 229	QMP schist	147/1
MWE 230	magnetite quartzite	150/8
MWE 231	QMP+talc-actin. schist	140/6.5
MWE 232	QMP schist	138/3.5
MWE 233	gossan talc-actinolite schist	130/3.5
MWE 234	QMP schist	131/1
MWE 235	QMP schist	123.3
MWE 236	QMP+actinolite schist	123/4
MWE 237	QMP schist	110/2.5
MWE 238	QMP schist	103/1.5
MWE 239	chlor.-actin.-talc schist	103/3.5
MWE 240	magnetite quartzite	98/4
MWE 241	amph.-rich magnetite quartzite	95/3.5
MWE 242	magnetite quartzite	90/3.5
MWE 243	chlorite actinolite schist	89/2.5
MWE 244	magnetite quartzite	80/0
MWE 245	talc-actin.-carb. schist	83/3.5
MWE 246	talc-actin.-carb. schist	78.5/3.5
MWE 247	magnetite quartzite	81/5
MWE 248	gossan talc-actin. schist	69/3
MWE 249	amphib.-rich magnetite quartzite	72/6
MWE 250	magnetite quartzite	72/7
MWE 251	magnetite quartzite	61/3
MWE 252	gossan. talc-chlor. schist	61/4
MWE 253	magnetite quartzite	58/8
MWE 254	magnetite quartzite	51/6
MWE 255	gossan. talc-actin.-carb. schist	50/7.5
MWE 256	magnetite quartzite	53/11.5
MWE 257	magnetite quartzite	44/6.5
MWE 258	gossan. talc-actin.-chlor. schist	42/10
MWE 259	marble-like rock	17/13.5
MWE 260	magnetite quartzite	17/15
MAB 261	Friedenau amphibolite	see attached map
MAB 262	Friedenau amphibolite	see attached map
MAB 263	Friedenau amphibolite	see attached map
MAB 264	Matchless Mine Horizon amphibolite	see attached map
MAB 265	Matchless Mine Horizon amphibolite	see attached map
MAB 266	Matchless Mine Horizon amphibolite	see attached map
MAB 267	Friedenau amphibolite	see attached map
MAB 268	Friedenau amphibolite	see attached map
MAB 269	Friedenau amphibolite	see attached map

MAFIC AND ULTRAMAFIC ROCKS FROM THE OTJIHASE AREA

sample no.	description	location
OTJ 675	talc-actin. schist (coarse-gr.)	Otjihase
OTJ 676	talc-actin. schist (fine-gr.)	Otjihase
OTJ 677	metagabbro	Otjihase
OTJ 678	talc-carb. schist	Elisenheim
OTJ 679	talc-carb.-chlor. schist	Elisenheim 68
OTJ 680	chlor. actin. schist	Elisenheim 68
OTJ 681	talc schist	Elisenheim 68
OTJ 682	chlorite schist	Otjihase
OTJ 683	epid.-rich chlorite schist	Otjihase
OTJ 684	actinolite schist	Von Francois Ost 6
OTJ 685	chlor.-talc schist	Von Francois Ost 6
OTJ 686	talc-olivine(?)-magn. schist	Von Francois Ost 6

OG 669	OGB 154 A T3	517.18-517.41 F/W
OG 670	OGB 154 A T1	517.41-517.66 F/W
OG 671	OGB 154 A T1 T2	517.66-517.91 F/W
OG 672	OGB 154 A T2 T3	517.91-518.95 F/W
OG 673	OGB 154 A T1 T2	518.95-519.29 F/W
OG 674	OGB 154 A T3	519.29-521.15 F/W

MATCHLESS WEST EXTENSION DEPOSIT

sample no.	description	grid reference
MWE 201	QMP schist	246/-5.5
MWE 202	QMP schist	246/-19
MWE 203	qtz-rich gossan	243/10
MWE 204	muscovite chlorite schist	240/-18
MWE 205	QMP schist	240/-13
MWE 206	QMP schist	235/-6
MWE 207	talc-rich gossan	235/10
MWE 208	magnetite quartzite	233/9.5
MWE 209	QMP schist	230/-11
MWE 210	QMP schist	221/-3.5
MWE 211	muscovite chlorite schist	224/1
MWE 212	qtz-rich gossan	218/10
MWE 213	qtz-rich gossan	208/6
MWE 214	QMP schist	208/-5
MWE 215	muscovite chlorite schist	210/-8
MWE 216	QMP schist	200/2.5
MWE 217	QMP schist	200/-3.5
MWE 218	qtz-rich massive gossan	192/6
MWE 219	QMP schist	190/5
MWE 220	QMP schist	191/-1
MWE 221	QMP schist	180/1
MWE 222	qtz-rich massive gossan	179/10
MWE 223	magnetite quartzite	179/12.5
MWE 224	QMP schist	171/6
MWE 225	magnetite quartzite	170/8.5
MWE 226	QMP schist	158/1
MWE 227	talc-actinolite schist	158/6
MWE 228	magnetite quartzite	160/8
MWE 229	QMP schist	147/1
MWE 230	magnetite quartzite	150/8
MWE 231	QMP+talc-actin. schist	140/6.5
MWE 232	QMP schist	138/3.5
MWE 233	gossan talc-actinolite schist	130/3.5
MWE 234	QMP schist	131/1
MWE 235	QMP schist	123.3
MWE 236	QMP+actinolite schist	123/4
MWE 237	QMP schist	110/2.5
MWE 238	QMP schist	103/1.5
MWE 239	chlor.-actin.-talc schist	103/3.5
MWE 240	magnetite quartzite	98/4
MWE 241	amph.-rich magnetite quartzite	95/3.5
MWE 242	magnetite quartzite	90/3.5
MWE 243	chlorite actinolite schist	89/2.5
MWE 244	magnetite quartzite	80/0
MWE 245	talc-actin.-carb. schist	83/3.5
MWE 246	talc-actin.-carb. schist	78.5/3.5
MWE 247	magnetite quartzite	81/5
MWE 248	gossan talc-actin. schist	69/3

OG 607	OGB 151 A T1 T2	353.56-354.00 H/W
OG 608	OGB 151 A chlor.-amph. schist	354.00-355.31 H/W
OG 609	OGB 151 A T1	355.31-355.38 H/W
OG 610	OGB 151 A T2 T3	355.38-355.93 H/W
OG 611	OGB 151 A T2 T3	362.66-363.05 F/W
OG 612	OGB 151 A T3	363.05-363.89 F/W
OG 613	OGB 151 A T2	363.89-364.12 F/W
OG 614	OGB 151 A T1	364.12-364.87 F/W
OG 615	OGB 151 A T2 T3	364.87-365.05 F/W
OG 616	OGB 151 A T1 T2	365.05-365.40 F/W
OG 617	OGB 151 A T3	365.40-365.82 F/W
OG 618	OGB 151 A T1	365.82-365.87 F/W
OG 619	OGB 151 A T3	365.87-367.18 F/W
OG 620	OGB 151 A T1	367.18-367.29 F/W
OG 621	OGB 151 A T3	367.29-367.63 F/W
OG 622	OGB 151 A T1 T2	367.63-368.00 F/W
OG 623	OGB 151 A T3	368.00-368.89 F/W
OG 624	OGB 151 A qtz vein + sulph.	368.63-368.73 F/W
OG 625	OGB 151 A T2	368.83-371.15 F/W
OG 626	OGB 151 A T1 T2	371.15-372.24 F/W
OG 627	OGB 151 A T2 T3	372.24-372.94 F/W
OG 628	OGB 151 A T1	372.94-373.44 F/W
OG 629	OGB 151 A T1 T2	373.44-375.32 F/W
OG 630	OGB 154 A T2	492.83-493.70 H/W
OG 631	OGB 154 A T2 T3	493.70-493.83 H/W
OG 632	OGB 154 A chlor. amph. schist	493.83-494.54 H/W
OG 632	OGB 154 A amphibolite	494.54-495.47 H/W
OG 633	OGB 154 A chlor. amph. schist	495.47-495.71 H/W
OG 634	OGB 154 A T2	495.71-496.70 H/W
OG 635	OGB 154 A T2 (magn.)	496.70-497.07 H/W
OG 636	OGB 154 A FA	497.07-497.12 H/W
OG 638	OGB 154 A T2 T3	497.12-497.68 H/W
OG 639	OGB 154 A T1	497.68-498.50 H/W
OG 640	OGB 154 A chlor.-amph. schist	498.50-498.62 H/W
OG 641	OGB 154 A T2	498.62-499.38 H/W
OG 642	OGB 154 A T2 (m)	499.38-499.56 H/W
OG 643	OGB 154 A amphibolite	499.56-501.15 H/W
OG 644	OGB 154 A amphibolite	501.15-502.64 H/W
OG 645	OGB 154 A chlor.-amph. schist + T1	502.64-502.73 H/W
OG 646	OGB 154 A T1	502.73-503.23 H/W
OG 647	OGB 154 A T2 T3	503.23-503.47 H/W
OG 648	OGB 154 A T1 T2	503.47-503.83 H/W
OG 649	OGB 154 A chlor. amph. schist	503.83-503.90 H/W
OG 650	OGB 154 A T1 T2	503.90-504.27 H/W
OG 651	OGB 154 A T2 T3	504.27-504.53 H/W
OG 652	OGB 154 A T1 T2	504.53-505.36 H/W
OG 653	OGB 154 A T2 T3	505.36-505.79 H/W
OG 654	OGB 154 A T3	505.79-506.48 H/W
OG 655	OGB 154 A T2 T3	506.48-507.40 H/W
OG 656	OGB 154 A T1 T2	507.40-507.68 H/W
OG 657	OGB 154 A T3	507.68-507.74 H/W
OG 658	OGB 154 A T1 T2	507.74-507.89 H/W
OG 659	OGB 154 A T2 T3	507.89-508.82 H/W
OG 660	OGB 154 A T2	510.21-511.00 F/W
OG 661	OGB 154 A T2 T3	511.00-511.71 F/W
OG 662	OGB 154 A T1 T2	511.71-512.04 F/W
OG 663	OGB 154 A T2 T3	512.04-512.19 F/W
OG 664	OGB 154 A T1	512.19-513.40 F/W
OG 665	OGB 154 A T2	513.40-514.49 F/W
OG 666	OGB 154 A T2 T3	514.49-515.48 F/W
OG 667	OGB 154 A T1	515.48-516.00 F/W
OG 668	OGB 154 A T2	516.00-517.18 F/W

MWE 249	amphib.-rich magnetite quartzite	72/6
MWE 250	magnetite quartzite	72/7
MWE 251	magnetite quartzite	61/3
MWE 252	gossan. talc-chlor. schist	61/4
MWE 253	magnetite quartzite	58/8
MWE 254	magnetite quartzite	51/6
MWE 255	gossan. talc-actin.-carb. schist	50/7.5
MWE 256	magnetite quartzite	53/11.5
MWE 257	magnetite quartzite	44/6.5
MWE 258	gossan. talc-actin.-chlor. schist	42/10
MWE 259	marble-like rock	17/13.5
MWE 260	magnetite quartzite	17/15
MAB 261	Friedenau amphibolite	see attached map
MAB 262	Friedenau amphibolite	see attached map
MAB 263	Friedenau amphibolite	see attached map
MAB 264	Matchless Mine Horizon amphibolite	see attached map
MAB 265	Matchless Mine Horizon amphibolite	see attached map
MAB 266	Matchless Mine Horizon amphibolite	see attached map
MAB 267	Friedenau amphibolite	see attached map
MAB 268	Friedenau amphibolite	see attached map
MAB 269	Friedenau amphibolite	see attached map

MAFIC AND ULTRAMAFIC ROCKS FROM THE OTJIHASE AREA

sample no.	description	location
OTJ 675	talc-actin. schist (coarse-gr.)	Otjihase
OTJ 676	talc-actin. schist (fine-gr.)	Otjihase
OTJ 677	metagabbro	Otjihase
OTJ 678	talc-carb. schist	Elisenheim
OTJ 679	talc-carb.-chlor. schist	Elisenheim 68
OTJ 680	chlor. actin. schist	Elisenheim 68
OTJ 681	talc schist	Elisenheim 68
OTJ 682	chlorite schist	Otjihase
OTJ 683	epid.-rich chlorite schist	Otjihase
OTJ 684	actinolite schist	Von Francois Ost 6
OTJ 685	chlor.-talc schist	Von Francois Ost 6
OTJ 686	talc-olivine(?)-magn. schist	Von Francois Ost 6

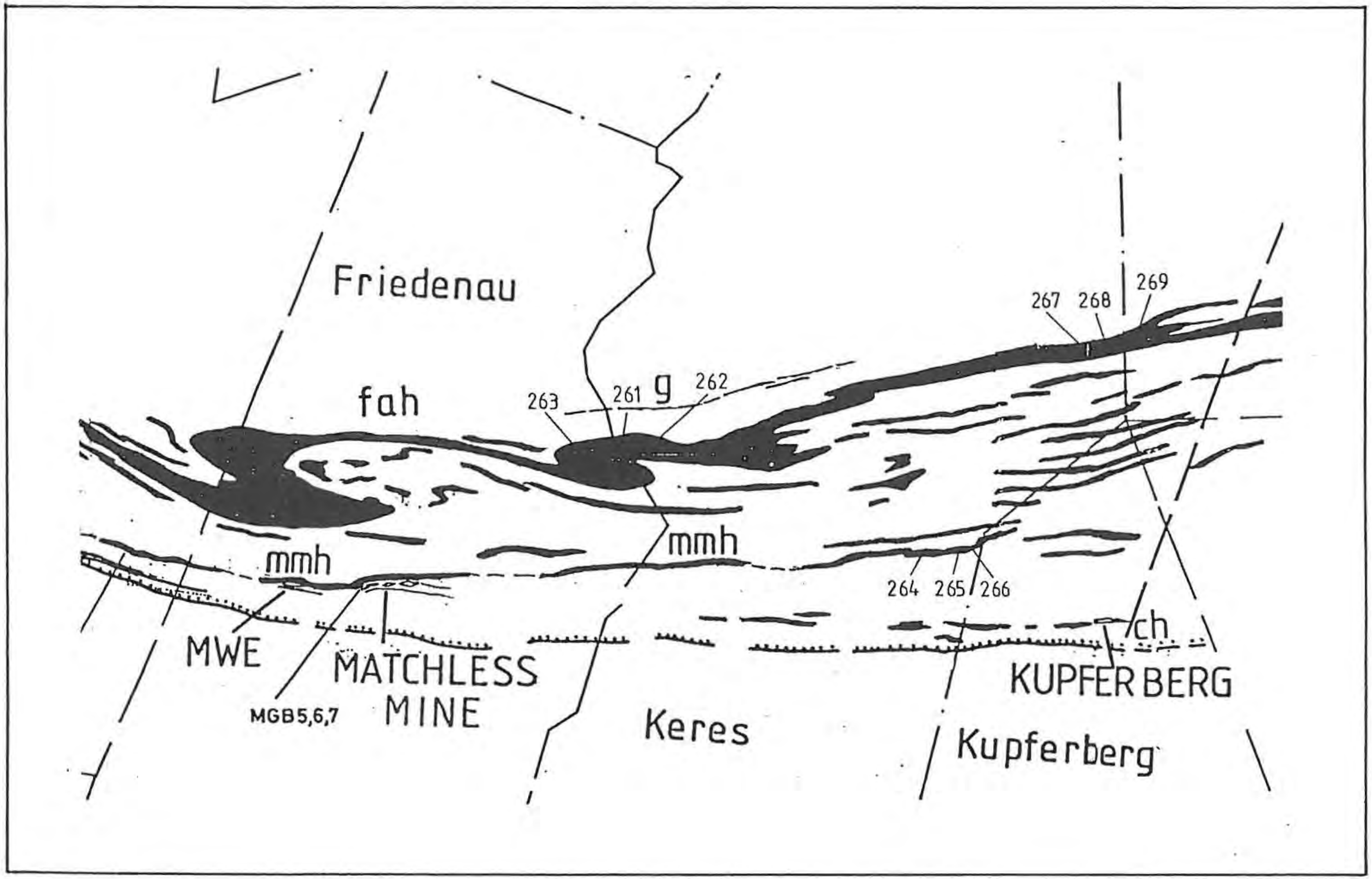

Location of the meta-lava samples. See legend in Fig. 12.

APPENDIX D

LIST OF THE THIN AND POLISHED SECTIONS

Sample no.	Location	Grid reference or depth (in drill holes)	Type of section	Remarks
OG 2	Ongeama gossan	11060E/10240N	P/S	qtz-rich massive gossan
OG 15	Ongeama gossan	10900E/10258.2N	P/S	qtz-rich massive gossan
OG 17	Ongeama gossan	10880E/10260.3N	T/S	magnetite quartzite
OG 19A	Ongeama gossan	10840E/10271N	T/S,P/S	magnetite quartzite
OG 19B	Ongeama gossan	10840E/10271N	T/S,P/S	magnetite quartzite
OG 25	Ongeama gossan	10720E/10253.3N	T/S	ferruginous schist
OG 38	Ongeama gossan	10420E/10220N	P/S	qtz-rich massive gossan
OG 47	Ongeama gossan	10360E/10206N	T/S,P/S	qtz-rich massive gossan
OG 63	Ongeama gossan	10260E/10197N	T/S,P/S	amph.-rich semi-mass. gossan
OG 64	Ongeama gossan	10260E/10193N	T/S	ferruginous schist
OG 77	Ongeama gossan	10180E/10178N	T/S	magnetic chloritoid-rich chlor.-qtz schist
OG 78	Ongeama gossan	10180E/10166N	T/S,P/S	magnetic chlor.-muscovite schist
OG 135	Ongeama grant	10290E/10255N	T/S	magnetic chloritoid-rich chlor.-qtz schist
OG 144	Ongombo gossan	11900E/10220N	P/S	sulph.-rich magnetite quartzite
OG 192A	Ongombo gossan	9360E/10055N	T/S	magnetite quartzite close to OG 192B
OG 192B	Ongombo gossan	9360E/10055N	T/S,P/S	amph.-rich gossan
OG 196	Ongombo gossan	9280E/10045N	T/S,P/S	amph.-rich magn. quartzite
MWE 204	MWE deposit	240/-18	T/S	muscovite-chlorite schist
MWE 207	MWE deposit	235/10	T/S,P/S	talc-bearing gossan
MWE 208	MWE deposit	233/9.5	T/S,P/S	sulph.-rich magn. quartzite
MWE 209	MWE deposit	230/-11	T/S	QMP schist
MWE 217	MWE deposit	200/-3.5	T/S	QMP schist
MWE 236	MWE deposit	123/4	T/S	actin.-talc-baryte-qtz schist
MWE 239	MWE deposit	103/3.5	T/S,P/S	chlor.-actin. schist
MWE 241A	MWE deposit	95/3.5	T/S,P/S	amph.-rich magnetite quartzite
MWE 241B	MWE deposit	95/3.5	T/S	amph.-rich magnetite quartzite
MWE245A	MWE deposit	83/3.5	T/S	talc-actin.-baryte quartz
MWE 245B	MWE deposit	83/3.5	T/S	actinolite schist
MWE 246	MWE deposit	78.5/3.5	T/S	talc-carbonate schist
MWE 253	MWE deposit	58/8	T/S,P/S	magnetite quartzite
MWE 259	MWE deposit	17/13.5	T/S	marble-like rock
MWE 261	MMH		T/S	Friedenau amphibolite
MWE 264	MMH		T/S	MMH amphibolite
OG 281	Ongombo gossan	8960E/10040N	T/S,P/S	amph.-rich magn. quartzite
OG 636	Ongombo - DH OGB 154A	497.07-497.12	T/S	T2 (magn.) schist (F/W of mafic unit)
OG 637	Ongombo - DH OGB 154A	493.7-494.17	2 T/S	T1 schist (F/W and H/W of mafic unit)
OG 682	Otjihase		T/S	mafic metalava
OG 684	Von Francois Ost 60		T/S	actinolite schist
OG 685	Von Francois Ost 60		T/S	chlorite-talc-carb. schist
OG 686 (A+B)	Von Francois Ost 60		2 T/S	talc-carb.-magn. schist
OG 688	Ongombo Prospect	377.56-377.86	T/S	T1 schist (F/W of mafic unit)
OG 690	Ongombo - DH OGB 153A	267.41-267.84	T/S	T1 (magn.) schist (H/W of mafic unit)
OG 691	Ongombo - DH OGB 135A	77.30-77.40	T/S	magnetic amphibolite
OG 692	Ongombo - DH OGB 131C	101.35-103.48	T/S	hbl-rich T1 (magn.) schist
OG 693	Ongombo - DH OGB 151A	347.05	T/S	T1 schist (H/W of mafic unit)
OG 694	Ongombo - DH OGB 151A	347.13	T/S	T1 schist (H/W of mafic unit)
OG 695	Ongombo - DH OGB 151A	347.55-347.60	T/S	chlorite-amphibole schist
OG 696	Ongombo - DH OGB 151A	357.90	T/S	T2 schist (F/W of mafic unit)
OG 697	Ongombo - DH OGB 151A	348.00	T/S	T1 (magn.) schist (F/W of mafic unit)
OG 698	Ongombo - DH OGB 151A	348.48	T/S	T1 schist (H/W of mafic unit)
OG 699	Ongombo - DH OGB 151A	348.60	T/S	T1 (magn.) schist (F/W of mafic unit)
OG 700	Ongombo - DH OGB 153A	355.00	T/S	metagabbro
OG 703	Ongombo - DH OGB 153A	357-358.17	T/S	T1-T2 schist
OG 704	Ongombo - DH OGB 153A	358.17-358.375	T/S	T2 schist
OG 705	Ongombo - DH OGB 153A	359.18-359.36	T/S	T1-T2 schist (close to thin mafic unit)
OG 706	Ongombo - DH OGB 153A	359.36-359.53	T/S	T2 (magn.) schist
OG 707	Ongombo - DH OGB 153A	359.53-359.70	T/S	T3 schist
OG 708	Ongombo - DH OGB 153A	359.70-360.00	T/S,P/S	T1-T2 (magn.) schist
OG 709	Ongombo - DH OGB 153A	360.00-360.25	T/S	T1-T2 (magn.) schist
OG 710A	Ongombo - DH OGB 153A	360.25-360.685	T/S,P/S	T1-T2 (magn.) schist
OG 710B	Ongombo - DH OGB 153A	360.25-360.685	T/S	qtz-chlor.-amph. schist (close to mafic uni
OG 711	Ongombo - DH OGB 153A	360.685-361.01	T/S	T3 schist (H/W of mafic unit)
OG 712	Ongombo - DH OGB 153A	361.01-361.18	T/S	chlorite-amph.-talc schist
OG 713	Ongombo - DH OGB 153A	361.31-362.34	T/S	metagabbro
OG 714	Ongombo - DH OGB 153A	362.34-362.44	T/S	T1-T2 schist (F/W of mafic unit)
OG 715	Ongombo - DH OGB 153A	362.44-362.88	T/S	T2-T3 schist (staur.-rich)
OG 716	Ongombo - DH OGB 153A	362.88-363.00	T/S	T3 schist (staur.-rich)
OG 718	Ongombo - DH OGB 153A	363.48-363.56	T/S,P/S	biotite selvedge zone
OG 719	Ongombo - DH OGB 153A	363.56-364.46	T/S	biot. schist, diss. sulph.
OG 720	Ongombo - DH OGB 153A	363.56-364.46	2 T/S,P/S	sulph.-rich lenses in biot. schist
OG 721	Ongombo - DH OGB 153A	363.56-364.46	T/S	biot. schist
OG 722	Ongombo - DH OGB 153A	364.46-364.82	P/S	sulph.-rich magnetite quartzite
OG 723	Ongombo - DH OGB 153A	364.46-364.82	P/S	remob. sulph. (qtz vein)
OG 725	Ongombo - DH OGB 153A	364.46-364.82	T/S	semi-mass. sulph. bands
OG 726	Ongombo - DH OGB 153A	364.46-364.82	P/S	semi-mass. sulph. bands
OG 727A	Ongombo - DH OGB 153A	364.46-364.82	T/S	biot.-rich schist (smeared sulph.)
OG 727B	Ongombo - DH OGB 153A	364.82-364.95	T/S	biot.-staur.-rich schist (smeared sulph.)
OG 728	Ongombo - DH OGB 153A	364.95-365.14	T/S	semi-mass. sulph. bands
OG 729	Ongombo - DH OGB 153A	364.95-365.14	P/S	semi-mass. sulph. bands
OG 730	Ongombo - DH OGB 153A	365.14-365.37	T/S	biot.-staur. schist
OG 731	Ongombo - DH OGB 153A	365.14-365.37	T/S	biot.-staur. schist
OG 732	Ongombo - DH OGB 153A	365.37-365.56	T/S	biotite-plag. schist
OG 733	Ongombo - DH OGB 153A	365.37-365.56	P/S	semi-mass. sulph. bands
OG 734	Ongombo - DH OGB 153A	365.37-365.56	T/S	semi-mass. sulph. bands
OG 735	Ongombo - DH OGB 153A	365.56-366.05	T/S,P/S	plag.-biot. schist (diss. sulph.)
OG 737	Ongombo - DH OGB 153A	365.56-366.05	P/S	semi-mass. sulph. bands
OG 738	Ongombo - DH OGB 153A	365.56-366.05	T/S	qtz-chlor. schist (diss. sulph.)
OG 739	Ongombo - DH OGB 153A	366.05-366.35	T/S	biot. selvedge zone (diss. sulph)
OG 740	Ongombo - DH OGB 153A	366.05-366.35	T/S	qtz-chlor. schist
OG 741	Ongombo - DH OGB 153A	366.05-366.35	P/S	semi-mass. sulph. bands
OG 743	Ongombo - DH OGB 153A	366.35-366.54	T/S	chlor.-biot.-musc. schist
OG 744	Ongombo - DH OGB 153A	366.54-367.00	P/S	biot. schist (diss. sulph.)
OG 745	Ongombo - DH OGB 153A	366.54-367.00	T/S	biot. schist (diss. sulph.)
OG 746	Ongombo - DH OGB 153A	367.00-367.83	T/S	biot.-chlor. schist (diss. sulph.)
OG 747	Ongombo - DH OGB 153A	367.83-368.29	P/S	semi-mass. sulph. bands
OG 748	Ongombo - DH OGB 153A	367.83-368.29	P/S	sulph.-rich magn. quartzite
OG 749	Ongombo - DH OGB 153A	367.83-368.29	T/S	magnetite quartzite
OG 750	Ongombo - DH OGB 153A	368.48-368.87	P/S	biotite selvedge zone
OG 751	Ongombo - DH OGB 153A	368.48-368.87	T/S	biotite selvedge zone
OG 752	Ongombo - DH OGB 153A	368.87-369.25	T/S	biot.-chlor schist (apatite)
OG 754	Ongombo - DH OGB 153A	368.87-369.25	T/S	T1 (magn.) schist
OG 755	Ongombo - DH OGB 153A	325.83-325.95	T/S	T2 schist
OG 756	Ongombo - DH OGB 153A	326.07-326.17	T/S	T3 schist
OG 757	Ongombo - DH OGB 151A	182.26-182.48	T/S	calc-silicate layer

Abbreviations used in the table:

MWE - Matchless West Extension
MMH - Matchless Mine Horizon amphibolite
DH - drillhole
T/S - thin section
P/S - polished section
T1 - massive quartz-biotite schist
T2 - foliated quartz-biotite-muscovite-chlorite schist
T3 - contorted biotite-muscovite-chlorite-quartz schist
remob. - remobilized
diss. - disseminated
semi-mass. - semi-massive

sulph. - sulphide
qtz - quartz
biot. - biotite
magn. - magnetite
actin. - actinolite
hbl - hornblende
staur. - staurolite
plag. - plagioclase

APPENDIX E

Tables of the geochemical data of mineralized and unmineralized rock types

Table 1 - Lower detection limits for trace element analyses.

element	detection limit (ppm)	element	detection limit (ppm)
Cu	5	Cr	2
Pb	5	Mo	10
Zn	5	Zr	10
Co	5	Nb	10
Ni	5	Y	10
Ag	0.5	Rb	10
Au	40 ppb	Sr	10
Mn	50	Bi	10
Ba	25	W	10
V	25		
TiO2	25		

Table 2 - Ongeama Prospect: trace element geochemistry of the gossan exposure.
(Note: ND means "below detection limit").

Abbreviations used in the table:

MS - massive sulphide gossan
MQ - magnetite quartzite
AS - amphibole-rich semi-massive sulphide gossan
FS - ferruginous schist
MM - magnetic muscovite schist
CS - magnetic chlorite schist

sample no. and rock type	Cu %	Pb ppm	Zn ppm	Ni ppm	Co ppm	Ag ppm	Au ppb	Mn ppm	Ba ppm	Cr ppm	V ppm	TiO2 ppm	As ppm	WO3 ppm	Mo ppm	Sn ppm	Zr ppm	Rb ppm	Sr ppm	Bi ppm	Nb ppm	Y ppm
OG 2 MS	0.33	88	388	36	34	21	144	482	274	35	40	1086	29	ND	ND	ND	ND	ND	ND	ND	ND	ND
OG 3 MS	0.28	87	176	34	32	18	168	401	296	37	108	2302	ND	ND	ND	ND	8	ND	16	ND	ND	ND
OG 4 MS	0.24	61	237	29	31	22	139	482	286	44	62	812	57	ND	ND	ND	ND	ND	4	ND	ND	ND
OG 5 MS	0.25	83	207	33	34	16	134	361	414	39	116	1080	ND	ND	ND	28	ND	ND	ND	ND	ND	ND
OG 6 MS	0.21	114	153	28	26	21	257	321	300	47	88	1996	14	ND	ND	ND	20	ND	26	ND	ND	ND
OG 7 FS	0.22	96	130	29	30	12	136	522	503	20	205	7700	17	ND	ND	24	115	ND	16	ND	ND	ND
OG 8 MS	0.31	104	355	34	34	26	430	652	338	40	84	1426	26	ND	ND	ND	8	ND	16	ND	ND	ND
OG 9 MS	0.31	86	116	27	30	14	304	522	320	38	58	2602	50	ND	ND	8	26	ND	2	ND	ND	ND
OG 10 MS	0.40	82	239	34	30	20	1510	522	230	46	70	2434	48	ND	ND	42	8	ND	6	ND	ND	ND
OG 11 MS	0.60	121	161	33	32	12	244	562	322	28	54	2008	ND	ND	ND	16	20	ND	6	ND	ND	ND
OG 12 MS	0.73	112	237	35	40	21	737	873	516	43	106	1632	19	ND	ND	ND	26	ND	14	ND	ND	ND
OG 13 MQ	0.29	303	132	30	26	27	323	502	306	43	ND	956	ND	ND	ND	62	16	ND	6	ND	ND	ND
OG 14 MQ	0.45	476	182	32	34	28	1154	582	452	55	58	2950	ND	ND	ND	10	28	ND	44	48	ND	ND
OG 15 MS	0.49	442	242	34	35	13	938	502	707	40	102	2877	71	ND	ND	ND	28	ND	24	ND	ND	ND
OG 16 MQ	0.36	318	112	33	33	20	737	401	232	48	40	1830	22	ND	ND	34	34	ND	12	ND	ND	ND
OG 17 MQ	0.41	1900	427	31	33	14	365	1164	312	30	52	852	13	ND	ND	86	ND	ND	8	ND	ND	ND
OG 18 MQ	0.29	364	258	31	34	30	530	381	250	48	58	1484	36	ND	ND	78	26	ND	12	24	ND	ND
OG 19 MQ	0.41	357	436	32	35	29	892	552	428	40	58	1000	41	40	ND	58	22	2	32	12	ND	ND
OG 20 MQ	0.48	391	300	34	29	36	519	682	480	45	36	624	14	ND	ND	22	10	ND	20	ND	ND	ND
OG 21 MQ	0.41	794	289	33	35	19	1244	783	520	28	58	1565	13	ND	ND	76	20	ND	22	ND	ND	ND
OG 22 MQ	0.47	593	471	35	38	19	732	883	504	28	52	346	16	ND	ND	16	6	ND	16	ND	ND	ND
OG 23 MQ	0.17	487	163	27	25	46	485	271	228	65	38	288	ND	56	ND	110	36	8	20	16	ND	ND
OG 24 MS	0.45	611	367	35	35	14	1651	1104	1360	43	118	1186	39	ND	ND	52	20	ND	32	ND	ND	ND
OG 25 FS	0.34	118	442	44	41	3	168	311	474	55	224	8400	ND	ND	ND	70	148	30	24	ND	ND	ND
OG 26 MS	0.29	96	205	37	38	8	517	452	147	58	51	2431	ND	ND	ND	24	20	ND	4	ND	ND	ND
OG 27 MS	0.34	55	182	34	38	13	868	431	364	45	88	2714	ND	ND	ND	32	24	ND	12	ND	ND	ND
OG 28 MS	0.33	46	173	36	32	19	466	522	378	53	126	3868	ND	ND	ND	ND	12	ND	8	ND	ND	ND
OG 29 MS	0.35	273	161	32	34	13	168	401	262	53	80	4536	ND	ND	ND	ND	36	ND	38	ND	ND	ND
OG 30 FS	0.28	105	111	27	34	18	130	452	1740	68	100	7400	ND	ND	ND	ND	94	ND	30	ND	ND	ND
OG 31 MS	0.3	149	206	35	40	13	647	492	392	23	76	3510	ND	ND	ND	ND	ND	ND	2	ND	ND	ND
OG 32 FS	0.37	143	270	30	23	5	351	542	828	60	116	6100	ND	ND	ND	ND	38	ND	14	ND	ND	ND
OG 33 MS	0.29	294	209	26	23	7	1770	552	458	30	42	972	66	ND	ND	22	ND	ND	8	ND	ND	ND
OG 34 MQ	0.12	473	157	33	20	47	316	401	194	60	123	467	70	ND	ND	44	28	ND	6	24	ND	ND
OG 35 MS	0.39	167	304	33	29	3	1438	622	244	28	52	1312	67	ND	ND	ND	ND	ND	2	ND	ND	ND
OG 36 MQ	0.22	513	125	28	20	14	3887	773	199	58	177	591	70	ND	ND	72	10	ND	2	28	ND	ND
OG 37 FS	0.32	117	287	30	20	5	321	1545	387	38	91	5464	15	ND	ND	18	26	ND	ND	ND	ND	ND
OG 38 MS	0.3	283	299	33	23	8	951	662	308	43	50	1224	54	ND	ND	ND	2	ND	4	ND	ND	ND
OG 39 MQ	0.07	141	168	23	9	70	232	221	128	60	116	438	12	ND	ND	122	12	ND	14	12	ND	ND
OG 40 FS	0.15	87	112	31	23	16	199	291	636	73	116	6900	ND	ND	ND	ND	108	ND	14	ND	ND	ND
OG 41 MS	0.37	334	324	35	26	9	598	2849	748	35	42	922	54	ND	ND	56	ND	ND	ND	ND	ND	ND
OG 42 MQ	0.23	642	365	36	54	2	262	2017	490	13	28	550	23	ND	ND	58	10	ND	4	8	ND	ND
OG 43 MM	0.13	110	140	30	29	0.5	162	439	2057	15	84	6600	22	82	ND	ND	136	16	28	20	ND	ND
OG 44 MQ	0.25	916	219	28	32	5	290	1298	310	23	ND	244	26	ND	ND	38	30	ND	22	18	ND	ND
OG 45 MS	0.38	354	225	32	30	2	733	1049	323	23	56	845	23	ND	ND	62	10	ND	2	ND	ND	ND
OG 46 MM	0.13	83	115	27	23	0.5	162	180	1308	60	172	6693	ND	ND	ND	ND	130	28	42	ND	ND	ND
OG 47 MS	0.42	235	277	33	37	3	247	1069	352	23	52	882	80	ND	ND	4	ND	ND	18	ND	ND	ND
OG 48 MQ	0.28	509	245	29	31	2	483	859	210	65	ND	236	48	ND	ND	44	18	ND	2	ND	ND	ND
OG 49 MM	0.2	111	144	29	31	0.5	167	290	988	52	108	7800	ND	ND	ND	32	116	22	32	ND	ND	ND
OG 50 MS	0.43	161	215	23	37	2	2116	629	242	37	ND	260	68	ND	ND	ND	ND	ND	ND	ND	ND	ND
OG 51 MQ	0.15	540	239	20	28	1	337	360	172	27	ND	236	20	ND	ND	74	10	ND	6	42	ND	ND
OG 52 MM	0.22	133	268	26	40	1	411	399	834	55	88	6800	ND	ND	ND	ND	60	10	8	ND	30	ND
OG 53 MS	0.49	242	177	17	25	1	591	799	284	30	34	1976	17	ND	ND	26	ND	ND	14	ND	ND	ND
OG 54 MQ	0.16	751	257	23	27	0.5	893	539	130	52	ND	104	23	54	ND	44	16	ND	2	22	ND	ND
OG 55 MM	0.17	118	249	27	34	0.5	234	260	1100	40	124	6500	ND	34	ND	40	100	38	40	2	ND	ND
OG 56 MS	0.5	251	500	26	37	4	758	989	332	30	36	666	49	ND	ND	ND	14	ND	4	88	ND	ND
OG 57 MQ	0.25	443	194	18	23	0.5	378	499	126	40	36	58	15	ND	ND	10	4	ND	ND	ND	ND	ND
OG 58 MM	0.23	84	181	27	29	0.5	362	300	1676	62	107	6200	ND	62	ND	ND	130	30	46	20	ND	ND
OG 59 MS	0.67	219	534	36	32	6	306	1967	450	25	68	666	39	ND	ND	ND	ND	ND	ND	ND	30	ND
OG 60 MQ	0.21	1600	154	32	30	2	290	1218	272	60	32	148	ND	ND	ND	64	30	6	14	32	ND	ND

sample no. and rock type		Cu %	Pb ppm	Zn ppm	Ni ppm	Co ppm	Ag ppm	Au ppb	Mn ppm	Ba ppm	Cr ppm	V ppm	TiO2 ppm	As ppm	WO3 ppm	Mo ppm	Sn ppm	Zr ppm	Rb ppm	Sr ppm	Bi ppm	Nb ppm	Y ppm
OG 61	MS	0.60	784	154	30	38	3	694	1228	148	30	54	290	61	ND	ND	46	6	ND	0	28	ND	ND
OG 62	MM	0.16	211	247	29	25	2	460	439	3130	50	68	6800	ND	ND	ND	56	160	28	66	38	ND	ND
OG 63	AS	0.50	101	848	37	37	0.5	1300	3485	866	17	ND	304	36	ND	ND	ND	ND	ND	ND	ND	ND	ND
OG 64	FS	0.23	87	432	30	32	0.5	226	619	1240	52	144	7400	ND	ND	ND	ND	86	2	4	ND	ND	ND
OG 65	MS	0.30	60	826	32	30	0.5	283	1168	238	27	120	2292	ND	ND	ND	ND	ND	10	16	ND	ND	ND
OG 66	MQ	0.33	2200	195	24	30	0.5	190	1927	674	57	61	778	ND	ND	ND	12	24	ND	28	30	ND	ND
OG 67	MM	0.38	77	188	21	26	0.5	288	200	2875	52	125	4800	ND	84	ND	ND	86	8	50	8	ND	ND
OG 68	AS	1.30	210	284	21	30	5	247	3176	1112	22	34	1136	28	ND	ND	ND	ND	ND	ND	ND	ND	ND
OG 69	MQ	0.24	687	358	27	33	0.5	391	879	286	40	30	66	ND	ND	ND	42	8	ND	ND	6	ND	ND
OG 70	MS	0.79	307	196	28	35	4	589	1109	230	35	ND	542	56	ND	ND	ND	ND	ND	ND	ND	ND	ND
OG 72	AS	1.58	415	208	25	35	2	932	1119	584	22	124	394	35	ND	ND	4	ND	ND	4	ND	ND	ND
OG 73	MQ	0.09	450	51	17	13	1	188	140	78	60	28	ND	ND	ND	ND	76	24	ND	ND	ND	ND	ND
OG 74	AS	0.55	260	282	18	21	1	314	1318	674	30	44	3200	58	ND	ND	ND	14	ND	ND	ND	ND	ND
OG 75	MM	0.11	31	145	21	23	0.5	237	389	4200	55	108	4800	49	58	ND	16	134	26	34	26	ND	ND
OG 76	MM	0.23	23	110	22	27	0.5	239	379	2324	42	122	5300	11	74	ND	14	152	16	34	20	ND	ND
OG 77	CS	0.10	21	48	37	28	0.5	121	250	414	62	132	6100	285	ND	ND	28	154	ND	20	36	ND	ND
OG 78	CS-MM	0.11	31	61	33	25	0.5	139	300	2662	55	130	5300	225	ND	ND	26	162	14	30	34	ND	ND
OG 79	AS	1.03	412	2000	27	36	8	704	2676	797	17	24	709	97	ND	ND	ND	ND	ND	ND	ND	ND	ND
OG 80	CS	0.08	28	53	37	18	0.5	118	340	706	52	150	5900	213	ND	ND	18	141	ND	22	12	ND	ND
OG 81	CS	0.07	28	54	31	17	0.5	126	270	2338	50	126	5900	146	ND	ND	64	158	10	24	50	ND	ND
OG 82	MS	0.54	440	349	29	25	9	244	1494	509	20	51	2792	48	ND	ND	ND	40	ND	ND	ND	ND	ND
OG 83	MQ	0.19	272	271	15	10	0.5	216	401	118	42	ND	634	16	ND	ND	32	22	2	ND	46	ND	ND
OG 84	CS	0.07	24	52	33	19	0.5	131	170	388	50	114	6000	262	ND	ND	40	170	6	14	30	ND	ND
OG 85	MM	0.21	78	81	26	24	0.5	190	361	3000	27	84	5700	133	ND	ND	ND	80	4	36	ND	ND	ND
OG 86	MS	0.35	202	344	23	18	5	226	942	646	30	48	2762	77	ND	ND	ND	4	ND	12	ND	ND	ND
OG 87	CS	0.06	38	55	35	20	0.5	175	221	1648	15	104	6700	60	ND	ND	36	177	16	34	22	ND	ND
OG 88	MM	0.25	50	79	28	33	0.5	188	301	1262	30	134	5400	384	ND	ND	34	102	24	42	30	ND	ND
OG 89	MM	0.34	111	116	28	33	1	195	1454	2452	39	88	5200	23	ND	ND	ND	96	6	42	ND	ND	ND
OG 90	MS	0.69	423	344	26	20	6	689	2236	516	32	90	3500	ND	64	ND	ND	30	ND	8	ND	ND	ND
OG 91	CS	0.07	22	33	30	14	0.5	131	291	106	15	82	5300	76	75	ND	22	132	ND	4	28	ND	ND
OG 92	MM	0.33	45	122	25	18	0.5	165	511	1276	12	96	6300	44	96	ND	ND	58	16	42	ND	ND	ND
OG 93	MM	0.32	115	81	28	27	0.5	139	672	2070	12	79	5400	14	32	ND	28	104	14	32	ND	ND	ND
OG 94	MS	0.55	247	420	20	14	7	424	1584	473	20	65	1499	ND	86	ND	ND	ND	ND	2	ND	ND	ND
OG 95	MS	0.60	328	113	23	27	4	308	1935	506	17	172	2846	10	40	ND	8	4	ND	ND	ND	ND	ND
OG 96	CS	0.07	20	32	33	20	0.5	149	291	204	7	82	5900	212	ND	ND	14	160	10	20	32	38	ND
OG 97	MS	0.45	200	108	30	27	7	524	1083	666	32	114	2474	ND	ND	ND	ND	28	ND	26	ND	ND	ND
OG 98	MM	0.26	111	57	37	34	0.5	165	802	1676	10	104	5600	12	ND	ND	ND	106	6	34	18	ND	ND
OG 99	MM	0.33	109	118	32	25	0.5	177	652	586	30	130	5000	ND	138	ND	ND	ND	ND	ND	ND	ND	ND
OG 100	MS	0.66	125	128	26	28	2	283	591	374	20	124	3226	ND	58	ND	10	244	ND	8	ND	ND	ND
OG 101	MM	0.24	64	85	29	37	0.5	126	531	1320	42	132	6200	ND	78	ND	ND	106	18	28	ND	ND	ND
OG 102	MS	0.45	162	154	19	16	7	362	912	434	27	85	1788	ND	ND	ND	ND	16	ND	ND	ND	ND	ND
OG 103	MQ	0.25	326	181	22	20	2	278	912	346	37	60	870	ND	ND	ND	26	32	ND	12	ND	ND	ND
OG 104	MM	0.28	69	92	25	26	0.5	152	612	695	25	157	6900	ND	88	ND	ND	104	ND	24	ND	ND	ND
OG 105	MS	0.36	164	344	24	27	0.5	373	1243	390	25	42	1978	ND	ND	ND	ND	ND	ND	ND	ND	ND	ND
OG 106	MQ	0.24	657	110	30	30	0.5	136	1383	300	12	40	486	ND	48	ND	ND	12	ND	ND	ND	ND	ND
OG 107	MM	0.21	61	102	31	34	0.5	103	752	1614	12	137	5600	ND	62	ND	16	130	18	42	28	ND	ND
OG 108	MS	0.49	140	103	32	39	2	216	1283	518	7	104	2498	ND	ND	ND	ND	42	ND	34	ND	ND	ND
OG 109	MM	0.33	41	75	24	31	0.5	113	371	974	15	140	6300	ND	ND	ND	ND	98	12	10	ND	ND	ND
OG 110	MS	0.55	80	182	30	36	3	193	1203	452	12	54	2110	ND	ND	ND	ND	16	ND	8	ND	ND	ND
OG 111	MM	0.16	33	68	23	25	1	131	251	1680	17	132	6100	ND	ND	ND	6	146	32	26	ND	ND	ND
OG 112	MS	0.41	40	212	22	21	1	231	561	222	12	66	3800	ND	36	ND	ND	26	ND	18	ND	ND	ND
OG 113	MM	0.1	11	111	22	19	1	211	381	668	22	72	5000	ND	94	ND	54	156	18	16	8	ND	ND
OG 114	MS	0.67	32	157	21	18	2	1672	1995	464	17	64	3250	ND	72	ND	16	16	ND	18	ND	ND	ND
OG 115	MS	0.51	149	199	23	26	4	4870	1594	526	25	58	5000	36	ND	ND	8	30	4	22	ND	ND	ND
OG 116	MM	0.37	32	422	27	23	2	334	451	458	12	118	6700	ND	ND	ND	ND	80	64	22	ND	ND	ND
OG 117	MS	0.51	49	284	30	26	2	563	251	220	15	188	4900	ND	ND	ND	ND	42	ND	14	ND	ND	ND
OG 118	MS	0.59	39	380	34	37	2	144	301	192	7	164	4000	14	ND	ND	ND	52	ND	ND	ND	ND	ND

sample no. and rock type	Cu %	Pb ppm	Zn ppm	Ni ppm	Co ppm	Ag ppm	Au ppb	Mn ppm	Ba ppm	Cr ppm	V ppm	TiO2 ppm	As ppm	WO3 ppm	Mo ppm	Sn ppm	Zr ppm	Rb ppm	Sr ppm	Bi ppm	Nb ppm	Y ppm
OG 61 MS	0.60	784	154	30	38	3	694	1228	148	30	54	290	61	ND	ND	46	6	ND	0	28	ND	ND
OG 62 MM	0.16	211	247	29	25	2	460	439	3130	50	68	6800	ND	ND	ND	56	160	28	66	38	ND	ND
OG 63 AS	0.50	101	848	37	37	0.5	1300	3485	866	17	ND	304	36	ND	ND	ND	ND	ND	ND	ND	ND	ND
OG 64 FS	0.23	87	432	30	32	0.5	226	619	1240	52	144	7400	ND	ND	ND	ND	86	2	4	ND	ND	ND
OG 65 MS	0.30	60	826	32	30	0.5	283	1168	238	27	120	2292	ND	ND	ND	ND	ND	10	16	ND	ND	ND
OG 66 MQ	0.33	2200	195	24	30	0.5	190	1927	674	57	61	778	ND	ND	ND	12	24	ND	28	30	ND	ND
OG 67 MM	0.38	77	188	21	26	0.5	288	200	2875	52	125	4800	ND	84	ND	ND	86	8	50	8	ND	ND
OG 68 AS	1.30	210	284	21	30	5	247	3176	1112	22	34	1136	28	ND	ND	ND	ND	ND	ND	ND	ND	ND
OG 69 MQ	0.24	687	358	27	33	0.5	391	879	286	40	30	66	ND	ND	ND	42	8	ND	ND	6	ND	ND
OG 70 MS	0.79	307	196	28	35	4	589	1109	230	35	ND	542	56	ND	ND	ND	ND	ND	ND	ND	ND	ND
OG 72 AS	1.58	415	208	25	35	2	932	1119	584	22	124	394	35	ND	ND	4	ND	ND	4	ND	ND	ND
OG 73 MQ	0.09	450	51	17	13	1	188	140	78	60	28	ND	ND	ND	ND	76	24	ND	ND	ND	ND	ND
OG 74 AS	0.55	260	282	18	21	1	314	1318	674	30	44	3200	58	ND	ND	ND	14	ND	ND	ND	ND	ND
OG 75 MM	0.11	31	145	21	23	0.5	237	389	4200	55	108	4800	49	58	ND	16	134	26	34	26	ND	ND
OG 76 MM	0.23	23	110	22	27	0.5	239	379	2324	42	122	5300	11	74	ND	14	152	16	34	20	ND	ND
OG 77 CS	0.10	21	48	37	28	0.5	121	250	414	62	132	6100	285	ND	ND	28	154	ND	20	36	ND	ND
OG 78 CS-MM	0.11	31	61	33	25	0.5	139	300	2662	55	130	5300	225	ND	ND	26	162	14	30	34	ND	ND
OG 79 AS	1.03	412	2000	27	36	8	704	2676	797	17	24	709	97	ND	ND	ND	ND	ND	ND	ND	ND	ND
OG 80 CS	0.08	28	53	37	18	0.5	118	340	706	52	150	5900	213	ND	ND	18	141	ND	22	12	ND	ND
OG 81 CS	0.07	28	54	31	17	0.5	126	270	2338	50	126	5900	146	ND	ND	64	158	10	24	50	ND	ND
OG 82 MS	0.54	440	349	29	25	9	244	1494	509	20	51	2792	48	ND	ND	ND	40	ND	ND	ND	ND	ND
OG 83 MQ	0.19	272	271	15	10	0.5	216	401	118	42	ND	634	16	ND	ND	32	22	2	ND	46	ND	ND
OG 84 CS	0.07	24	52	33	19	0.5	131	170	388	50	114	6000	262	ND	ND	40	170	6	14	30	ND	ND
OG 85 MM	0.21	78	81	26	24	0.5	190	361	3000	27	84	5700	133	ND	ND	ND	80	4	36	ND	ND	ND
OG 86 MS	0.35	202	344	23	18	5	226	942	646	30	48	2762	77	ND	ND	ND	4	ND	12	ND	ND	ND
OG 87 CS	0.06	38	55	35	20	0.5	175	221	1648	15	104	6700	60	ND	ND	36	177	16	34	22	ND	ND
OG 88 MM	0.25	50	79	28	33	0.5	188	301	1262	30	134	5400	384	ND	ND	34	102	24	42	30	ND	ND
OG 89 MM	0.34	111	116	28	33	1	195	1454	2452	39	88	5200	23	ND	ND	ND	96	6	42	ND	ND	ND
OG 90 MS	0.69	423	344	26	20	6	689	2236	516	32	90	3500	ND	64	ND	ND	30	ND	8	ND	ND	ND
OG 91 CS	0.07	22	33	30	14	0.5	131	291	106	15	82	5300	76	75	ND	22	132	ND	4	28	ND	ND
OG 92 MM	0.33	45	122	25	18	0.5	165	511	1276	12	96	6300	44	96	ND	ND	58	16	42	ND	ND	ND
OG 93 MM	0.32	115	81	28	27	0.5	139	672	2070	12	79	5400	14	32	ND	28	104	14	32	ND	ND	ND
OG 94 MS	0.55	247	420	20	14	7	424	1584	473	20	65	1499	ND	86	ND	ND	ND	ND	2	ND	ND	ND
OG 95 MS	0.60	328	113	23	27	4	308	1935	506	17	172	2846	10	40	ND	8	4	ND	ND	ND	ND	ND
OG 96 CS	0.07	20	32	33	20	0.5	149	291	204	7	82	5900	212	ND	ND	14	160	10	20	32	38	ND
OG 97 MS	0.45	200	108	30	27	7	524	1083	666	32	114	2474	ND	ND	ND	ND	28	ND	26	ND	ND	ND
OG 98 MM	0.26	111	57	37	34	0.5	165	802	1676	10	104	5600	12	ND	ND	ND	106	6	34	18	ND	ND
OG 99 MM	0.33	109	118	32	25	0.5	177	652	586	30	130	5000	ND	138	ND	ND	ND	ND	ND	ND	ND	ND
OG 100 MS	0.66	125	128	26	28	2	283	591	374	20	124	3226	ND	58	ND	10	244	ND	8	ND	ND	ND
OG 101 MM	0.24	64	85	29	37	0.5	126	531	1320	42	132	6200	ND	78	ND	ND	106	18	28	ND	ND	ND
OG 102 MS	0.45	162	154	19	16	7	362	912	434	27	85	1788	ND	ND	ND	ND	16	ND	ND	ND	ND	ND
OG 103 MQ	0.25	326	181	22	20	2	278	912	346	37	60	870	ND	ND	ND	26	32	ND	12	ND	ND	ND
OG 104 MM	0.28	69	92	25	26	0.5	152	612	695	25	157	6900	ND	88	ND	ND	104	ND	24	ND	ND	ND
OG 105 MS	0.36	164	344	24	27	0.5	373	1243	390	25	42	1978	ND	ND	ND	ND	ND	ND	ND	ND	ND	ND
OG 106 MQ	0.24	657	110	30	30	0.5	136	1383	300	12	40	486	ND	48	ND	ND	12	ND	ND	ND	ND	ND
OG 107 MM	0.21	61	102	31	34	0.5	103	752	1614	12	137	5600	ND	62	ND	16	130	18	42	28	ND	ND
OG 108 MS	0.49	140	103	32	39	2	216	1283	518	7	104	2498	ND	ND	ND	ND	42	ND	34	ND	ND	ND
OG 109 MM	0.33	41	75	24	31	0.5	113	371	974	15	140	6300	ND	ND	ND	ND	98	12	10	ND	ND	ND
OG 110 MS	0.55	80	182	30	36	3	193	1203	452	12	54	2110	ND	ND	ND	ND	16	ND	8	ND	ND	ND
OG 111 MM	0.16	33	68	23	25	1	131	251	1680	17	132	6100	ND	ND	ND	6	146	32	26	ND	ND	ND
OG 112 MS	0.41	40	212	22	21	1	231	561	222	12	66	3800	ND	36	ND	ND	26	ND	18	ND	ND	ND
OG 113 MM	0.1	11	111	22	19	1	211	381	668	22	72	5000	ND	94	ND	54	156	18	16	8	ND	ND
OG 114 MS	0.67	32	157	21	18	2	1672	1995	464	17	64	3250	ND	72	ND	16	16	ND	18	ND	ND	ND
OG 115 MS	0.51	149	199	23	26	4	4870	1594	526	25	58	5000	36	ND	ND	8	30	4	22	ND	ND	ND
OG 116 MM	0.37	32	422	27	23	2	334	451	458	12	118	6700	ND	ND	ND	ND	80	64	22	ND	ND	ND
OG 117 MS	0.51	49	284	30	26	2	563	251	220	15	188	4900	ND	ND	ND	ND	42	ND	14	ND	ND	ND
OG 118 MS	0.59	39	380	34	37	2	144	301	192	7	164	4000	14	ND	ND	ND	52	ND	ND	ND	ND	ND

Table 4 - Ongombo Prospect: trace element geochemistry of the gossan exposure.
(Note: ND means "below detection limit").

Sample no.	Cu ppm	Pb ppm	Zn ppm	Ni ppm	Co ppm	Ag ppm	Au ppb	Mn ppm	Ba ppm	Cr ppm	V ppm	TiO2 %	As ppm	WO3 ppm	Mo ppm	Sn ppm	Zr ppm	Rb ppm	Sr ppm	Bi ppm	Nb ppm	Y ppm
OG 144	0.21%	73	76	40	19	3	88	293	160	ND	126	983	ND	30	92	ND	ND	ND	ND	ND	ND	ND
OG 145	566	71	50	21	10	3	149	115	636	22	58	387	ND	ND	52	ND	ND	ND	ND	ND	ND	ND
OG 146	0.46%	57	46	27	13	2	182	272	247	12	80	213	ND	ND	ND	ND	ND	ND	ND	ND	ND	ND
OG 147	307	52	43	21	13	ND	137	293	1980	10	62	293	ND	ND	ND	ND	20	ND	15	ND	ND	ND
OG 148	283	48	61	23	15	ND	81	335	215	7	57	236	ND	ND	ND	ND	ND	ND	ND	ND	ND	ND
OG 149	412	36	104	30	22	ND	88	356	101	2	86	256	ND	ND	ND	ND	ND	ND	ND	ND	ND	ND
OG 150	182	36	34	36	18	ND	81	283	115	24	85	378	ND	ND	ND	ND	ND	ND	ND	ND	ND	ND
OG 151	236	22	58	31	11	2	119	115	3806	24	45	215	ND	ND	ND	ND	27	ND	39	ND	ND	ND
OG 152	90	38	27	24	10	ND	76	105	5221	2	71	179	ND	ND	ND	ND	36	ND	40	ND	ND	ND
OG 153	117	25	29	14	10	ND	88	105	662	41	58	146	ND	58	ND	ND	ND	ND	17	ND	ND	ND
OG 154	0.16%	46	39	23	28	2	116	220	4636	29	102	465	ND	ND	ND	ND	35	ND	53	ND	ND	ND
OG 155	0.17%	30	75	22	19	3	432	105	3822	24	69	295	ND	ND	34	20	31	ND	40	ND	ND	ND
OG 156	127	36	20	12	10	ND	73	388	495	19	50	195	ND	ND	ND	ND	16	ND	ND	ND	ND	ND
OG 157	234	47	22	12	8	ND	66	168	88	31	55	326	ND	ND	ND	ND	ND	ND	ND	ND	ND	ND
OG 158	135	38	21	13	10	ND	56	335	513	22	36	122	ND	ND	ND	ND	ND	ND	ND	ND	ND	ND
OG 159	114	23	20	10	6	ND	88	388	112	31	40	75	ND	ND	ND	ND	ND	ND	ND	ND	ND	ND
OG 160	399	42	23	16	12	2	349	189	4138	24	55	225	ND	ND	ND	ND	28	ND	42	ND	ND	ND
OG 161	405	45	28	18	16	ND	405	314	2080	22	44	182	ND	ND	ND	ND	ND	ND	28	ND	ND	ND
OG 162	333	50	31	15	13	ND	147	168	218	12	62	255	ND	ND	ND	ND	ND	ND	ND	ND	ND	ND
OG 163	518	36	23	21	16	ND	165	115	140	2	48	441	ND	ND	ND	ND	ND	ND	16	ND	ND	ND
OG 164	579	36	37	16	21	ND	159	136	124	2	36	358	ND	ND	ND	ND	ND	ND	ND	ND	ND	ND
OG 165	203	36	18	20	18	ND	144	241	91	ND	94	261	ND	86	ND	ND	ND	ND	ND	ND	ND	ND
OG 166	367	33	27	16	18	ND	167	189	1912	15	86	183	ND	ND	ND	ND	16	ND	16	ND	ND	ND
OG 167	231	55	22	21	17	2	233	189	591	22	46	479	ND	ND	ND	ND	ND	ND	ND	ND	ND	ND
OG 168	630	87	33	21	14	ND	175	105	1121	2	61	841	ND	ND	ND	ND	18	ND	ND	ND	ND	ND
OG 169	120	28	25	14	11	ND	147	105	1058	17	ND	393	ND	ND	ND	ND	ND	ND	ND	ND	ND	ND
OG 170	374	56	50	24	19	ND	301	189	224	19	119	528	ND	ND	39	ND	ND	ND	ND	ND	ND	ND
OG 171	271	33	42	24	14	ND	144	388	82	27	88	305	ND	ND	ND	ND	ND	ND	ND	ND	ND	ND
OG 172	204	24	47	29	10	ND	129	136	75	12	94	293	ND	ND	ND	ND	ND	ND	ND	ND	ND	ND
OG 173	235	35	16	17	10	ND	137	136	647	24	35	180	ND	ND	ND	ND	ND	ND	ND	ND	ND	ND
OG 174	622	66	14	18	22	ND	215	178	542	7	71	935	21	ND	ND	ND	ND	ND	ND	ND	ND	ND
OG 175	0.24%	123	28	12	43	1	210	199	326	29	108	1685	ND	ND	67	ND	19	ND	ND	ND	ND	ND
OG 176	0.19%	45	22	21	28	1	195	230	1142	10	113	361	ND	ND	47	ND	ND	ND	ND	ND	ND	ND
OG 177	200	25	15	15	15	1	152	94	4695	29	46	124	ND	ND	ND	ND	35	ND	84	ND	ND	ND
OG 178	326	37	15	11	22	1	180	220	539	22	37	182	ND	ND	ND	ND	ND	ND	ND	ND	ND	ND
OG 179	699	44	18	18	21	1	223	220	1020	12	63	277	ND	ND	ND	ND	ND	ND	ND	ND	ND	ND
OG 180	652	50	19	19	16	1	245	126	2160	2	63	396	ND	ND	ND	ND	23	ND	15	ND	ND	ND
OG 181	627	45	20	21	17	1	189	241	2640	7	55	244	ND	ND	ND	ND	18	ND	ND	ND	ND	ND
OG 182	427	41	16	21	17	1	169	230	1206	19	73	721	ND	ND	ND	ND	16	ND	ND	ND	ND	ND
OG 183	545	44	19	19	19	1	215	210	1289	22	101	558	ND	ND	ND	ND	26	ND	ND	ND	ND	ND
OG 184	472	57	17	19	17	ND	172	105	1377	15	110	495	ND	ND	ND	ND	ND	ND	19	ND	ND	ND
OG 185	0.21%	57	23	20	25	ND	220	168	446	12	157	939	ND	ND	ND	ND	ND	ND	ND	ND	ND	ND
OG 186	725	43	25	23	24	ND	152	450	305	15	353	588	ND	ND	ND	ND	ND	ND	ND	ND	ND	ND
OG 187	0.12%	44	18	24	22	ND	182	189	358	5	314	647	ND	ND	ND	17	ND	ND	31	ND	ND	ND
OG 188	517	35	20	21	38	ND	172	189	299	10	146	597	ND	44	ND	ND	ND	ND	ND	ND	ND	ND
OG 189	327	29	16	20	15	ND	167	147	302	15	119	609	ND	ND	ND	ND	ND	ND	ND	ND	ND	ND
OG 190	233	38	16	19	12	ND	179	178	696	15	133	400	ND	ND	ND	ND	ND	ND	ND	ND	ND	ND
OG 191	227	21	28	14	33	ND	121	136	194	20	55	287	ND	44	ND	ND	ND	ND	ND	ND	ND	ND
OG 192	310	41	18	20	21	ND	215	168	544	12	145	469	ND	ND	ND	ND	ND	ND	ND	ND	ND	ND
OG 193	384	30	22	28	43	ND	159	178	283	5	113	364	ND	ND	ND	ND	ND	ND	ND	ND	ND	ND
OG 194	304	33	19	26	33	ND	174	272	236	2	119	676	ND	ND	35	ND	ND	ND	ND	ND	ND	ND
OG 195	454	33	29	22	43	ND	182	210	181	2	166	1195	ND	ND	ND	ND	ND	ND	ND	ND	ND	ND
OG 196	209	29	24	26	31	ND	134	230	167	2	82	889	ND	ND	ND	ND	ND	ND	ND	ND	ND	ND
OG 197	264	23	29	14	34	ND	152	189	199	15	136	365	ND	ND	ND	ND	ND	ND	ND	ND	ND	ND
OG 198	395	30	30	26	38	ND	136	356	236	10	147	254	ND	ND	ND	ND	ND	ND	25	ND	ND	ND
OG 199	184	29	19	21	23	ND	136	178	311	20	72	722	ND	ND	ND	ND	ND	ND	17	ND	ND	ND
OG 200	258	34	24	26	27	ND	182	168	119	15	81	476	ND	ND	ND	ND	ND	ND	ND	ND	ND	ND
OG 270	220	40	21	24	31	1	146	126	533	42	105	1002	ND	48	ND	ND	ND	ND	ND	ND	ND	ND

Sample no.	Cu ppm	Pb ppm	Zn ppm	Ni ppm	Co ppm	Ag ppm	Au ppb	Mn ppm	Ba ppm	Cr ppm	V ppm	TiO2 %	As ppm	WO3 ppm	Mo ppm	Sn ppm	Zr ppm	Rb ppm	Sr ppm	Bi ppm	Nb ppm	Y ppm
OG 271	338	30	20	26	30	ND	116	178	180	25	107	642	ND	ND	ND	ND	ND	ND	ND	ND	ND	ND
OG 272	735	64	46	44	100	ND	134	419	225	22	354	779	ND	ND	ND	ND	ND	ND	15	ND	ND	ND
OG 273	479	36	51	46	113	ND	139	210	166	32	182	1037	ND	ND	ND	ND	ND	ND	ND	ND	ND	ND
OG 274	401	52	25	34	44	ND	141	168	513	30	178	2816	ND	ND	ND	ND	24	ND	ND	ND	ND	ND
OG 275	611	34	96	41	110	ND	141	241	221	32	101	292	ND	ND	ND	ND	ND	ND	ND	ND	ND	ND
OG 276	222	29	21	21	20	ND	91	157	100	15	24	315	ND	ND	ND	ND	ND	ND	ND	ND	ND	ND
OG 277	884	43	101	50	175	ND	167	272	209	30	124	616	ND	ND	42	ND	ND	ND	ND	ND	ND	ND
OG 278	0.26%	48	148	76	110	ND	157	492	610	7	140	334	ND	ND	36	ND	ND	ND	ND	ND	ND	ND
OG 279	778	69	95	49	79	ND	182	199	746	30	100	382	ND	ND	ND	ND	ND	ND	ND	ND	ND	ND
OG 280	850	46	34	29	39	ND	134	220	470	22	59	543	ND	ND	ND	ND	ND	ND	ND	ND	ND	ND
OG 281	848	36	102	52	74	ND	141	168	180	32	66	256	ND	ND	ND	ND	ND	ND	ND	ND	ND	ND
OG 282	0.32%	37	47	37	49	ND	182	199	174	40	103	600	ND	ND	42	18	ND	ND	ND	ND	ND	ND
OG 283	658	31	119	46	81	ND	162	168	140	47	59	238	ND	ND	ND	ND	ND	ND	ND	ND	ND	ND
OG 284	0.38%	39	104	47	66	ND	149	220	126	35	69	354	ND	ND	ND	ND	ND	ND	ND	ND	ND	ND
OG 285	476	35	84	33	65	ND	139	220	145	35	52	169	ND	ND	ND	ND	ND	ND	ND	ND	ND	ND
OG 286	564	38	112	29	75	ND	157	356	787	35	127	779	ND	ND	ND	ND	ND	ND	ND	ND	ND	ND
OG 287	404	37	215	45	198	ND	167	1006	232	42	79	253	ND	ND	ND	ND	ND	ND	ND	ND	ND	ND
OG 288	376	34	40	24	25	ND	146	147	137	32	71	258	ND	ND	ND	19	ND	ND	ND	ND	ND	ND
OG 289	285	27	91	34	112	ND	124	283	3282	35	200	315	ND	ND	ND	ND	25	ND	57	ND	ND	ND
OG 290	0.32%	44	315	109	502	ND	162	765	567	27	86	326	ND	ND	ND	ND	ND	ND	ND	ND	ND	ND
OG 291	680	36	44	33	52	ND	159	335	297	27	286	486	ND	ND	ND	ND	ND	ND	ND	ND	ND	ND
OG 292	691	29	44	33	40	ND	146	189	236	24	194	525	ND	ND	ND	28	ND	ND	ND	ND	ND	ND
OG 293	0.19%	31	28	30	32	ND	152	105	294	29	145	776	ND	ND	ND	ND	17	ND	57	ND	ND	ND
OG 294	0.2	23	30	25	42	ND	139	105	343	22	228	589	ND	ND	35	ND	ND	ND	ND	ND	ND	ND
OG 295	741	32	70	32	47	ND	121	94	326	24	201	374	ND	ND	ND	27	ND	ND	22	ND	ND	ND
OG 296	521	30	47	27	28	ND	139	147	264	26	170	586	ND	ND	ND	ND	ND	ND	ND	ND	ND	ND
OG 297	0.25%	39	223	47	110	ND	164	346	250	22	187	411	ND	ND	ND	30	ND	ND	ND	ND	ND	ND
OG 298	766	43	53	34	66	ND	162	105	178	22	191	822	ND	ND	ND	ND	ND	ND	ND	ND	ND	ND
OG 299	573	39	26	21	19	ND	154	126	368	41	251	360	ND	ND	ND	ND	ND	ND	ND	ND	ND	ND
OG 300	0.23%	61	76	36	51	ND	149	199	393	22	187	985	ND	ND	ND	ND	22	ND	ND	ND	ND	ND
OG 301	600	35	36	24	20	ND	308	251	343	29	227	772	ND	ND	ND	ND	ND	ND	ND	ND	ND	ND
OG 302	307	24	20	17	12	ND	212	136	368	36	150	358	ND	ND	44	ND	ND	ND	ND	ND	ND	ND
OG 303	406	19	25	15	14	ND	162	84	341	34	77	402	ND	ND	ND	ND	ND	ND	ND	ND	ND	ND
OG 304	348	16	21	14	5	ND	232	168	3102	34	67	310	ND	ND	ND	18	22	ND	38	ND	ND	ND
OG 305	117	16	26	16	5	ND	167	73	8741	38	165	175	ND	100	ND	18	69	ND	192	ND	ND	ND
OG 306	192	19	19	18	11	ND	154	115	1402	41	162	182	ND	ND	ND	15	ND	ND	ND	ND	ND	ND
OG 307	110	13	24	19	10	ND	146	94	4127	34	228	216	ND	ND	ND	15	24	ND	69	ND	ND	ND
OG 308	330	28	22	31	31	ND	136	178	1739	31	214	491	ND	ND	ND	ND	ND	ND	ND	ND	ND	ND
OG 309	246	24	29	31	31	ND	131	84	1433	31	221	346	ND	ND	ND	ND	ND	ND	ND	ND	ND	ND
OG 310	451	34	28	37	73	ND	172	283	1371	34	301	551	ND	67	ND	ND	25	ND	20	ND	ND	ND
OG 311	122	31	25	27	13	ND	225	199	513	34	125	139	ND	ND	ND	ND	ND	ND	ND	ND	ND	ND
OG 312	109	21	16	15	14	ND	136	199	257	36	264	243	ND	ND	ND	ND	ND	ND	ND	ND	ND	ND
OG 313	135	21	14	18	10	ND	106	210	697	26	88	345	ND	ND	ND	ND	ND	ND	ND	ND	ND	ND
OG 314	212	18	22	21	26	ND	119	367	308	50	160	57	ND	ND	ND	ND	ND	ND	ND	ND	ND	ND
OG 315	119	29	26	21	10	ND	131	147	17200	34	119	267	ND	156	ND	16	114	ND	248	53	ND	ND
OG 316	185	102	29	30	14	ND	141	189	5933	43	185	511	ND	ND	ND	24	41	ND	100	22	ND	ND
OG 317	278	155	20	24	11	ND	197	210	1588	41	148	540	ND	ND	ND	ND	ND	ND	ND	ND	ND	ND
OG 318	171	86	21	21	7	ND	141	157	16000	41	92	170	ND	136	34	40	126	ND	364	51	ND	ND
OG 319	376	91	96	25	18	ND	232	105	13100	43	175	794	24	56	ND	ND	106	ND	255	48	ND	ND
OG 320	69	158	22	19	9	ND	220	84	19800	50	110	345	32	148	ND	ND	138	ND	352	74	ND	ND
OG 321	159	107	54	20	12	ND	179	115	15400	10	120	756	23	68	ND	36	115	ND	199	51	ND	ND

Table 5 - Ongombo Prospect: trace element geochemistry of the ore-bearing sequence in drill cores.
(Boreholes no. OGB 151A, OGB 153A, OGB 154A).

BOREHOLE OGB 151A

Sample no.	Cu ppm	Pb ppm	Zn ppm	Ni ppm	Co ppm	Ag ppm	Au ppb	Mn ppm	Ba ppm	Cr ppm	V ppm	TiO2 %	As ppm	WO3 ppm	Mo ppm	Sn ppm	Zr ppm	Rb ppm	Sr ppm	Bi ppm	Nb ppm	Y ppm
OG 384	27	19	57	41	13	ND	ND	232	799	96	133	1.03	ND	34	ND	ND	230	130	106	23	ND	59
OG 385	65	17	44	34	14	ND	ND	211	340	96	90	0.92	ND	48	ND	ND	261	92	144	ND	20	54
OG 386	54	17	53	40	16	ND	50	282	552	89	153	1.13	ND	77	ND	ND	284	123	143	ND	31	59
OG 387	35	19	60	36	17	ND	ND	302	462	105	107	0.99	ND	72	ND	ND	242	104	153	21	33	46
OG 388	6	22	66	44	25	ND	42	362	416	96	118	0.96	ND	92	ND	ND	224	89	184	ND	ND	59
OG 389	5	19	57	84	32	ND	50	483	53	185	257	1.09	ND	84	25	ND	82	119	63	ND	ND	84
OG 390	21	19	73	34	22	ND	ND	544	534	91	105	1.00	ND	58	ND	ND	287	94	170	20	26	47
OG 391	30	20	110	48	23	ND	50	544	717	96	144	1.06	ND	79	ND	ND	225	143	116	ND	20	61
OG 392	10	20	79	36	17	ND	ND	574	597	98	92	1.05	ND	51	ND	ND	389	139	181	ND	35	62
OG 393	3	16	67	31	17	ND	ND	483	574	64	70	0.90	ND	69	ND	ND	270	81	171	ND	ND	42
OG 394	4	14	66	32	15	ND	ND	473	562	74	86	0.93	ND	33	ND	ND	258	92	188	ND	23	53
OG 395	3	15	81	148	21	ND	ND	252	55	167	134	0.71	ND	85	ND	ND	99	18	23	ND	ND	24
OG 396	146	21	90	45	21	ND	ND	362	349	108	102	0.96	ND	89	ND	ND	214	73	129	ND	ND	38
OG 397	9	25	118	134	35	ND	47	644	74	130	170	0.89	ND	ND	ND	ND	144	15	36	ND	23	40
OG 398	752	21	82	45	19	ND	40	574	219	84	138	0.95	ND	98	ND	ND	220	29	95	ND	ND	39
OG 399	47	19	87	46	16	ND	ND	674	219	93	164	0.96	ND	57	ND	ND	207	44	82	20	21	27
OG 400	28	15	85	42	14	ND	ND	473	384	88	140	1.04	ND	42	ND	ND	262	49	100	ND	30	37
OG 601	399	13	88	50	21	1	ND	581	504	63	134	0.93	ND	80	ND	21	212	66	131	ND	ND	31
OG 602	0.21%	15	101	145	17	1	47	551	119	101	85	0.83	ND	31	ND	ND	170	18	107	ND	27	34
OG 603	110	16	106	53	18	ND	42	571	371	91	133	0.99	ND	62	ND	ND	246	49	135	ND	ND	43
OG 604	194	14	134	108	17	ND	42	921	107	166	134	0.68	ND	62	ND	ND	113	17	36	ND	ND	22
OG 605	58	17	83	35	17	ND	ND	559	221	87	115	1.03	ND	72	ND	ND	311	34	142	ND	ND	41
OG 606	14	19	110	90	27	ND	ND	838	154	140	198	1.02	ND	ND	ND	31	177	39	88	ND	26	36
OG 607	37	20	70	47	22	ND	ND	569	204	67	133	0.96	ND	57	ND	ND	243	43	150	ND	36	53
OG 608	33	19	55	71	23	ND	ND	778	132	103	289	1.25	ND	50	25	ND	134	25	104	ND	ND	37
OG 609	67	19	56	50	17	ND	40	469	215	94	129	0.98	ND	60	ND	ND	223	43	139	ND	24	30
OG 610	96	20	60	40	14	ND	ND	379	683	84	139	0.96	ND	79	ND	ND	198	91	117	ND	ND	48
ore zone																						
OG 611	47	23	46	42	20	ND	ND	279	660	75	156	1.11	ND	91	ND	ND	218	129	131	ND	ND	54
OG 612	40	22	36	47	17	ND	ND	319	635	84	114	1.07	ND	100	ND	ND	231	127	107	ND	25	56
OG 613	6	19	61	44	16	ND	ND	269	704	87	127	1.13	ND	76	ND	ND	227	130	126	ND	33	58
OG 614	13	20	61	34	12	ND	ND	409	561	75	49	1.06	ND	47	20	ND	249	102	189	ND	30	68
OG 615	9	20	75	38	14	ND	ND	289	522	58	100	1.02	ND	101	ND	ND	237	97	162	22	ND	46
OG 616	80	30	65	139	24	ND	ND	359	603	65	127	1.08	ND	63	ND	ND	232	130	129	ND	32	54
OG 617	29	25	93	55	23	ND	40	339	767	87	141	1.26	ND	72	ND	ND	253	161	157	24	26	65
OG 618	6	27	105	54	25	ND	57	309	540	59	145	1.49	ND	53	ND	ND	381	155	310	ND	48	76
OG 619	31	23	81	50	18	ND	47	309	736	67	183	1.19	ND	68	ND	ND	239	171	133	30	46	73
OG 620	51	19	46	42	12	ND	ND	319	284	79	91	0.94	ND	37	ND	ND	232	91	129	ND	30	51
OG 621	118	22	84	53	15	ND	60	354	831	87	179	1.22	ND	65	21	ND	240	173	140	21	25	66
OG 622	20	19	89	43	15	ND	ND	364	418	77	123	1.06	ND	ND	ND	ND	285	108	162	ND	ND	68
OG 623	42	23	108	60	20	ND	58	304	1268	67	186	1.23	ND	55	ND	ND	257	191	163	32	31	67
OG 624	160	18	95	66	20	1	63	283	878	65	173	0.94	ND	79	25	ND	209	161	196	ND	ND	54
OG 625	54	25	95	42	27	ND	ND	324	991	60	142	1.18	ND	99	ND	ND	246	159	140	ND	ND	67
OG 626	39	22	62	38	22	ND	ND	506	880	70	122	1.12	ND	80	21	ND	320	114	158	ND	23	56
OG 627	12	20	73	33	22	ND	48	597	831	70	118	1.10	ND	74	23	ND	300	131	179	29	ND	55
OG 628	48	24	60	33	19	ND	ND	445	548	53	134	0.97	ND	51	22	ND	298	103	169	ND	ND	54
OG 629	96	21	78	42	21	ND	ND	395	738	48	155	1.10	ND	53	ND	ND	259	131	156	ND	26	55

BOREHOLE OGB 153A

Sample no.	Cu ppm	Pb ppm	Zn ppm	Ni ppm	Co ppm	Ag ppm	Au ppb	Mn ppm	Ba ppm	Cr ppm	V ppm	TiO2 %	As ppm	WO3 ppm	Mo ppm	Sn ppm	Zr ppm	Rb ppm	Sr ppm	Bi ppm	Nb ppm	Y ppm
OG 322	26	24	63	48	28	ND	49	292	769	62	180	1.00	ND	80	ND	ND	235	132	125	ND	27	67
OG 323	44	25	76	29	18	ND	ND	232	521	101	70	1.01	ND	74	ND	ND	278	93	161	ND	ND	59
OG 324	33	20	83	38	20	ND	ND	282	551	77	121	0.99	ND	70	ND	ND	239	108	139	ND	27	55
OG 325	9	28	60	49	21	ND	ND	242	783	84	167	1.07	ND	57	ND	ND	225	142	104	ND	ND	64
OG 326	36	21	68	33	12	ND	ND	212	311	94	122	0.89	ND	98	ND	ND	257	91	129	ND	ND	44
OG 327	24	30	73	56	21	ND	54	232	919	69	217	0.91	ND	109	ND	ND	177	149	72	22	ND	63
OG 328	46	24	95	45	22	ND	ND	272	455	42	127	1.03	ND	75	ND	ND	277	120	150	ND	ND	67
OG 329	31	24	70	44	25	ND	ND	212	826	69	182	0.94	ND	103	ND	ND	218	142	103	ND	24	75
OG 330	33	21	80	40	17	ND	ND	242	390	91	102	0.96	ND	55	ND	ND	265	105	132	26	ND	54
OG 331	75	24	118	47	19	ND	ND	282	645	79	158	1.02	ND	36	ND	ND	228	133	123	ND	ND	53
OG 332	21	23	89	37	17	ND	ND	232	456	84	107	0.97	ND	74	ND	ND	252	98	143	22	ND	56
OG 333	15	25	93	42	18	ND	ND	242	559	72	96	0.98	ND	46	ND	ND	227	118	128	ND	37	62
OG 334	33	24	70	36	11	ND	ND	232	337	96	78	1.05	ND	47	20	ND	288	89	149	ND	ND	40
OG 335	27	24	71	45	19	ND	ND	252	713	84	96	1.09	ND	51	ND	ND	221	139	106	ND	ND	59
OG 336	14	23	120	52	23	ND	61	282	936	89	178	1.14	ND	79	ND	ND	256	157	108	ND	ND	70
OG 337	33	23	96	42	21	ND	ND	343	707	89	143	1.02	ND	ND	ND	ND	269	120	115	ND	35	57
OG 338	19	22	92	36	15	ND	46	353	568	81	109	0.96	ND	82	ND	ND	250	105	122	ND	ND	37
OG 339	24	25	89	36	17	ND	ND	393	809	74	145	0.98	ND	85	ND	ND	223	121	109	ND	ND	52
OG 340	18	28	83	39	18	ND	ND	373	631	59	80	1.05	ND	65	ND	ND	248	113	125	ND	32	40
OG 341	59	24	70	64	21	ND	ND	373	593	77	86	1.32	ND	59	ND	ND	435	109	229	ND	42	73
OG 342	9	22	79	161	25	ND	ND	464	455	319	161	0.75	ND	57	ND	ND	97	113	14	ND	ND	47
OG 343	20	20	74	49	18	ND	ND	393	682	74	99	1.11	ND	63	ND	ND	251	80	129	ND	50	46
OG 344	4	22	45	42	17	ND	ND	353	528	240	131	0.83	ND	97	ND	ND	115	106	82	ND	32	36
OG 345	7	21	323	27	9	ND	ND	322	153	104	303	1.34	ND	ND	ND	ND	119	24	135	ND	24	74
OG 346	3	25	58	38	14	ND	ND	393	551	64	325	1.56	ND	74	ND	ND	119	88	83	ND	ND	61
OG 347	19	25	70	43	17	ND	58	393	629	81	96	1.20	ND	83	ND	ND	243	140	186	24	ND	54
OG 348	5	20	72	40	23	ND	58	433	648	77	121	0.98	ND	43	ND	ND	233	71	87	ND	ND	41
OG 349	8	20	67	33	21	ND	40	524	294	86	95	1.07	ND	42	ND	ND	228	38	75	ND	26	47
OG 350	15	22	73	34	19	ND	ND	423	401	77	100	1.01	ND	77	ND	ND	212	85	122	ND	38	31
OG 351	14	15	40	34	13	ND	ND	504	186	84	352	1.61	ND	ND	21	ND	131	23	115	ND	ND	52
OG 352	56	18	75	50	23	ND	43	484	449	77	141	1.07	ND	69	ND	ND	221	102	139	ND	36	49
OG 353	14	18	68	37	14	ND	40	383	226	114	81	0.81	ND	38	ND	ND	229	46	129	ND	23	42
OG 354	115	18	131	59	26	ND	58	695	311	146	184	1.17	ND	88	25	ND	182	59	106	ND	ND	39
OG 355	19	18	64	35	15	ND	ND	413	300	106	60	0.91	ND	48	ND	ND	258	41	114	ND	42	48
OG 356	38	18	57	38	15	ND	ND	403	414	109	89	0.92	ND	31	ND	ND	225	45	111	ND	ND	33
OG 357	34	18	66	38	12	ND	55	393	234	106	86	0.87	ND	ND	ND	ND	234	26	130	ND	20	43
OG 358	81	23	120	73	24	ND	48	433	906	99	161	1.16	ND	40	24	ND	227	142	164	ND	27	55
OG 359	7	27	132	136	53	ND	65	524	680	373	333	1.21	ND	ND	ND	ND	87	97	ND	ND	20	55
OG 360	85	14	44	38	14	ND	40	333	144	128	185	1.15	ND	38	ND	ND	82	22	59	ND	ND	50
OG 361	75	16	44	34	20	ND	ND	494	110	79	349	1.74	ND	53	ND	ND	139	ND	117	ND	ND	65
OG 362	65	28	128	43	21	ND	ND	308	291	NS	111	0.94	ND	52	ND	ND	204	49	169	ND	22	51
OG 363	33	21	42	38	21	ND	ND	318	585	105	128	1.09	ND	71	ND	ND	260	79	116	ND	34	49
OG 364	31	25	157	45	17	ND	42	368	550	122	157	1.12	ND	ND	ND	ND	215	114	110	ND	ND	44
ore zone																						
OG 365	16	26	77	37	19	ND	ND	269	610	NS	108	0.92	ND	76	20	ND	213	112	133	ND	28	63
OG 366	5	20	84	33	17	ND	ND	318	684	NS	171	1.08	ND	65	ND	ND	232	135	131	ND	ND	58
OG 367	12	23	64	43	18	ND	ND	249	394	NS	70	0.93	ND	84	ND	ND	228	86	168	ND	ND	40
OG 368	13	24	40	47	20	ND	ND	249	676	NS	129	1.15	ND	83	ND	ND	233	132	133	ND	ND	56
OG 369	25	24	73	34	15	ND	ND	209	400	96	100	0.99	ND	ND	ND	ND	250	97	169	ND	20	43
OG 370	23	20	53	43	20	ND	ND	209	640	86	139	0.99	ND	79	ND	ND	195	125	114	ND	24	50
OG 371	11	20	64	50	17	ND	ND	239	707	72	132	1.15	ND	86	29	ND	235	168	147	ND	ND	57
OG 372	15	19	47	55	18	ND	42	279	636	89	196	1.17	ND	ND	ND	ND	215	153	112	22	25	48
OG 373	3	21	43	43	15	ND	ND	299	371	67	95	1.03	ND	53	ND	ND	225	114	146	ND	ND	65

BOREHOLE OGB 153A

Sample no.	Cu ppm	Pb ppm	Zn ppm	Ni ppm	Co ppm	Ag ppm	Au ppb	Mn ppm	Ba ppm	Cr ppm	V ppm	TiO2 %	As ppm	WO3 ppm	Mo ppm	Sn ppm	Zr ppm	Rb ppm	Sr ppm	Bi ppm	Nb ppm	Y ppm
OG 374	14	21	48	40	16	ND	ND	393	670	70	133	1.17	ND	36	ND	ND	231	149	129	ND	ND	58
OG 375	13	16	62	44	16	ND	ND	413	687	70	127	1.15	ND	83	23	ND	235	140	123	ND	ND	55
OG 376	12	23	93	39	17	ND	ND	634	548	77	95	1.06	ND	49	ND	ND	268	113	145	ND	22	44
OG 377	9	24	132	51	25	ND	ND	745	858	96	154	1.15	ND	87	32	ND	216	176	95	ND	36	68
OG 378	15	20	71	32	15	ND	ND	695	571	120	71	1.16	ND	36	ND	ND	317	93	140	ND	38	49
OG 379	4	20	84	28	15	ND	ND	664	591	93	134	1.06	ND	32	ND	ND	231	106	120	ND	29	34
OG 380	30	20	64	33	18	ND	ND	564	495	105	67	1.09	ND	77	ND	ND	318	104	141	ND	39	63
OG 381	10	20	108	42	10	ND	ND	564	764	98	155	1.08	ND	64	ND	ND	266	147	128	ND	ND	60
OG 382	33	21	80	36	16	ND	ND	372	417	77	121	1.05	ND	47	ND	ND	294	104	151	ND	27	47
OG 383	9	19	110	42	15	ND	ND	393	744	89	100	1.33	ND	40	ND	ND	389	141	135	ND	ND	52

BOREHOLE OGB 154A

Sample no.	Cu ppm	Pb ppm	Zn ppm	Ni ppm	Co ppm	Ag ppm	Au ppb	Mn ppm	Ba ppm	Cr ppm	V ppm	TiO2 %	As ppm	WO3 ppm	Mo ppm	Sn ppm	Zr ppm	Rb ppm	Sr ppm	Bi ppm	Nb ppm	Y ppm
OG 630	16	20	92	38	17	ND	ND	395	687	63	124	1.12	ND	69	ND	ND	285	109	120	ND	26	60
OG 631	108	19	113	44	21	ND	45	526	432	46	163	0.99	ND	62	ND	ND	239	81	196	ND	24	52
OG 632	35	16	71	177	28	ND	ND	210	ND	150	205	0.81	ND	43	ND	ND	69	ND	19	ND	ND	26
OG 633	6	15	35	48	14	ND	ND	213	22	130	222	0.87	ND	ND	ND	ND	104	ND	174	ND	ND	32
OG 634	248	19	101	202	43	ND	ND	496	56	113	235	1.04	ND	105	ND	ND	97	ND	44	ND	ND	20
OG 635	19	19	82	38	20	ND	ND	536	319	65	132	0.96	ND	55	ND	ND	308	48	112	ND	23	61
OG 636	7	19	92	44	20	ND	ND	719	136	44	120	0.93	ND	48	ND	ND	247	25	113	ND	38	38
OG 637	66	22	131	60	25	ND	45	941	351	67	237	0.14	ND	63	ND	ND	197	73	78	ND	22	31
OG 638	61	17	84	41	21	ND	ND	658	232	64	123	0.93	ND	83	ND	ND	241	43	117	ND	ND	44
OG 639	13	15	80	31	15	ND	ND	455	129	59	98	0.87	ND	41	ND	27	276	24	82	ND	35	29
OG 640	150	18	124	65	21	1	ND	830	232	86	299	1.71	ND	79	36	ND	149	51	65	ND	23	45
OG 641	36	18	105	44	20	ND	50	577	254	40	117	1.01	ND	62	ND	ND	240	29	94	ND	50	20
OG 642	16	13	96	40	28	ND	55	466	673	25	149	0.99	ND	70	ND	ND	241	58	145	ND	ND	51
OG 643	59	13	46	23	15	ND	ND	213	ND	7	380	1.52	ND	34	38	ND	142	ND	134	ND	ND	61
OG 644	31	13	80	20	12	ND	ND	253	ND	20	397	1.77	ND	ND	27	ND	147	ND	144	ND	ND	42
OG 645	3	15	92	89	27	ND	48	466	113	79	300	1.38	ND	82	ND	ND	130	33	110	ND	ND	43
OG 646	5	15	68	40	19	ND	ND	395	251	30	140	0.94	ND	80	ND	ND	242	47	131	ND	ND	40
OG 647	11	15	78	89	24	ND	ND	455	272	101	184	0.99	ND	40	ND	ND	186	52	121	ND	39	44
OG 648	21	14	52	44	18	ND	ND	466	210	62	156	0.94	ND	47	ND	ND	263	36	101	ND	37	53
OG 649	16	42	405	94	18	ND	ND	607	182	74	132	0.89	ND	43	ND	ND	251	37	126	ND	ND	59
OG 650	30	19	51	43	21	ND	ND	506	183	72	116	0.90	ND	86	ND	ND	259	35	125	ND	ND	30
OG 651	96	25	102	63	27	ND	ND	850	317	59	214	1.04	ND	46	ND	25	226	57	118	ND	27	48
OG 652	42	17	61	49	22	ND	45	466	262	69	113	0.91	ND	57	ND	ND	248	39	121	ND	ND	31
OG 653	11	18	28	40	16	ND	ND	409	425	79	114	1.06	ND	52	ND	ND	248	81	99	24	ND	43
OG 654	55	25	25	54	24	ND	43	370	815	72	169	1.10	ND	97	23	ND	216	133	82	ND	21	62
OG 655	61	22	30	44	17	ND	50	469	773	67	117	1.02	ND	81	ND	ND	235	96	87	20	34	67
OG 656	10	19	45	30	6	ND	ND	389	705	74	79	0.78	ND	65	ND	ND	210	49	17	ND	ND	27
OG 657	6	17	71	33	12	ND	ND	639	488	54	107	1.05	ND	84	ND	ND	335	93	212	ND	ND	61
OG 658	81	24	60	36	17	ND	40	389	778	69	104	0.65	ND	82	ND	23	126	56	ND	ND	32	23
OG 659	489	22	73	27	19	ND	45	449	328	77	76	0.61	ND	50	ND	ND	141	32	ND	ND	ND	41
ore zone																						
OG 660	88	21	41	38	19	ND	43	280	600	64	138	0.94	ND	112	ND	ND	230	96	91	ND	25	38
OG 661	105	25	25	45	24	ND	48	350	849	30	147	1.09	ND	70	ND	ND	215	133	53	ND	33	56

BOREHOLE OGB 154A

Sample no.	Cu ppm	Pb ppm	Zn ppm	Ni ppm	Co ppm	Ag ppm	Au ppb	Mn ppm	Ba ppm	Cr ppm	V ppm	TiO2 %	As ppm	WO3 ppm	Mo ppm	Sn ppm	Zr ppm	Rb ppm	Sr ppm	Bi ppm	Nb ppm	Y ppm
OG 662	114	18	31	38	18	ND	ND	280	1129	62	129	1.04	ND	83	ND	ND	266	120	61	ND	45	50
OG 663	27	21	53	36	16	ND	50	340	1405	74	152	1.01	ND	69	ND	ND	208	124	52	ND	ND	61
OG 664	26	15	66	37	18	ND	ND	260	559	54	114	1.01	ND	60	ND	ND	263	110	97	ND	ND	48
OG 665	29	25	53	42	19	ND	ND	260	724	69	138	1.10	ND	71	ND	ND	238	146	100	ND	34	64
OG 666	13	23	67	40	24	ND	ND	230	704	57	152	1.05	ND	76	ND	ND	230	132	100	ND	ND	59
OG 667	19	18	73	34	19	ND	ND	300	406	72	84	0.98	ND	37	ND	24	273	92	159	ND	ND	59
OG 668	14	21	102	44	22	ND	ND	280	660	64	159	1.07	ND	83	ND	ND	228	136	150	ND	31	57
OG 669	5	22	104	48	22	ND	ND	240	1071	69	212	1.17	ND	73	ND	ND	228	161	114	ND	ND	56
OG 670	25	18	75	34	18	ND	ND	200	387	104	72	0.94	ND	55	21	ND	243	90	151	ND	29	48
OG 671	42	16	45	33	20	ND	ND	190	405	104	106	0.79	ND	ND	ND	ND	218	76	114	ND	ND	47
OG 672	10	24	61	40	26	ND	ND	280	397	94	145	1.08	ND	72	ND	ND	237	117	152	ND	29	41
OG 673	9	22	76	40	21	ND	ND	200	486	79	72	1.00	ND	80	ND	ND	249	98	176	ND	22	58
OG 674	7	26	37	56	22	ND	ND	280	765	74	204	1.17	ND	94	ND	ND	218	17	33	ND	ND	69

Table 6 - Ongombo Prospect: trace element geochemistry
of the ore-zone rock types (analyses by Scientific Services
and Tsumeb Corporation Ltd. laboratories).

BOREHOLE No. OGB 151A

Sample no.	Cu	Pb	Zn	Ni	Co	Ag	Au	Mn	Ba	Cr	V	TiO2	As	WO3	Mo	Sn	Zr	Rb	Sr	Bi	Nb	Y
	%	ppm	ppm	ppm	ppm	ppm	ppm	ppm	ppm	ppm	ppm	ppr	ppm	ppm	ppm	ppm	ppm	ppm	ppm	ppm	ppm	ppm
448 GF	0.13	30	208	36	23	1	N/S	268	486	21	76	552	N/D	34	N/D	N/D	110	31	22	N/D	N/D	19
449 GF	0.45	32	265	36	33	3	0.11	318	557	6	130	779	N/D	77	22	N/D	142	58	54	N/D	N/D	N/D
450 GF	1.58	28	315	31	114	9	0.28	377	704	56	64	538	N/D	N/D	31	N/D	97	62	12	N/D	N/D	22
451 GF	1.48	16	261	37	99	8	0.63	298	435	11	83	612	N/D	N/D	N/D	N/D	99	36	13	N/D	N/D	N/D
452 GF	2.42	41	199	42	244	13	0.12	59	UR	15	UR	U	UR	UR	UR	UR	UR	UR	UR	UR	UR	UR
453 GF	0.18	39	138	38	30	2	0.04	333	UR	168	UR	U	UR	UR	UR	UR	UR	UR	UR	UR	UR	UR
454 GF	2.72	20	949	28	127	21	1.08	199	962	29	32	352	N/D	N/D	27	N/D	56	39	N/D	N/D	N/D	N/D
455 GF	0.13	30	206	38	33	2	0.01	298	1900	23	70	870	N/D	55	N/D	N/D	164	43	69	N/D	20	24
456 GF	0.27	28	215	30	29	2	0.05	308	2157	50	77	776	N/D	60	27	N/D	176	49	48	N/D	N/D	27
457 GF	3	22	323	25	119	20	0.31	199	1125	19	23	179	N/D	N/D	48	N/D	30	12	N/D	N/D	N/D	N/D
458 GF	0.93	32	168	21	47	8	0.14	137	UR	186	UR	U	UR	UR	UR	UR	UR	UR	UR	UR	UR	UR
459 GF	0.05	26	98	48	27	1	N/S	228	1444	34	126	110	N/D	76	N/D	N/D	233	111	129	N/D	24	39

BOREHOLE No. OGB 153A

Sample no.	Cu	Pb	Zn	Ni	Co	Ag	Au	Mn	Ba	Cr	V	TiO2	As	WO3	Mo	Sn	Zr	Rb	Sr	Bi	Nb	Y
	%	ppm	ppm	ppm	ppm	ppm	ppm	ppm	ppm	ppm	ppm	ppr	ppm	ppm	ppm	ppm	ppm	ppm	ppm	ppm	ppm	ppm
460 GF	0.04	38	83	47	23	N/D	N/S	288	678	38	150	110	N/D	53	N/D	N/D	206	105	100	N/D	32	45
461 GF	2.71	20	405	24	67	11	0.14	99	IS	IS	IS	I	IS	IS	IS	IS	IS	IS	IS	IS	IS	IS
462 GF	0.22	24	170	43	42	2	0.06	338	1046	63	122	887	N/D	44	N/D	N/D	161	69	37	N/D	N/D	34
463 GF	3.89	28	561	22	112	16	0.25	228	333	46	61	191	N/D	N/D	23	N/D	24	11	N/D	N/D	N/D	N/D
464 GF	0.52	74	275	27	24	3	0.06	407	1552	6	77	855	N/D	77	22	N/D	212	106	66	N/D	N/D	36
465 GF	11.75	44	1700	43	41	66	3.78	139	253	11	N/D	163	N/D	N/D	31	N/D	10	N/D	N/D	N/D	N/D	N/D
466 GF	0.03	56	159	36	13	N/D	0.08	248	1257	25	83	990	N/D	60	N/D	N/D	252	65	156	N/D	21	41
467 GF	8.45	33	1900	26	120	37	0.16	199	N/S	34	N/S	N/:	N/S	N/S	N/S	N/S	N/S	N/S	N/S	N/S	N/S	N/S
468 GF	3.13	47	914	30	64	UR	1.13	196	UR	66	UR	UI	UR	UR	UR	UR	UR	UR	UR	UR	UR	UR
469 GF	0.18	49	314	23	22	UR	0.04	255	UR	234	UR	UI	UR	UR	UR	UR	UR	UR	UR	UR	UR	UR
470 GF	1.72	84	566	25	136	UR	0.75	167	UR	30	UR	UI	UR	UR	UR	UR	UR	UR	UR	UR	UR	UR
471 GF	0.14	60	247	36	40	UR	0.04	284	UR	216	UR	UF	UR	UR	UR	UR	UR	UR	UR	UR	UR	UR
472 GF	0.56	51	334	32	43	UR	0.19	206	UR	204	UR	UF	UR	UR	UR	UR	UR	UR	UR	UR	UR	UR
473 GF	0.61	46	240	16	42	UR	0.4	167	UR	192	UR	UF	UR	UR	UR	UR	UR	UR	UR	UR	UR	UR
474 GF	1.41	61	325	30	60	UR	0.4	167	UR	174	UR	UR	UR	UR	UR	UR	UR	UR	UR	UR	UR	UR
475 GF	0.82	31	339	31	93	UR	0.24	343	UR	138	UR	UR	UR	UR	UR	UR	UR	UR	UR	UR	UR	UR
476 GF	0.15	35	138	36	21	UR	0.05	225	UR	162	UR	UR	UR	UR	UR	UR	UR	UR	UR	UR	UR	UR

BOREHOLE No. OGB 154A

Sample no.	Cu	Pb	Zn	Ni	Co	Ag	Au	Mn	Ba	Cr	V	TiO2	As	WO3	Mo	Sn	Zr	Rb	Sr	Bi	Nb	Y
	%	ppm	ppm	ppm	ppm	ppm	ppm	ppm	ppm	ppm	ppm	ppm	ppm	ppm	ppm	ppm	ppm	ppm	ppm	ppm	ppm	ppm
425 GF	0.12	18	160	42	20	ND	0.03	288	447	17	95	7839	N/D	N/D	N/D	N/D	174	48	46	N/D	N/D	21
426 GF	1.05	22	411	39	38	8	0.32	348	575	21	76	6635	N/D	N/D	N/D	N/D	115	87	41	N/D	N/D	33
427 GF	2.77	32	1100	29	121	17	0.39	89	107	29	24	1133	21	N/D	23	N/D	13	N/D	N/D	N/D	N/D	N/D
428 GF	0.25	29	313	40	31	2	0.07	407	549	186	82	6427	N/D	62	N/D	N/D	132	89	32	N/D	24	25
429 GF	0.03	24	85	46	25	ND	0.07	218	777	25	113	9972	N/D	52	N/D	N/D	225	106	80	N/D	N/D	35

Note: UR - unavailable result; N/S - insufficient sample; N/D - below detection limit.

Table 7 - Trace element geochemistry of the unmineralized schists.

sample no.	Cu ppm	Pb ppm	Zn ppm	Ni ppm	Co ppm	Ag ppm	Au ppb	Mn ppm	Ba ppm	Cr ppm	V ppm	Ti ppm	As ppm	WO3 ppm	Mo ppm	Sn ppm	Zr ppm	Rb ppm	Sr ppm	Bi ppm	Nb ppm	Y ppm
OG 71	80	29	92	41	29	ND	116	310	724	62	146	9900	ND	56	ND	63	252	128	128	36	ND	ND
OG 119	160	24	131	58	33	2	95	351	838	7	204	11000	ND	107	ND	32	242	130	98	36	ND	ND
OG 129	34	36	79	52	27	ND	66	260	750	17	119	10600	ND	ND	ND	ND	209	131	105	ND	ND	60
OG 130	42	41	108	67	28	ND	46	260	971	10	227	10200	ND	ND	ND	ND	203	157	86	ND	ND	ND
OG 131	54	41	95	85	25	ND	46	150	952	7	213	9480	ND	46	ND	ND	245	149	85	ND	ND	65
OG 132	21	26	77	59	26	ND	63	210	909	7	205	9757	ND	ND	ND	ND	254	141	83	ND	ND	ND
OG 133	44	38	114	39	27	ND	63	190	776	10	227	10400	ND	ND	ND	ND	213	133	107	ND	ND	ND
OG 134	59	36	122	47	24	ND	74	130	732	17	183	10800	ND	ND	ND	ND	229	139	111	ND	ND	56
OG 135	64	38	115	56	20	ND	61	190	940	27	218	9945	ND	ND	ND	ND	204	139	90	ND	ND	ND
OG 136	32	34	111	51	21	ND	63	160	672	22	152	9836	ND	ND	ND	ND	212	128	96	ND	ND	ND
$\bar{x}$	59	30.6	104.4	55.3	26	0.1	69.3	221.1	758.4	18.6	189.4	10200	ND	20.9	ND	9.5	226.3	137.5	98.9	7.2	ND	18

Table 8 - Ongeama Prospect: trace element geochemistry of the magnetic schists from the "I anomaly" area.

sample no.	Cu ppm	Pb ppm	Zn ppm	Ni ppm	Co ppm	Ag ppm	Au ppb	Mn ppm	Ba ppm	Cr ppm	V ppm	Ti ppm	As ppm	WO3 ppm	Mo ppm	Sn ppm	Zr ppm	Rb ppm	Sr ppm	Bi ppm	Nb ppm	Y ppm
OG 137	44	32	90	56	17	ND	58	350	568	12	124	10400	ND	ND	ND	ND	264	100	91	ND	ND	ND
OG 138	92	33	84	43	16	ND	53	579	201	17	146	8873	ND	38	ND	ND	192	25	81	ND	ND	ND
OG 139	38	33	78	34	13	ND	46	300	532	12	133	9583	ND	ND	ND	ND	231	100	93	ND	ND	67
OG 140	43	30	104	44	17	ND	51	459	715	17	141	10600	ND	ND	ND	ND	235	108	93	ND	ND	ND
OG 141	43	31	85	45	11	ND	43	409	533	7	101	9985	ND	ND	ND	ND	294	104	111	ND	ND	ND
OG 142	38	31	76	29	11	ND	56	330	624	12	97	9269	ND	ND	ND	ND	246	96	107	ND	ND	55
OG 143	45	30	74	34	11	ND	66	310	487	7	110	10400	ND	ND	ND	ND	259	96	122	ND	ND	ND

Table 9 - X-Ray fluorescence analytical conditions and rock standards used.

Element	Emission Line	Tube	kV	mA	Crystal	Time	Counter	Collimator	Specimen
Si	K	Cr	55	40	PET	40	flow	coarse	fusion disc
Ti	K	Cr	55	40	LIF (200)	10	flow	fine	fusion disc
Al	K	Cr	55	40	PET	40	flow	coarse	fusion disc
Fe	K	Cr	55	40	LIF (200)	20	flow	fine	fusion disc
Mn	K	Cr	55	40	LIF (200)	20	flow	coarse	fusion disc
Mg	K	Cr	55	40	TLAP	100	flow	fine	fusion disc
Ca	K	Cr	55	40	LIF (200)	10	flow	fine	fusion disc
Na	K	Cr	55	40	TLAP	100	flow	fine	powder pellet
K	K	Cr	55	40	LIF (200)	10	flow	fine	fusion disc
P	K	Cr	55	40	Ge	20	flow	coarse	fusion disc

Rock standards

Major elements AGV-1, BCR-1, GSP-1, NIM-D, NIM-N

Na BCR-1, GSP-1, AGV-1, G-2

Table 10 - Ongeama Prospect:major element geochemistry of selected samples from the alteration pipe.

	OG 37 (FS)	OG 43 (MM)	OG 52 (MM)	OG 62 (MM)	OG 75 (MM)	OG 77 (CS)	OG 80 (CS)	OG 84 (CS)	OG 87 (CS)
SiO2	19.176	58.314	36.315	72.412	64.328	60.672	63.178	64.164	65.983
TiO2	0.417	0.606	0.54	0.67	0.639	0.793	0.785	0.773	0.773
Al2O3	3.618	7.931	4.171	7.258	9.838	13.516	12.107	11.494	12.075
Fe2O3	66.407	30.103	50.594	16.395	19.032	19.951	19.772	17.675	16.099
FeO	0	0	0	0	0	0	0	0	0
MnO	0.61	0.091	0.083	0.091	0.071	0.171	0.083	0.11	0.091
MgO	0.246	0.277	0.699	0.354	2.053	3.42	2.955	3.085	2.576
CaO	0.231	0	0.105	0	0	0.034	0	0.018	0.003
Na2O	4.198	0.381	0.118	0.542	0.331	0.091	0.142	0.09	0.308
K2O	0	1.125	0.856	1.274	1.047	0.054	0.153	0.054	0.0726
P2O5	0.285	0.146	0.214	0.082	0.087	0.136	0.131	0.101	0.102
LOI	7.68	3.55	6.07	2.54	2.5	2.6	2.71	2.54	2.71
H2O-	1.2	0.6	1	0.4	0.18	0.18	0.17	0.16	0.15
	103.619	103.125	100.496	102.018	100.106	101.617	102.186	101.265	101.598

Note: FS = ferruginous schist; MM = magnetic muscovite schist; CS = magnetic chlorite schist.

Table 11 - Matchless West Extension deposit:major element geochemistry of selected samples from the alteration pipe.

	MWE 202	MWE210	MWE 219	MWE 226	MWE 234
SiO2	70.529	94.834	63.606	51.81	76.579
TiO2	0.802	0.021	0.312	0.741	0.302
Al2O3	11.71	0.274	3.687	8.837	1.451
Fe2O3	7.611	3.257	26.514	29.701	18.931
FeO	0	0	0	0	0
MnO	0.095	0.014	0.045	0.096	0.031
MgO	3.446	0.013	0.214	0.414	0.016
CaO	0.047	0	0.02	0.02	0.011
Na2O	0.373	0.013	0.176	0.321	0.0529
K2O	2.125	0	0.806	2.425	0
P2O5	0.184	0.077	0.16	0.208	0.05
LOI	3.04	0.53	3.65	3.85	1.87
H2O-	0.52	0.17	0.7	0.91	0.49
	100.482	99.318	99.892	99.312	100.26

Note:

MWE 202 = phlogopite-bearing muscovite-chlorite schist (marginal zone)
MWE 210 = pyrite-bearing muscovite quartzite (axial zone)
MWE 219 = pyrite-bearing quartz-muscovite schist (marginal zone)
MWE 226 = pyrite-bearing quartz-muscovite schist (marginal zone)
MWE 234 = pyrite-bearing quartz-muscovite schist (marginal zone)

Table 12 - Major element geochemistry of unmineralized metapelitic schists (Kuiseb Formation).

	OG 131	OG 135	OG 138
SiO2	55.323	6.079	69.912
TiO2	1.048	1.02	0.856
Al2O3	19.298	17.215	12.339
Fe2O3	9.189	8.264	7.996
FeO	0	0	0
MnO	0.151	0.093	0.111
MgO	4.146	3.701	2.273
CaO	0.993	0.982	2.62
Na2O	0.916	1.251	2.597
K2O	4.185	3.87	0.492
P2O5	0.211	0.276	0.254
LOI	3.07	2.37	1.64
H2O-	0.93	0.22	0.24
	99.458	100.052	101.33

Table 13 - Subdivision of the alteration pipe at Ongeama in sectors:average of the trace element content for each sector.

Sector	Cu ppm	Pb ppm	Zn ppm	Ni ppm	Co ppm	Ag ppm	Au ppm	Cr ppm	Mn ppm	Ba ppm	V ppm	Ti ppm	Rb ppm	Sr ppm	Zr ppm	Sn ppm	W ppm	Mo ppm	As ppm	Nb ppm	Y ppm	Bi ppm
I	1530	101.3	133	28.7	27.7	0.03	0.164	42.3	303	1451	107.7	7031	22	34	127.3	10.7	27.3	0	7.3	0	0	6.7
II	2070	111.7	232.7	26.7	34.3	0.36	0.336	52.3	319.7	1203	142	6500	26	31.3	96.7	13.33	0	0	0	10	0	14
III	2170	106.3	193.3	23.7	24.7	0.7	0.328	52.3	342.7	3402	100.3	5466.7	20.7	50	126.7	25.7	47.3	0	16.3	0	0	24
IV	1470	22	73	30.7	26.7	0.05	0.166	53	309.7	1800	128	4175	10	28	156	22.7	24.7	0	173.7	0	0	41.3
V	750	28	53.5	34	17.5	0.05	0.122	51	305	1522	138	5900	5	23	149.5	41	0	0	179.5	0	0	31
VI	650	31	53.5	34	19.5	0.05	0.153	32.5	195.5	1018	109	6350	11	24	173.5	38	0	0	161	0	0	26
VII	700	21	32.5	31.5	17	0.05	0.14	11	291	155	82	5600	5	12	146	18	37.5	0	144	19	0	30

Note:

Sector I includes samples OG 43, OG 46, OG 49
Sector II includes samples OG 52, OG 55, OG 58
Sector III includes samples OG 62, OG 67, OG 75
Sector IV includes samples OG 76, OG 77, OG 78
Sector V includes samples OG 80, OG 81

Table 14 - Subdivision of the alteration pipe at Matchless West Extension in sectors: average of the trace element content in each sector.

Sector	Cu ppm	Pb ppm	Zn ppm	Ni ppm	Co ppm	Ag ppm	Au ppm	Cr ppm	Mn ppm	Ba ppm	V ppm	Ti ppm	Rb ppm	Sr ppm	Zr ppm	Sn ppm	WO3 ppm	Mo ppm	As ppm	Nb ppm	Y ppm	Bi ppm
I	1600	37	43	27.25	18.75	0.75	0.052	10.25	159.5	246.35	109.5	7440.5	58.75	19.75	206.5	0	19.5	8.25	0	0	0	0
II	1600	61	23.5	19.5	12.5	0.05	0.054	27	65	1710.5	127.5	8172	71	16	196	0	0	0	0	0	0	0
III	1900	174.5	54.3	22.25	14.75	5.25	0.064	18.5	294.25	1681.5	90	5207.75	39.75	12	132.25	0	0	7.8	12.25	0	0	9.5
IV	1800	82.25	34.25	26.5	17.75	0.5	0.11	23	72.5	2758.5	136	6101.3	57.5	0	145	0	55.25	86.75	12	0	0	0
V	5400	65.5	101.25	22.5	18.5	1.25	0.095	23.5	169.25	3947	249.25	7967.75	38.25	36.75	145.25	30.25	13.5	60.25	18.5	0	15	0
VI	4100	574.6	851.16	24.2	17.4	1.4	0.095	20	141.8	4135.8	105.8	3806.8	3	32	84.8	13.2	28.2	24	12.4	0	0	27.2

Note:

Sector I includes samples MWE 201, MWE 202, MWE 204, MWE 205
Sector II includes samples MWE 206, MWE 209
Sector III includes samples MWE 210, MWE 211, MWE 214, MWE 215
Sector IV includes samples MWE 216, MWE 217, MWE 219, MWE 220
Sector V includes samples MWE 221, MWE 224, MWE 226, MWE 229
Sector VI includes samples MWE 232, MWE 234, MWE 235, MWE 237, MWE 238

Table 15 - Ongeama Prospect: barium and zinc contents in the schists of the alteration pipe.

ONGEAMA TRACE ELEMENT GEOCHEMISTRY - ALTERATION PIPE

distance	Ba ppm	Zn ppm
-101.4	204	32
-84.3	106	33
-61.4	1648	55
-47.1	388	52
-32.9	2338	54
-25.7	706	53
-16.7	2662	61
-10	414	48
-8.6	2324	110
5.7	4200	145
37.1	2875	188
62.9	3130	247
78.6	1676	181
95.7	1100	249
112.9	834	268
134.3	988	144
150	1308	115
170	2057	140

Table 16.a

UNMINERALIZED SCHISTS

sample no.	I trace	TZ
OG 71	0.802	0.39
OG 119	0.818	0.45
OG 129	0.792	0.51
OG 130	0.827	0.5
OG 131	0.83	0.39
OG 132	0.822	0.38
OG 133	0.802	0.49
OG 134	0.791	0.47
OG 135	0.835	0.49
OG 136	0.791	0.46

Table 16.b

ONGEAMA PROSPECT: MAGNETIC SCHISTS FROM THE "I ANOMALY" AREA

sample no.	I trace	TZ
OG 137	0.793	0.39
OG 138	0.794	0.46
OG 139	0.779	0.41
OG 140	0.816	0.45
OG 141	0.763	0.34
OG 142	0.791	0.38
OG 143	0.745	0.4

Table 16.c

ONGEAMA PROSPECT - ALTERATION PIPE

sample no.	I trace	TZ
OG 7	0.995	0.669
OG 25	0.988	0.568
OG 30	0.993	0.787
OG 32	0.997	1.61
OG 37	1	2.1
OG 40	0.994	0.639
OG 43	0.988	0.485
OG 46	0.976	0.515
OG 49	0.981	0.672
OG 52	0.995	1.13
OG 55	0.976	0.65
OG 58	0.982	0.477
OG 62	0.982	0.425
OG 64	0.998	0.86
OG 67	0.992	0.558
OG 75	0.989	0.358
OG 76	0.992	0.349
OG 77	0.987	0.396
OG 78	0.989	0.327
OG 80	0.986	0.418
OG 81	0.989	0.373
OG 84	0.983	0.376
OG 85	0.992	0.712
OG 87	0.979	0.378
OG 88	0.983	0.529
OG 89	0.992	0.542
OG 91	0.995	0.401
OG 92	0.988	1.09
OG 93	0.992	0.519
OG 96	0.97	0.369
OG 98	0.991	0.528
OG 99	1	0.205
OG 101	0.994	0.585
OG 104	0.993	0.663
OG 107	0.985	0.431
OG 109	0.995	0.643
OG 111	0.983	0.418
OG 113	0.981	0.32

Table 16.d

MATCHLESS WEST EXTENSION

sample no.	I trace	TZ
MWE 201	0.99	0.41
MWE 202	0.97	0.35
MWE 204	0.97	0.32
MWE 205	0.99	0.44
MWE 206	0.97	0.47
MWE 209	0.97	0.37
MWE 210	1	0.17
MWE 211	0.98	0.47
MWE 214	0.99	0.49
MWE 215	0.98	0.34
MWE 216	0.98	0.5
MWE 217	0.98	0.39
MWE 219	0.99	0.57
MWE 220	0.99	0.38
MWE 221	0.99	0.43
MWE 224	0.99	1.2
MWE 226	0.99	0.49
MWE 229	0.99	0.4
MWE 232	0.99	0.47
MWE 234	0.99	0.57
MWE 235	1	0.5
MWE 237	0.99	0
MWE 238	0.99	0.43

ONGOMBO PROSPECT - THE ORE-HOSTING SEQUENCE IN DRILL CORES

Table 16.e

BOREHOLE OGB 151A

sample no.		I trace	TZ
OG 384	(H/W)	0.79	0.448
OG 385	(H/W)	0.36	0.352
OG 386	(H/W)	0.72	0.398
OG 387	(H/W)	0.69	0.408
OG 388	(H/W)	0.65	0.43
OG 390	(H/W)	0.71	0.347
OG 391	(H/W)	0.77	0.471
OG 392	(H/W)	0.69	0.27
OG 393	(H/W)	0.72	0.335
OG 394	(H/W)	0.7	0.362
OG 396	(H/W)	0.75	0.45
OG 398	(H/W)	0.9	0.43
OG 399	(H/W)	0.75	0.463
OG 400	(H/W)	0.78	0.397
OG 601	(H/W)	0.84	0.438
OG 602	(H/W)	0.94	0.487
OG 603	(H/W)	0.75	0.402
OG 604	(H/W)	0.89	0.604
OG 605	(H/W)	0.72	0.331
OG 606	(H/W)	0.7	0.576
OG 607	(H/W)	0.64	0.395
OG 609	(H/W)	0.66	0.438
OG 610	(H/W)	0.8	0.483
-------------- ore zone ---------			
OG 611	(F/W)	0.75	0.509
OG 612	(F/W)	0.76	0.463
OG 613	(F/W)	0.75	0.498
OG 614	(F/W)	0.69	0.426
OG 615	(F/W)	0.71	0.43
OG 616	(F/W)	0.75	0.465
OG 617	(F/W)	0.74	0.498
OG 618	(F/W)	0.59	0.391
OG 619	(F/W)	0.74	0.498
OG 620	(F/W)	0.65	0.403
OG 621	(F/W)	0.77	0.508
OG 622	(F/W)	0.67	0.372
OG 623	(F/W)	0.8	0.479
OG 625	(F/W)	0.8	0.48
OG 626	(F/W)	0.79	0.35
OG 627	(F/W)	0.75	0.367
OG 628	(F/W)	0.72	0.327
OG 629	(F/W)	0.76	0.39

Table 16.f

BOREHOLE NO. OGB 153A

sample no.		I trace	TZ
OG 322	(H/W)	0.744	0.426
OG 323	(H/W)	0.724	0.363
OG 324	(H/W)	0.735	0.412
OG 325	(H/W)	0.781	0.475
OG 326	(H/W)	0.665	0.348
OG 327	(H/W)	0.826	0.512
OG 328	(H/W)	0.697	0.372
OG 329	(H/W)	0.795	0.433
OG 330	(H/W)	0.689	0.362
OG 331	(H/W)	0.771	0.447
OG 332	(H/W)	0.71	0.387
OG 333	(H/W)	0.738	0.433
OG 334	(H/W)	0.661	0.365
OG 335	(H/W)	0.773	0.493
OG 336	(H/W)	0.805	0.445
OG 337	(H/W)	0.785	0.379
OG 338	(H/W)	0.755	0.382
OG 339	(H/W)	0.805	0.44
OG 340	(H/W)	0.761	0.423
OG 341	(H/W)	0.688	0.303
OG 343	(H/W)	0.792	0.442
OG 347	(H/W)	0.695	0.494
OG 348	(H/W)	0.825	0.422
OG 349	(H/W)	0.775	0.469
OG 350	(H/W)	0.712	0.476
OG 352	(H/W)	0.713	0.452
OG 353	(H/W)	0.651	0.352
OG 354	(H/W)	0.777	0.643
OG 355	(H/W)	0.721	0.351
OG 356	(H/W)	0.772	0.41
OG 357	(H/W)	0.693	0.373
OG 358	(H/W)	0.787	0.51
OG 362	(H/W)	0.701	0.46
OG 363	(H/W)	0.777	0.419
OG 364	(H/W)	0.773	0.521
------- ore zone ---------------			
OG 365	(F/W)	0.748	0.431
OG 366	(F/W)	0.749	0.465
OG 367	(F/W)	0.66	0.408
OG 368	(F/W)	0.74	0.49
OG 369	(F/W)	0.662	0.39
OG 370	(F/W)	0.755	0.51
OG 371	(F/W)	0.718	0.489
OG 372	(F/W)	0.73	0.544
OG 373	(F/W)	0.627	0.458
OG 374	(F/W)	0.73	0.506
OG 375	(F/W)	0.747	0.489
OG 376	(F/W)	0.724	0.395
OG 377	(F/W)	0.791	0.532
OG 378	(F/W)	0.769	0.366
OG 379	(F/W)	0.756	0.459
OG 380	(F/W)	0.713	0.343
OG 381	(F/W)	0.766	0.406
OG 382	(F/W)	0.684	0.357
OG 383	(F/W)	0.762	0.342

Table 16.g

BOREHOLE OGB 154A

sample no.		I trace	TZ
OG 630	(H/W)	0.78	0.393
OG 631	(H/W)	0.71	0.414
OG 635	(H/W)	0.73	0.312
OG 636	(H/W)	0.65	0.374
OG 638	(H/W)	0.71	0.385
OG 639	(H/W)	0.69	0.315
OG 641	(H/W)	0.77	0.42
OG 642	(H/W)	0.8	0.411
OG 646	(H/W)	0.66	0.386
OG 647	(H/W)	0.68	0.531
OG 648	(H/W)	0.68	0.356
OG 650	(H/W)	0.64	0.349
OG 651	(H/W)	0.75	0.46
OG 652	(H/W)	0.7	0.368
OG 653	(H/W)	0.73	0.427
OG 654	(H/W)	0.81	0.509
OG 655	(H/W)	0.83	0.434
OG 656	(H/W)	0.92	0.373
OG 657	(H/W)	0.66	0.313
OG 658	(H/W)	0.94	0.519
OG 659	(H/W)	0.97	0.433
------------ ore zone ------------			
OG 660	(F/W)	0.8	0.408
OG 661	(F/W)	0.84	0.507
OG 662	(F/W)	0.87	0.391
OG 663	(F/W)	0.83	0.486
OG 664	(F/W)	0.76	0.384
OG 665	(F/W)	0.77	0.462
OG 666	(F/W)	0.78	0.456
OG 667	(F/W)	0.67	0.359
OG 668	(F/W)	0.74	0.469
OG 669	(F/W)	0.81	0.513
OG 670	(F/W)	0.68	0.386
OG 671	(F/W)	0.73	0.363
OG 672	(F/W)	0.65	0.456
OG 673	(F/W)	0.68	0.401
OG 674	(F/W)	0.87	0.537

Table 16.h

I major FOR SCHISTS FROM ALTERATION ZONE (*) AND UNMINERALIZED SCHISTS (x)

sample no.	I major	TZ
OG 37 *	0.938	2.1
OG 43 *	0.952	0.485
OG 52 *	0.979	1.13
OG 62 *	0.903	0.425
OG 75 *	0.939	0.358
OG 77 *	0.992	0.396
OG 80 *	0.987	0.418
OG 84 *	0.988	0.376
OG 87 *	0.948	0.378
*		
MWE 202 *	0.814	0.35
MWE 210 *	0.962	0.17
MWE 219 *	0.964	0.57
MWE 226 *	0.917	0.49
OG 131 x	0.689	0.39
OG 135 x	0.663	0.49
OG 138 x	0.645	0.46

Tables 16 a-h - Alteration index for trace elements (I trace) and for major elements (I major), and the TiO2/Zr index (TZ) for unmineralized and mineralized rock types.

Table 17 - Trace element geochemistry of the Alpine-type ultramafic rocks from the Otjihase Mine area and Elisenheim.

sample no.	Cu ppm	Pb ppm	Zn ppm	Ni ppm	Co ppm	Ag ppm	Au ppb	Mn ppm	Ba ppm	Cr ppm	V ppm	Ti ppm
OTJ 675	17	22	35	252	32	ND	ND	230	10	417	159	5813
OTJ 676	19	21	38	256	41	ND	42	180	10	548	185	6233
OTJ 677	131	16	22	107	21	ND	ND	200	20	116	157	6155
OTJ 678	371	36	56	102	24	ND	ND	790	10	508	45	2340
OTJ 679	25	3	16	31	3	ND	ND	50	10	412	10	8300
OTJ 680	166	12	3	43	3	ND	ND	290	10	157	35	1630
OTJ 681	4	37	9	56	18	ND	ND	745	10	280	22	1910
OTJ 684	11	16	36	372	35	ND	ND	402	43	730	134	4344
OTJ 685	13	30	46	409	31	ND	ND	520	64	975	133	4759
OTJ 686	26	25	37	415	40	ND	ND	78	10	985	144	2527

sample no	As ppm	W03 ppm	Mo ppm	Sn ppm	Zr ppm	Rb ppm	Sr ppm	Bi ppm	Nb ppm	Y ppm
OTJ 675	ND	ND	ND	ND	57	ND	ND	ND	ND	ND
OTJ 676	ND	45	ND	ND	44	ND	ND	ND	ND	27
OTJ 677	ND	94	ND	ND	116	ND	316	ND	ND	ND
OTJ 678	ND	52	ND	ND	20	19	52	ND	ND	ND
OTJ 679	ND	ND	ND	ND	ND	ND	ND	ND	ND	ND
OTJ 680	ND	63	ND	ND	20	ND	15	ND	ND	ND
OTJ 681	ND	56	ND	ND	27	ND	71	ND	ND	ND
OTJ 684	ND	70	23	ND	45	ND	15	ND	ND	20
OTJ 685	ND	36	ND	ND	44	ND	15	ND	ND	24
OTJ 686	ND	76	ND	ND	29	ND	ND	ND	ND	ND

Table 18 - Major element geochemistry of ultramafic rock types.

	MWE 239	MWE 245	OTJ 686
SiO2	44.843	55.134	47.809
TiO2	0.079	0.044	0.374
Al2O3	4.883	1.903	7.164
Fe2O3	21.899	10.595	10.488
MnO	0.191	0.262	0.063
MgO	15.399	18.277	26.99
CaO	6.292	11.201	0.15
Na2O	0.295	0.494	0.08
K2O	0.272	0	0.034
P2O5	0.087	0.097	0.024
LOI	5.59	1.57	6.67
H2O-	0.73	0.26	0.33
	98.885	99.836	100.175

1 gossanous talc-actinolite schist (Matchless West Extension)

2 gossanous talc-actinolite schist (ultramafic body, Von Francois Ost 60)

Table 19 - Concentrations of selected elements in different ultramafic rock types from Matchless West Extension, Ongombo and Otjihase, and values of the Ex and Um indices.

sample no.	Cr ppm	V ppm	Ni ppm	Co ppm	Ba ppm	Cu ppm	Zn ppm	Pb ppm	Um	Ex
MWE 227	12	37	20	19	3799	4100	156	242	88	8143
MWE 233	17	18	29	18	27500	14200	382	162	82	42164
MWE 236	2	272	23	7	77400	2300	201	241	304	80205
MWE 239	7	97	26	26	2160	12600	3200	1800	156	18116
MWE 243	13	57	18	6	2695	2800	341	148	94	5930
MWE 245	8	56	8	5	1549	2100	208	143	77	3934
MWE 246	13	38	14	33	1542	4500	2400	49	98	8540
MWE 248	23	375	30	132	2857	35600	8700	207	560	47717
MWE 252	15	78	30	18	65046	11800	6200	203	141	83187
MWE 255	20	196	24	25	3861	3400	3100	285	265	10626
MWE 258	20	30	19	6	2215	2900	370	42	75	5560
OG 359	373	333	136	53	680	7	132	27	895	1714
OTJ 675	417	159	252	32	10	17	35	22	860	922
OTJ 676	548	185	256	41	10	19	38	21	1030	1097
OTJ 677	116	157	107	21	20	131	22	16	401	574
OTJ 678	508	45	102	24	10	371	56	36	679	1116
OTJ 679	412	10	31	3	10	25	16	3	456	507
OTJ 680	157	35	43	3	10	166	3	12	238	417
OTJ 681	280	22	56	18	10	4	9	37	376	399
OTJ 684	730	134	372	35	43	11	36	16	1271	1361
OTJ 685	975	133	409	31	64	13	46	30	1548	1671
OTJ 686	985	144	415	40	10	26	37	25	1584	1657

APPENDIX F

Ongeama Prospect: geochemical profiles along the minor gossan outcrop

Charts 1 to 15

Elements: Cu, Pb, Zn, Co, Ni, Ag, Au, Mn, Ba, Cr, V, Ti, As, Bi, Sn Zr, Rb, Sr

Legend

massive sulphide gossan

trench

magnetite quartzite

grid reference

11000E

ferruginous schist

Kuiseb formation

351

concentration of the considered element (Note: ND indicates "below detection limit")

Key for the profiles

massive gossan

magnetite quartzite

ferruginous schist

$\bar{x}$ *country rocks (average content)*

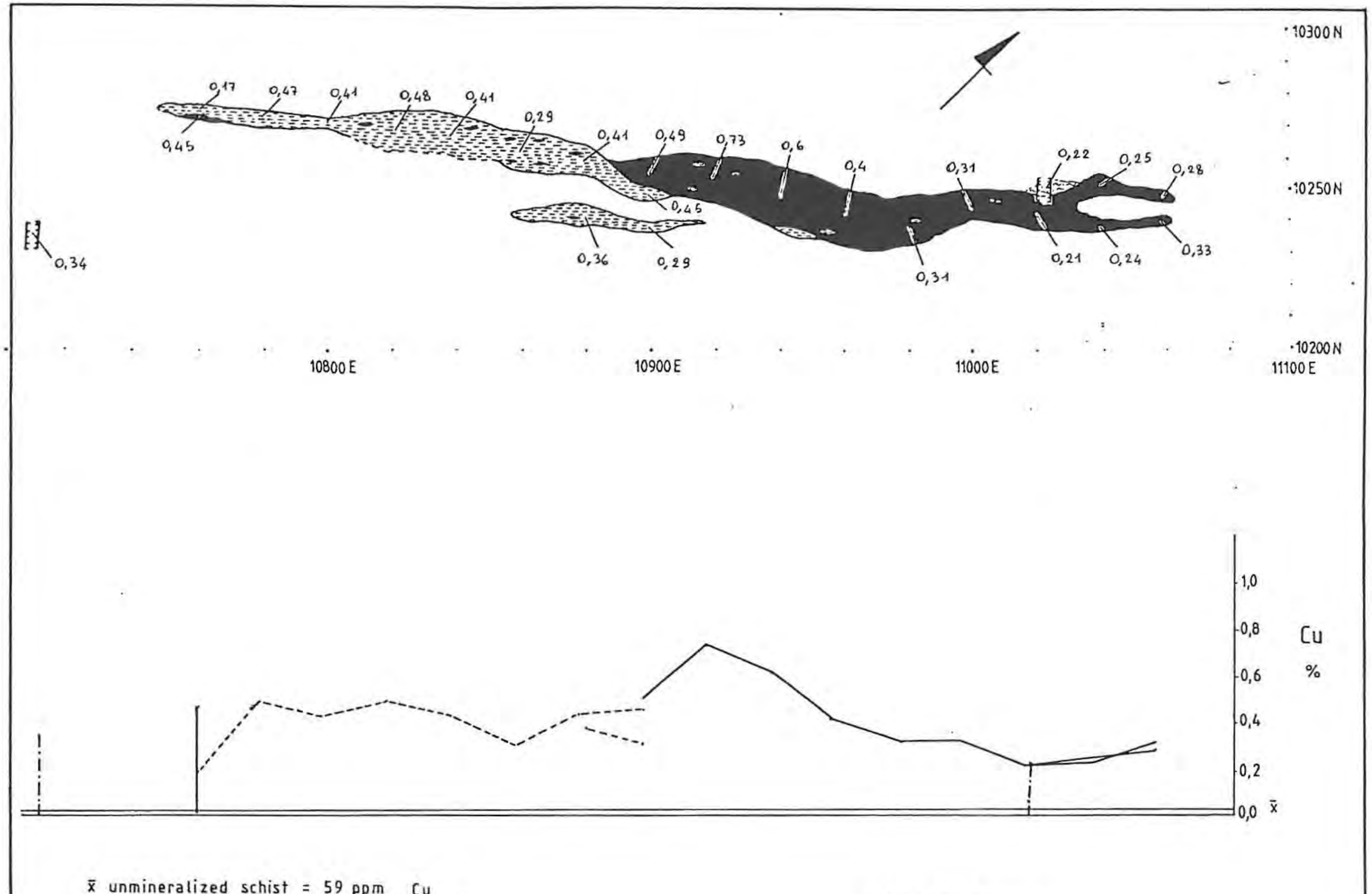

Chart 1: Copper

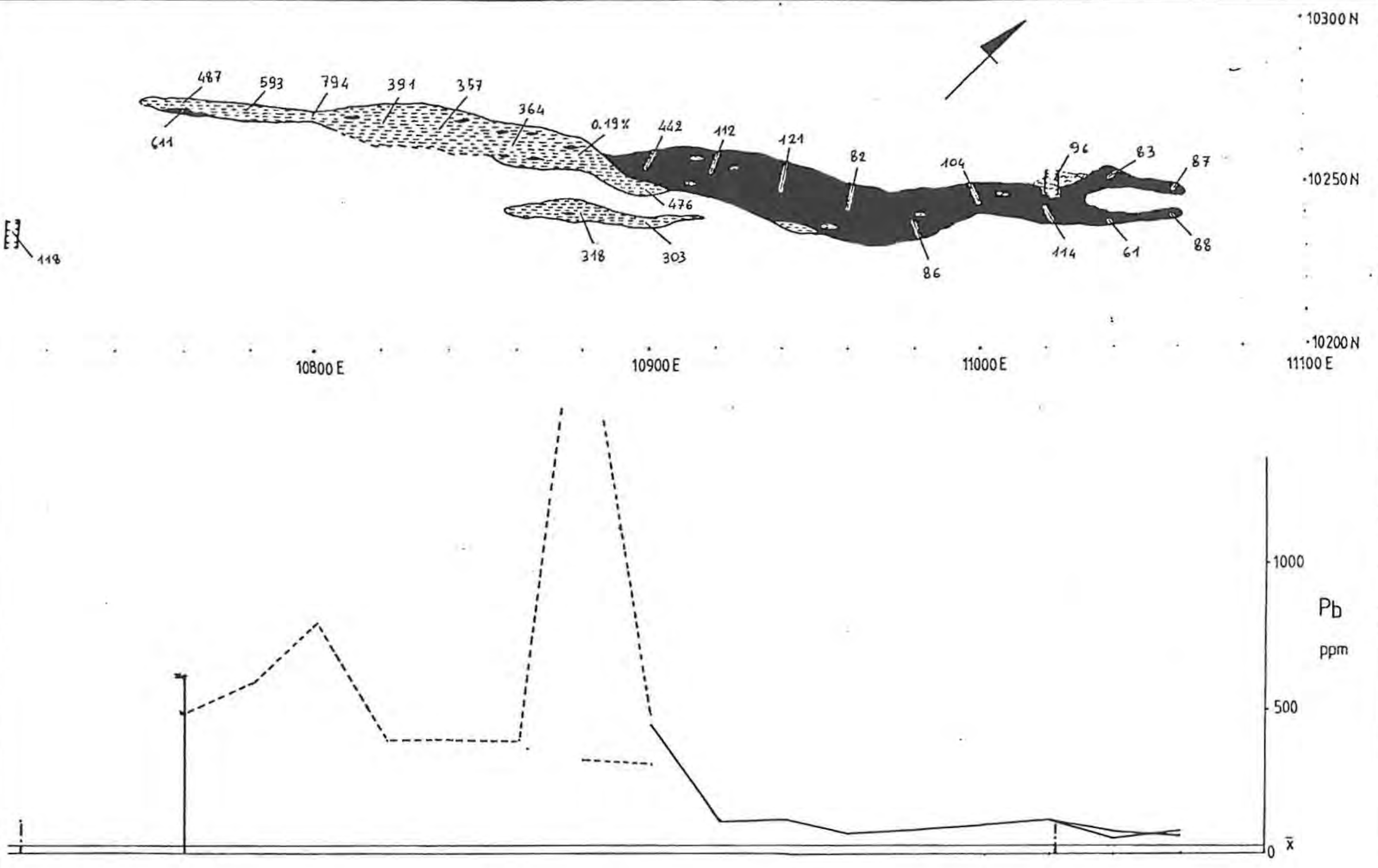

$\bar{x}$ unmineralized schist = 30,6 ppm Pb .

Chart 2: Lead

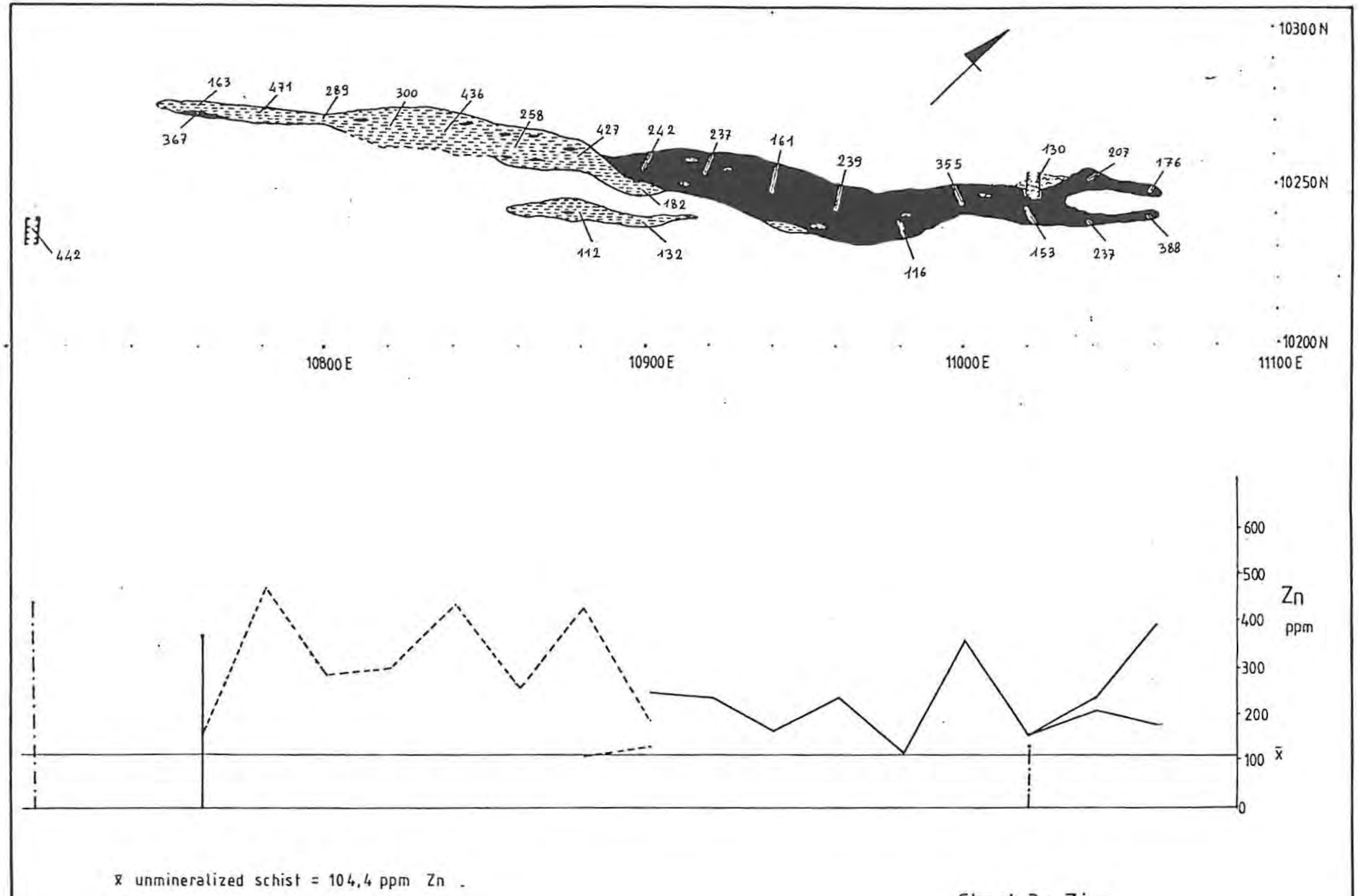

10300 N
10250 N
10200 N
10800 E
10900 E
11000 E
11100 E
163
471
289
300
436
258
427
242
237
161
239
355
130
207
176
367
182
112
132
116
153
237
388
442
Zn
ppm
600
500
400
300
200
100
0
x̄
x̄ unmineralized schist = 104,4 ppm Zn .

Chart 3: Zinc

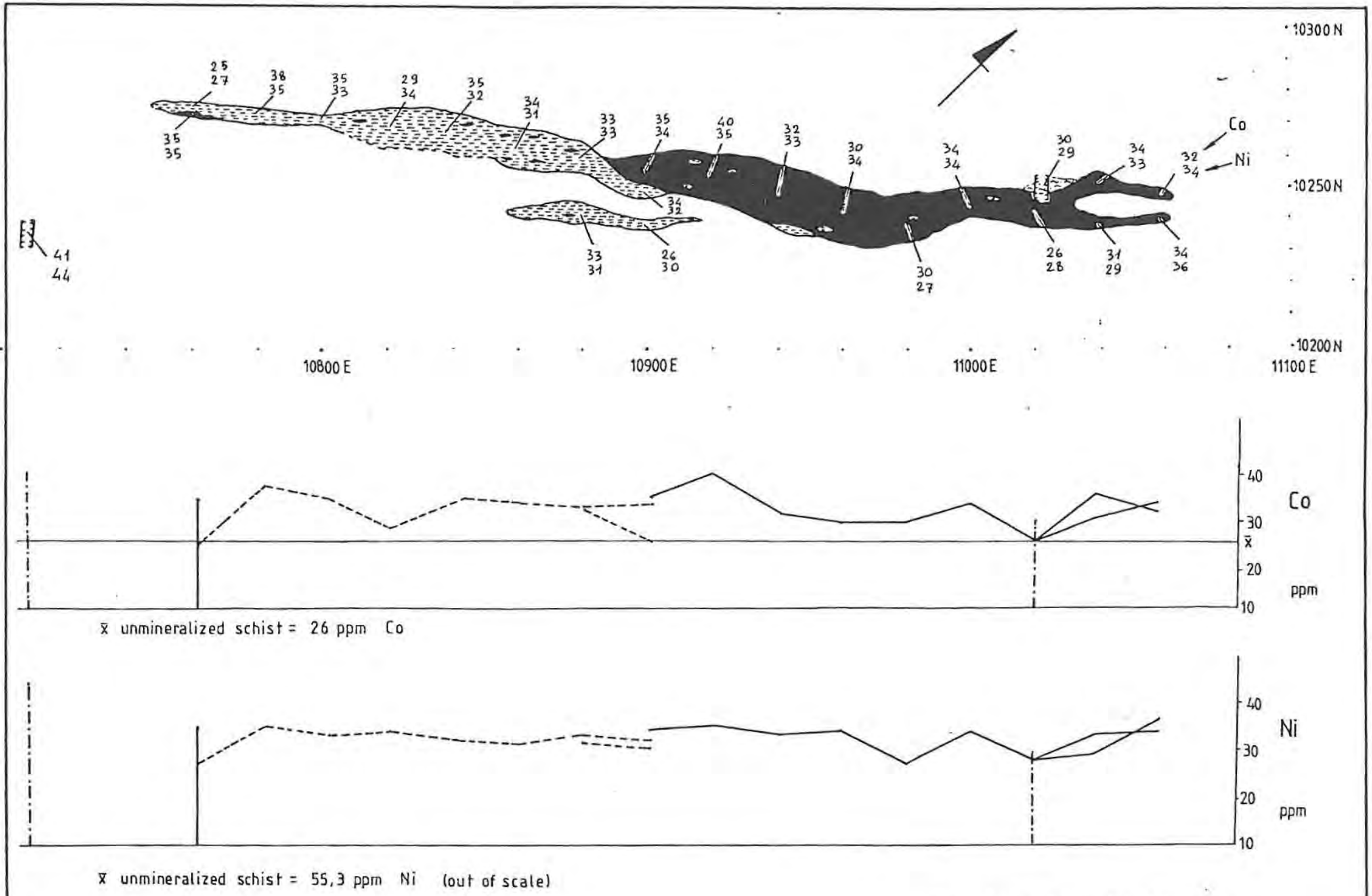

Chart 4 : Cobalt - Nickel

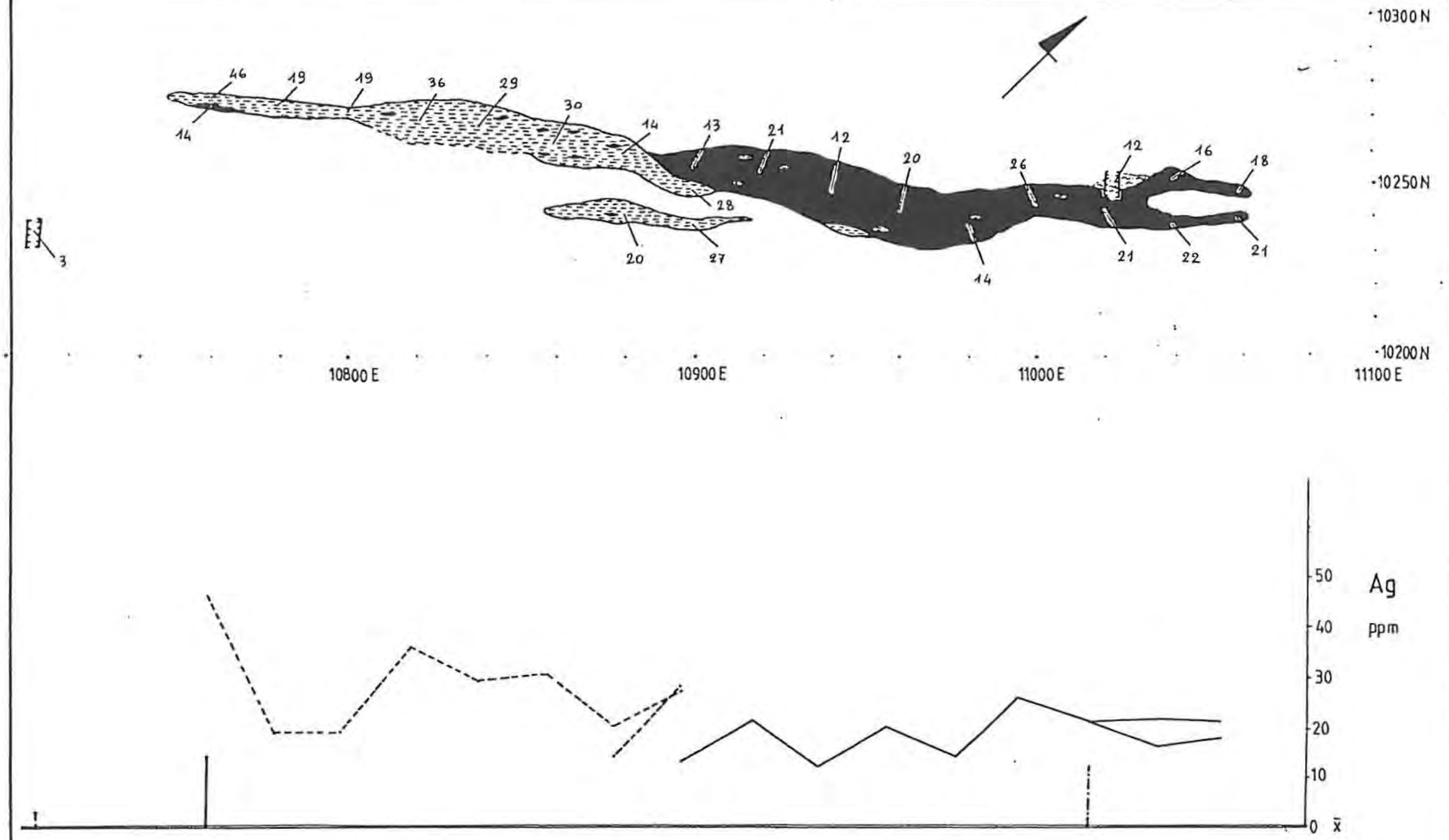

$\bar{x}$ unmineralized schist = 0,2 ppm Ag

Chart 5: Silver

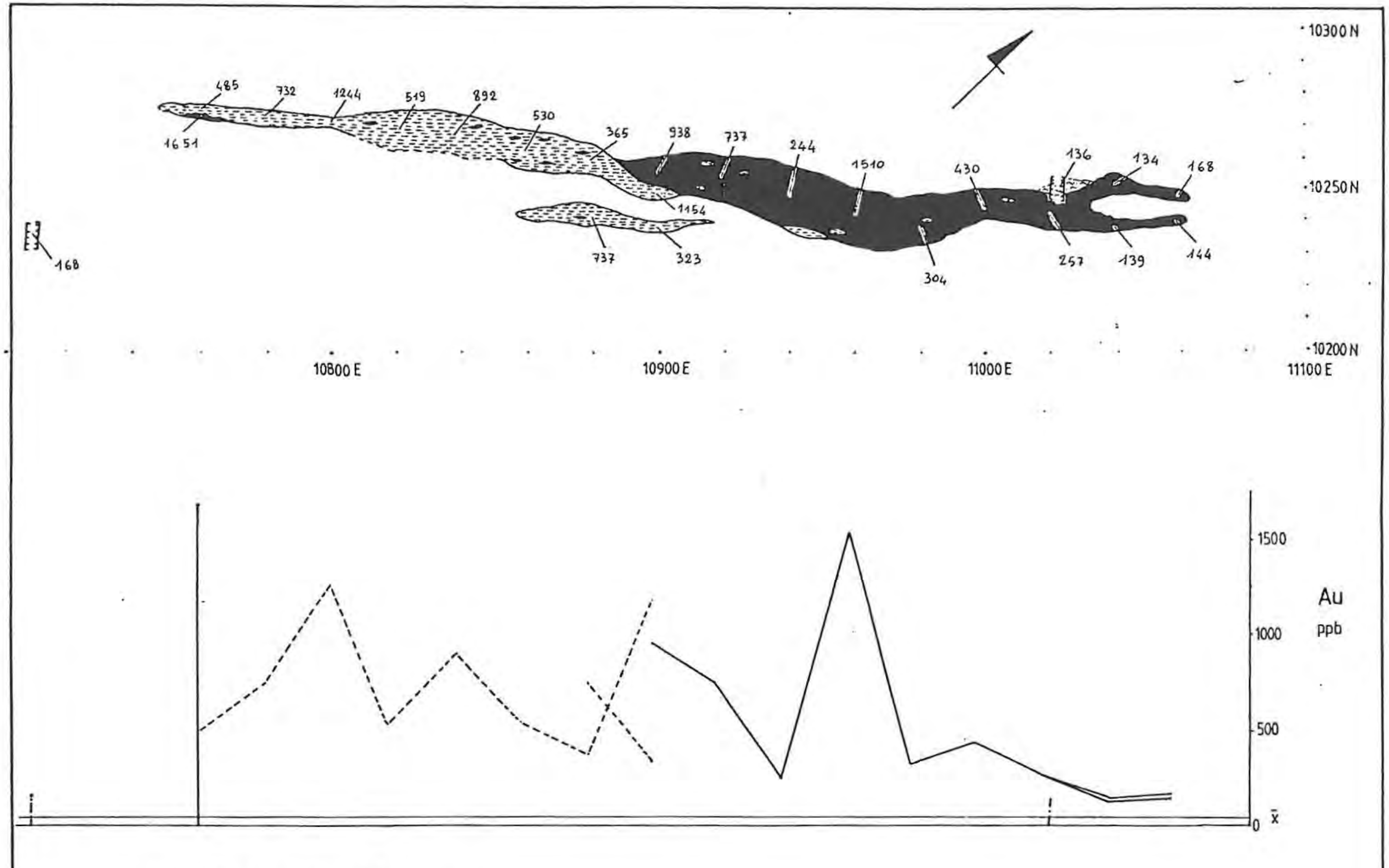

x̄ unmineralized schist = 69,3 ppb Au

Chart 6: Gold

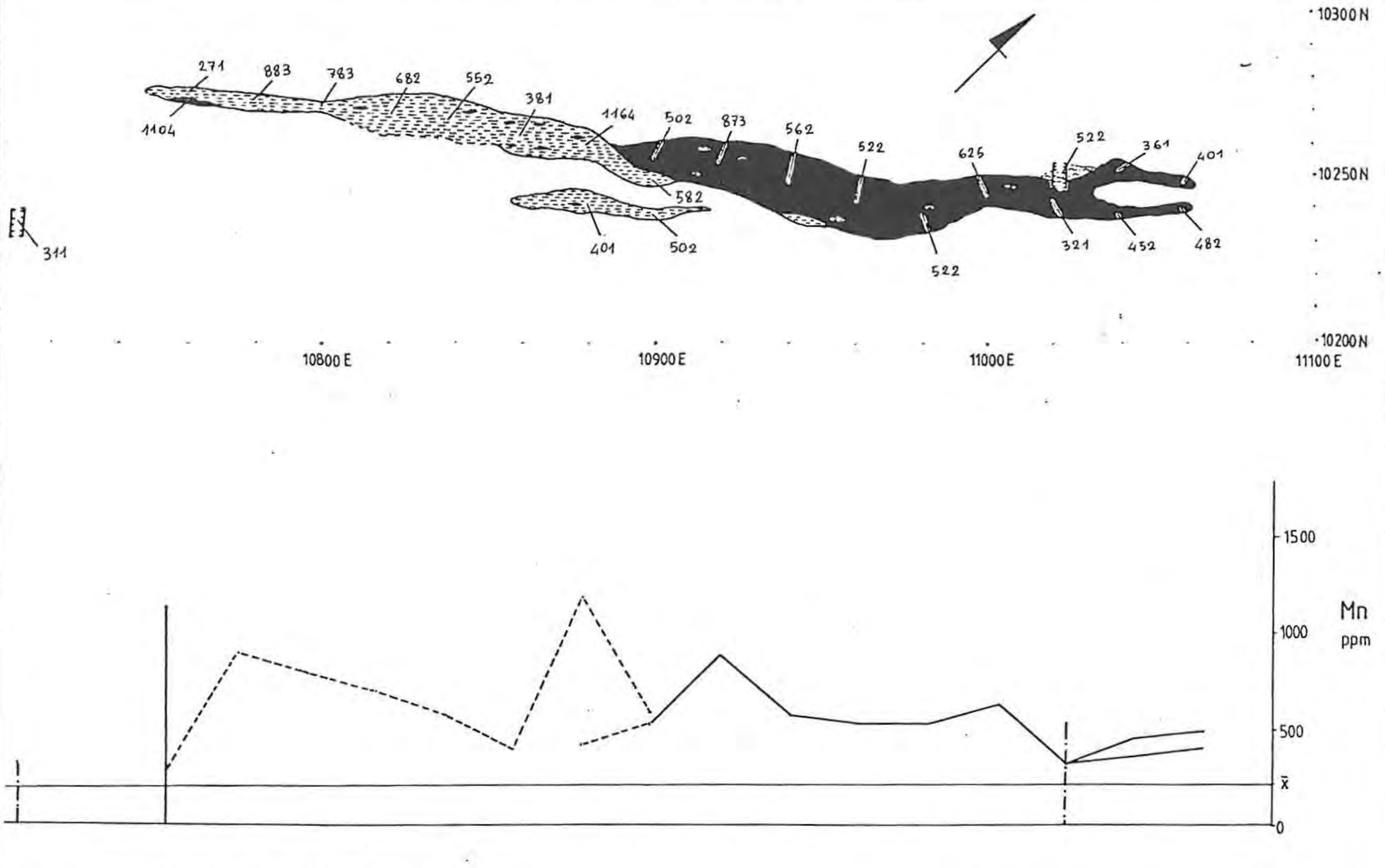

$\bar{x}$ unmineralized schist = 221,1 ppm Mn

Chart 7: Manganese

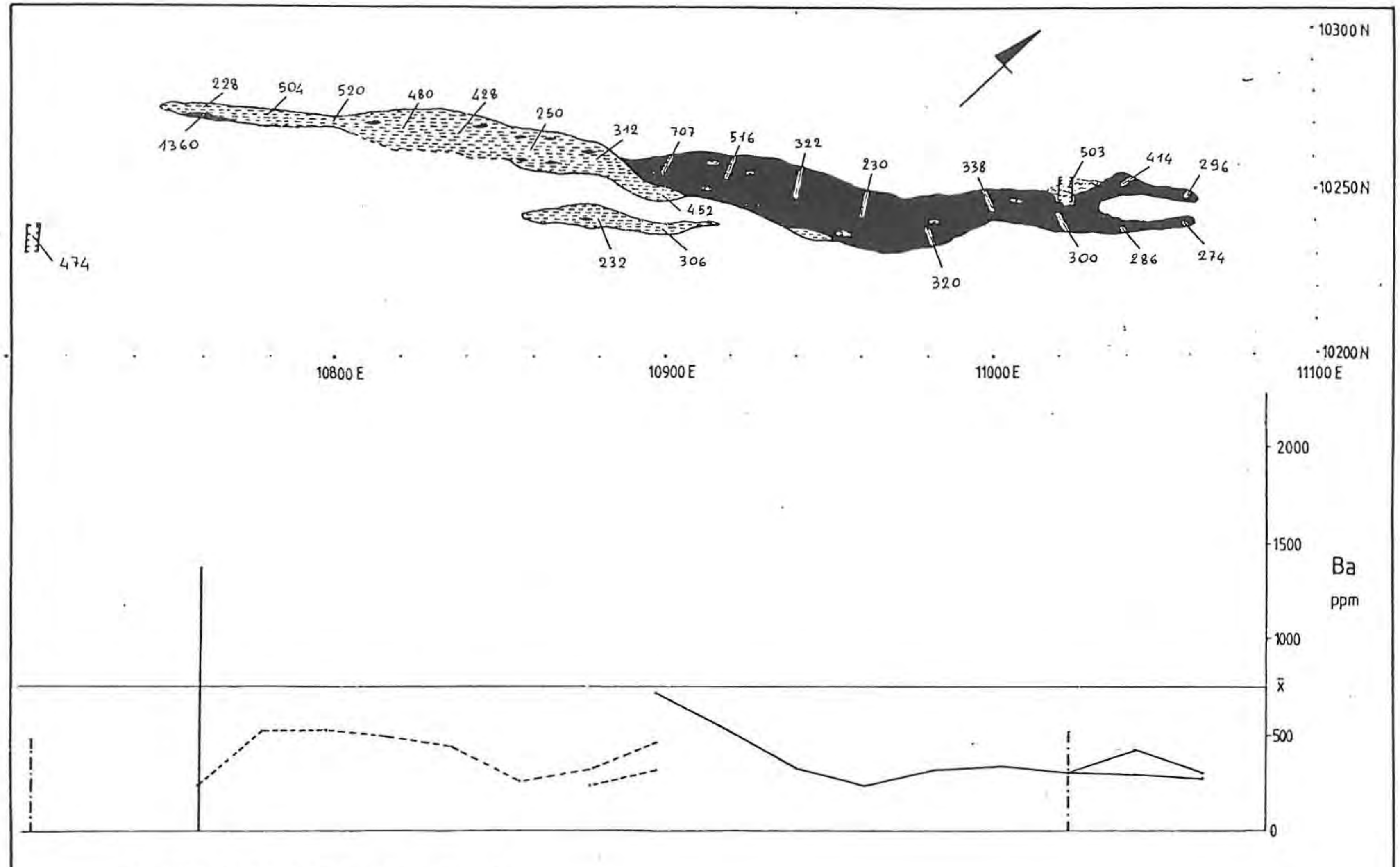

x̄ unmineralized schist = 758,4 ppm Ba

Chart 8: Barium

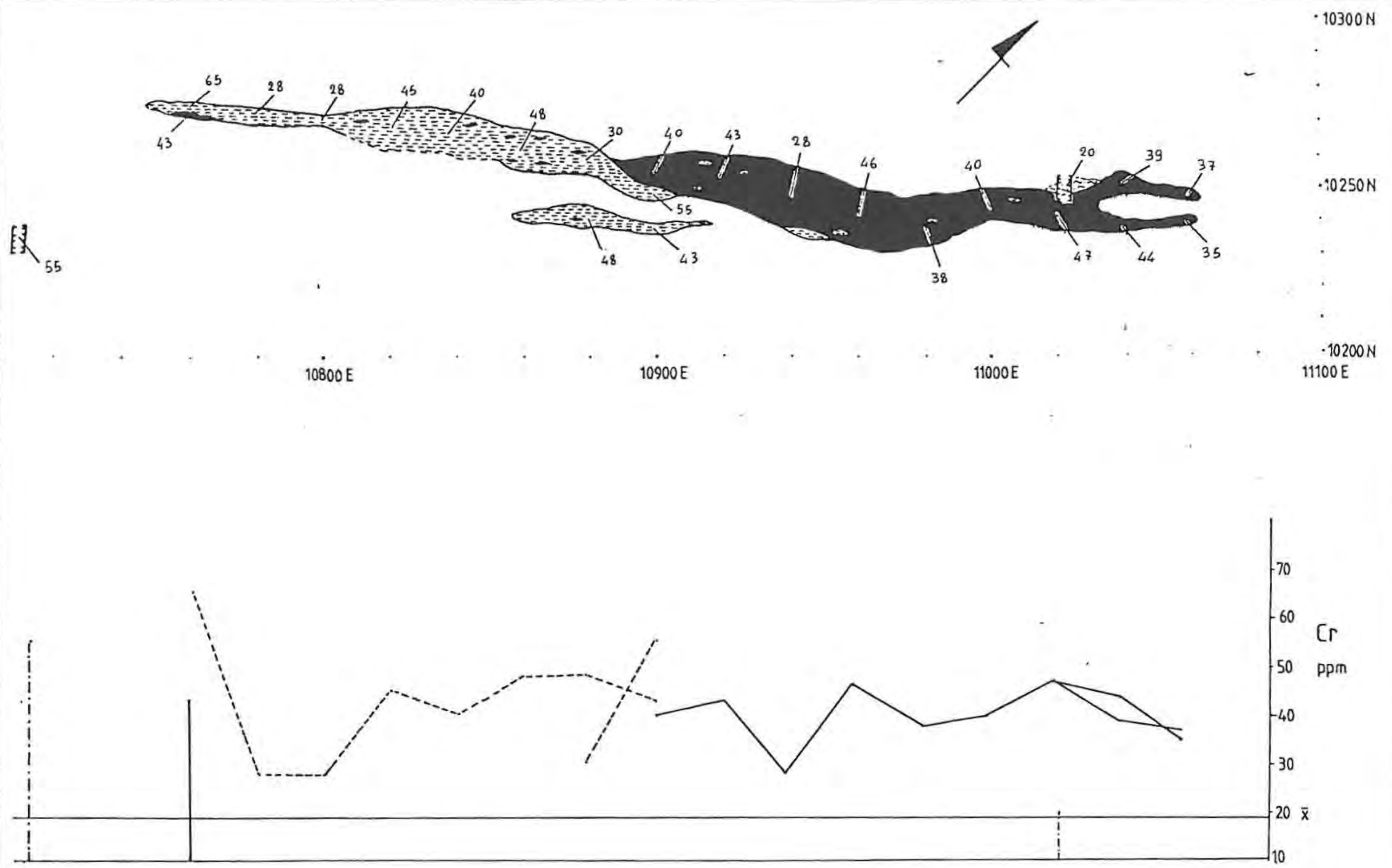

x̄ unmineralized schist = 18,6 ppm Cr

Chart 9: Chromium

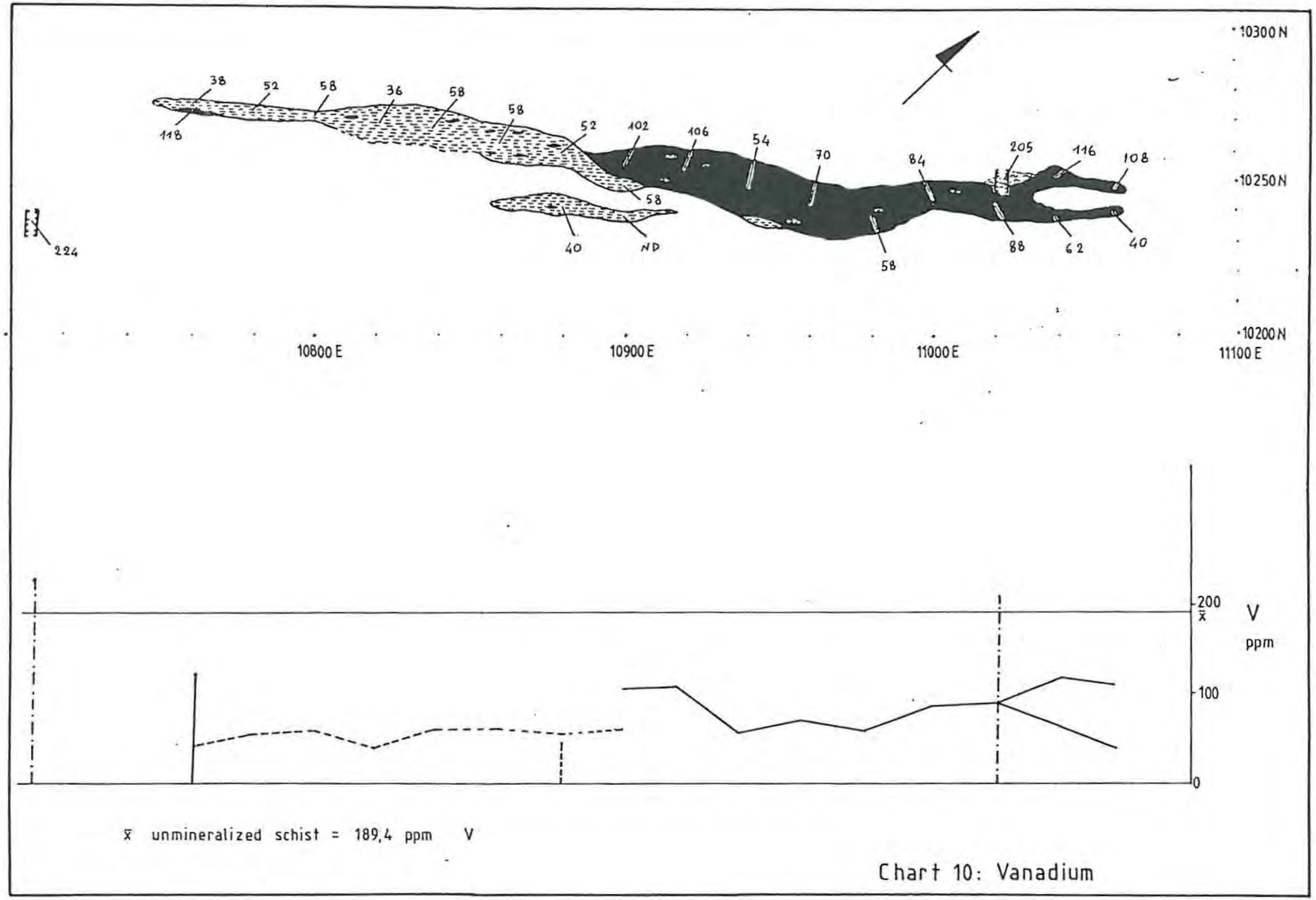

Chart 10: Vanadium

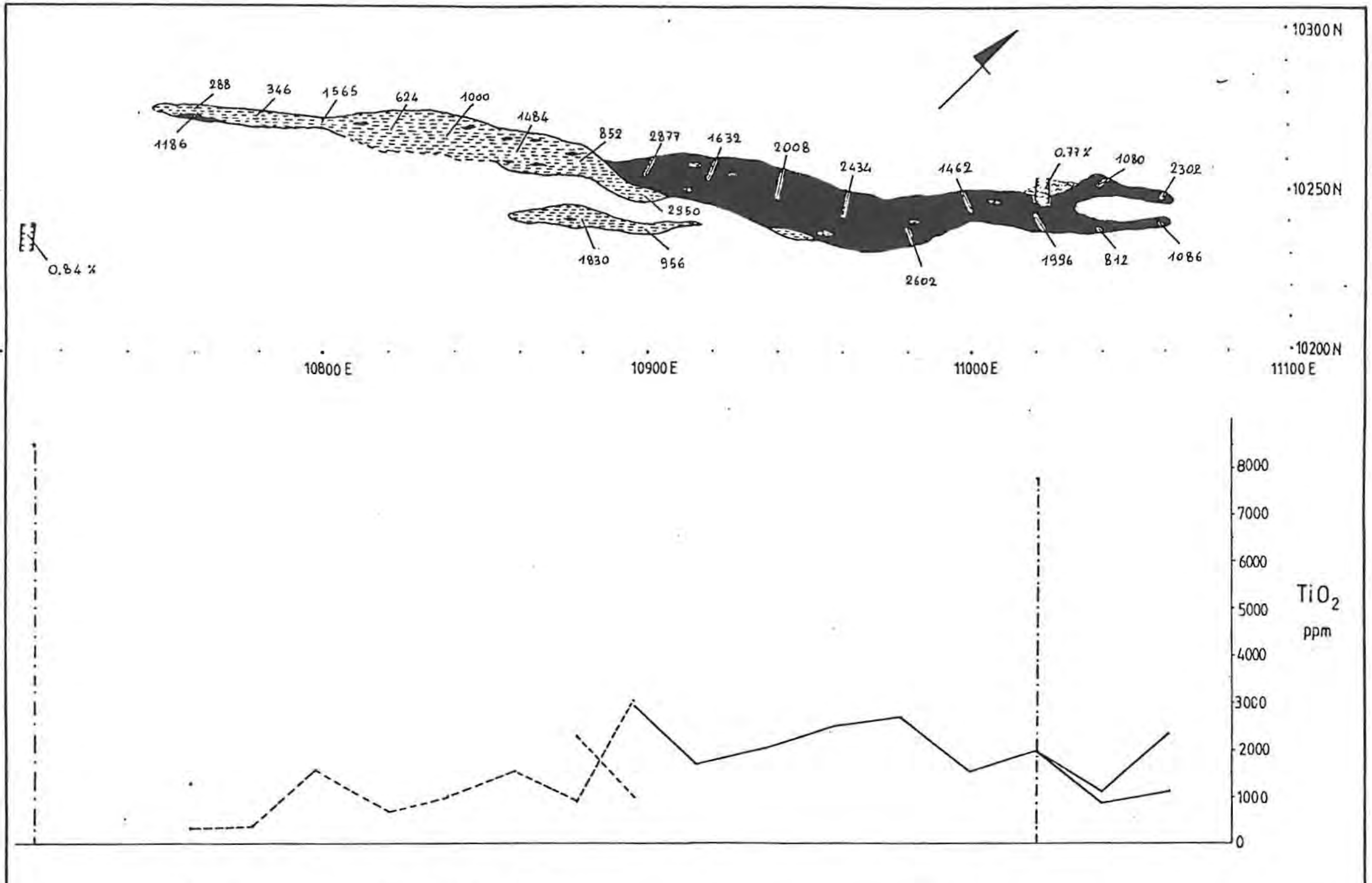

x̄ unmineralized schist = 10 200 ppm TiO_2 (out of scale)

Chart 11: Titanium

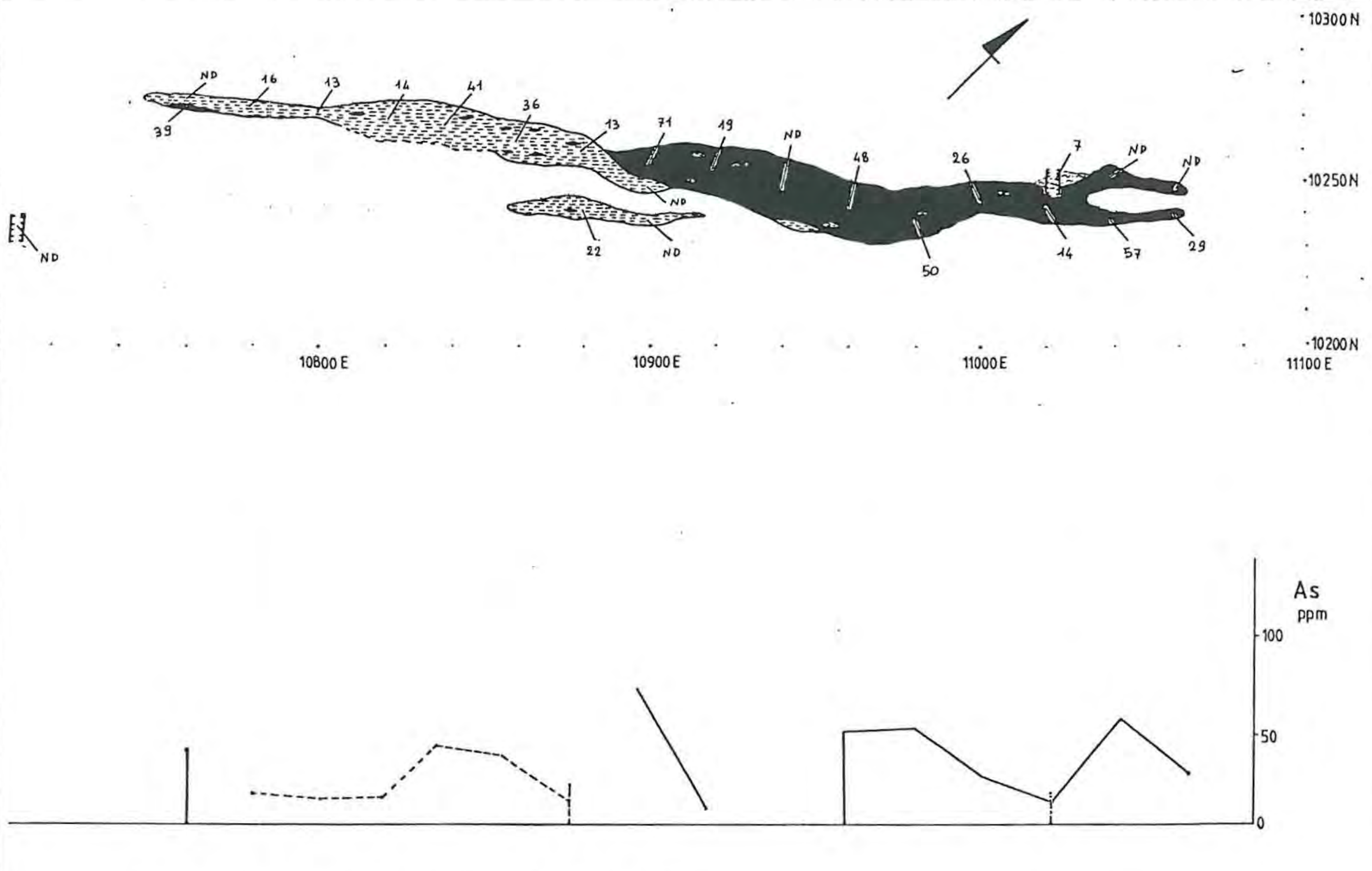

x̄ unmineralized schist below detection limit (10 ppm As)

Chart 12: Arsenic

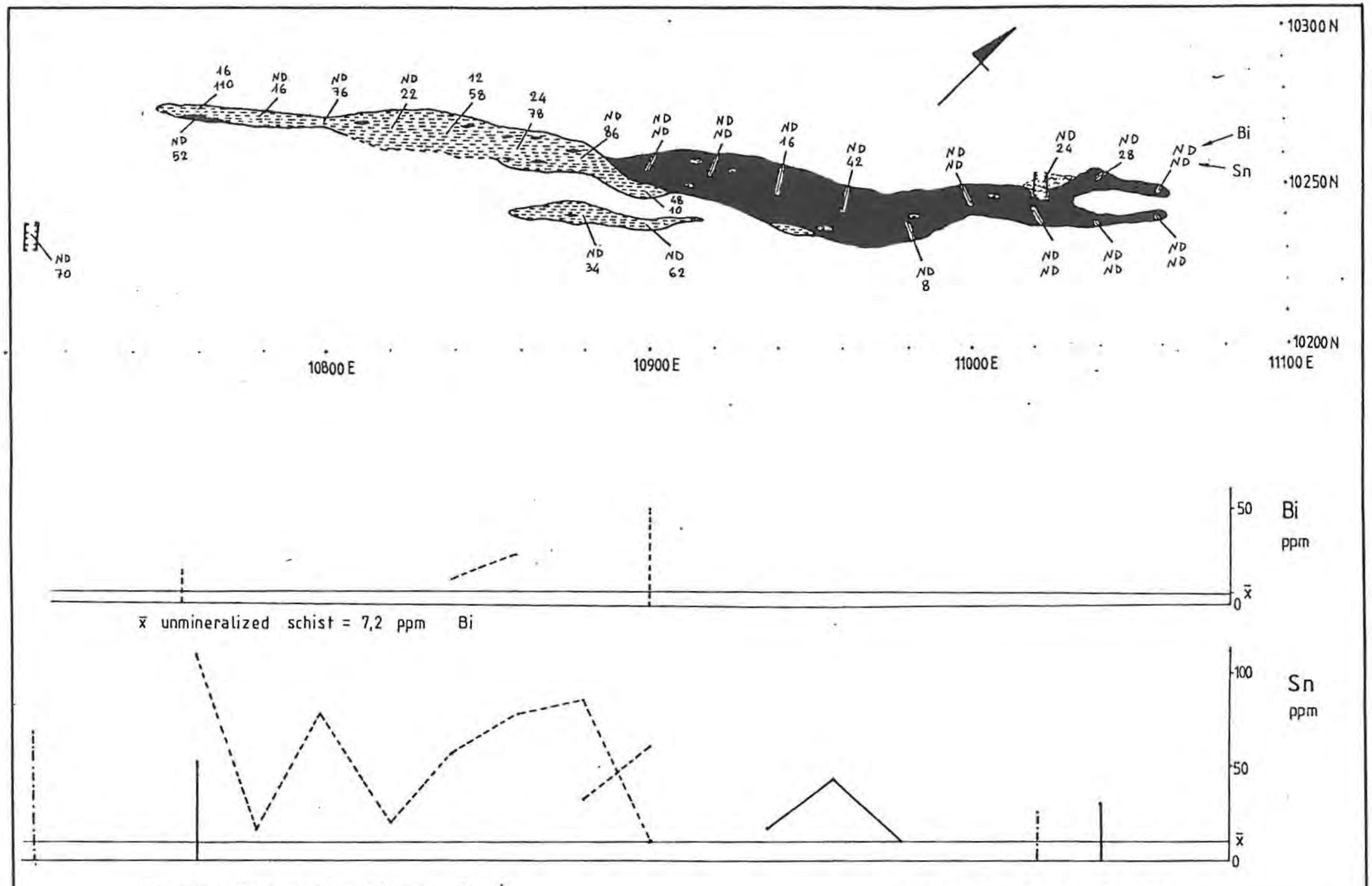

Chart 13: Bismuth - Tin

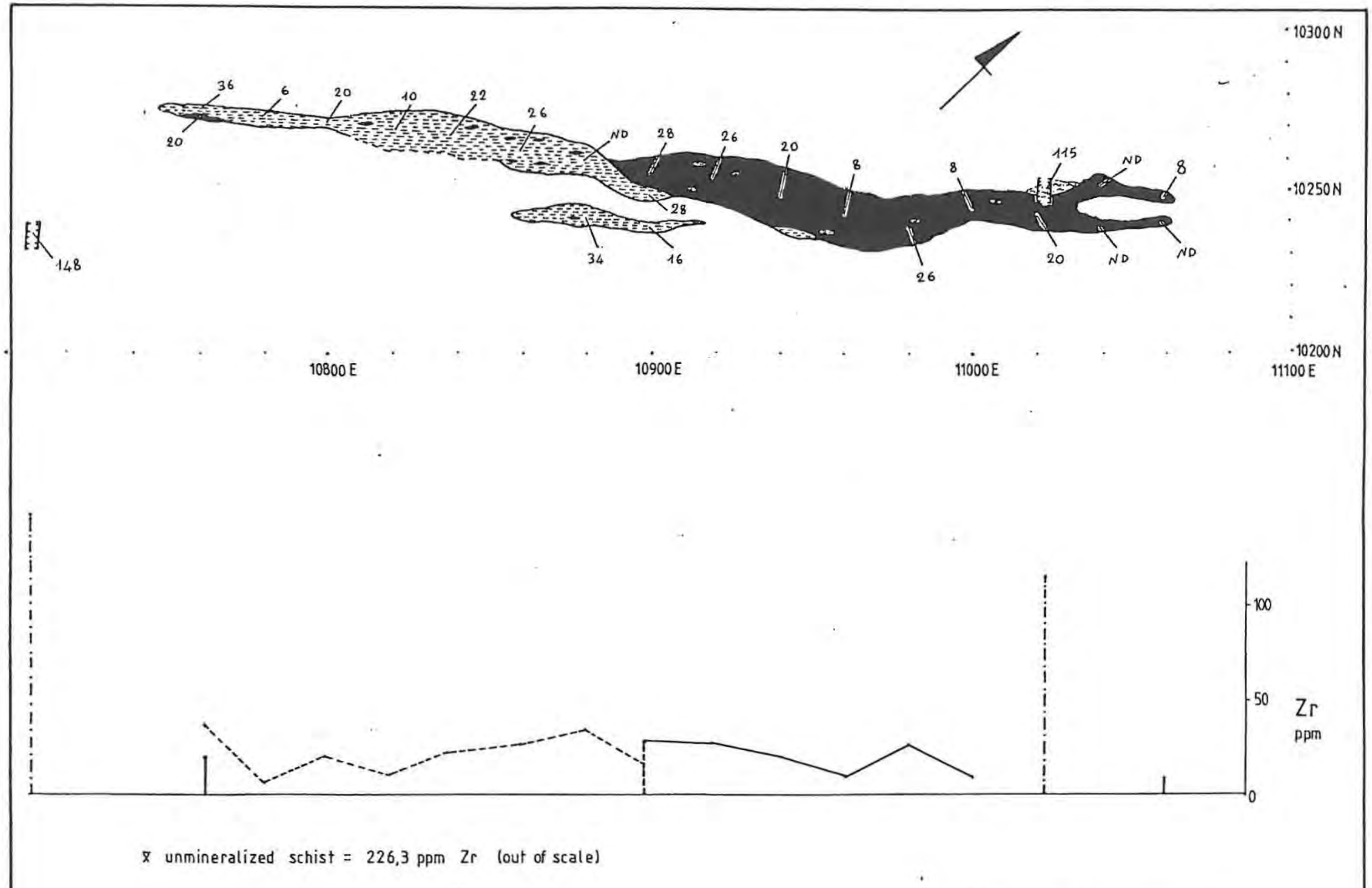

Chart 14: Zirconium

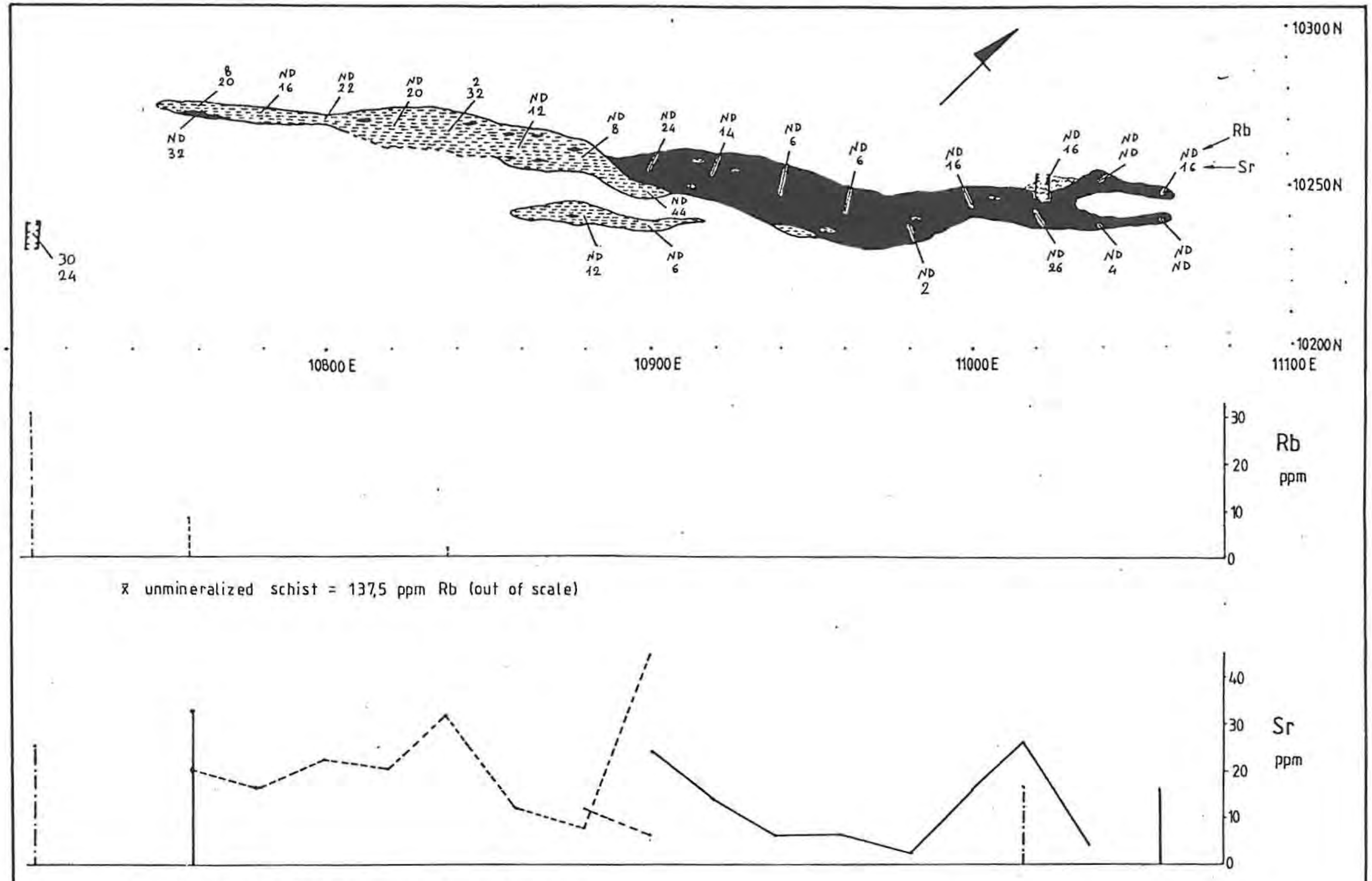

x̄ unmineralized schist = 137,5 ppm Rb (out of scale)

x̄ unmineralized schist = 98,9 ppm Sr - (out of scale)

Chart 15: Rubidium - Strontium

APPENDIX G

Ongeama Prospect: geochemical profiles along the major gossan outcrop

Charts 1 to 16

Elements: Cu, Pb, Zn, Co, Ni, Ag, Au, Mn, Ba, Cr, V, Ti, As, W, Zr, Rb, Bi, Nb

Legend

massive sulphide gossan

trench

semi-massive gossan (anthophyllite)

farm track

magnetite quartzite

10300E *grid reference*

ferruginous schist

250 *concentration of the considered element (Note: ND indicates "below detection limits)*

magnetic muscovite schist

magnetic chlorite schist

Key for the profiles

massive sulphide gossan

semi-massive gossan (anthophyllite)

magnetic muscovite schist

magnetite quartzite

magnetic chlorite schist

ferruginous schist

x̄ *country rocks (average content)*

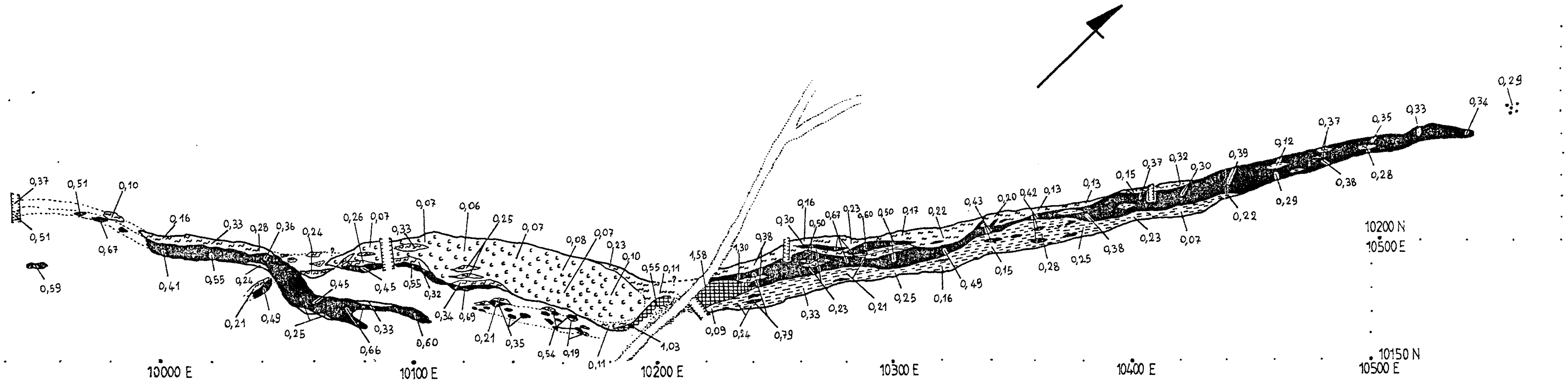

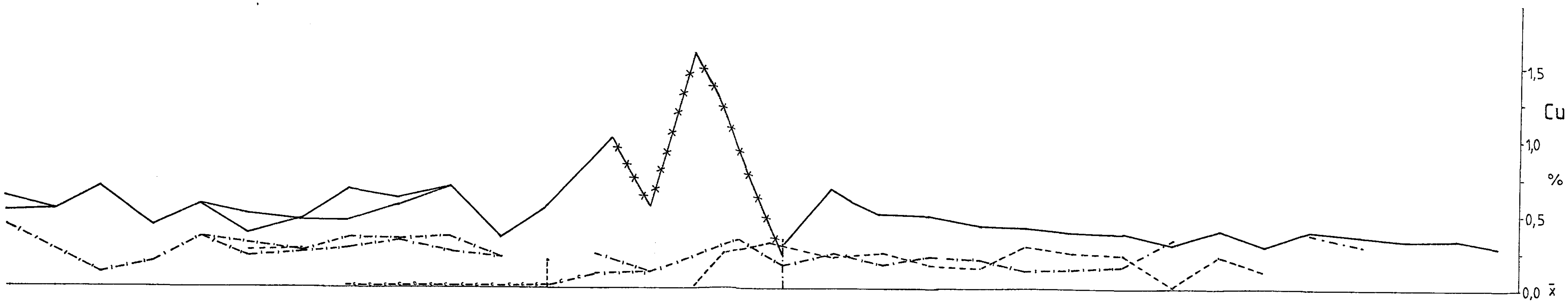

x̄ unmineralized schist = 59 ppm Cu

Chart 1: Copper

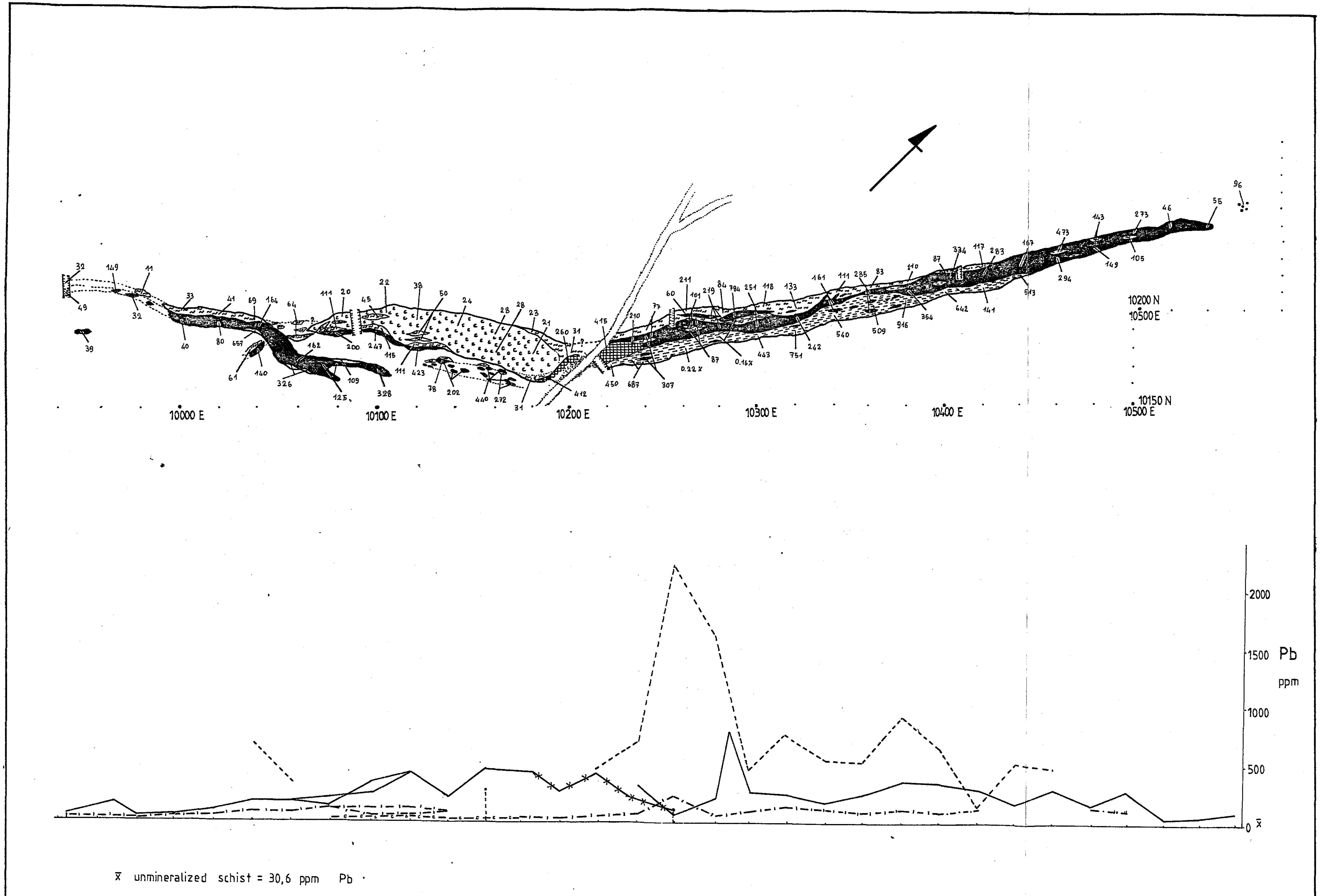

10000 E
10100 E
10200 E
10300 E
10400 E
10500 E
10200 N
10500 E
10150 N
10500 E
2000
1500
1000
500
0
Pb
ppm
x̄ unmineralized schist = 30,6 ppm Pb

Chart 2: Lead

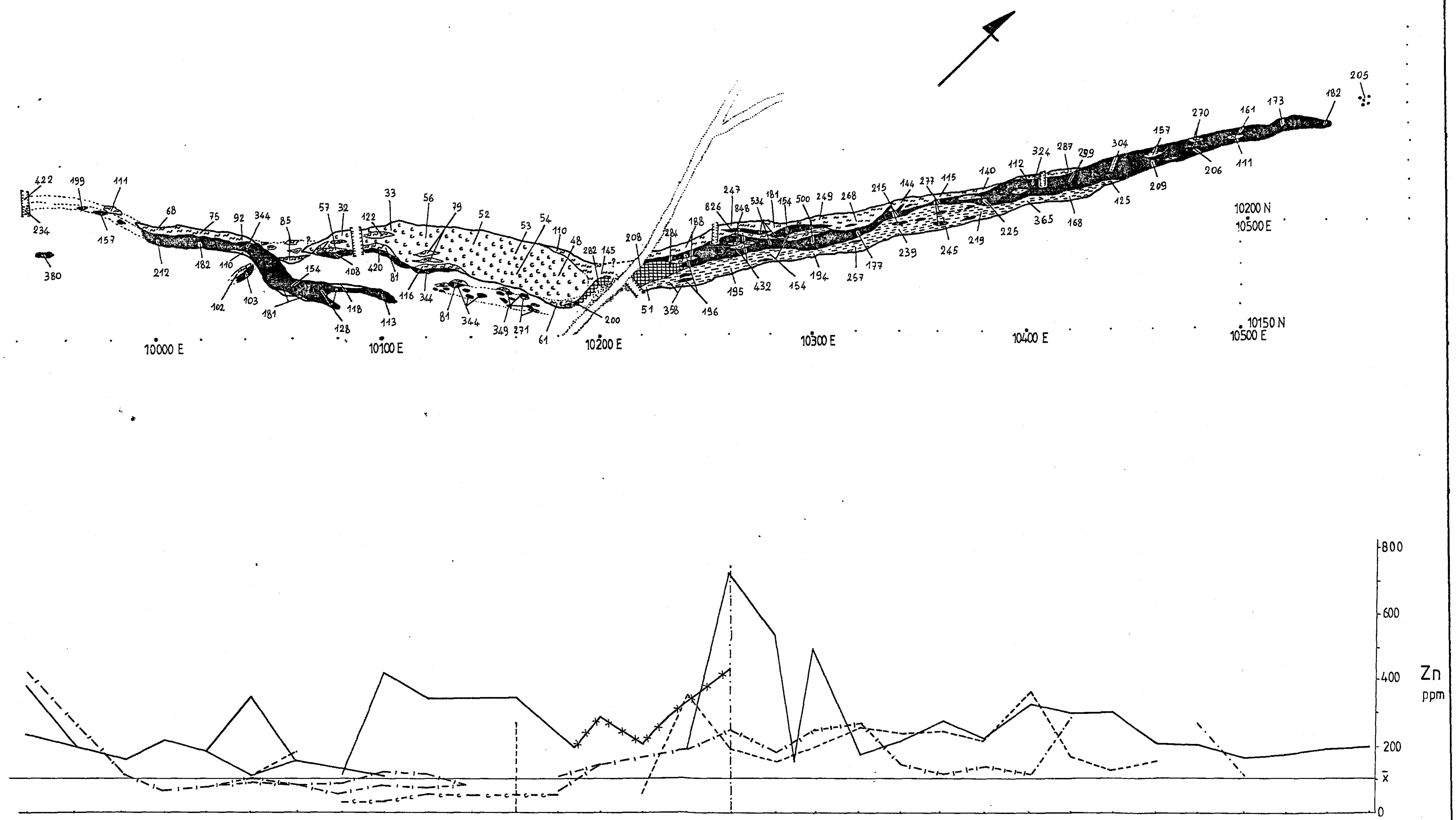

$\bar{x}$ unmineralized schist = 104,4 ppm Zn

Chart 3: Zinc

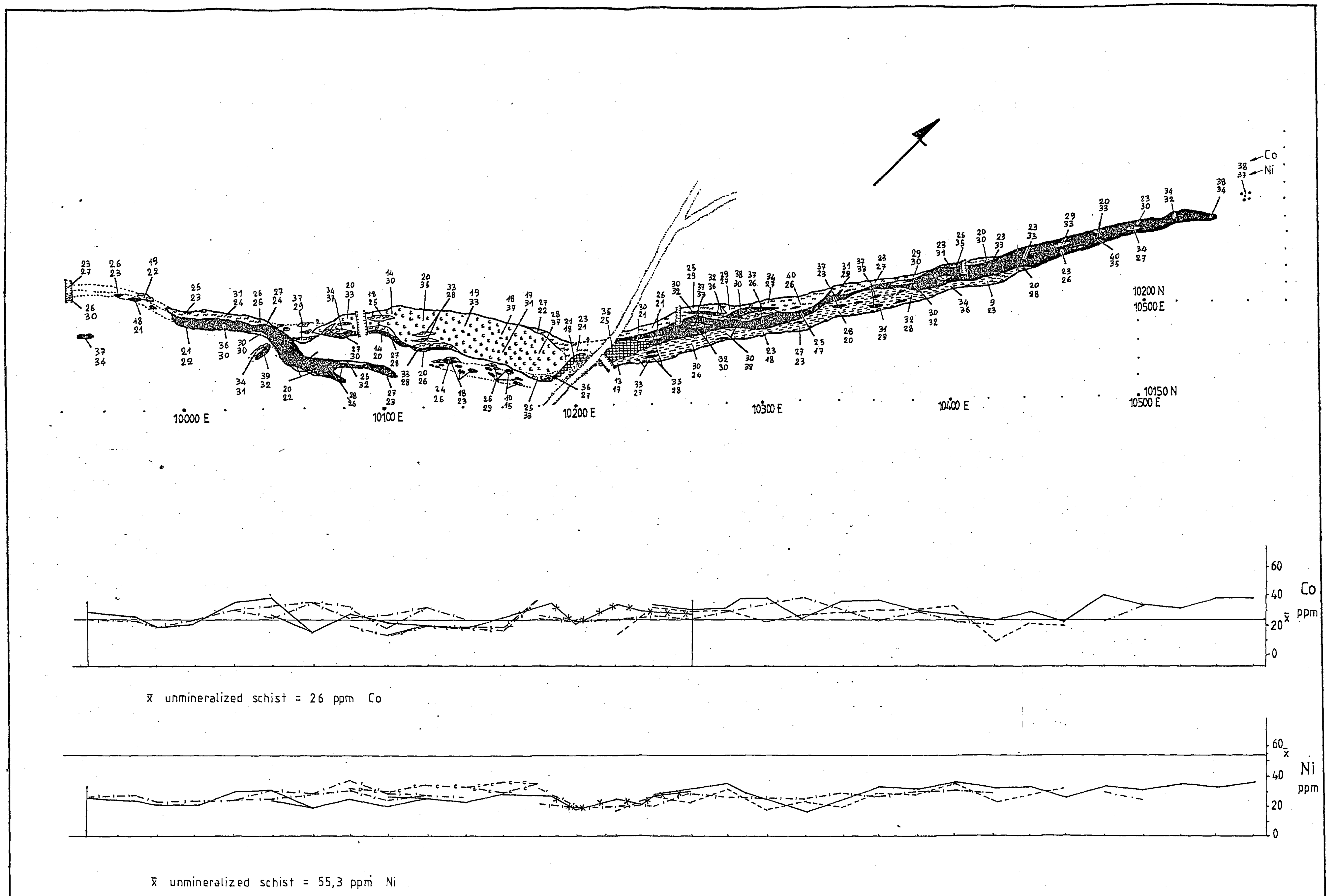

Chart 4: Cobalt-Nickel

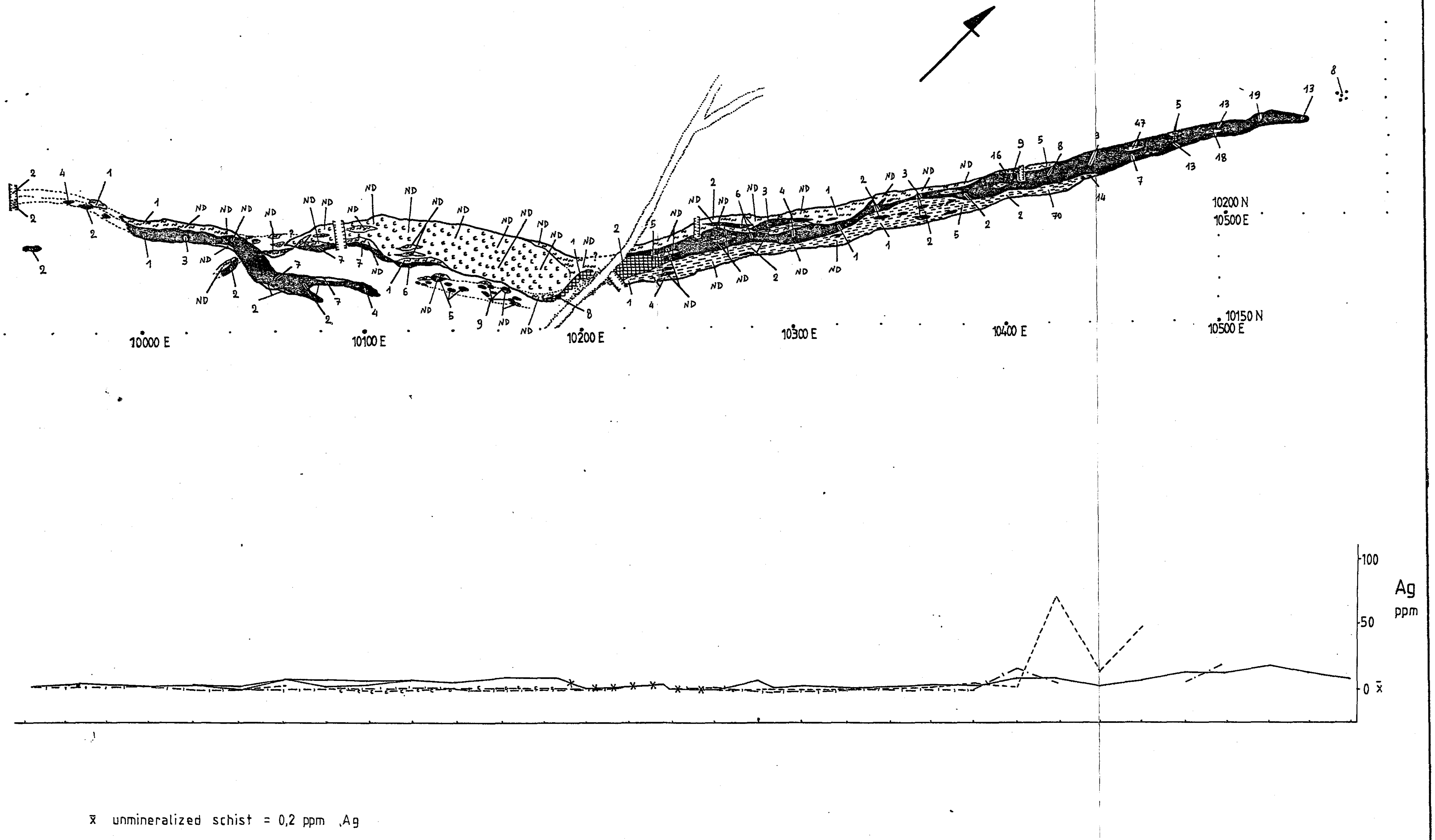

Chart 5: Silver

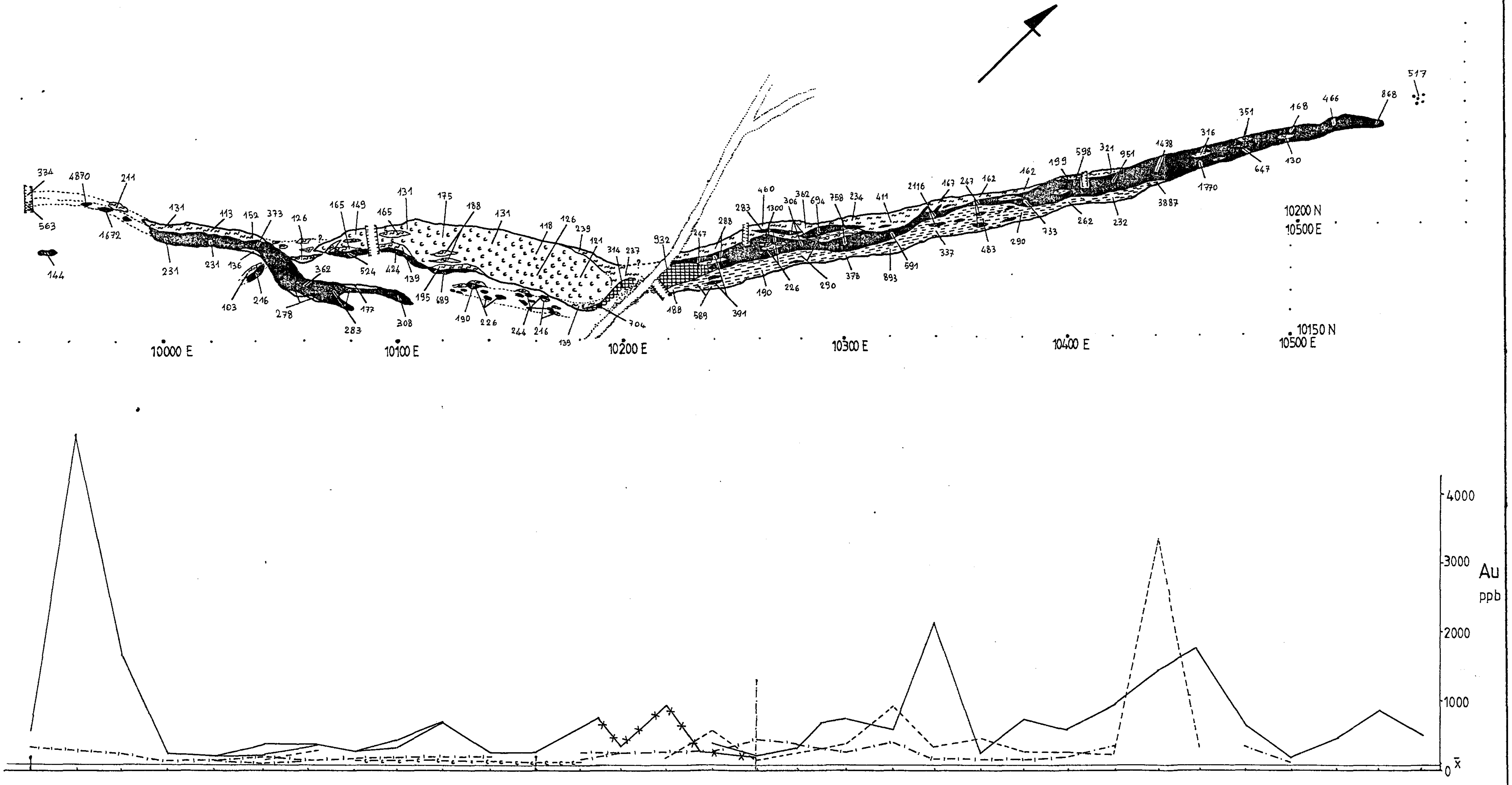

x̄ unmineralized schist = 69,3 ppb Au

Chart 6: Gold

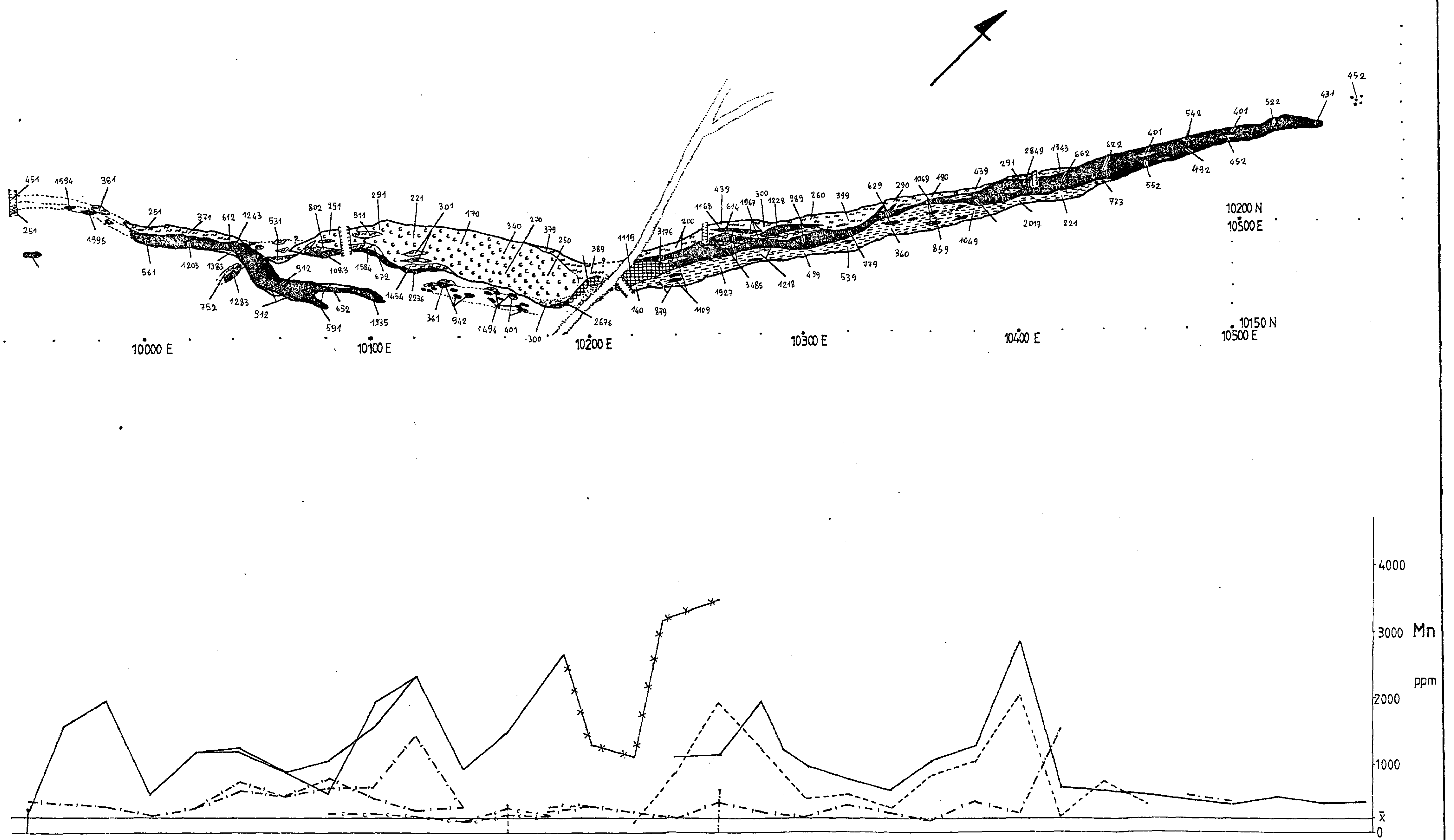

x̄ unmineralized schist = 221,1 ppm Mn

Chart 7: Manganese

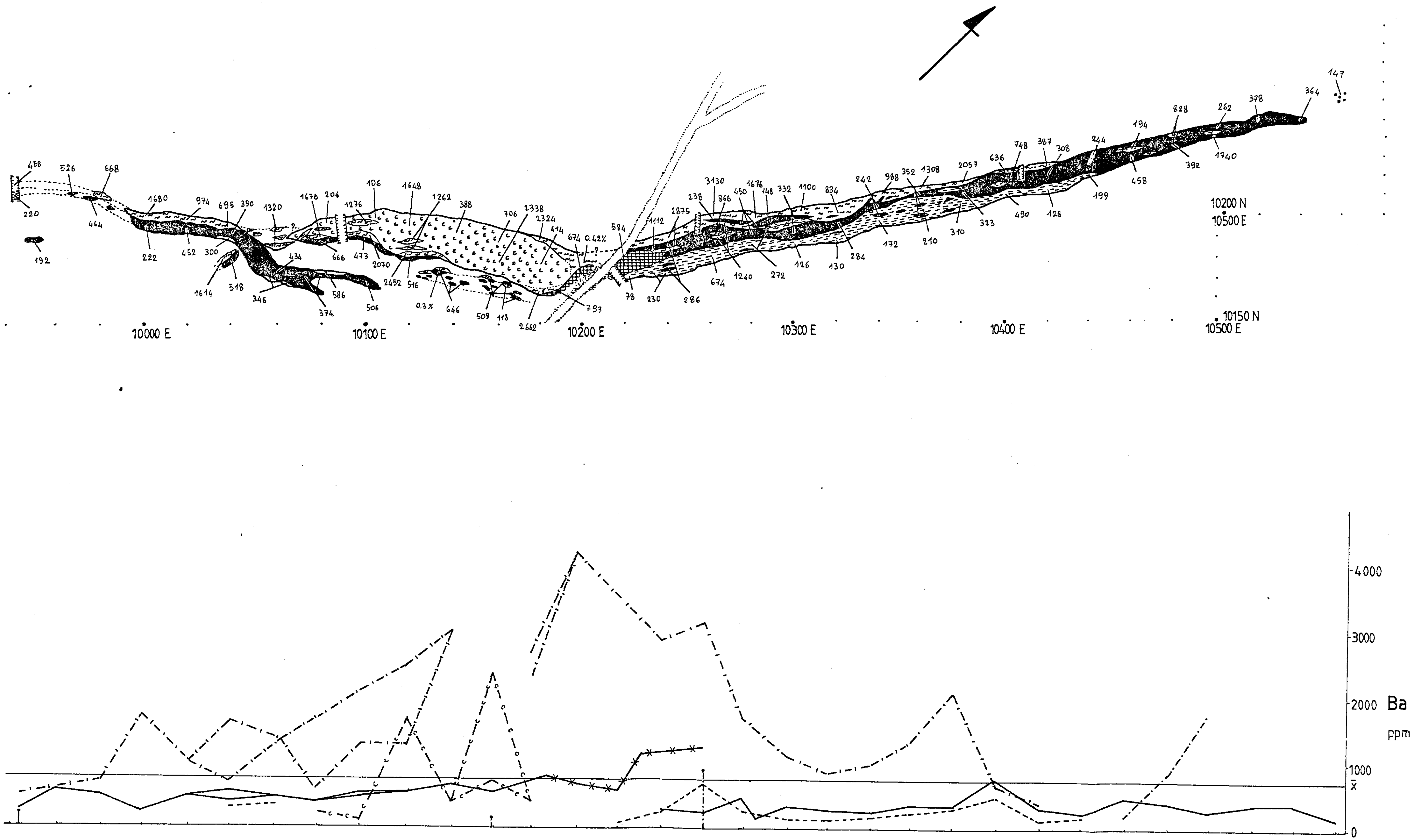

$\bar{x}$ unmineralized schist = 758,4 ppm Ba

Chart 8: Barium

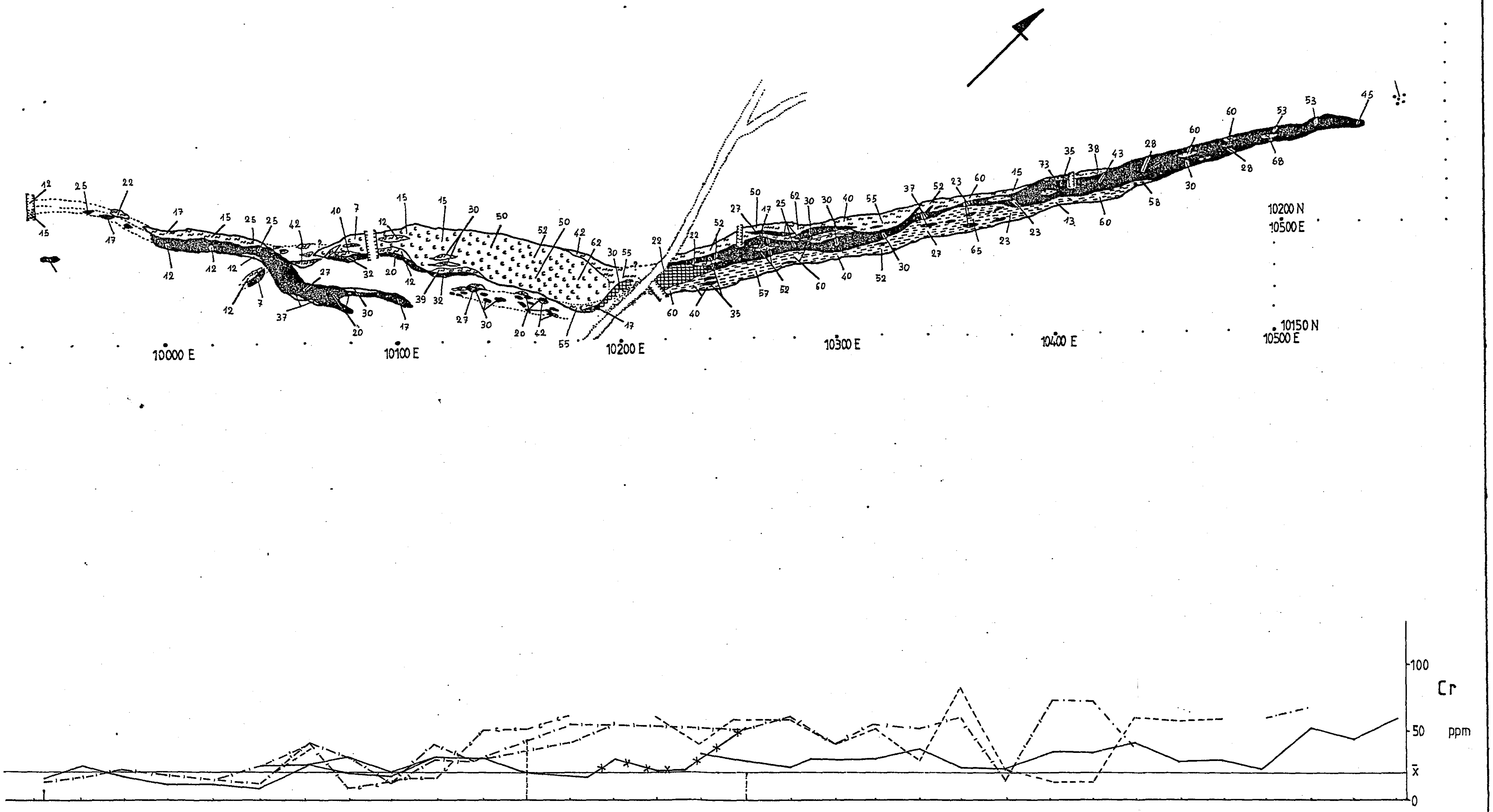

x̄ unmineralized schist = 18,6 ppm Cr

Chart 9: Chromium

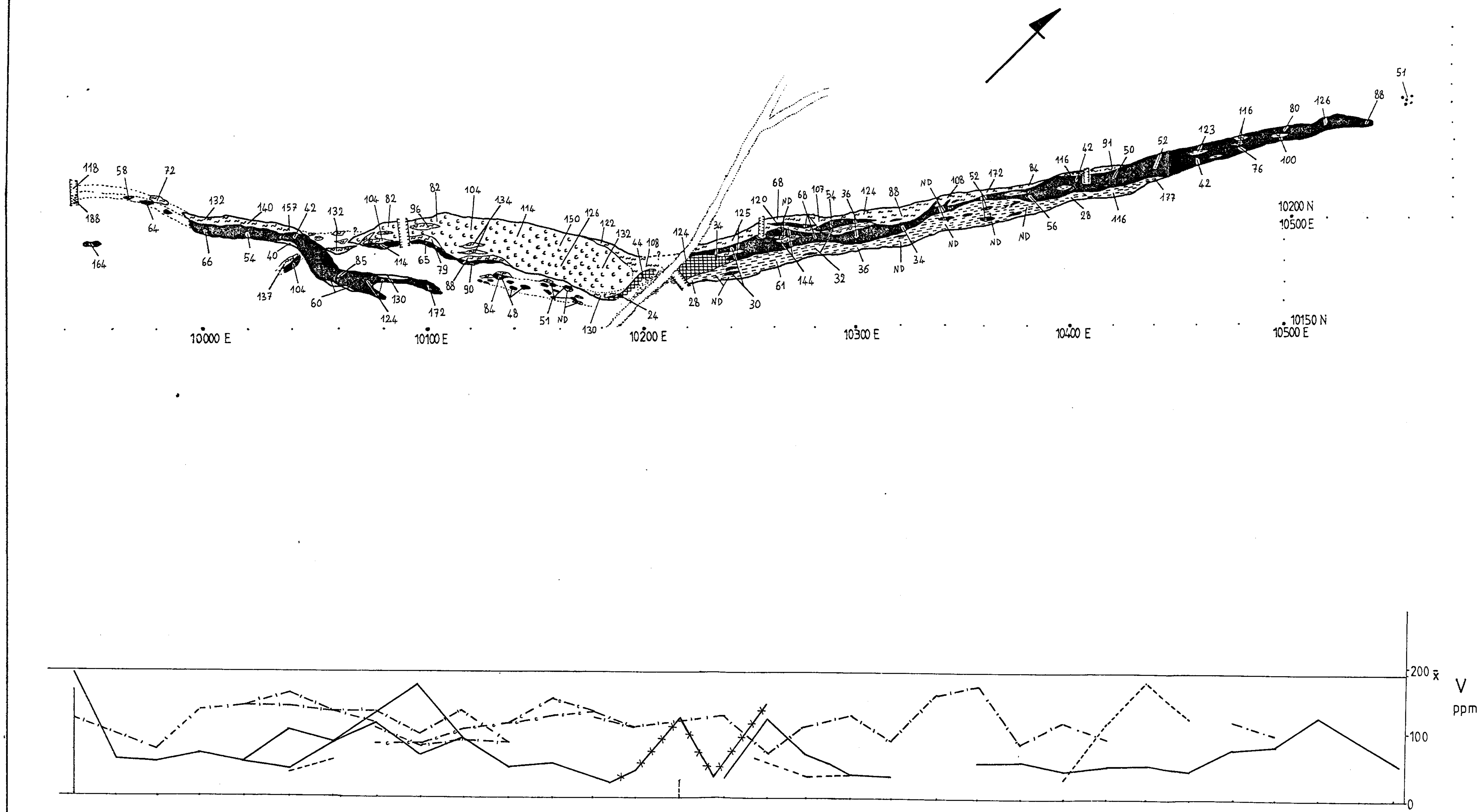

x̄ unmineralized schist = 189,4 ppm V

Chart 10: Vanadium

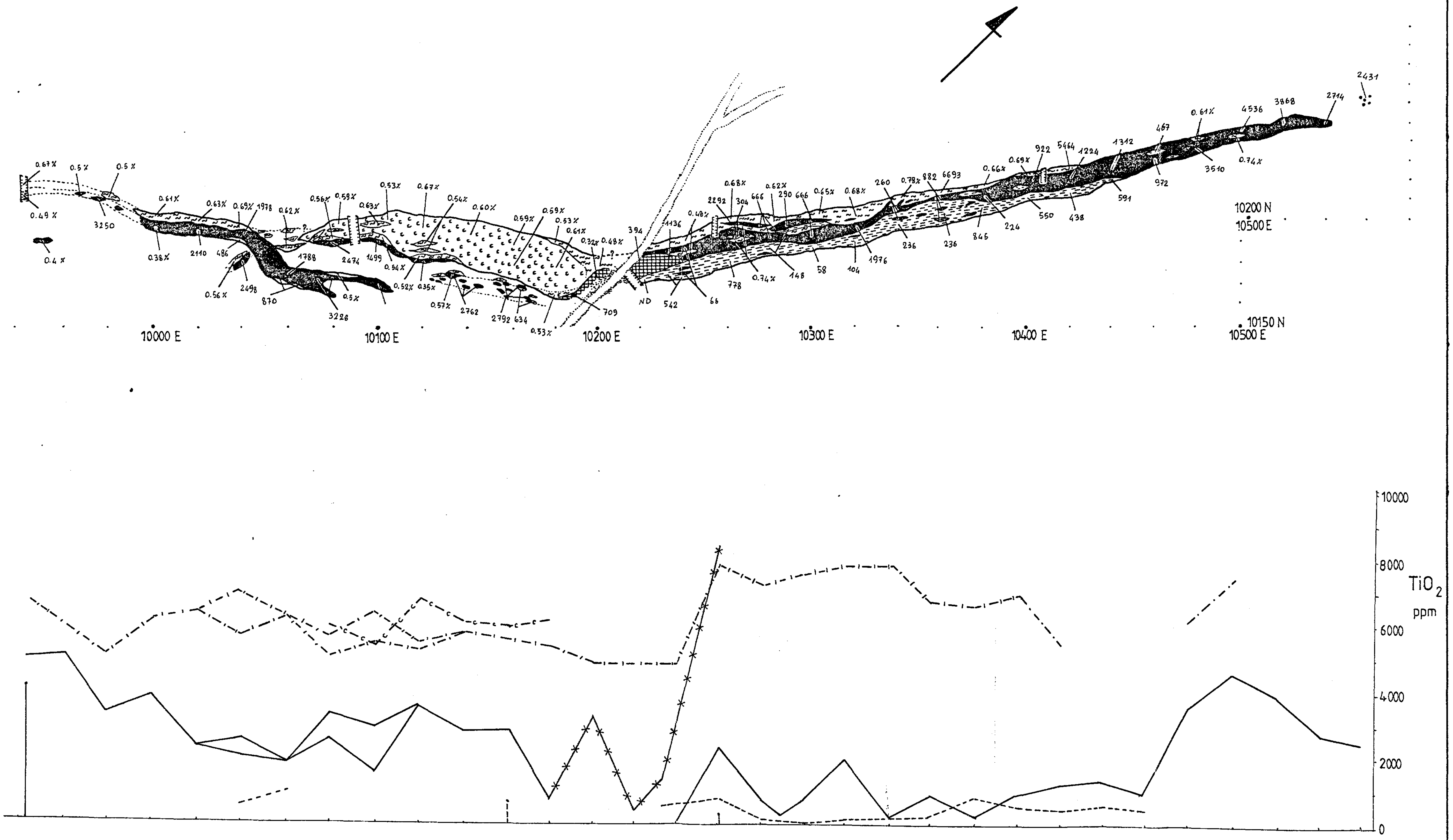

$\bar{x}$ unmineralized schist = 10200 TiO_2 (out of scale)

Chart 11: Titanium

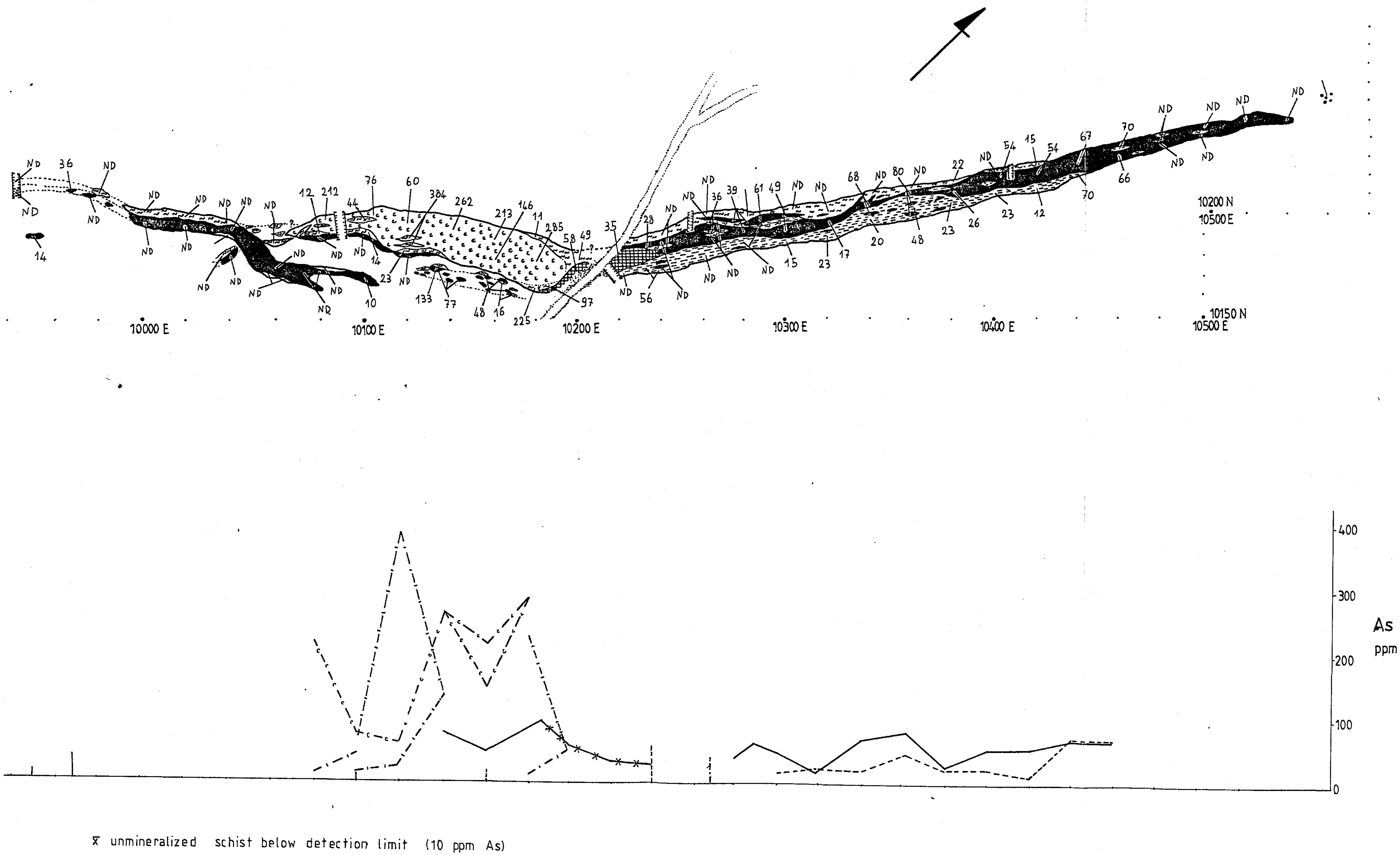

Chart 12: Arsenic

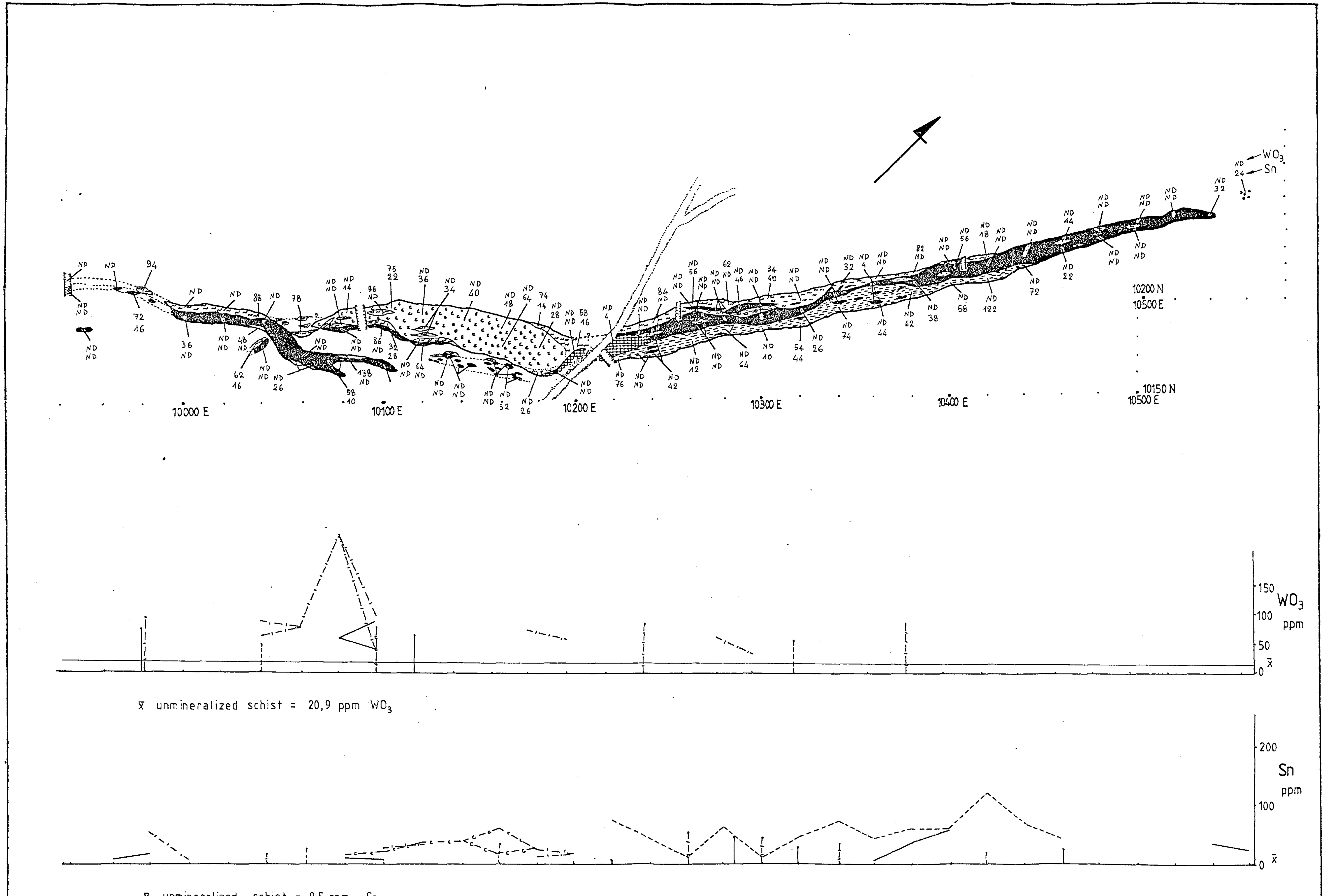

Chart 13: Tungsten - Tin

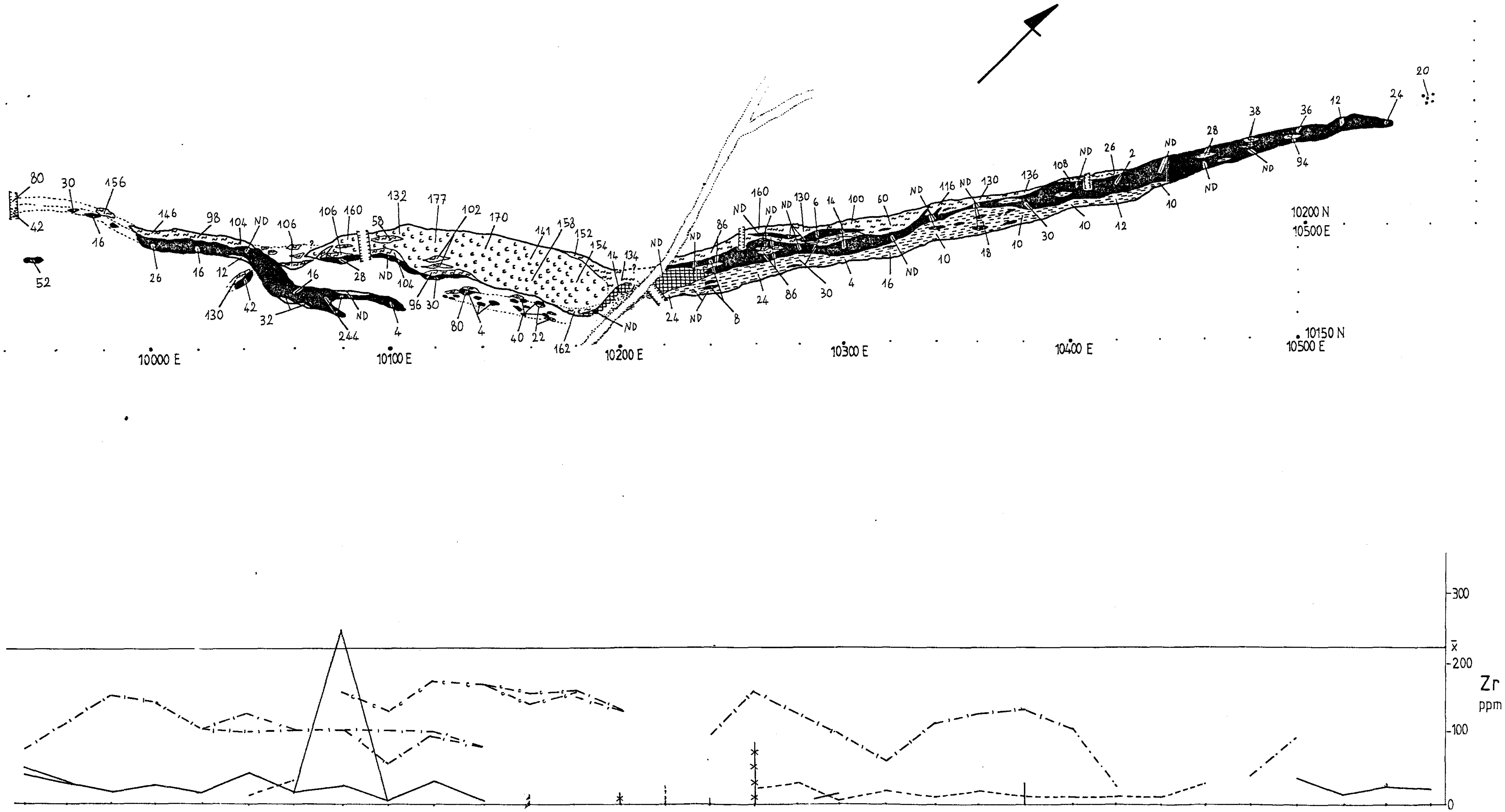

$\bar{x}$ unmineralized schist = 226,3 ppm Zr

Chart 14: Zirconium

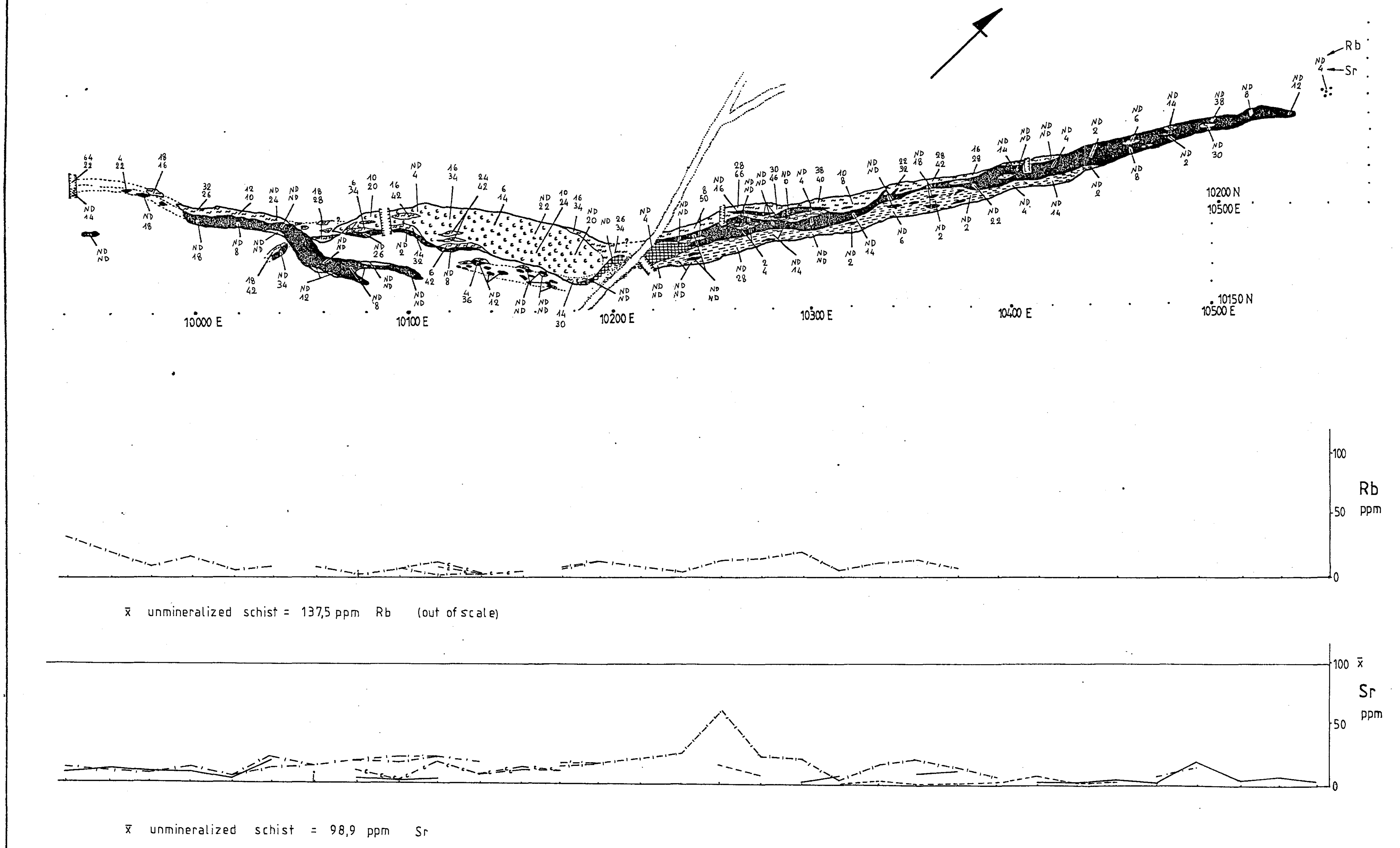

Chart 15: Rubidium - Strontium

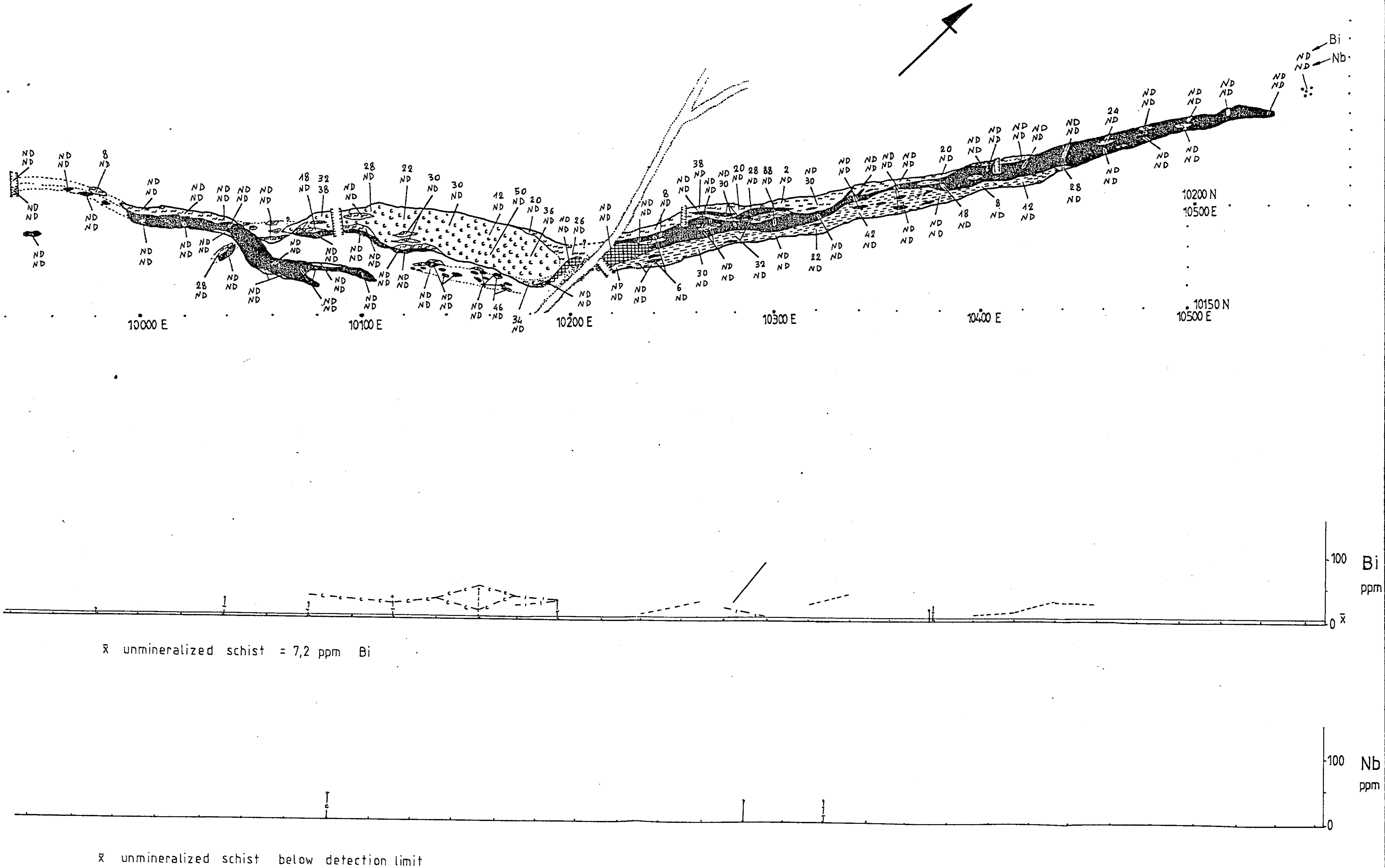

Chart 16: Bismuth- Niobium

APPENDIX H

Ongombo Prospect: geochemical profiles along the gossan outcrop

Charts 1 to 11

Elements: Cu, Pb, Zn, Ni, Co, Ag, Au, Mn, Ba, V, Ti, Sn, W, Zr, Sr, Mo, Bi

Legend

gossan surface outcrop

outcrop trace

fault

358 *concentration of the considered element (Note: ND indicates "below detection limit")*

Key for the profiles

mineralization

$\bar{x}$ *country rocks (average content)*

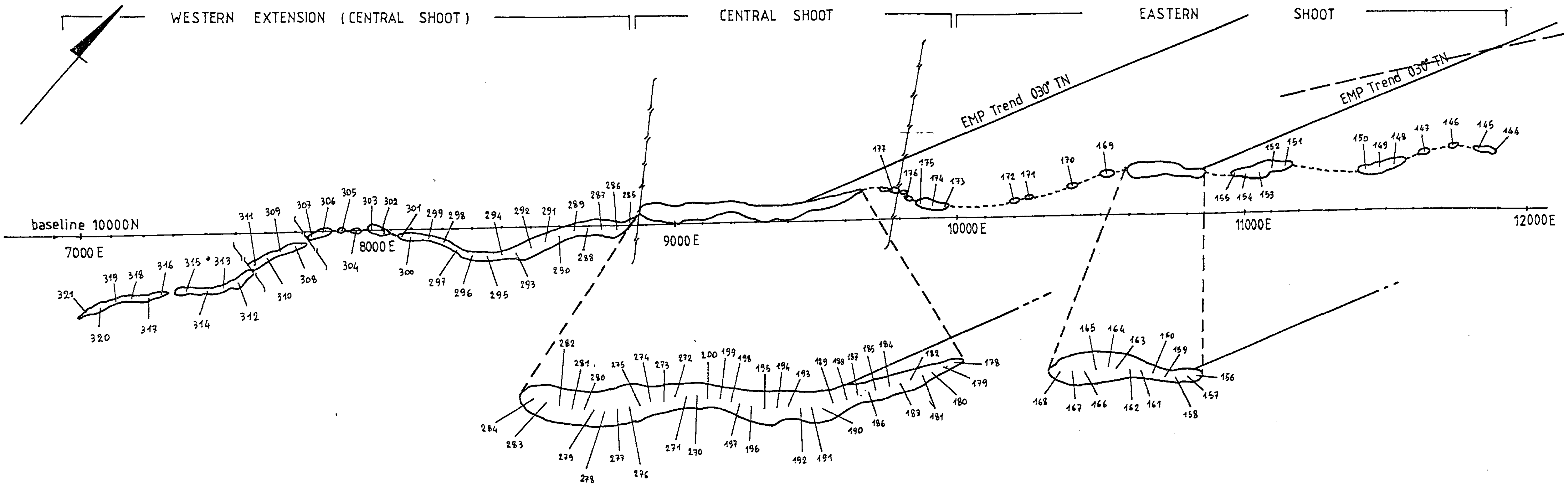

ONGOMBO PROSPECT - Schematic map with the location of the samples along the gossan outcrop

Samples OG 144 - OG 200 and OG 270 - OG 321

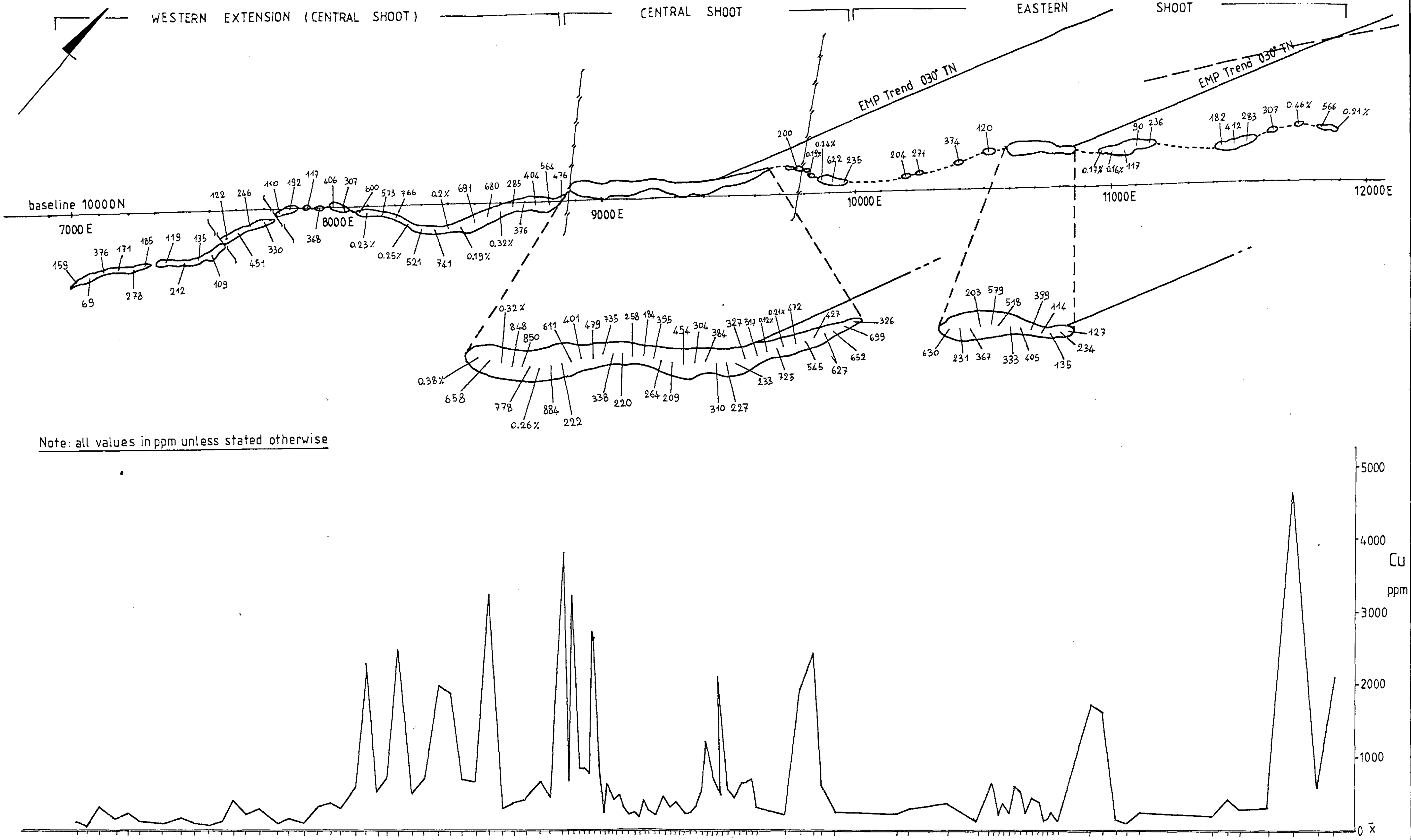

x̄ unmineralized schist = 59 ppm Cu

Chart 1: Copper

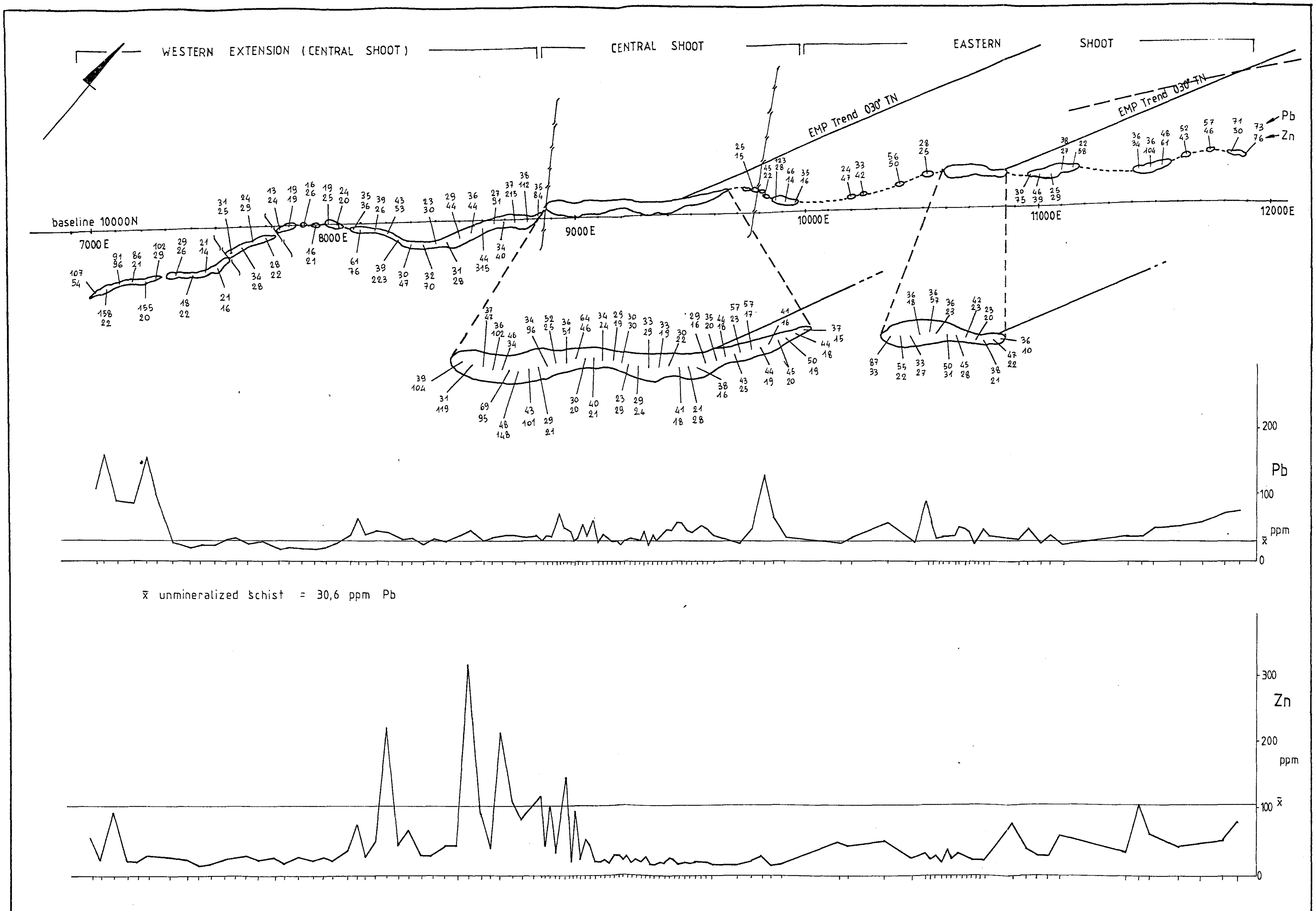

Chart 2: Lead - Zinc

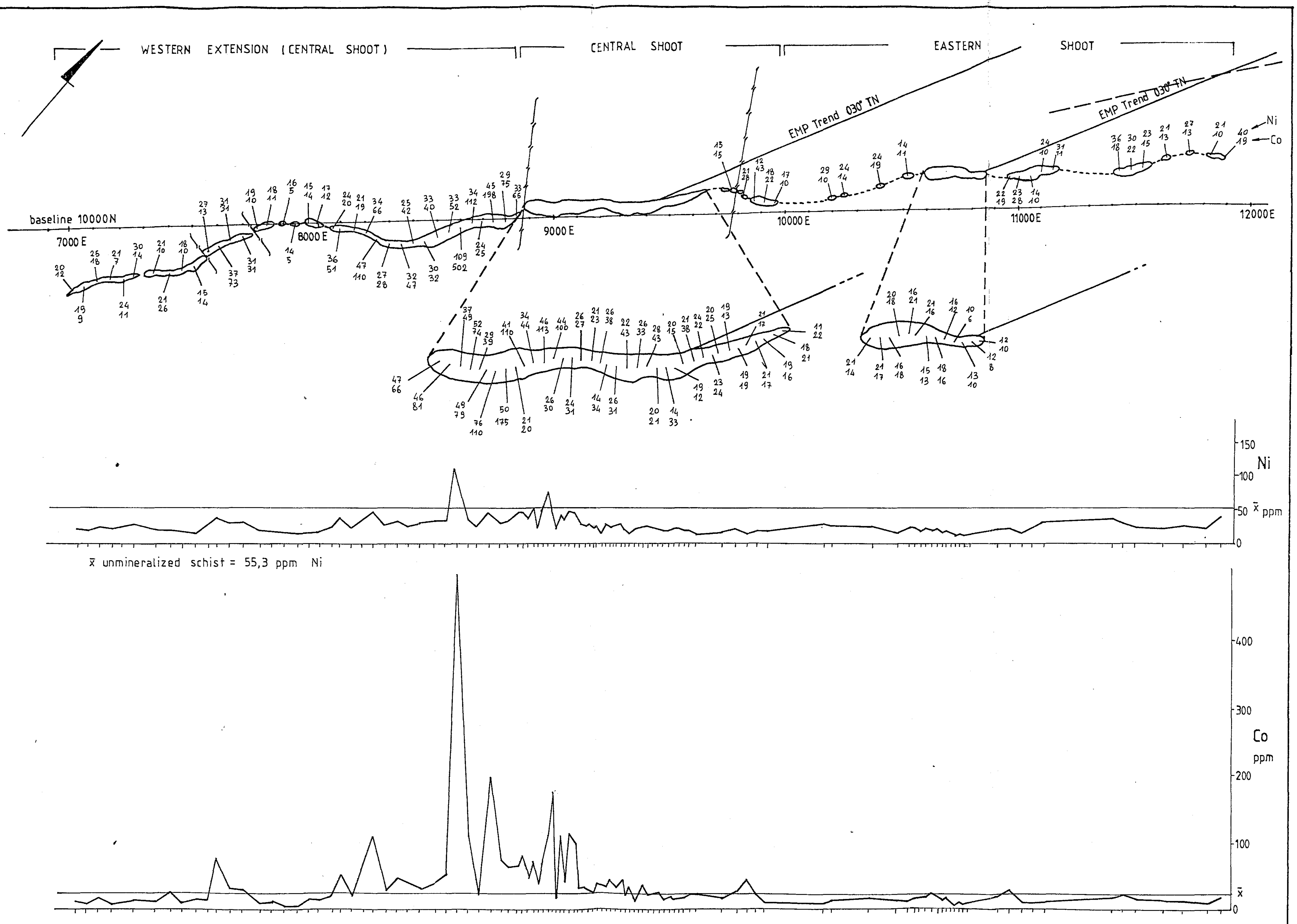

Chart 3: Nickel - Cobalt

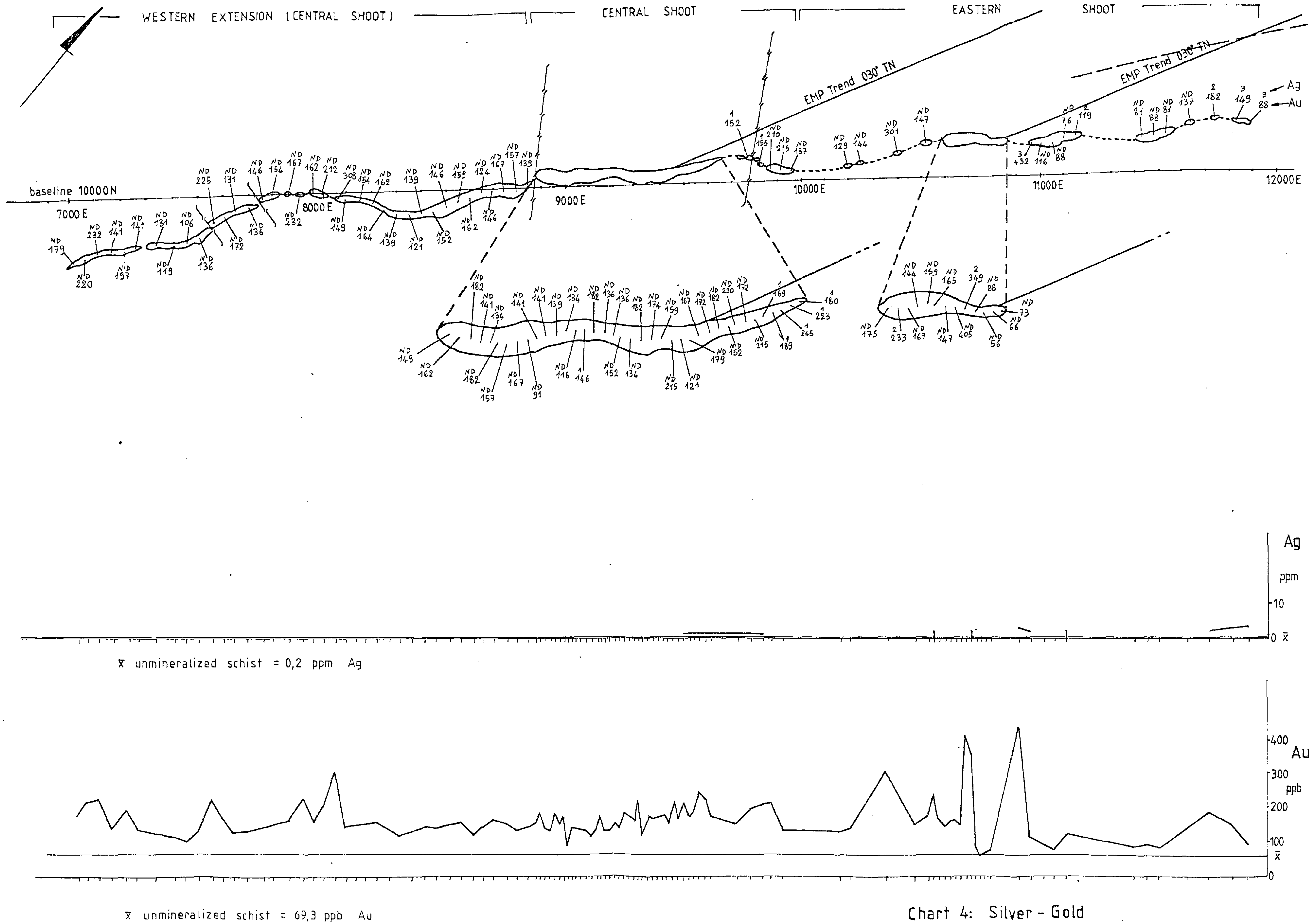

Chart 4: Silver - Gold

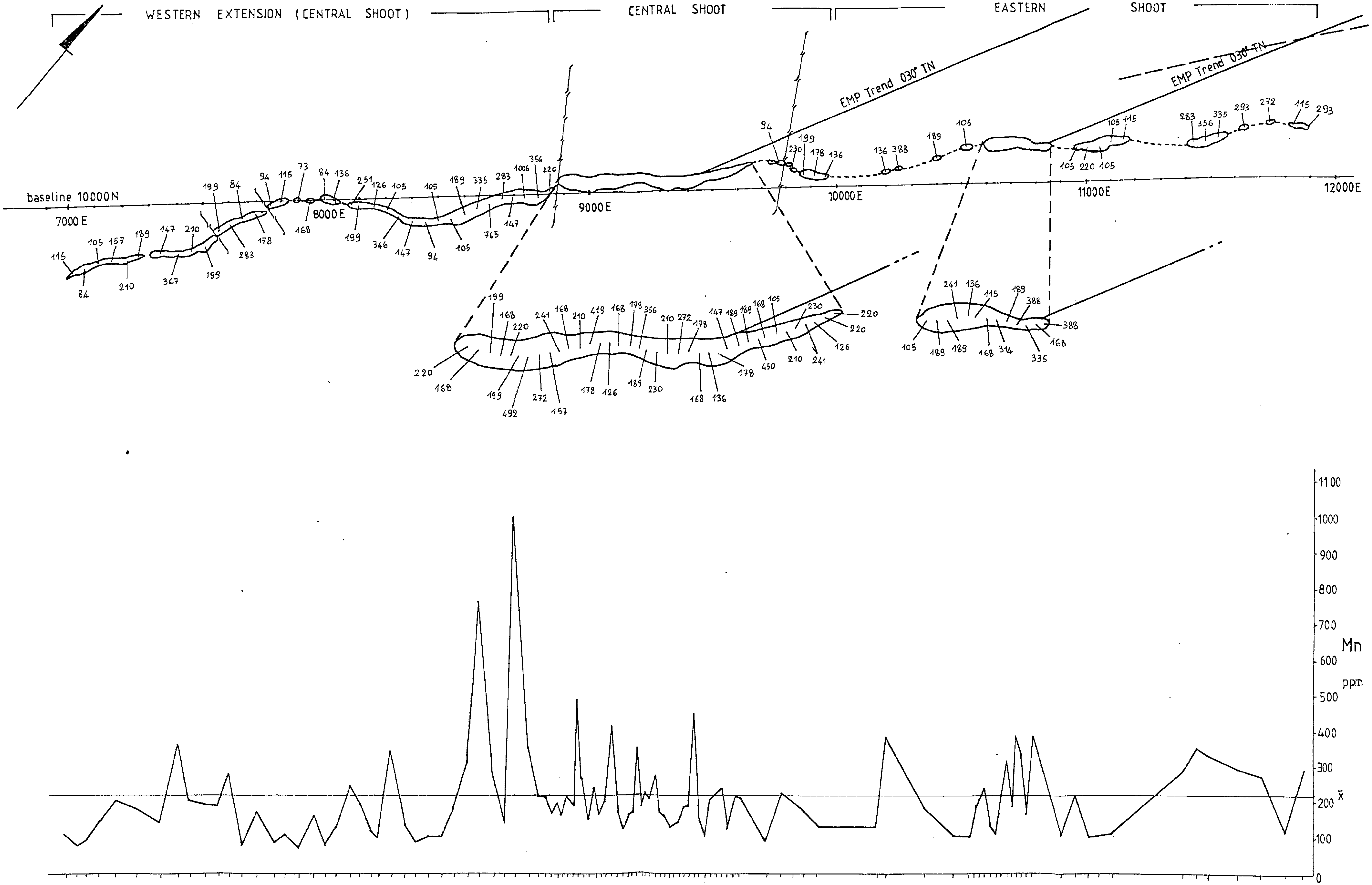

x̄ unmineralized schist = 221,1 ppm Mn

Chart 5: Manganese

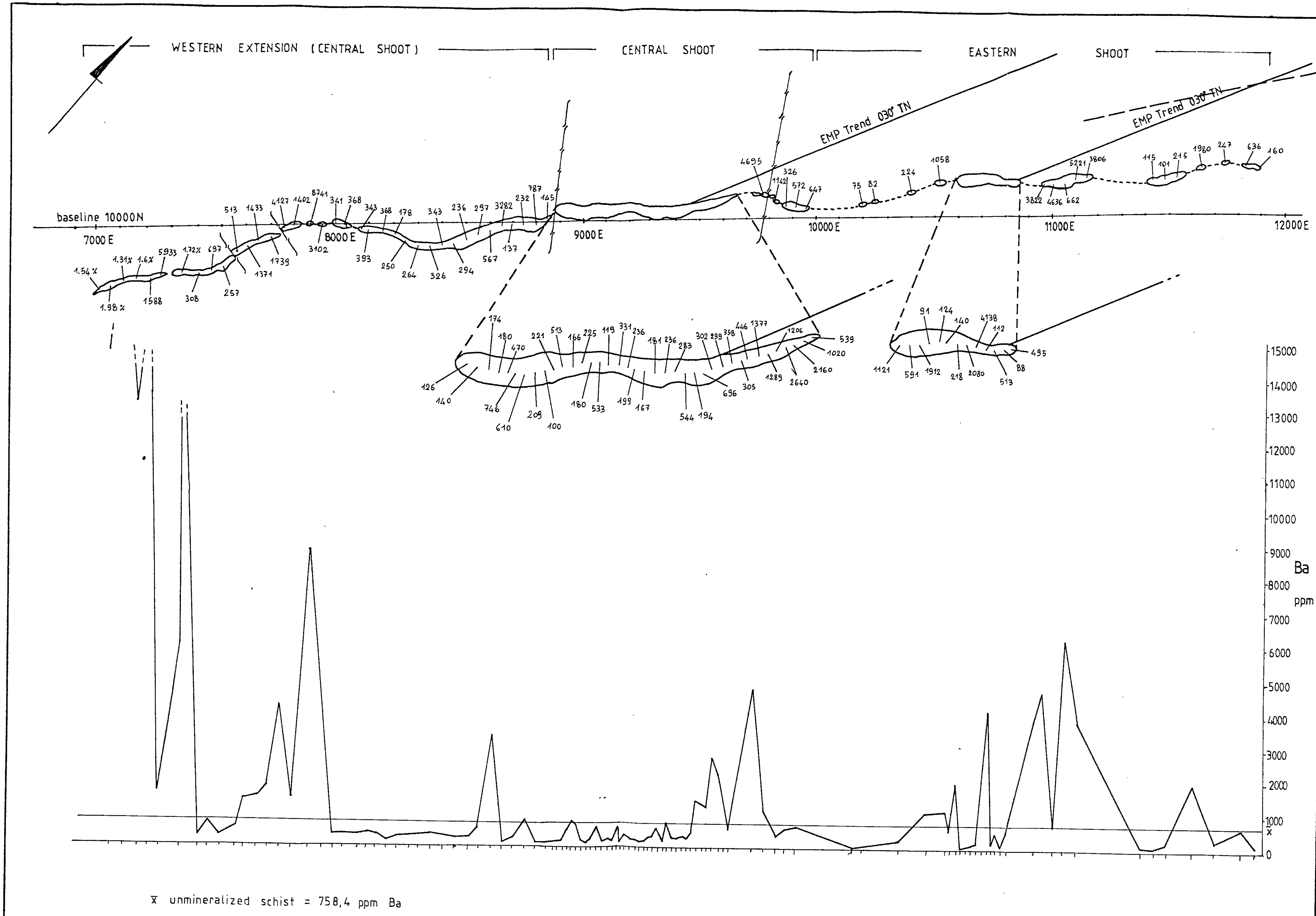

Chart 6: Barium

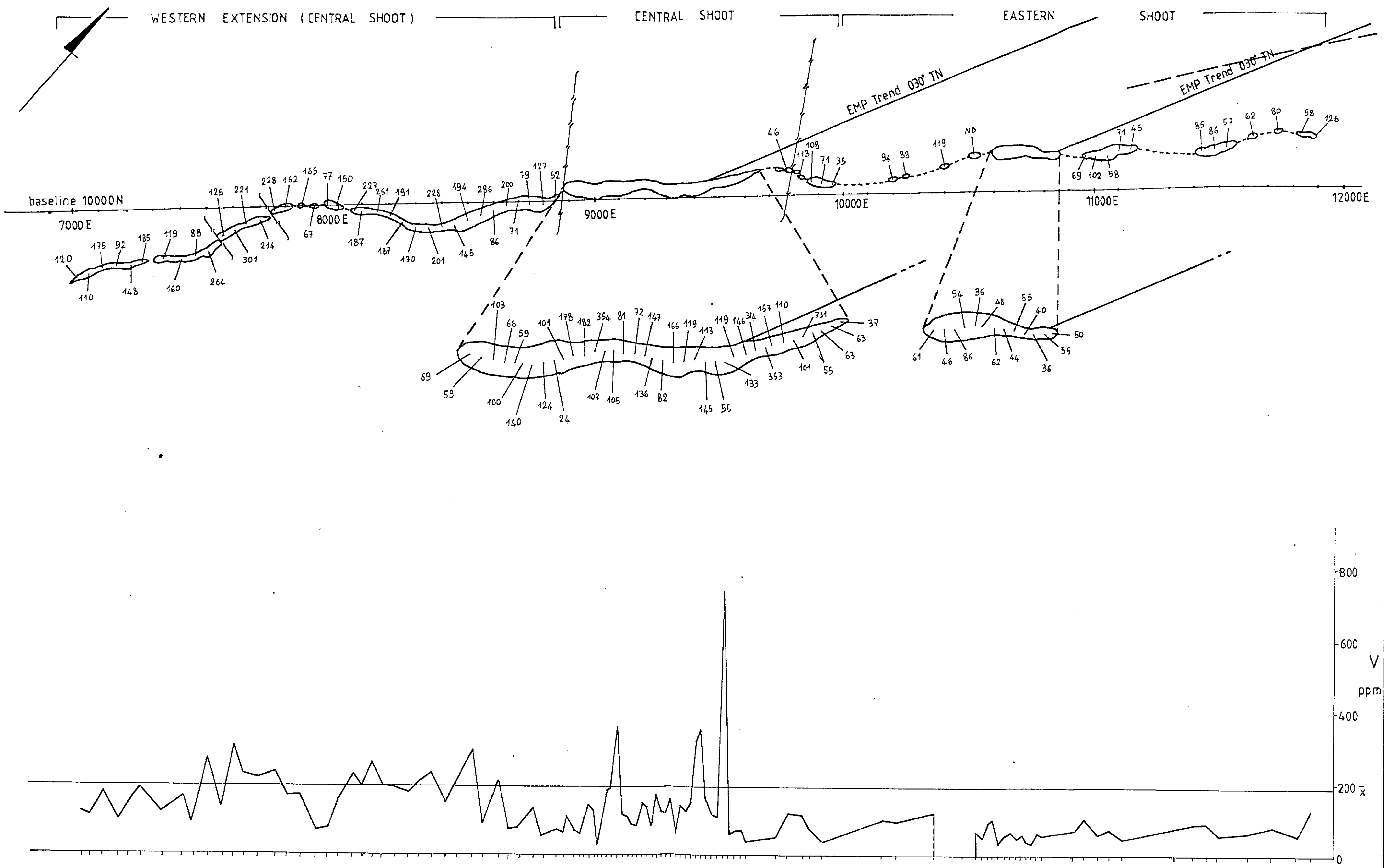

$\bar{x}$ unmineralized schist = 189,4 ppm V

Chart 7: Vanadium

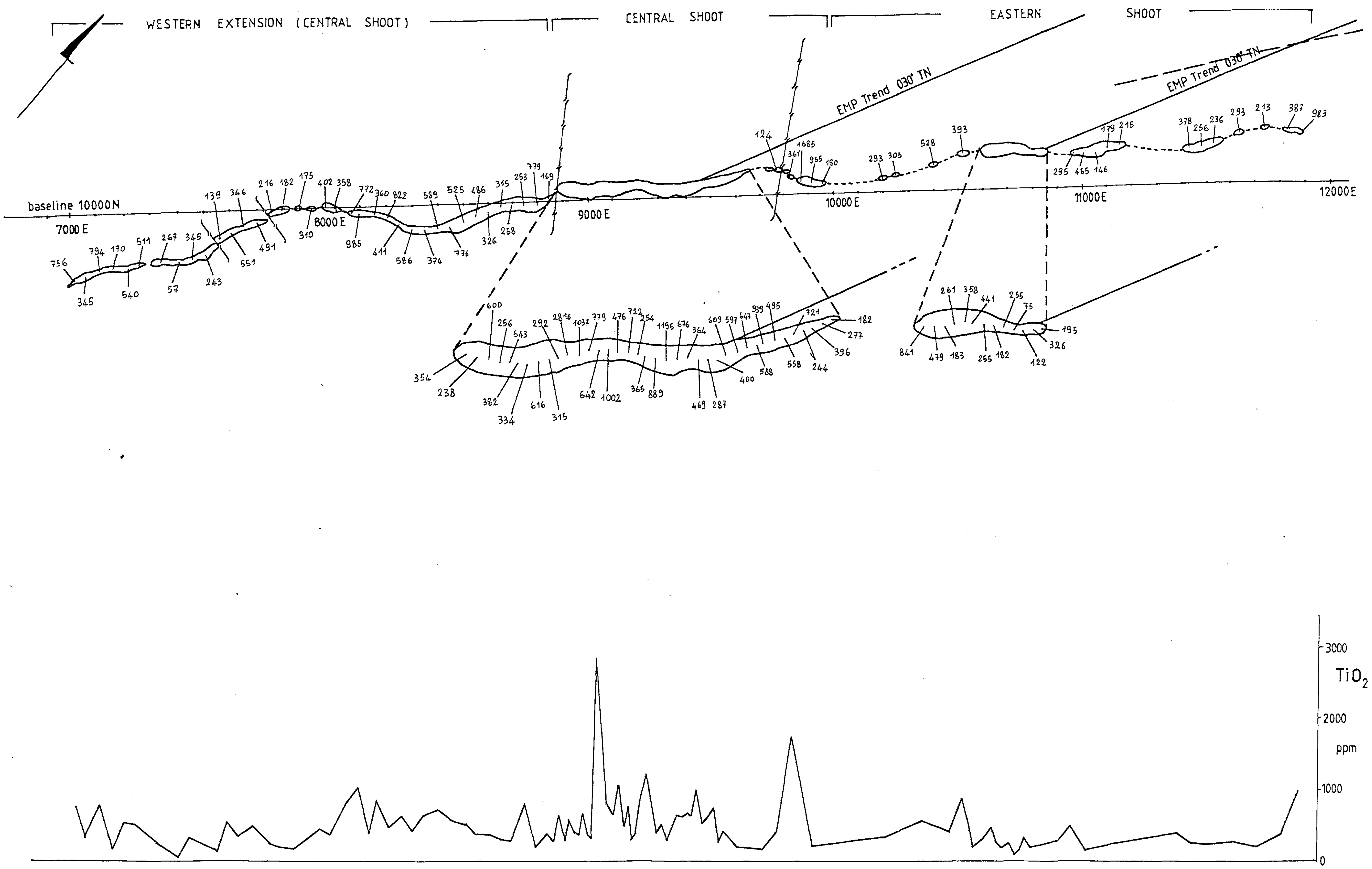

$\bar{x}$ unmineralized schist = 10200 TiO_2 (out of scale)

Chart 8: Titanium

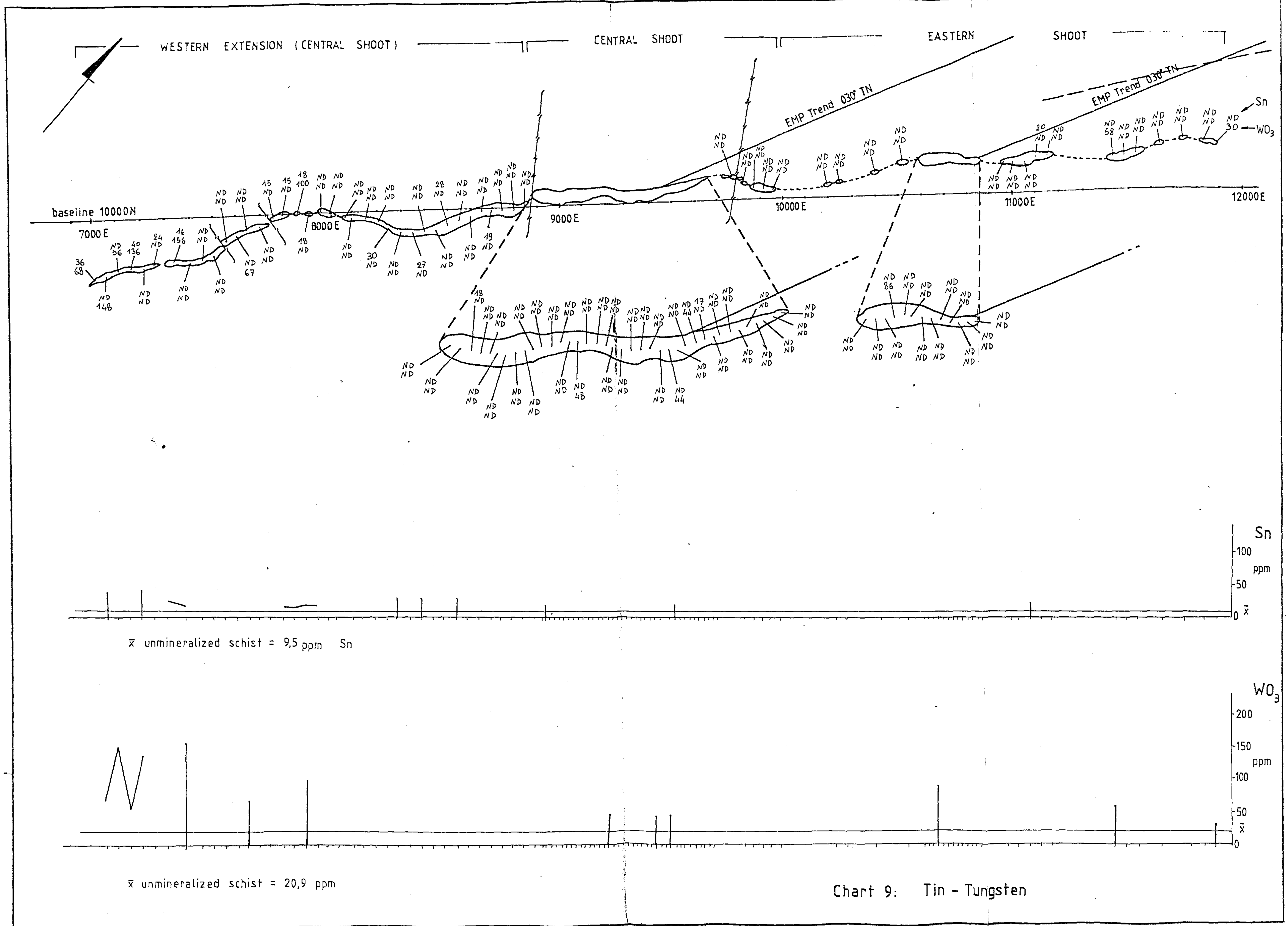

$\bar{x}$ unmineralized schist = 9,5 ppm Sn

$\bar{x}$ unmineralized schist = 20,9 ppm

Chart 9: Tin - Tungsten

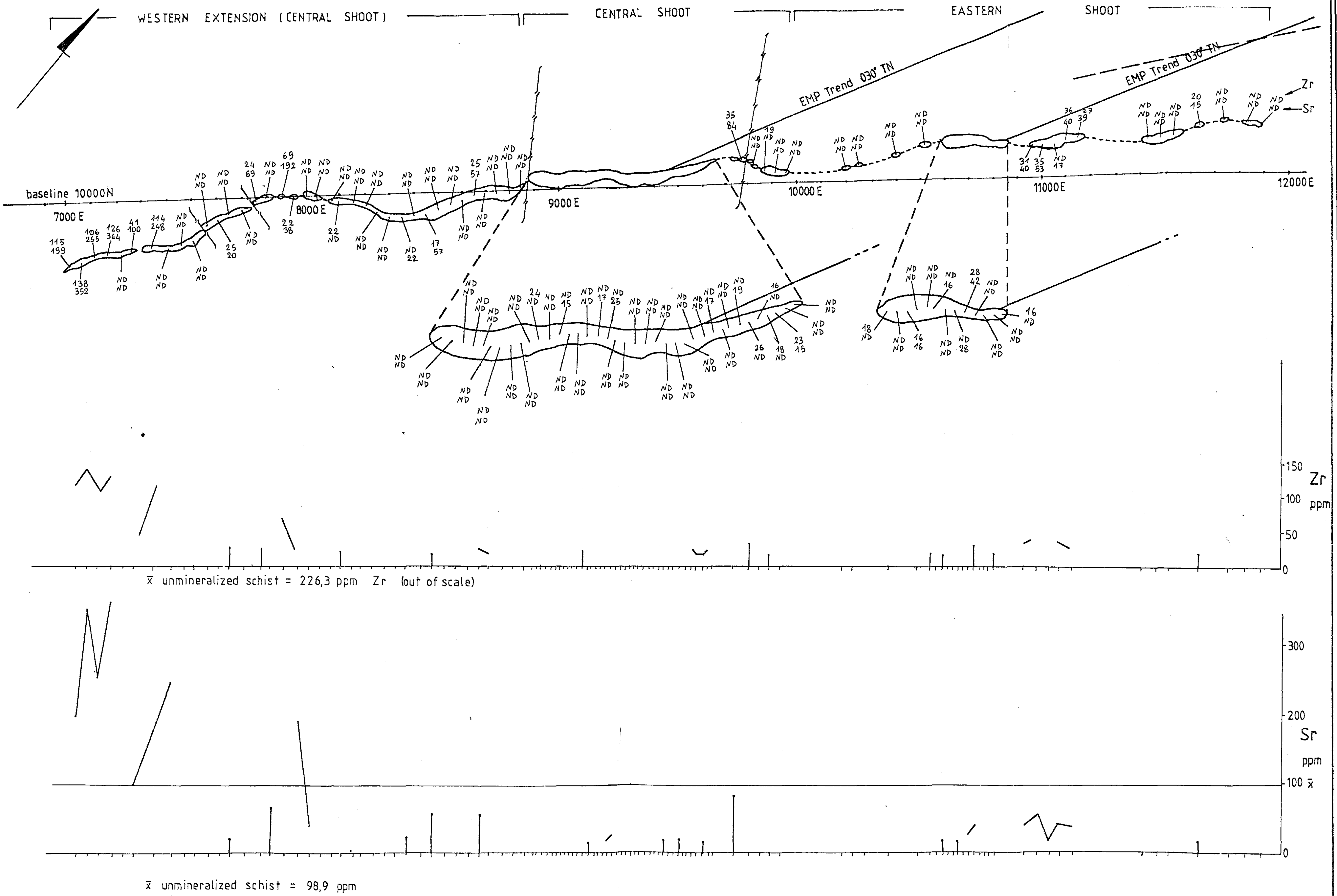

Chart 10: Zirconium - Strontium

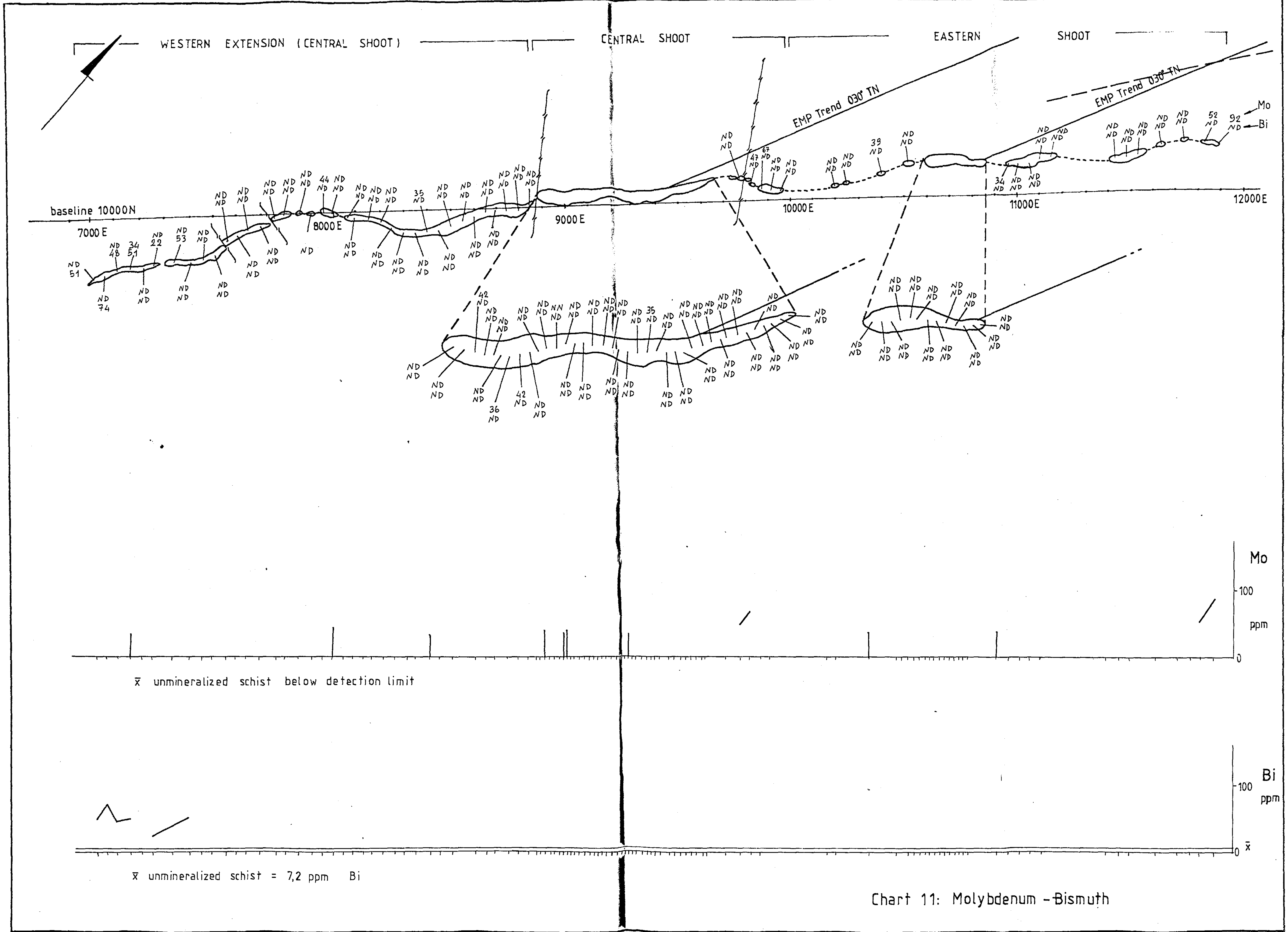

Chart 11: Molybdenum - Bismuth

APPENDIX I

ONGOMBO PROSPECT

Geochemical profiles of the ore-bearing sequence in drillcores

Boreholes no. OGB 151A, OGB 153A, OGB 154A

(in the back pocket)

APPENDIX J

ONGOMBO PROSPECT

Geochemical profiles of the ore zone in drill cores

Boreholes no. OGB 151A, OGB 153A, OGB 154A

Charts 1 to 3

<u>Legend</u>

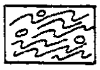	*BS*	*biotite selvedge zone*
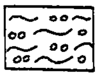	*SD*	*sulphides in lenses and disseminations in schists (stringer-type ore)*
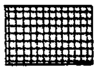	*SM*	*semi-massive sulphide layers*
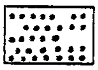	*MQ*	*(sulphide-bearing) magnetite quartzite*
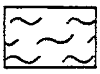	*hw sch* *fw sch* *bsc*	*quartz-biotite-staurolite-chlorite schist*
	474	*sample number*

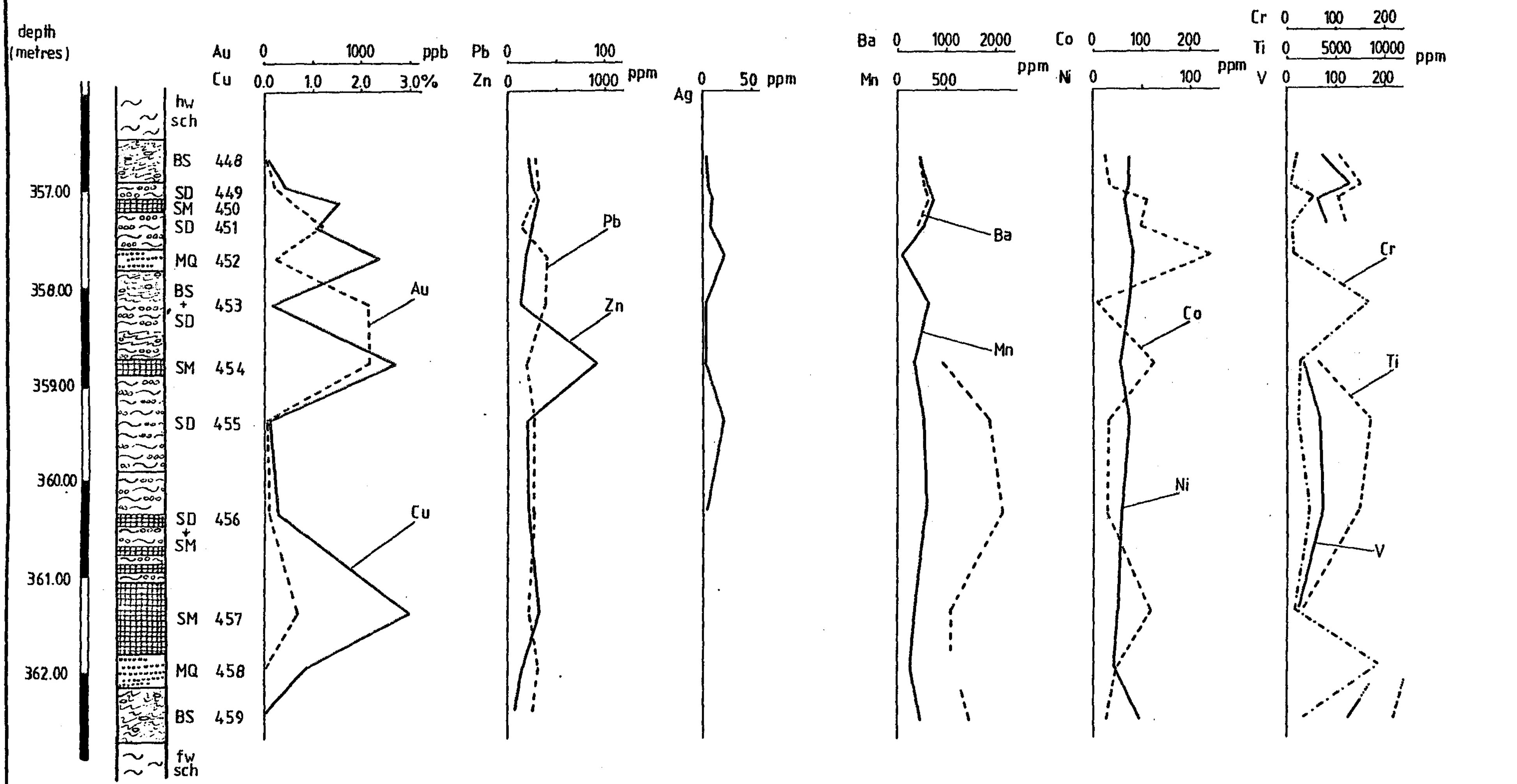

Chart 1 - Borehole no. OGB 151A

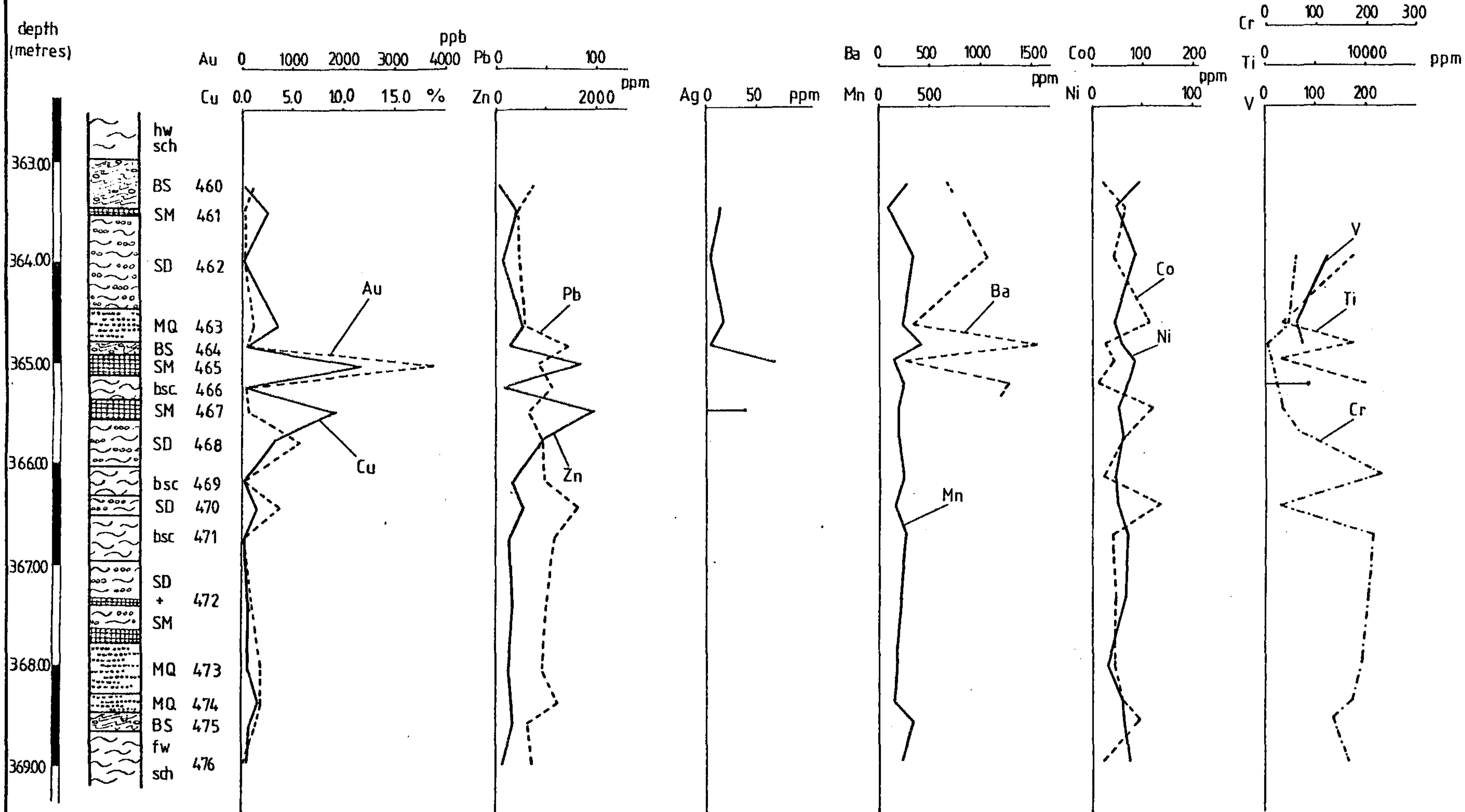

Chart 2 - Borehole no. OGB 153A

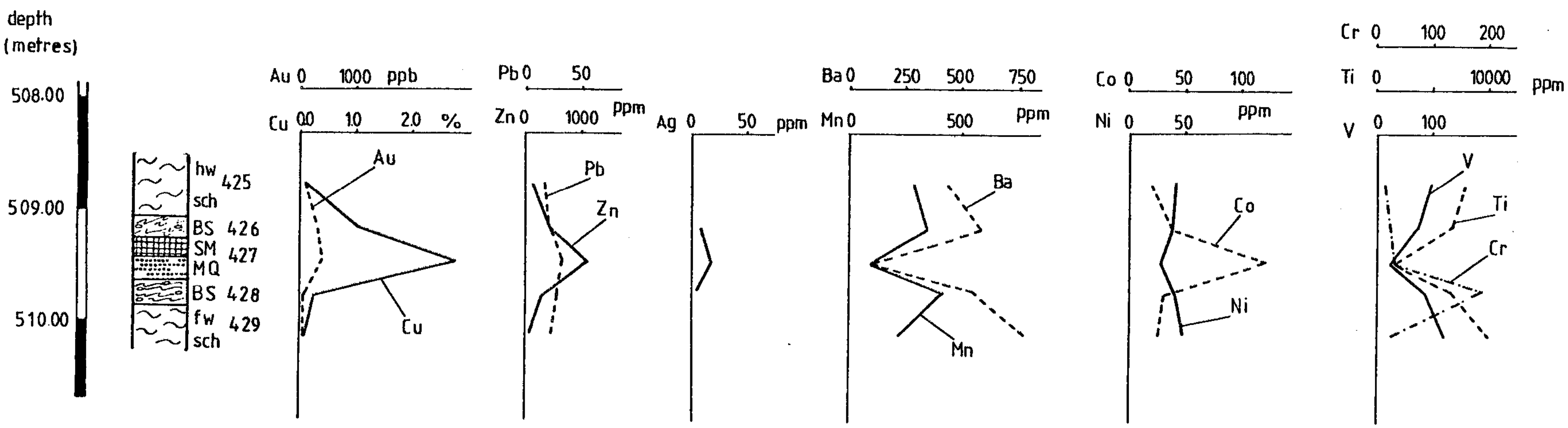

Chart 3 - Borehole no. OGB 154A

APPENDIX L

Plates

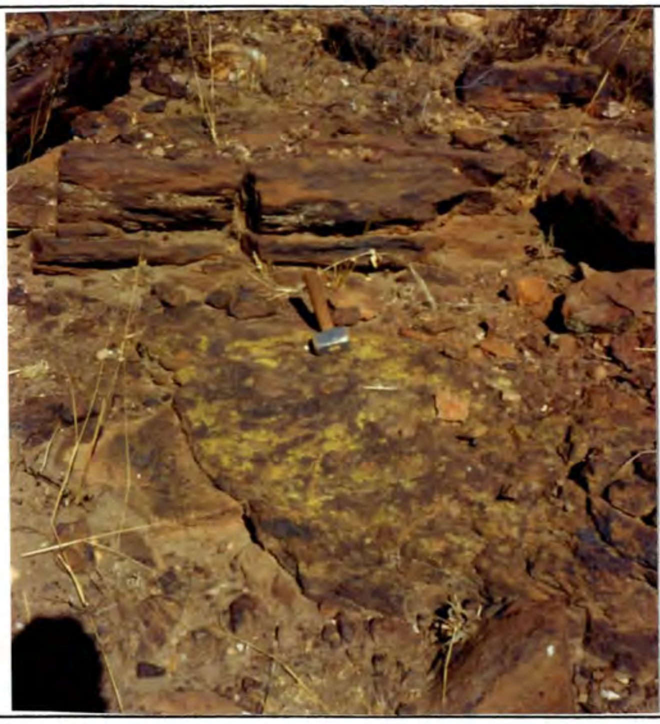

Plate 1

Ongeama gossan outcrop: gossan after massive sulphide mineralization (below) overlain by rusty magnetic muscovite schist of the alteration zone.

Plate 2

Ongeama gossan outcrop: close-up of banded magnetite quartzite showing small-scale tight fold-like structures.

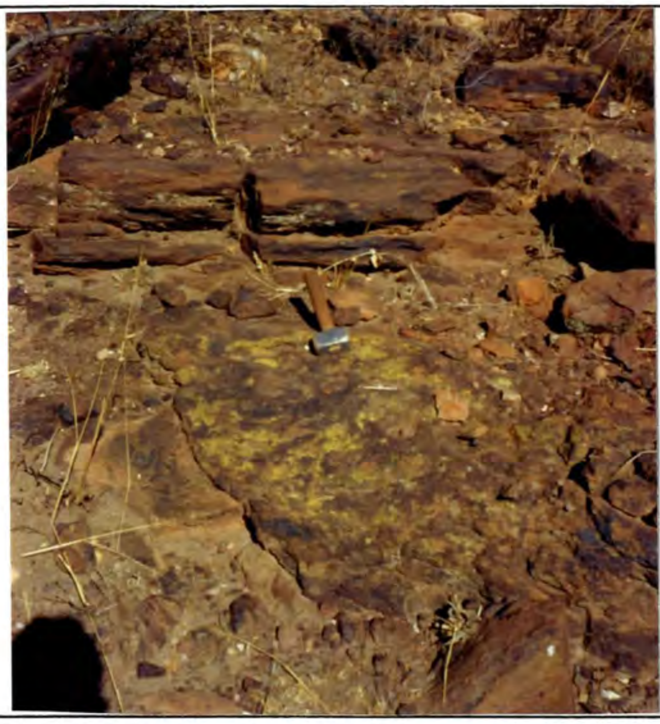

Plate 1

Ongeama gossan outcrop: gossan after massive sulphide mineralization (below) overlain by rusty magnetic muscovite schist of the alteration zone.

Plate 2

Ongeama gossan outcrop: close-up of banded magnetite quartzite showing small-scale tight fold-like structures.

Plate 3

Ongeama gossan outcrop, alteration zone: mottled magnetic staurolite- and garnet-bearing chlorite schist.

Plate 4

Ongombo Prospect: outcrop of magnetite quartzite in the sandy bed of the White Nossob River.

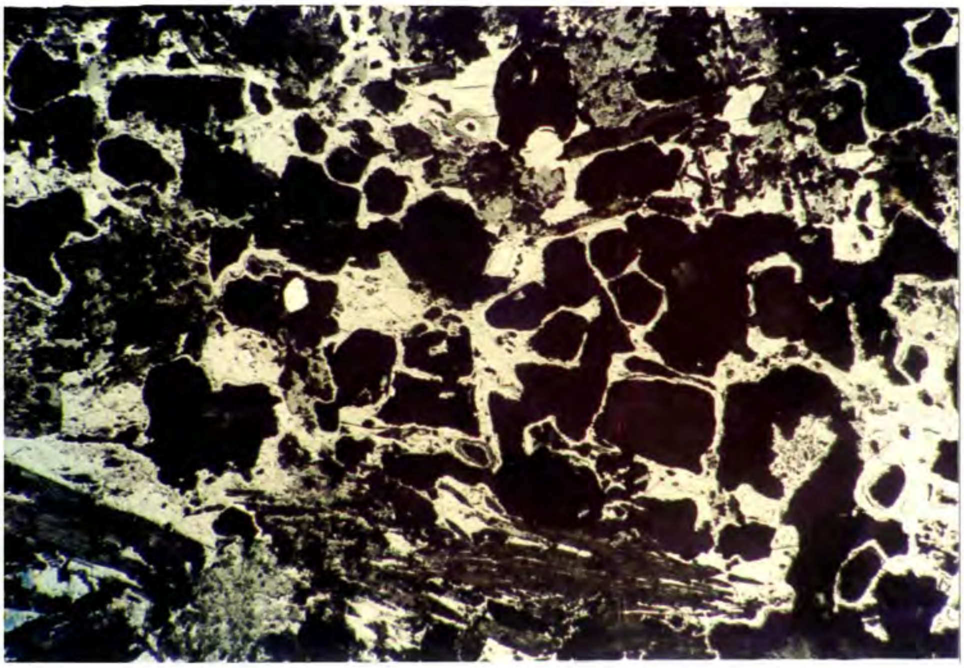

Plate 5

Ongeama gossan: coarse boxwork structure after pyrite. Note a small patch with fine-grained ladder-like boxwork after chalcopyrite towards the bottom-right corner. Acicular traces are probably anthophyllite crystals. White-grey material is Fe-hydroxide.
(Polished section OG 63; // Nicols; field of view = 2.5 mm).

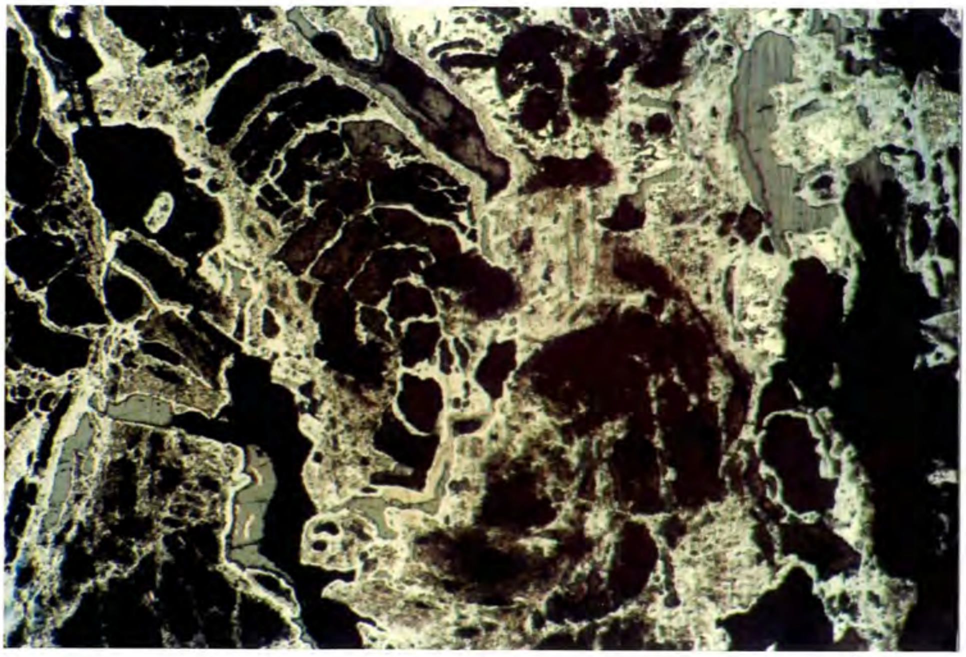

Plate 6

Ongeama gossan: boxwork structure after shrinkage cracks, typical of bird's eye weathering in pyrrhotite. The light grey material is Fe-hydroxide.
(Polished section OG 38; // Nicols; field of view = 2.5 mm).

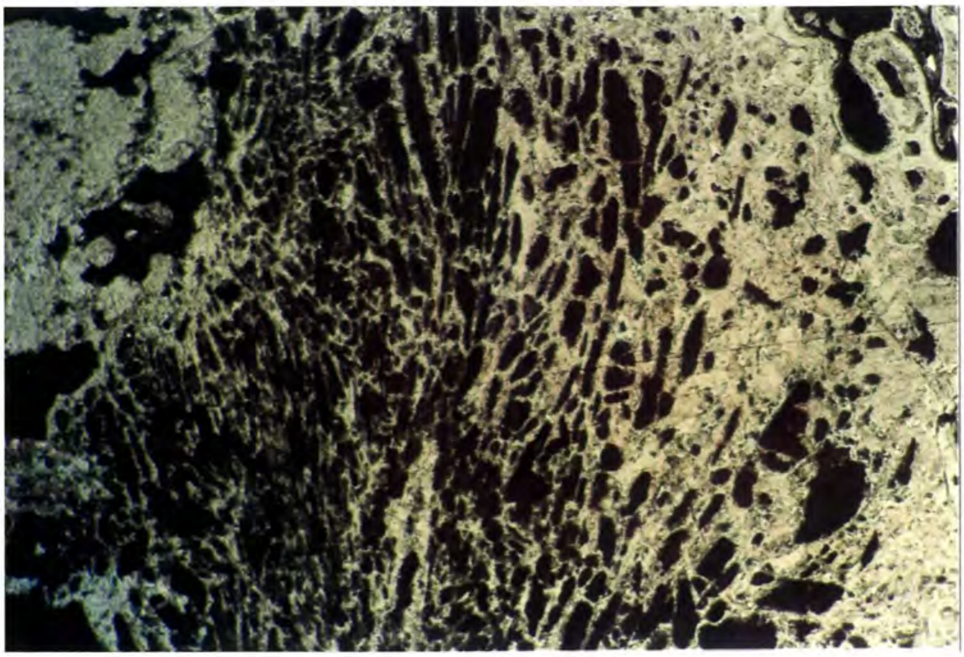

Plate 7

Ongombo gossan: boxwork structures after anthophyllite aggregates. The light grey material is Fe-hydroxide.
(Polished section OG 196; // Nicols; field of view = 2.5 mm).

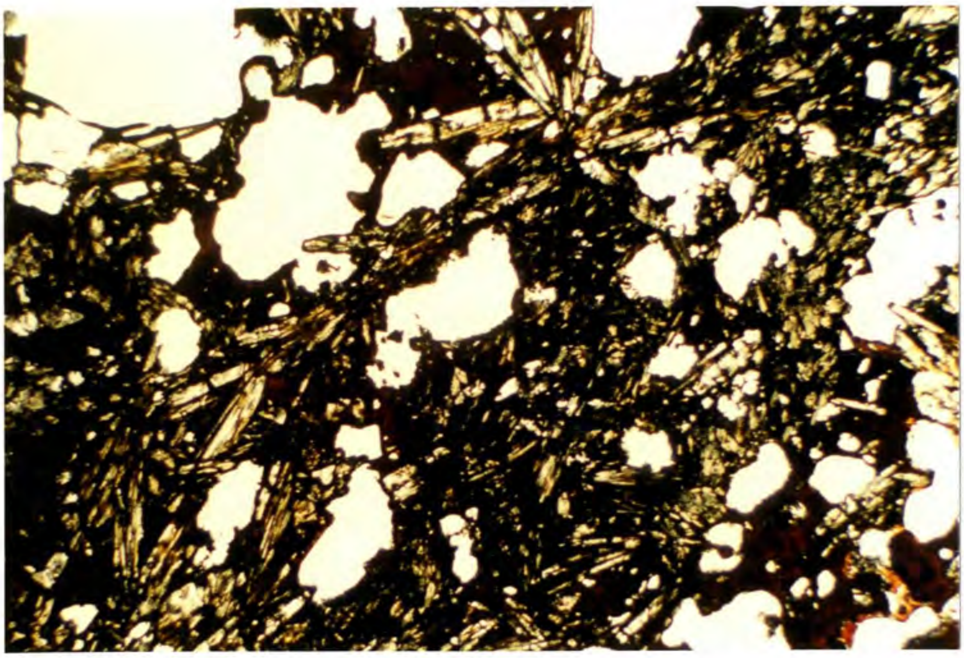

Plate 8

Ongeama gossan: radiating anthophyllite aggregates impregnated with Fe-hydroxides. White areas indicate voids.
(Thin section OG 63; // Nicols; field of view = 4 mm).

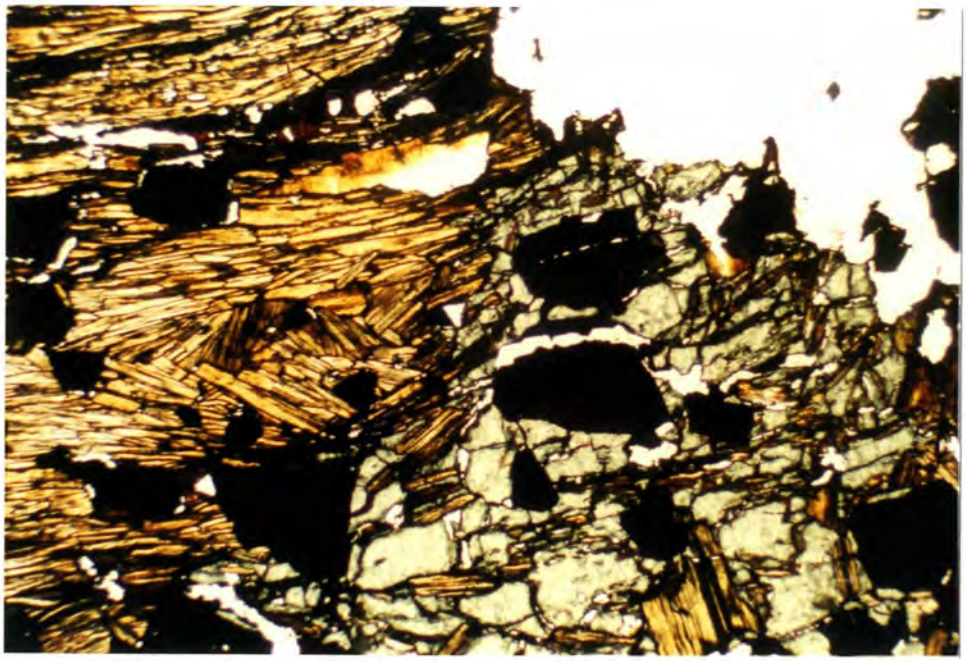

Plate 9

Ongeama gossan: phlogopite (?)-bearing ferruginous schist (brownish) containing gahnite (?) (greenish transparent, fractured) and magnetite (opaque).
(Thin section OG 64; + Nicols; field of view = 4 mm).

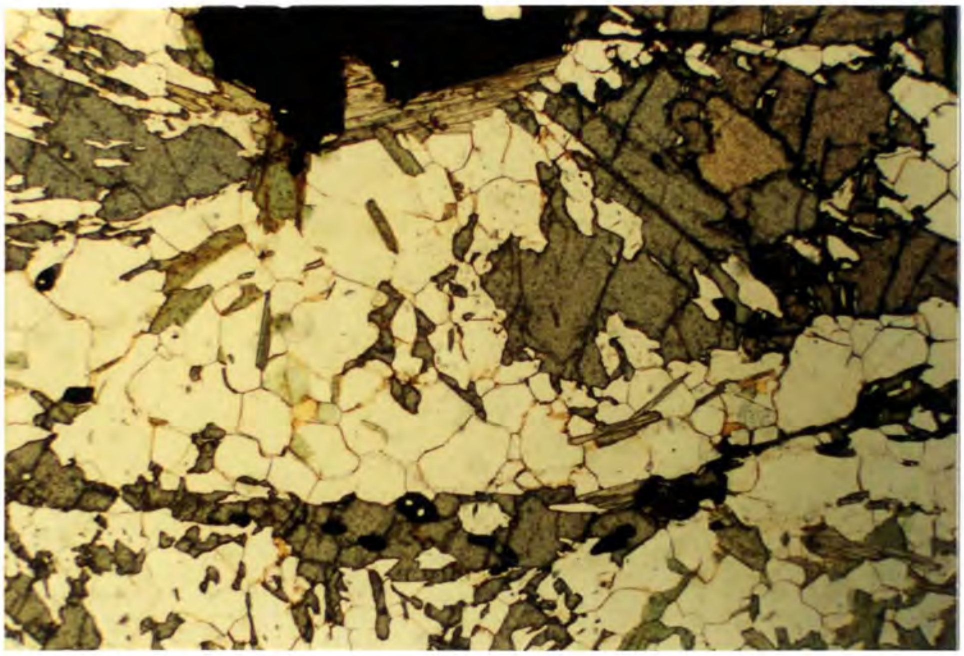

Plate 10

Ongeama deposit, alteration pipe, magnetic quartz-chlorite schist facies: aggregate of garnet (dark brown, containing light brown staurolite) and chloritoid (greenish-grey) in chlorite-bearing quartz-rich groundmass. The opaque mineral is magnetite.
(Thin section OG 77B; // Nicols; field of view = 4 mm).

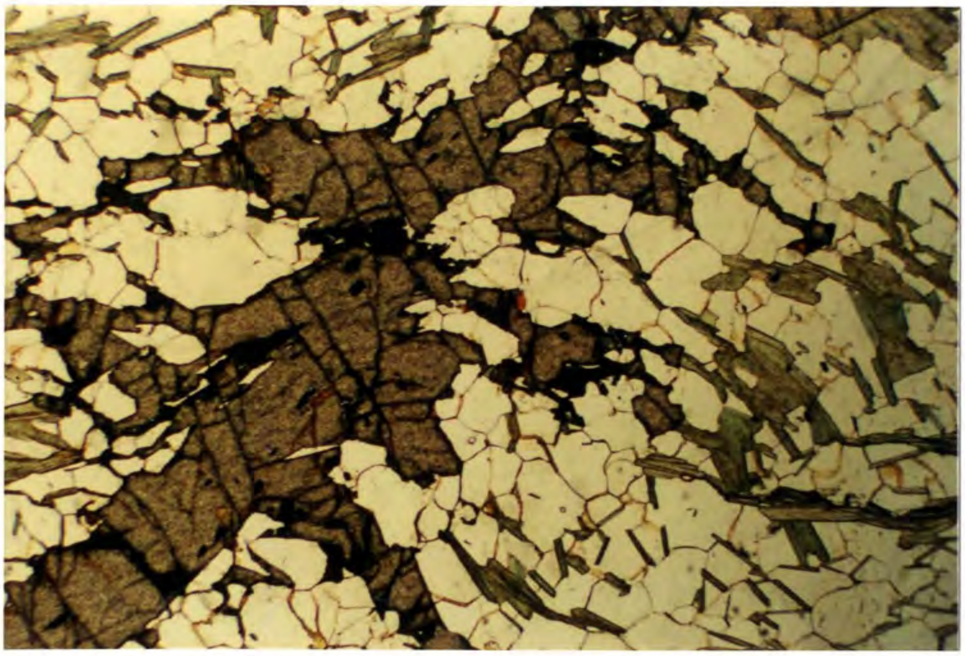

Plate 11

Ongeama deposit, alteration pipe, magnetic quartz-chlorite schist facies: coarse-grained skeletal garnet porphyroblast in chlorite-bearing quartzose groundmass.
(Thin section OG 77B; // Nicols; field of view = 4 mm).

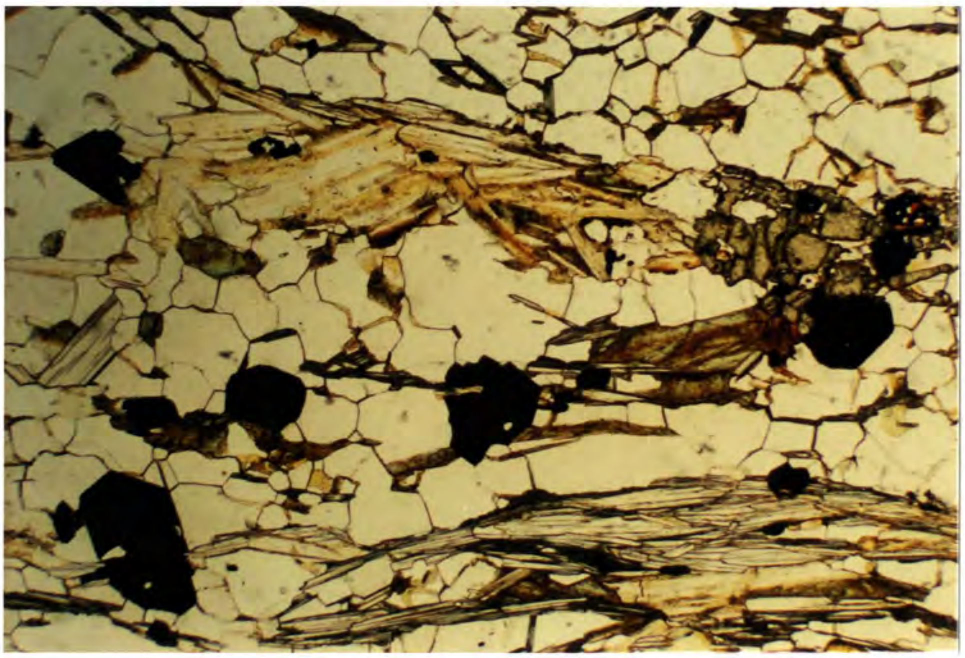

Plate 12

Ongeama deposit, alteration pipe magnetic muscovite facies: Fe-hydroxide-stained quartz-muscovite schist, with disseminated magnetite (opaque). Sporadic staurolite (brownish, high relief, cracked) and chlorite (greenish, lamellar).
(Thin section OG 62; // Nicols; field of view = 4 mm).

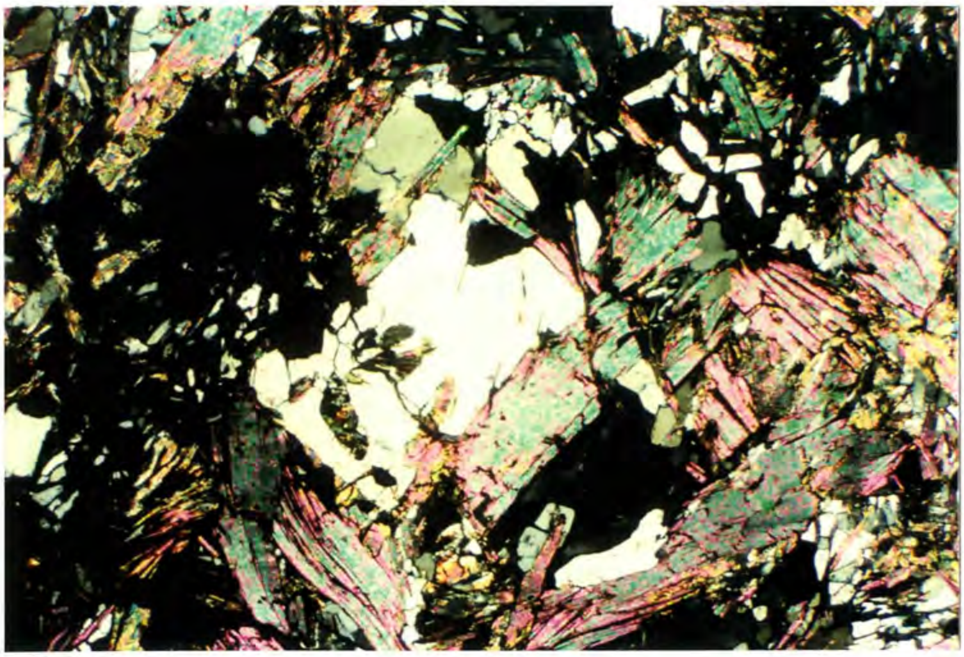

Plate 13

Matchless West Extension deposit: particular of a talc-quartz-rich patch of the massive sulphide gossan. Talc flakes (pink to green) randomly grow on the Fe-hydroxide-impregnated quartz-rich groundmass.
(Thin section MWE 207; + Nicols; field of view = 4 mm).

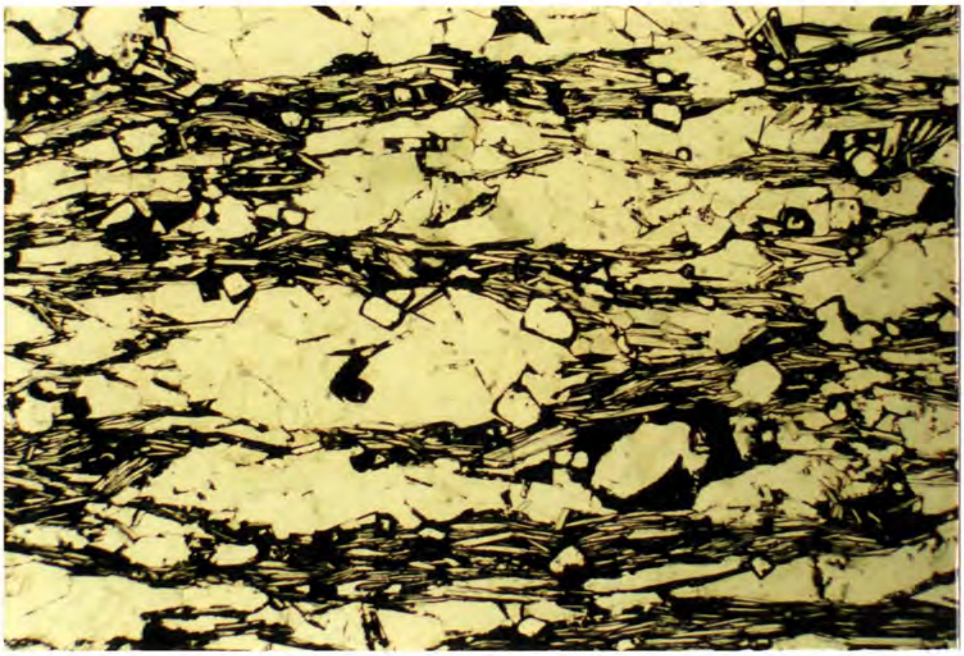

Plate 14

Matchless West Extension deposit: quartz-muscovite schist from the axial zone of the alteration pipe. Fe-hydroxide-rimmed cavities after euhedral pyrite crystals are disseminated. Fe-hydroxides impregnate the groundmass.
(Thin section MWE 205; // Nicols; field of view = 4 mm).

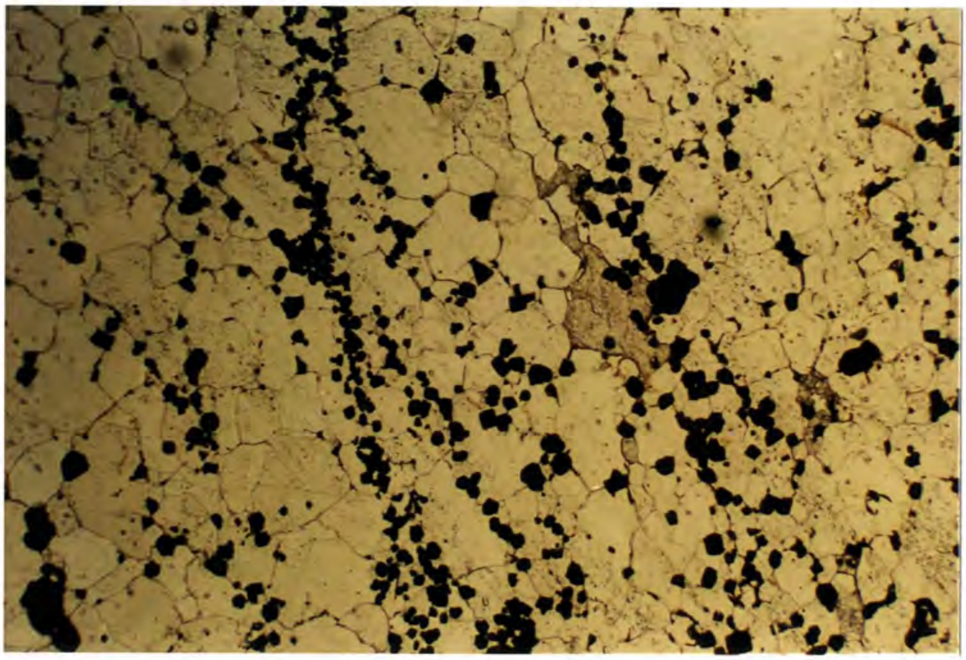

Plate 15

Matchless West Extension deposit, upper magnetite quartzite layer: thin magnetite strings and anhendral baryte blebs (colourless, high relief) in the sulphide-devoid quartz-rich groundmass.
(Thin section MWE 253; // Nicols; field of view = 4 mm).

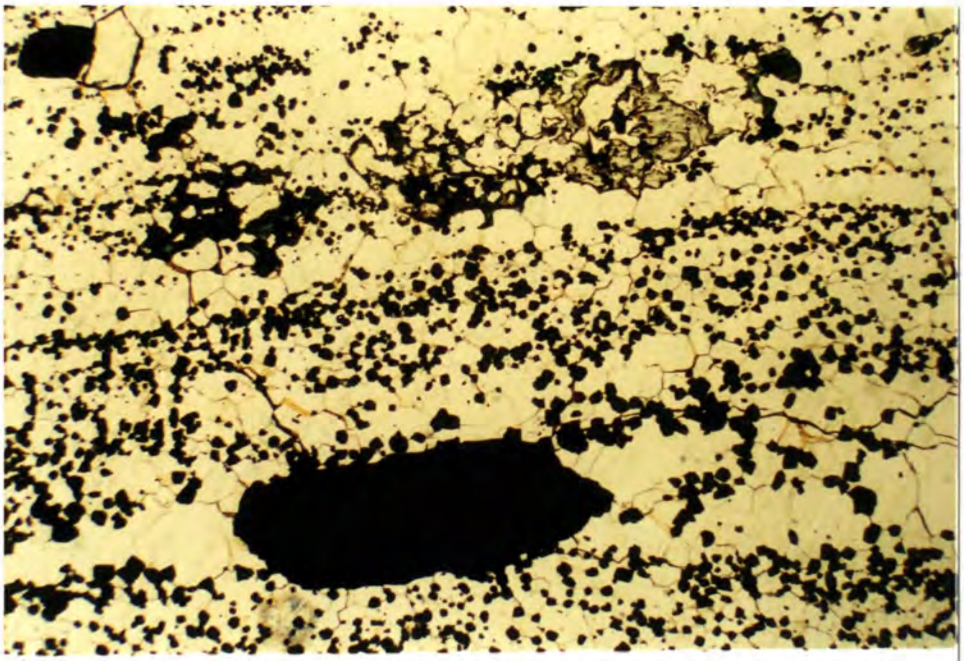

Plate 16

Matchless West Extension deposit, lower magnetite quartzite layer: typical banding induced by magnetite-rich laminae. Irregular sulphide and malachite patches and a weathered, anhedral amphibole grain are also shown.
(Thin section MWE 241A; // Nicols; field of view = 4 mm).

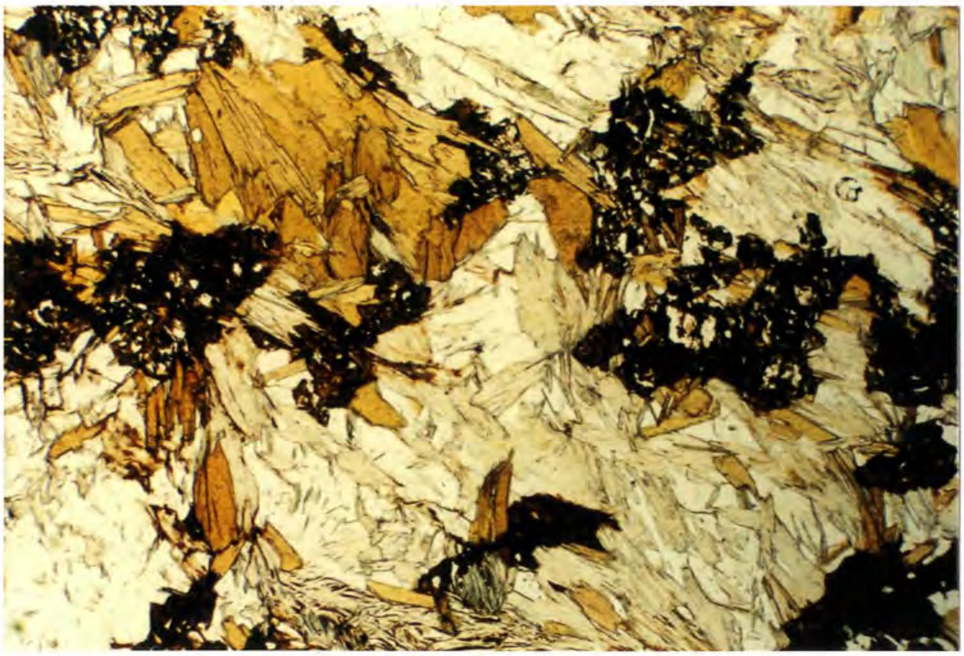

Plate 17

Matchless West Extension deposit, ultramafic exhalites: talc-phlogopite-carbonate schist. Talc and phlogopite lamellae grow on a quartzose groundmass. Carbonate porphyroblasts are repleced by Fe-hydroxides.
(Thin section MWE 246A; // Nicols; field of view = 4 mm).

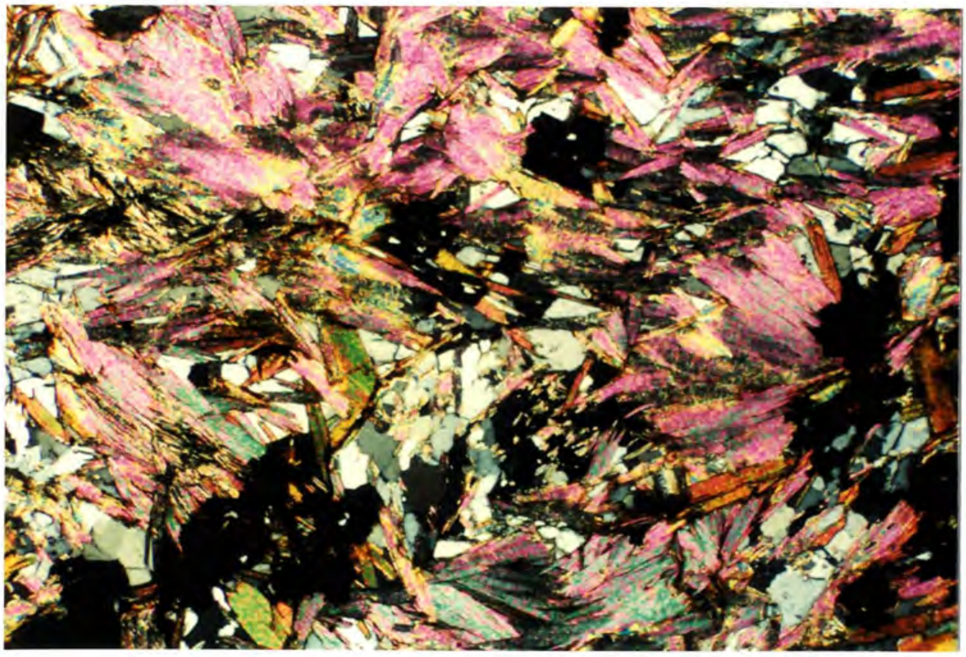

Plate 18

Matchless West Extension deposit: same rock type as in Plate 17.
(Thin section MWE 246A; + Nicols; field of view = 4 mm).

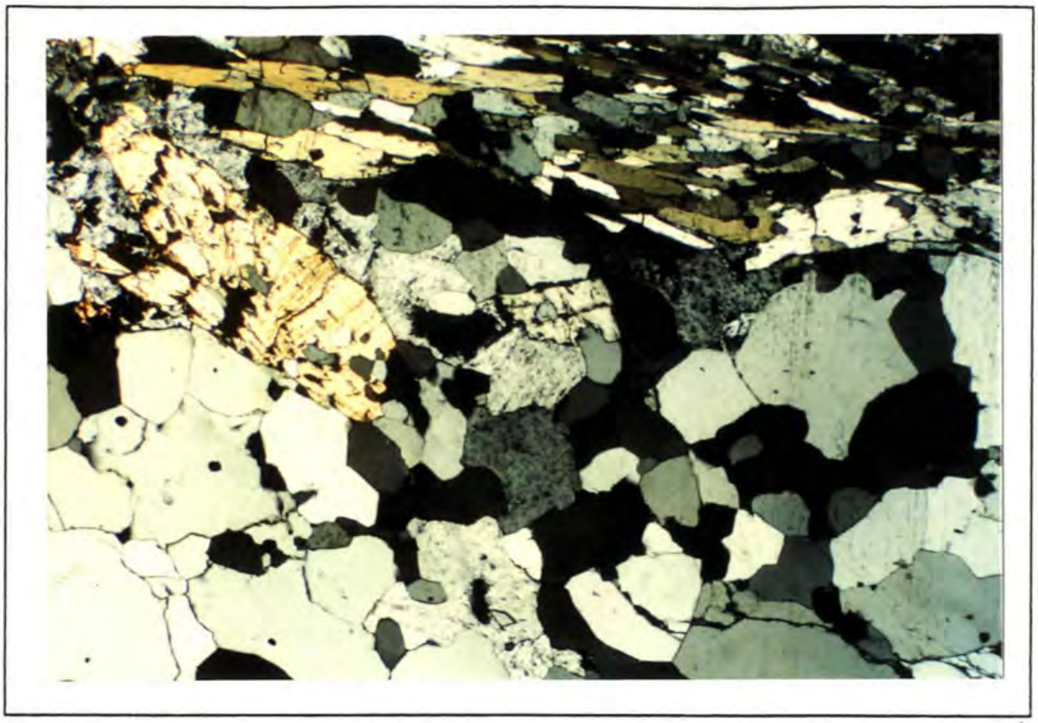

Plate 19

Matchless West Extension deposit, ultramafic exhalites: assemblage of actinolite (yellowish), quartz (white to grey) and baryte (grey, in centre).
(Thin section MWE 236; + Nicols; field of view = 4 mm).

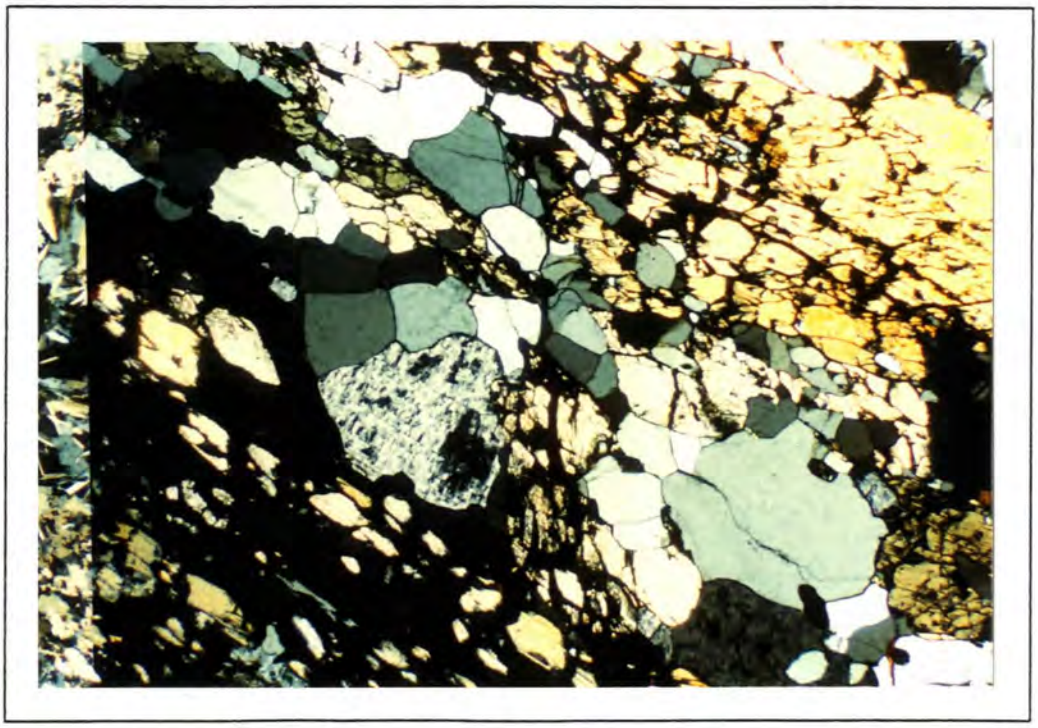

Plate 20

Matchless west Extension deposit, ultramafic exhalites: actinolite (yellowish) and baryte (grey, mottled) in gossanous quartzite.
(Thin section MWE 245A; + Nicols; field of view = 4 mm).

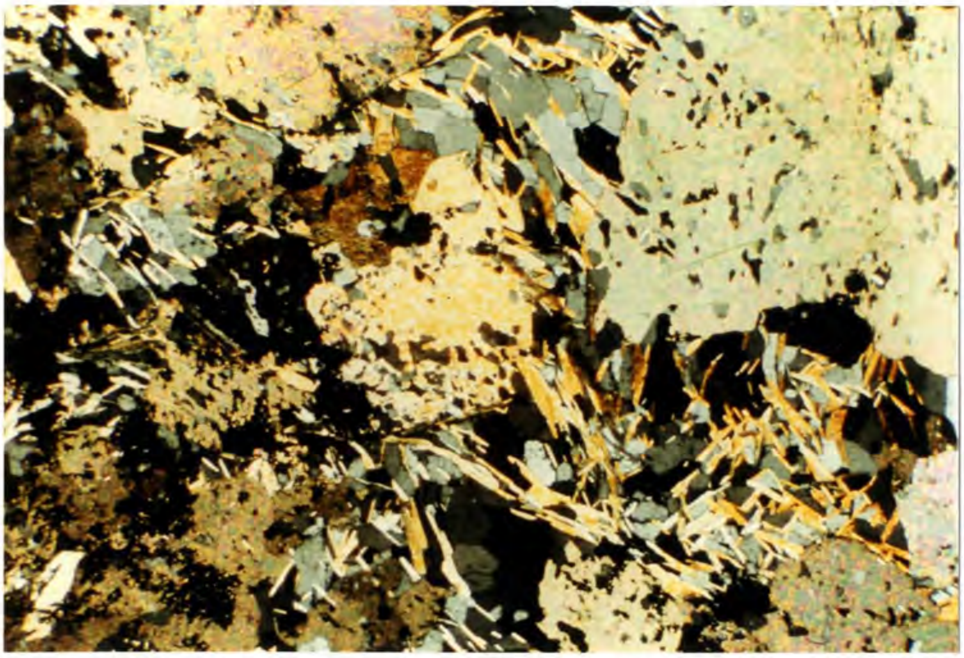

Plate 21

Matchless West extension deposit, marble-like rock: anhedral, sieve-textured carbonate crystals replacing the muscovite-bearing quartzitic-groundmass.
(Thin section MWE 259; + Nicols; field of view = 4 mm).

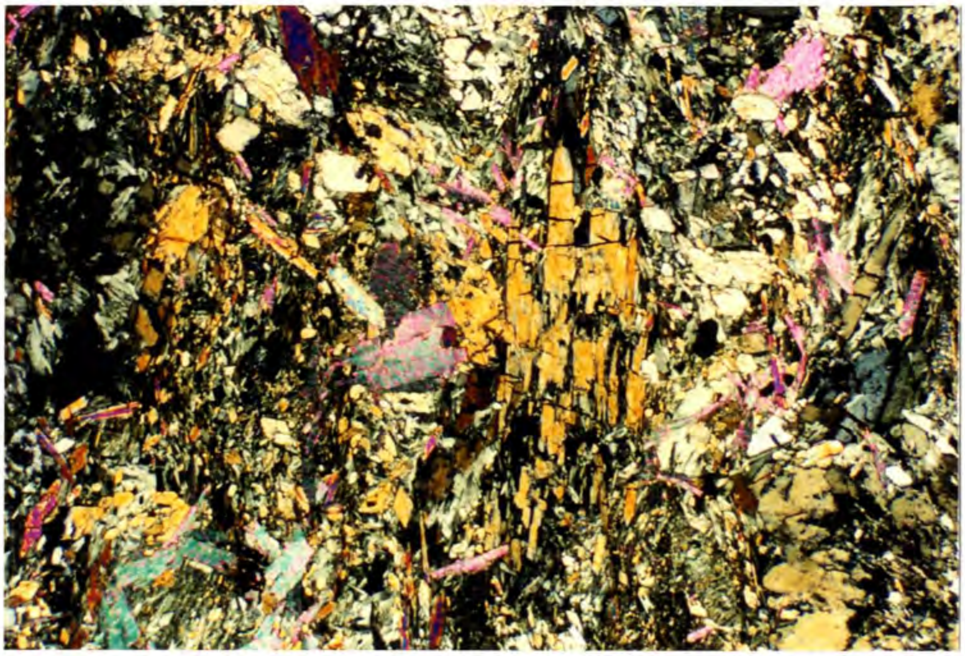

Plate 22

Von Francois Ost 60 farm area, massive talc-chlorite-actinolite schist: subhedral actinolite crystals (yellowish) and talc lamellae (pink to green) included in a fine-grained chlorite-rich groundmass.
(Thin section OTJ 685; + Nicols; field of view = 4 mm).

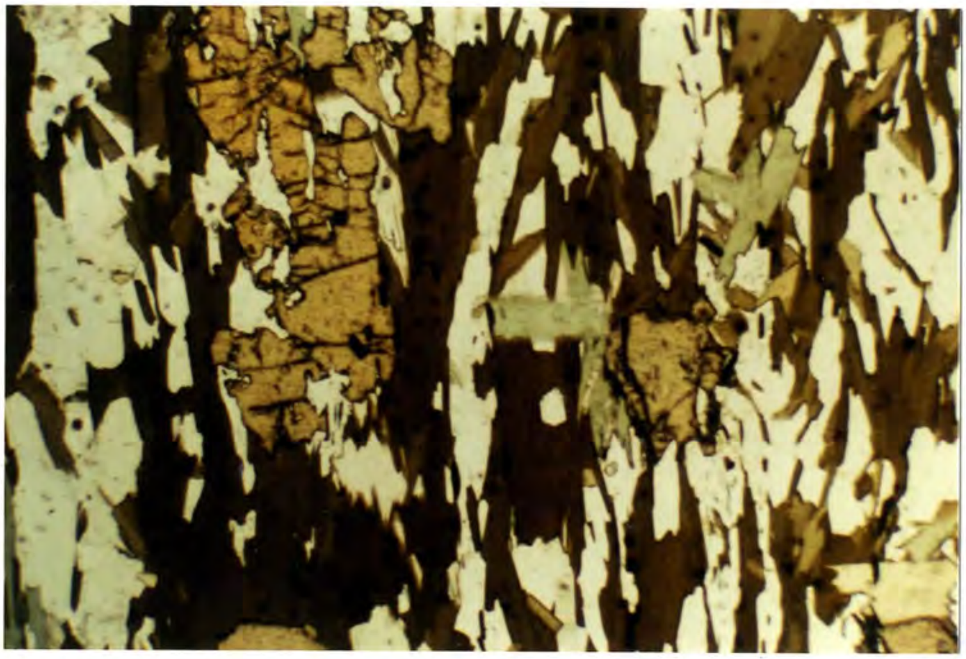

Plate 23

Ongombo deposit, borehole no. OGB 153A: staurolite-bearing quartz-biotite-muscovite-chlorite schist in the hangingwall next to the ore zone. Note the brown colour of the biotite lamellae.
(Thin section OG 716; // Nicols; field of view = 4 mm).

Plate 24

Ongombo deposit, borehole no. OGB 153A: biotite selvedge zone showing the coarse biotite groundmass, subhedral staurolite grains, coarse apatite crystals and part of pyrite "augen". Note the reddish-brown tinge of the biotite lamellae.
(Thin section OG 718; // Nicols; field of view = 4 mm).

Plate 25

Ongombo deposit, borehole no. OGB 153A: plagioclase-rich biotite schist facies within the ore zone.
(Thin section OG 735; + Nicols; field of view = 4 mm).

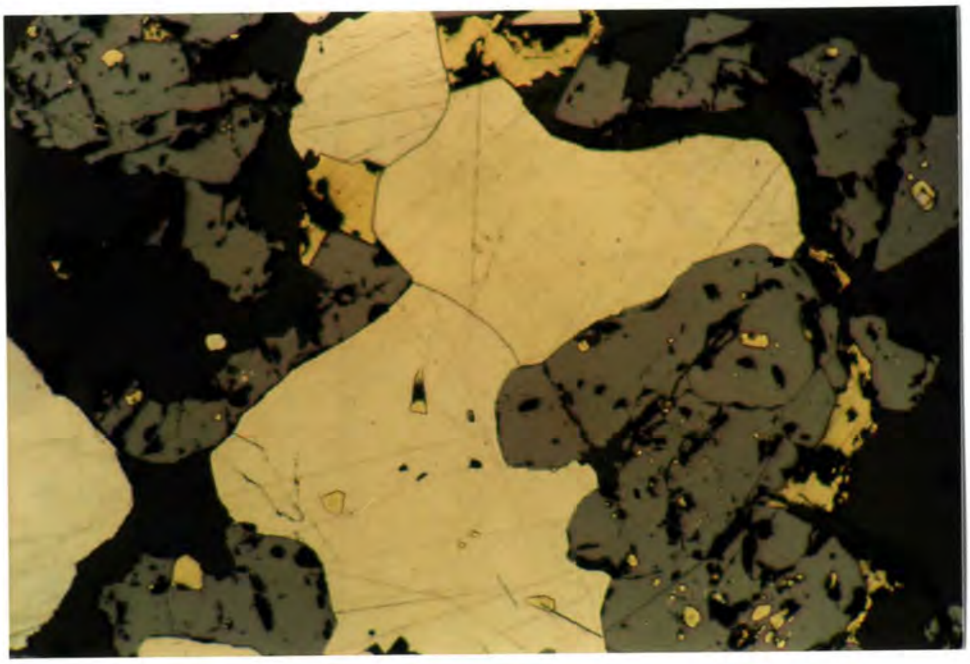

Plate 26

Ongombo deposit, borehole no. OGB 153A, sulphide-bearing magnetite quartzite: embayed intergrowth between recrystallized pyrite (white) and magnetite (grey). Chalcopyrite (greeny yellow) occurs as interstitial patches and inclusions within pyrite and magnetite.
(Polished section OG 747; // Nicols; field of view = 2.5 mm).

Plate 25

Ongombo deposit, borehole no. OGB 153A: plagioclase-rich biotite schist facies within the ore zone.
(Thin section OG 735; + Nicols; field of view = 4 mm).

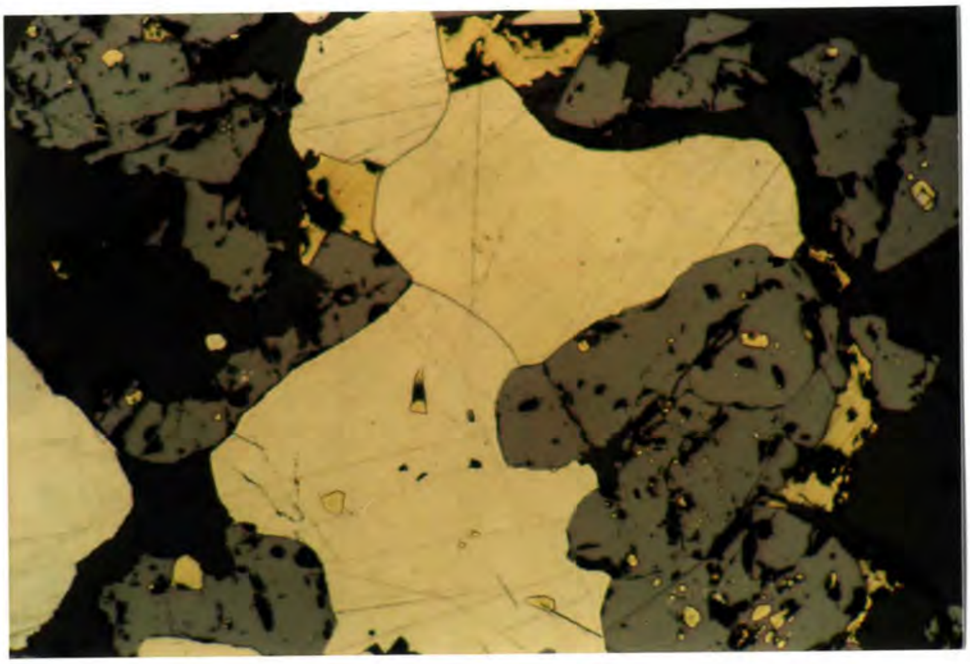

Plate 26

Ongombo deposit, borehole no. OGB 153A, sulphide-bearing magnetite quartzite: embayed intergrowth between recrystallized pyrite (white) and magnetite (grey). Chalcopyrite (greeny yellow) occurs as interstitial patches and inclusions within pyrite and magnetite.
(Polished section OG 747; // Nicols; field of view = 2.5 mm).